

**APPENDIX B.1**  
**PRELIMINARY GEOLOGIC HAZARDS ASSESSMENT**

# Technical Memorandum

---

<b>To:</b>	Javier Toro Rosemont Copper Company Tucson, Arizona	<b>Project No:</b>	1720214024
<b>By:</b>	Blake Easby and Jared Mullenbach Wood Environment & Infrastructure Solutions, Inc. (Wood)	<b>Reviewed by:</b>	Dan Johnson PE, RG, SME-RM
<b>Tel:</b>	775-398-7187	<b>CC:</b>	File
<b>Date:</b>	January 12, 2022		
<b>Re:</b>	<b>Preliminary Geologic Hazard Assessment Rosemont Copper World Project</b>		

---

## 1.0 Introduction

This Technical Memorandum presents the results of a preliminary Geologic Hazard Assessment performed by Wood Environment & Infrastructure Solutions, Inc. (Wood) to support Rosemont Copper Company's (Rosemont) Rosemont Copper World Project (Project). The Project consists of six open pits and related facilities located on the west and east flanks of the Santa Rita Mountain Range, approximately 28 miles southeast of Tucson, Arizona, in Pima County in the Rosemont and Helvetia mining districts. The purpose of this report is to present a preliminary summary and evaluation of geologic hazards in the vicinity of the Project based on available references.

## 2.0 Project Description

The Project will be developed as a conventional open pit truck and shovel surface mining operation with a milling and processing plant for sulfide ore, heap leach for oxide ore, and associated facilities. The mine life is estimated to be 15 years. The open pits will be mined in a sequence that generally progresses from west to east, facilitating the use of the available land to construct the waste rock facilities and other infrastructure. The six open pits named from west to east are Peach Pit, Elgin Pit, Heavy Weight Pit, Copper World Pit, Broadtop Butte Pit, and Rosemont Pit. Tailings from milling and sulfide ore processing will be deposited in two cyclone tailings impoundments. A heap leach facility (HLF) and waste rock facilities (WRFs) will be constructed as part of the mining operation. The Heavy Weight Pit, Copper World Pit, and Broadtop Butte Pit will be backfilled with waste rock after mining in each of the pits is completed. Figure 1 shows the location of facilities, open pits, and infrastructure.

## 3.0 Site Conditions

### 3.1 Regional Physiographic and Geologic Setting

The Project is located in the southern portion of the Basin and Range physiographic province. The Basin and Range is characterized by extensional tectonism with significant displacement along normal faults and contains discontinuous, semi-parallel mountain ranges separated by alluvial basins.

Located in the Santa Rita Mountain Range in Southern Arizona, the Project is underlain by Precambrian granite and north striking Cambrian to Permian marine sediments generally consisting of quartzite,

limestone, and dolomite, many of which have been metamorphosed. The sediments have been deformed by broad to locally tight and generally southeast-plunging folds. Overlying the marine sediments are Mesozoic clastic units which include conglomerates, sandstones, and siltstones. The Precambrian granite and sedimentary rocks are intruded locally by younger granitic rocks, including the Helvetia granite quartz monzonite porphyry and quartz latite porphyry. Faulting is generally north-trending and steeply-dipping, forming several major structural blocks (Ferguson, 2019; Meagher, 2017; Johnson, 2007).

### **3.2 Quaternary and Tertiary Surficial Deposits**

Alluvial deposits underlie significant portions of the Tailings Storage Facilities (TSFs) and HLF. The alluvium consists of sands and gravels with low and variable amounts of silt and clay, and varying amounts of cobbles and boulders. Cementation of some of the alluvial deposits were noted during recent geotechnical investigations (Wood, 2021a). The alluvial deposits are incised where ephemeral washes and drainages occur. Upgradient from the alluvial deposits in the steeper hillslope terrain, colluvium and talus deposits are present which generally consist of angular to subangular gravels with scattered boulders and cobbles (Ferguson, 2019). Historic areas of human disturbance on site include small-scale mine workings, road cuts and fills, and slag deposits.

## **4.0 Geologic Hazards**

Geologic hazards are geologic conditions that pose a potential hazard to life and/or property. In the context of geologic hazards, risk is the chance that the identified hazard will result in harm or damage to property. The following geologic hazards were identified at the Project property.

### **4.1 Rock Fall Hazards**

Rock fall occurs when rocks become dislodged from and descend down slopes. Rock fall typically originates on steep terrain, particularly where there are bare rock outcrops (Wyllie, 2015). The Project property traverses the Santa Rita Mountains, and some portions of the mining operations and infrastructure will be located in potential rock fall runout areas below and adjacent to steep hillslopes and rock outcrops (Photograph 1).

To define rock fall hazard areas in the vicinity of the Project facilities, Wood performed the following tasks:

- Project site topography of the area was displayed, and pixels were categorized by slope angle in ArcGIS (2020). Slopes at an angle of 30 degrees or greater were noted as the likely maximum runout of rock fall (Wyllie, 2015)
- Areas with slopes of 30 degrees or greater were reviewed in Google Earth (2022) and photographs taken during a site visit performed on August 11, 2021, for a rock fall source up gradient, such as exposed bedrock, and were selected as potential rock fall hazard areas if a rock fall source was identified in the aerial images
- Rock fall hazard areas in and around the facilities and pits were plotted in Figure 2

A large area along the crest of the Santa Rita Mountains and other steep terrain in the foothills of the mountain range were identified as potential source and runout areas for rock fall. The facilities that could be impacted by rock fall either during construction or during operations are TSF-2, the WRF, and the open pits. The potential hazard area of TSF-2 includes the far eastern portion of the facility where it is located adjacent to the base of the Santa Rita Mountains (Photograph 2). Rock fall hazards can be a risk for the open pit operations during mining. The risk of rock fall is most likely to exist early in development of the pits since many of the rock fall source areas (exposed rock outcrops) will largely be mined out during operations. Rock fall within the pits is managed by the incorporation of rock fall catchment benches. Various portions of the WRF will be located adjacent to steep slopes in the Santa Rita Mountains which could be

impacted by rock fall during early development. Additionally, rock fall hazards could exist for access roads and haul roads and at temporary facilities such as laydown yards and electrical substations.

Additional areas of rock fall hazard not shown on the map include steeply incised alluvial channels and valleys, in which loose cobbles or boulders can become dislodged from the channel slopes.

## **4.2 Historic Mine Workings**

Historic mining has occurred in the Helvetia mining district since the late 1800s and many historic mine working features are located in the footprint of the Project facilities and pits. To summarize historic mine workings hazards in the vicinity of the Project, Wood referenced the USGS (2021) Abandoned Mine Lands (AML) database. The AML database includes information on location, feature type, and the topographic map the feature was initially identified on. The size of the feature and extent of underground workings is not included in the AML database. Features included in the USGS (2021) AML database on the Project site are shown in Figure 2. Identified historic mine workings in the vicinity of the Project generally consist of adits, mine shafts, open pit mines, and prospect pits. Of those, adits and mine shafts may contain underground features of unknown size (USGS, 2021).

Most historic mine workings on the eastern flanks of the Santa Rita Mountains in the vicinity of the Rosemont Pit are shallow pits that are no more than a few feet in diameter and depth (Tetra Tech, 2007), and the same appears to be true for the western flanks of the Santa Rita Mountains based on review of Google Earth images and observations made during the August 11, 2021, site visit. However, some extensive developments may be present on both the eastern and western flanks of the Santa Rita Mountains such as underground mine workings and waste rock dumps which may require further investigation and mitigation, such as backfilling, to reduce risks. As shown in Figure 2, several historic mine working features are located within the footprint of the TSF-1, the WRF, and the open pits. Mine shafts under TSF-1 and the WRF were measured in Google Earth (2022) to be circular and have a surface diameter of approximately 10 to 15 ft. Further investigation of underground workings could include geophysical techniques or physical inspection with a drone or cavity monitoring system (CMS).

## **4.3 Seismic Hazard**

A site-specific Seismic Hazard Analysis was performed by Lettis Consultants International, Inc. (LCI) to support the Project (LCI, 2021). The following is a summary of the findings of the LCI (2021) report.

The Project is located in the Southern Basin and Range province near the southern US border in a region characterized by relatively few late Quaternary faults and low rates of seismicity. LCI reviewed active and potentially active faults within 90 miles of the Project site which include faults showing evidence of activity in the late Quaternary ( $\leq 130,000$  years) or repeated activity in the Quaternary ( $\leq 1.6$  million years). LCI Identified the Santa Rita fault zone, the southern Cerro Prieto, and southern San Andreas faults as significant fault sources to the seismic hazard to the Project. A catalog of historical seismicity that encompasses an area of over 90 miles around the Project was also used by LCI. The catalog includes 26 moment magnitude (M) events of M 5 to 5.9, three events of M 6 to 6.9, and three events of M 7 and greater. Only five events in the historic record have occurred within 30 miles of the Project, the largest being an M 5.7 earthquake that occurred on November 11, 1887, about 15 miles northeast of the site. LCI performed a probabilistic seismic hazard analysis (PSHA) and deterministic seismic hazard analysis (DSHA), and the ground motion hazard results were used in the design of the facilities at the Project.

Based on the findings of the LCI (2021) study, including the lack of mapped surface fault traces with evidence of latest Quaternary displacement in the vicinity of the Project, Wood considers the risk of surface fault rupture to directly impact the proposed facilities to be low.



#### **4.4 Landslides**

Wood's review of available published references (Arizona Geological Survey [AZGS], 2010) and reconnaissance level site observations conducted during the geotechnical investigations at the Project by Wood in 2021 indicate there are no existing landslides mapped in the Project area. As such, the risk of existing landslides directly impacting the proposed facilities is considered low. However, the potential for construction activities, including excavation in steep terrain, to initiate slope instabilities should be considered in the design of the facilities.

#### **4.5 Flooding**

Wood referenced the Federal Emergency Management Agency (FEMA) flood zone maps to evaluate flooding hazards at the Project site. FEMA has assigned flood zones to identify areas with potential for flood hazards. Most of the Project site is located in Zone D which is defined by FEMA as "an area with a potentially moderate to high risk of flooding, but the probability has not been determined" (FEMA, 2011). The nearest published high potential flood area is to the east of the Project site in Davidson Canyon along State Highway 83 about 5 miles to the east-northeast of the Broadtop Butte Pit (FEMA, 2011). Local flooding of ephemeral washes and drainages can occur during and immediately after heavy rains, particularly during the monsoon season in Southern Arizona (approximately June through September) so surface water and flood management should be incorporated in the design of the surface facilities.

#### **4.6 Erosion**

Erosion potential was determined using the "K-factor" from the United States Department of Agriculture (USDA) web soil database (2021). The K-factor ranges from 0.02 to 0.69 with 0.69 being the highest potential for erosion, and the soil with the highest K-factor on the Project property was located in the alluvium and had a K-factor of 0.24, indicating low erodibility. Erosion sufficient to create a hazard to the Project facilities is most likely to occur during short, intense periods of rainfall at the Project site. The USDA web soil database (2021) has a rating assigned to soil types based on wind erodibility group (WEG). A rating of 1 defines a highly erodible soil from wind and 8 defines soil that is least susceptible to wind. The lowest rating on the Project property is in the alluvium and had a WEG of 3, indicating moderate erodibility. Erosion due to wind may occur, but it will likely not be a hazard due to the significant magnitude of erosion required to affect facilities. While there are no areas identified as unusually highly susceptible to accelerated erosion (USDA, 2021), construction activities and modifications to the natural ground surface have the potential to create conditions favorable to accelerated erosion during heavy precipitation events. Thus, the potential for erosion should be considered in the design of the facilities.

#### **4.7 Ground Subsidence and Earth Fissures**

Ground subsidence can occur from both natural processes and human activities. Some human activities that cause subsidence are mining activity, withdrawing groundwater or other fluids, and saturating collapsible sediments that are near surface. Ground subsidence and related earth fissures due to groundwater withdrawal in basin fill alluvial sediments are geologic hazards that have been identified in multiple basins in Arizona (Slaff, 1993). Larger amounts of subsidence can occur where soils are thickest in alluvium filled valleys. Earth fissures are cracks in the ground surface that form when the water table is lowered, and sediment consolidates (settles) differentially. One common cause of differential settlement can be differences in the depth to bedrock, such as where faults have displaced bedrock or along the margins of alluvial basins where alluvial sediment thicknesses decrease. Earth fissures can damage facilities or foundations for buildings due to differential settlement and the presence of air voids.

To evaluate the risk for ground subsidence and earth fissures to occur at the Project site, Wood reviewed the AZGS Hazard Maps which includes existing earth fissuring and ground subsidence. The AZGS Hazard Maps do not contain any recorded earth fissures in the Project area (AZGS, 2010). Additionally, the presence

of groundwater in the Project area is primarily in the bedrock and not in the relatively thin alluvial cover present within the footprint of the surface facilities (less than about 100 ft). Therefore, the risk of ground subsidence and earth fissuring is considered low.

#### **4.8 Expansive Soils**

Different soil types have a different affinity for absorbing water. Soils that intake more water can swell and cause damage to structures. Soils that contain clay are more likely to swell from surface water and those that have a high liquid limit and plasticity index have the highest swelling potential (FHWA, 1977). Soils with a high potential for swelling (i.e., high clay content) have not been identified on the Project site during geotechnical studies and surficial soil mapping (Wood, 2021a; USDA, 2021).

#### **4.9 Karst**

Karst is a topography composed of limestone or other soluble rocks that is formed by the dissolution of the minerals contained in the rocks by fluids either on the surface or subsurface, sometimes causing a surface collapse or sinkhole which could result in harm or loss of property. Although there are limestone and other carbonate units in the Project site, Wood's field investigations conducted in 2021 and discussions with Rosemont staff are that there is no visible evidence of karst terrain at the Project site, and karst has not been identified in the available geologic maps and resources (Ferguson et al., 2019; Drewes, 1971). Although a detailed investigation for karst features has not been conducted to date at the Project site and it is possible that unidentified karst could be present, Wood considers the risk for karst features to impact construction operations and facilities to be low.

### **5.0 Conclusions**

This Technical Memorandum presents a summary of identified geologic hazards based on review of the available data and limited field investigations. The following principal geologic hazards have been identified that should be considered in the design, construction, and operations of the facilities of the Rosemont Copper World Project:

- Rock fall hazards were identified within and adjacent to areas of relatively steep topography that also contain potential rockfall sources. Affected facilities include the WRF (see Figure 2), the open pits, and relatively small, localized portions of the east slope of TSF-2. Possible mitigation for rock fall hazards may include catchment ditches, berms, and offsets
- Historic mine workings have been identified within the footprint of the TSF-1, WRF, and the open pits. The majority of the features are small surface prospect workings that are no more than a few feet in diameter and depth and would likely have little impact on mining activity. However, some more extensive developments may require additional evaluation and mitigation. Mitigation of existing historic underground mine workings within the footprint of the TSF-1, WRF, and open pits may require backfilling and detailed operational procedures for work around voids. If extensive underground workings are identified in the open pit areas, a Hazard Mitigation Plan for underground voids may be required that includes void identification and safe working procedures
- The Project is located in a geographical province characterized by relatively few late Quaternary surface fault traces and low rates of seismicity. The risk of surface fault rupture to directly impact the facilities is considered low. Ground motion hazard results have been used in the design of the facilities at the Project
- Flooding, existing landslides, expansive soils, and erosion are considered relatively low potential risks

## 6.0 Recommendations

- Rock fall mitigation measures and engineering may be necessary to reduce the risk to infrastructure and personnel where identified. As needed, rock fall studies should be completed for facilities, access roads, infrastructure, and pits where rock fall is identified as a risk
- Historic mine workings should be further investigated and engineering designs for mitigation may be required where historic workings are located within the footprint of permanent or temporary infrastructure
- Surface water should be managed to mitigate the risk of flooding and accelerated erosion to infrastructure
- This study is intended to provide a preliminary assessment of geologic hazards at the Project site based on Wood's review of available published data, the Tetra Tech (2007) Geologic Hazard Assessment, observations made by Wood staff during geotechnical field investigations, and discussions with and information provided by Rosemont personnel. More detailed investigations of specific hazards should be performed as needed at future stages of design, construction, and operations

## 7.0 References

- Arizona Geological Survey (AZGS), 2010. Natural Hazards in Arizona. Earth Fissures Map. Viewed online at [Natural Hazards in Arizona \(arcgis.com\)](http://arcgis.com).
- Cook, J.P., Ferguson, C.A., 2019. Geologic Map of Empire Ranch 7.5' Quadrangle, Pima County, Arizona. Arizona Geological Survey Digital Maps, DGM 143, 1 map sheet, map scale 1:24,000.
- Esri, 2020. ArcGIS Desktop, ArcMap™ Version 10.5.
- Federal Emergency Management Agency [FEMA], 2011. FEMA's National Flood Hazard Layer (NFHL) Viewer. viewed online at <https://www.fema.gov/flood-maps/national-flood-hazard-layer>.
- Federal Highway Administration (FHWA), 1977. An Evaluation of Expedient Methodology for Identification of Potentially Expansive Soils. Report No. FHWA-RD-77-94.
- Ferguson, C.A., Johnson, B.J., Pearthree, P.A., Spencer, J.E., Shipman, T.C., and J.P. Cook, 2019. Geologic map of the Helvetia 7½' Quadrangle, Pima County, Arizona: Arizona Geological Survey Digital Geologic Map DGM-77, scale 1:24,000.
- Ferguson, C.A., Youberg, A., Gilbert, W.G., Orr, T.R., Richard, S.M., and J.E. Spencer, 2019. Geologic Map of the Mount Fagan 7.5' Quadrangle, Eastern Pima County, Arizona: Arizona Geological Survey Digital Geologic Map DGM-11, version 2.0, map scale 1:24,000.
- Google, 2022. Google Earth Pro. Version 7.3.4.8248
- Johnson, B.J., Pearthree, P.A., and C.A. Ferguson, 2016, Geologic map of the Corona de Tucson 7 1/2" Quadrangle, Pima County, Arizona: Arizona Geological Survey Digital Geologic Map DGM-115, scale 1:24,000.
- Lettis Consultants International, [LCI], (2021), Site-Specific Seismic Hazard Analysis and Development of Design Ground Motions for Hudbay's Rosemont Pre-Feasibility Study, dated November 11, 2021.
- Meagher, 2017. Rosemont Copper Project: NI 43-101 Technical Report, Feasibility Study, Updated Mineral Resource, Mineral Reserve and Financial Estimates, Pima County, Arizona, USA. Revision 3. Prepared for Hudbay Minerals Inc. Tucson, AZ: March 30, 2017.
- Slaff, S., 1993, Land Subsidence and Earth Fissures in Arizona. Arizona Geological Survey, Down-to-Earth Series 3, 32 p.
- Tetra Tech, 2007. Geologic Hazard Assessment. Prepared for Augusta Resource Corporation.
- United States Department of Agriculture (USDA), 2021. Web Soil Survey from Natural Resources Conservation Service. Downloaded from [Web Soil Survey \(usda.gov\)](http://usda.gov).
- United States Geological Survey (USGS), 2021. Prospect- and mine-related features on USGS topographic maps. Downloaded from <https://mrdata.usgs.gov/usmin/> on December 9, 2021.

- Weary, D.J., and Doctor, D.H., 2014, Karst in the United States: A digital map compilation and database: U.S. Geological Survey Open-File Report 2014–1156, 23 p., <https://dx.doi.org/10.3133/ofr20141156>. ISSN 2331-1258 (online)
- Wood, 2021a. Geotechnical Site Investigation Memorandum, Heap Leach, Tailings and Waste Rock Facilities, Project, prepared for Rosemont Copper Company, by Wood, December 1.
- Wood, 2021b. Stability Analysis Memorandum, Waste Rock Facility, Project, prepared for Rosemont Copper Company, by Wood, November 29.
- Wyllie, D., 2015. Rock Fall Engineering. CRC Press Taylor and Francis Group, Boca Raton, FL.

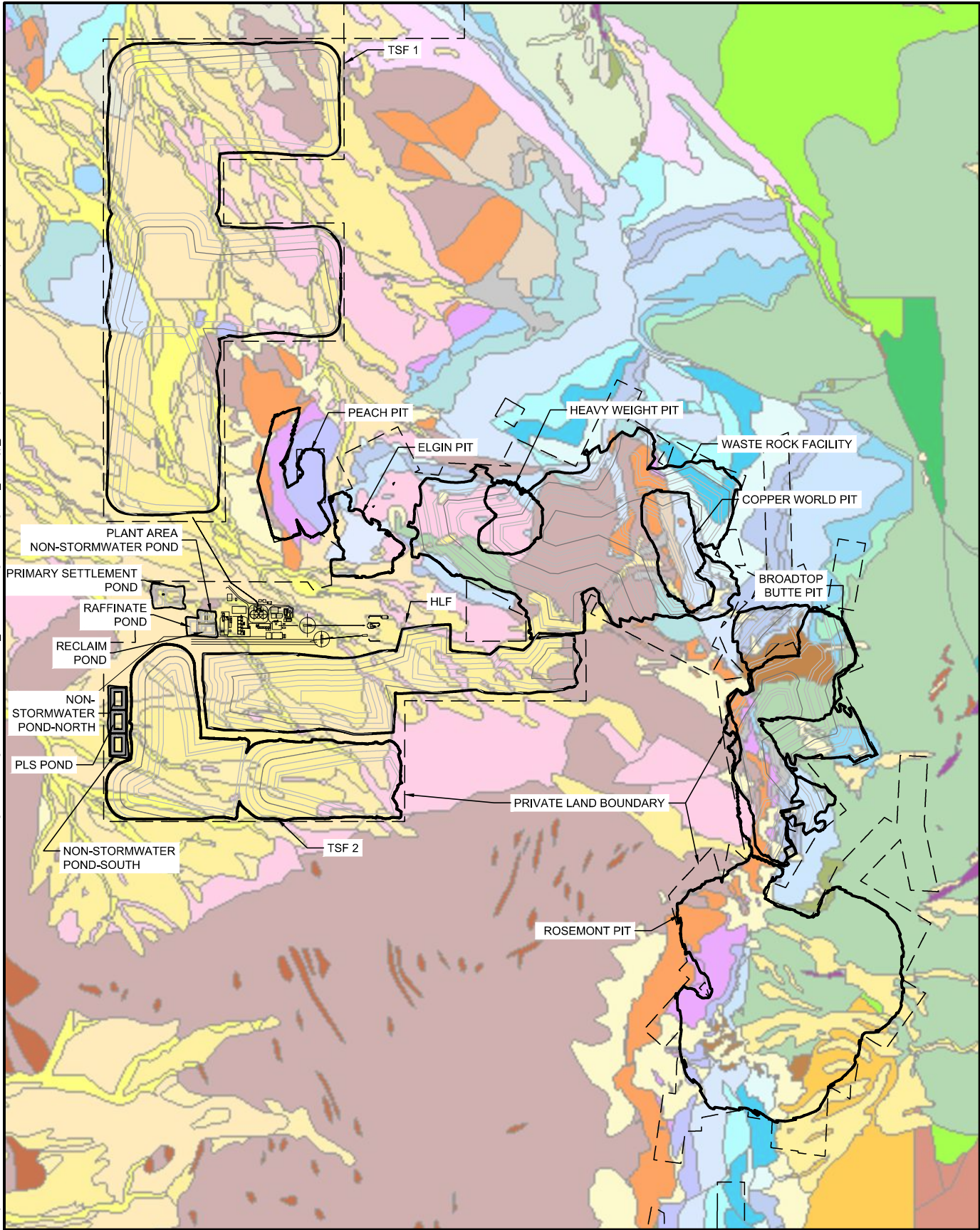
## ACRONYMS AND ABBREVIATIONS

%	%
AML	Abandoned Mine Lands
AZGS	Arizona Geological Survey
CMS	Cavity Monitoring System
DSHA	deterministic seismic hazard analysis
FEMA	Federal Emergency Management Agency
HLF	Heap Leach Facility
LCI	Lettis Consultants International, Inc.
M	Magnitude
Mt	Million Tons
Project	Rosemont Copper World Project
PSHA	Probabilistic Seismic Hazard Analysis
Rosemont	Rosemont Copper Company
TSF	Tailings Storage Facility
USDA	United States Department of Agriculture
USGS	United States Geological Survey
WEG	Wind Erosion Group
Wood	Wood Environment & Infrastructure Solutions, Inc.
WRF	Waste Rock Facility

Figures



Drawing Path: C:\Users\jared.mullenbach\Wood PLC\Rosemont RP21 - Private Land Studies - General\04 Eng Tech\Geologic Hazard Assessment\3\_CAD - Drawing Name: Figure 1\_Geology\_gileaud.dwg Plot Date: 01/06/22 - 3:35pm



SITE PLAN  
SCALE: 1"=3000'

LEGEND

- FACILITY OR PIT BOUNDARY
- PRIVATE LAND BOUNDARY
- 50 AND 250 FT CONTOURS USED ON FACILITIES

d Disturbed Ground

Surficial Deposits

- Qtc Talus and Colluvium
- Qy3 Deposits in active channels
- Qy2 Deposits in low terraces and active fans
- Qy1 Deposits in low terraces and young fans
- Qy Young alluvial deposits, undivided
- Qyx Eroded fine deposits
- Qi4 Deposits in young intermediate deposits and alluvial fans
- Qi3 Deposits in intermediate terraces and relic alluvial fans
- Qi2 Deposits in higher intermediate fans and terraces
- Qi1 Deposits in highest intermediate fans and terraces
- Qo Deposits in highest preserved alluvial fans
- QTa Old alluvial fan deposits

Bedrock Units

- Tc Gila Conglomerate (Miocene)
- Tcl Unit of Adobe Tank (Gila Group)
- Tp Pantano Formation (Oligocene to Miocene)
- TKs Lower Pantano megabreccia (U. Cretaceous - Oligocene)
- Tgp Porphyritic granite of Sycamore Canyon
- Tg Helvetia granite
- TKp Fine grained felsic porphyry (Tertiary - U. Cretaceous)
- Kr Rhyolite of Mt. Fagan
- Krz Heterolithic mesobreccia
- Krg Heterolithic megabreccia
- Kra Andesite megabreccia
- Krb Bisbee group megabreccia
- Krc Well-rounded conglomerate megabreccia
- Kaj Andesitic lava
- Kai Andesitic porphyry
- Kd Crystal-rich dacite ash-flow tuff
- Kdl Dacitic lava
- Kfc Fort Crittenden Formation
- Kfcv Fort Crittenden Formation, volcanic facies
- KJr Rhyolite Intrusions

Bisbee Group

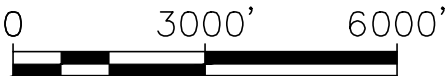
- Kt Turney Formation
- Ks Shellenburg Formation
- Ksl Lower Shellenburg Formation
- Ka Apache Canyon Formation
- Kw Willow Canyon Formation
- Kwm Willow Canyon Formation, mafic lava
- KJg Glance Conglomerate
- KJgs Glance Conglomerate (quartz sandstone-carbonate dominant)
- KJgg Glance Conglomerate (granite dominant)
- K^u Undifferentiated Mesozoic clastic rocks
- J^g Gardner Canyon Formation
- JPs Quartz sandstone

Naco Group

- Pr Rainvalley Formation
- Pch Concha Limestone
- Psu Sherrer Formation, upper division
- Psl Sherrer Formation, lower division
- Pe Epitaph Formation, undivided
- Pc Colina Limestone
- \*Pe Earp Formation
- \*h Horquilla Limestone
- Me Escabrosa Limestone
- MDu Escabrosa Limestone and Martin Limestone, undifferentiated
- Dm Martin Formation
- D\_u Martin Limestone and Abrigo Formation, undifferentiated
- Pz Marble, hornfels and skarn
- \_a Abrigo Formation
- \_b Bolsa quartzite
- YXa Megacrystic granite
- YXg Continental Granodiorite

GEOLOGY FILE PROVIDED BY PITEAU. FROM THE FOLLOWING SOURCES.

- Johnson, B.J., Pearthree, P.A., and Ferguson, C.A., 2016, Geologic map of the Corona de Tucson 7 1/2" Quadrangle, Pima County, Arizona: Arizona Geological Survey Digital Geologic Map DGM-115, scale 1:24,000.
- Ferguson, C.A., Youberg, A., Gilbert, W.G., Orr, T.R., Richard, S.M., and J.E. Spencer, 2019, Geologic Map of the Mount Fagan 7.5' Quadrangle, Eastern Pima County, Arizona: Arizona Geological Survey Digital Geologic Map DGM-11, version 2.0, map scale 1:24,000.
- Ferguson, C.A., Johnson, B.J., Pearthree, P.A., Spencer, J.E., Shipman, T.C., and Cook, J.P., 2019, Geologic Map of the Helvetia 7.5' Quadrangle, Pima County, Arizona: Arizona Geological Survey Digital Geologic Maps, DGM-144, 1 map sheet, map scale 1:24,000.
- Cook, J.P., Ferguson, C.A., 2019, Geologic Map of Empire Ranch 7.5' Quadrangle, Pima County, Arizona: Arizona Geological Survey Digital Maps, DGM 143, 1 map sheet, map scale 1:24,000.



ROSEMONT COPPER WORLD PROJECT  
SURFACE GEOLOGY

**wood.**

WOOD ENVIRONMENT & INFRASTRUCTURE SOLUTIONS  
9460 DOUBLE R BLVD SUITE 201  
RENO, NEVADA, 89521  
PHONE: 775-329-6123

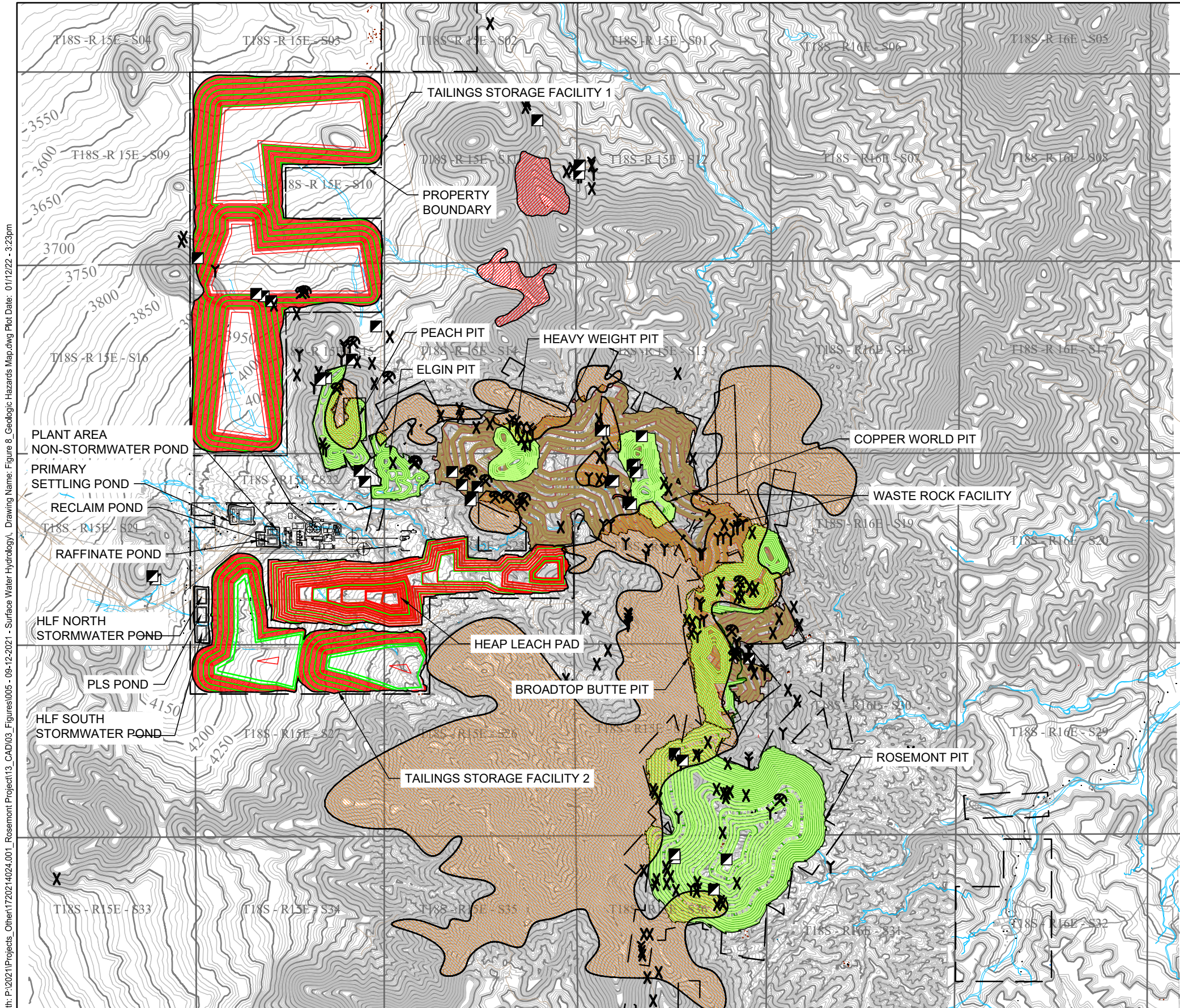
Figure:

1

By: JM Date: 1/6/2021 Project No: 17-2021-4024



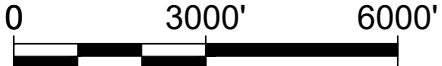
Drawing Path: P:\2021\Projects\_Other\1720214024.001\_Rosemont Project\13\_CAD\03\_Figures\005 - 09-12-2021 - Surface Water Hydrology\ Drawing Name: Figure 8. Geologic Hazards Map.dwg Plot Date: 01/12/22 - 3:23pm



**SITE PLAN**  
SCALE: 1" = 3000'

**LEGEND:**

- PROPERTY BOUNDARY
- MINE WORKING AREAS - MEASURED POLYGONS WHERE HISTORIC OR CURRENT MINE WORKINGS ARE PRESENT (USGS 2021)
- ROCKFALL AREA - AREA OF HIGH RELIEF OR PREDICTED RUNOUT DISTANCE OF ROCKFALL FROM PEAKS
- OPEN PIT MINE (USGS 2021)
- PROSPECT PIT (USGS 2021)
- ADIT(USGS 2021)
- MINE SHAFT (USGS 2021)



ROSEMONT COPPER WORLD PROJECT  
GEOLOGIC HAZARDS MAP



WOOD ENVIRONMENT & INFRASTRUCTURE SOLUTIONS  
4600 E WASHINGTON ST. SUITE 600  
PHOENIX, ARIZONA 85034  
PHONE: 602-733-6000

Figure:

2

By: OAS Date: 11/11/21 Project No: 17-2021-4024



**Attachment**



**Photograph 1 - View of rock outcrops along the crest of the Santa Rita Mountain Range (Looking East)**



**Photograph 2 - View of rock outcrops on slope abutted to the east slope of proposed TSF-2 (Looking East)**

**APPENDIX B.2**  
**BASELINE AND FINAL FACILITY CONFIGURATION HYDROLOGY**  
**MODELING REPORT**

# Bowman

**Copper World Project  
Baseline and Final Facility Configuration  
Hydrology Modeling Report  
Revision 3**

Prepared for:

Piteau Associates  
9090 Double Diamond Parkway, Suite 1  
Reno, NV 89521

Prepared By:

Bowman Consulting Group  
7464 N La Cholla Blvd  
Tucson, Arizona 85741



August 18, 2022

Bowman Project No. 051034-01-001

Table of Contents

1. Introduction..... 1

2. Modeling Methodology Overview..... 1

    2.1 Design Storm Model ..... 4

    2.2 Continuous Flow Model ..... 4

3. Baseline Model Results ..... 5

    3.1 Design Storm Model ..... 5

    3.2 Continuous Flow Model ..... 6

4. Life of Mine Year 15 Facility Configuration Model Results ..... 7

    4.1 Design Storm Model ..... 7

    4.2 Continuous Flow Model ..... 11

    4.3 Other Design Storm Events ..... 14

List of Tables

Table 1: Monthly evaporation (Nogales, AZ) ..... 2

Table 2: Basin areas, canopy, and surface parameter values..... 3

Table 3: Loss and transformation parameter values ..... 3

Table 4: Helvetia station precipitation statistics ..... 4

Table 5: Baseline drainage results – 100-year, 24-hour design storm ..... 4

Table 6: Baseline drainage results – continuous flow model ..... 6

Table 7: SCS curve numbers for project facilities ..... 7

Table 8: Final configuration drainage results – 100-year, 24-hour design storm..... 8

Table 9: Project Facility contact water - design storm model ..... 10

Table 10: Final configuration drainage results – 1000-year, 24-hour design storm..... 11

Table 11: Final facility configuration drainage –Contact water - Continuous flow ..... 14

Table 12: Project facility contact water - Continuous flow ..... 17



## List of Appendices

### Appendix A Report Figures

- Figure 1 Delineation of drainage basins
- Figure 2 Site vegetation
- Figure 3 Site soils
- Figure 4 Aerial with major site drainages outlined
- Figure 5 HEC-HMS baseline model schematics
- Figure 6 Helvetia Weather Station - gage precipitation plot
- Figure 7 Helvetia precipitation Table and Intensity-Duration-Frequency Graph
- Figure 8 Basin delineations for final drainage configuration with contact water separation
- Figure 9 Mine facility areas with existing soils
- Figure 10 HEC-HMS model schematics for final drainage configuration

### Appendix B Annualized summaries for project facility final configuration - continuous mode

### Appendix C Other design storm events

## 1.0 Introduction

Surface water hydrology studies for the Rosemont Aquifer Protection Permit (APP) and Pre-feasibility Study (PFS) were performed to predict peak and total volume flow for the following Life-of-Mine (LOM) scenarios:

- Site baseline conditions
- 15-year - final facility drainage configuration

The two types of surface water model simulations included the following:

- Design Storm Model

The design storm model used the 100-year, 24-hour design storm event to provide peak flow information that will be used to size temporary hydraulic structures (e.g., storm water channels, erosion control structures, etc.). The 1,000-year, 24-hour design storm model results will be used to design permanent hydraulic structures (final facility configuration). Design storm models used the point precipitation frequency estimates of the Helvetia weather station obtained from NOAA Atlas 14, Volume 1, Version 5.

- Continuous Flow Model

The continuous flow model used 25-years of continuous precipitation data from the Helvetia weather station. The primary objective of the Continuous Mode flow models provides information used to develop estimates of seepage and infiltration, perform mine water balance calculations.

- Other design storm models

Additional design storm models were run and included the 100-year, 3-hour, and 1,000-year, 3-hour events. The 100-year, 3-hour design storm event is recommended by the Pima County Flood Control District.

## 2.0 Modeling Methodology Overview

The drainage basins for the Site were delineated to determine the Concentration Points (CP), or the points where surface water discharges off the Site. The existing drainage basins for the project Site are shown in Appendix A, Figure 1. As shown in Appendix A, there are five major points of flow on the West slope of the Site, which include CP 01, CP 06, CP 07, CP 09, and CP 10. CP 01 includes Basins 01 and 02 with a total of 4.2 square miles (mi<sup>2</sup>). CP 06 is comprised of Basin 06 with a total of 1.4 mi<sup>2</sup>. CP 07 includes Basins 07 and 08 with a total of 1.8 mi<sup>2</sup>. CP 09 includes Basin 04, Basin 05, and Basin 09 with a total of 5.5 mi<sup>2</sup>. CP 10 includes Basin 10 with a total of 1.0 mi<sup>2</sup>. CP 03, CP 11, CP13, 14 and CP15 associated to the same Basin name discharge on the East slope of the Site and each basin has an area of less than 1 mi<sup>2</sup>.



The surface water modeling methodology employed herein utilized the Hydrological Engineering Center (HEC), Hydrological Modeling Software (HMS) sponsored by the US Corps of Engineers. The modeling software and modeling results are widely accepted by public and private sector entities. The results from these models are a technical approximation of potential real events.

The hydrological runoff methodology used within HEC-HMS is the one developed by the Soil Conservation Service (SCS) which assigns a curve number (CN) to different surfaces given the nature of the soil and physiographic conditions.

For both the Design Storm and Continuous Flow models, SCS curve numbers were selected from the Pima County SCS tables, which are based on soil type, vegetation type and cover density.

Table 2 provides Basin areas, canopy, and surface parameter values. Table 3 provides SCS curve numbers, loss and transformation parameter values. The values used for the lag and transformation were derived from the SCS standard hydrograph with lag time for Site drainages shown in light blue in Appendix A, Figure 4. HEC-HMS baseline model schematics are shown in Appendix A, Figure 5.

The HEC-HMS models also requires other climatological inputs such as precipitation and pan evaporation (PE). Precipitation data from the Helvetia weather station within the project area for the period 1925 to 1980) were used. The Helvetia weather station location is shown in Appendix A, Figure 4.

The PE data were obtained from the Nogales weather station. These PE data were used for hydrological studies at similar properties and are reliable data available within a reasonable proximity and elevation for the Site models. The PE data are summarized in Table 1 for the period 1952-2007. Precipitation data from the Helvetia weather station for the period, and PE data for the Nogales weather station are summarized in Table 1.

*Table 1 Monthly Pan Evaporation (Nogales, AZ)*

Month	Precipitation (inches)	PE (inches)
January	1.58	3.59
February	1.72	4.46
March	1.14	7.01
April	0.52	9.35
May	0.28	11.91
June	0.67	13.31
July	4.05	10.00
August	4.15	8.28
September	2.19	8.06
October	0.68	7.17
November	1.22	4.49
December	1.52	3.57
Total / Annual Average	19.73	91.2

Surface parameter values are influenced by Site vegetation, soils, and slopes. Appendix A, Figures 2 and 3, provide maps of Site vegetation and soils, respectively used for the Design Event and Continuous Flow models.

*Table 2 Basin areas, canopy, and surface parameter values*

<b>BASIN #</b>	<b>AREA (mi<sup>2</sup>)</b>	<b>Canopy maximum storage (in)</b>	<b>Surface maximum storage (in)</b>
Basin01	2.6327	0.02	0.4688
Basin02	1.5729	0.03	0.3750
Basin03	0.9329	0.07	0.3438
Basin04	0.541	0.03	0.3750
Basin05	2.2137	0.06	0.3125
Basin06	1.3932	0.05	0.3750
Basin07	1.0554	0.03	0.4375
Basin08	0.7373	0.03	0.4063
Basin09	2.7658	0.01	0.5000
Basin10	0.9576	0.01	0.5000
Basin11	0.658	0.08	0.3125
Basin12	0.9518	0.07	0.3438
Basin13	0.1297	0.08	0.3125
Basin14	0.1035	0.08	0.3125
Basin15	0.0602	0.08	0.3125

*Table 3 Loss and transformation parameter values*

<b>BASIN #</b>	<b>Loss- SCS Curve Number</b>	<b>Loss- Impervious Area (%)</b>	<b>Trans- Lag time (min)</b>
Basin01	86.40	2	53.34
Basin02	88.50	2	19.47
Basin03	86.80	2	19.29
Basin04	88.35	2	22.37
Basin05	85.33	2	30.77
Basin06	81.79	2	36.31
Basin07	81.99	2	22.48
Basin08	83.99	2	12.34
Basin09	81.37	2	60.89
Basin10	79.75	2	60.16
Basin11	86.70	2	9.73
Basin 12	82.28	2	11.69
Basin13	86.70	2	6.24
Basin14	86.70	2	3.40
Basin15	86.70	2	2.13

## 2.1 Design Storm Model

Using the methodologies described in Section 1, the HEC HMS model was used to evaluate peak flow results. The 100-year, 24-hour storm event rain depth of 4.64 inches (median with 90% confidence intervals) and the 1,000-year, 24-hour storm with a rain depth of 6.42 inches was obtained from the NOAA Atlas 14, Volume 1, Version 5 HELVETIA SANTA RITA RANGE shown in Appendix A, Figure 7. The basin delineation for the baseline analysis is in Appendix A, Figure 8, and the HEC- HMS model schematics are presented in Figure 5. Basin areas, canopy, and surface storage, SCS Curve Numbers, loss, and transformation data in Figures 2 and 3 were used for model simulations.

## 2.2 Continuous Flow Model

The Continuous Flow Model used daily precipitation data for 25 years from the Helvetia weather station. This is done using the HEC-HMS control specification component of the model, which determines the dates for the start and end of the simulation and the calculation interval (5-minute intervals were used).

Another step in the formulation of the hydrological model for the continuous flow method was to determine or calculate the value of parameters such as basin surface area, soils, vegetation-canopy cover, surface storage / loss and associated transformations.

For the continuous flow model, 25 years of continuous precipitation data from the Helvetia weather station are shown in Appendix A, Figure 6.

Raw data obtained from NOAA was adjusted to replace 17 days of missing precipitation data from the Helvetia Weather Station for the continuous flow model. Statistics for the adjusted precipitation results are in Table 4.

Precipitation data from the Helvetia weather station were selected by the Project team because it is most representative of the Site with most Project facilities impacted by Site drainage on the Western slope of the Santa Rita Mountains.

*Table 4 Helvetia Station Precipitation Statistics*

Number of valid Values:	9617	
Number of missing	0	
Last Valid Value:	0.0	at 30APR1950, 24:00
Minimum Value:	0.0	at 01JAN1924, 24:00
Mean Value:	0.0545378	
Maximum Value:	2.89	at 31AUG1935, 24:00
Accumulated Amount	524.49	
Standard Deviation	0.20071046	
Skew Coefficient	5.681595	
Data Type	PER-CUM	
Units	IN	

## 3.0 Baseline Model Results

### 3.1 Design Storm Model

Baseline peak flow results and surface areas for basins for the 100-year, 24-hour design storm model are summarized in Table 5 below.

*Table 5 Baseline drainage results – 100-year, 24-hour design storm*

Rosemont Copper World Project 2.1 simulation run: initial design event		
Basin model: Baseline 100yr-24hr		
Meteorologic Model: 100yr-24hr		
Control Specification: 24hr-5min		
Hydrologic Element	Drainage Area(mi <sup>2</sup> )	Peak flow (cfs)
Basin01	2.6327	1874.8
Basin02	1.5729	2783
Basin03	0.9329	1525.1
Basin04	0.541	877.3
Basin05	2.2137	2494.9
Basin06	1.3932	1022.1
Basin07	1.0554	1052.8
Basin08	0.7373	1366.9
Basin09	2.7658	1132.8
Basin10	0.9576	337
Basin11	0.658	1564.5
Basin12	0.9518	1717.4
Basin13	0.1297	371.7
Basin14	0.1035	334.7
Basin15	0.0602	208.7
Junction-1	0.7373	1366.9
Junction-2	2.7547	3236.2
Reach-1	1.5729	2783
Reach-2	0.7373	1366.9
Reach-7	2.7547	3236.2
Sink-1	1.7927	2016.5
Sink-2	1.3932	1022.1
Sink-3	0.9576	337
Sink-4	5.5205	4331
Sink-5	4.2056	4596.8
Sink-6	0.9329	1525.1
Sink-7	0.658	1564.5
Sink-8	0.9518	1717.4
Sink-9	0.1297	371.7
Sink-10	0.1035	334.7
Sink-11	0.0602	208.7

## 3.2 Continuous Flow Model

The Continuous flow model results and surface areas for basins for the baseline scenario are provided in Table 6.

*Table 6 Baseline drainage results – Continuous flow model*

Rosemont Copper World Project 2.1 simulation run: initial design event		
Basin model: Basin Initial		
Meteorologic Model: Met 2 – Hyetograph PE Nogales		
Control Specification: Control 1 -1925-1980		
Hydrologic Element	Drainage Area(mi <sup>2</sup> )	Volume (ac-ft)
Basin01	2.6327	15189.6
Basin02	1.5729	10146.7
Basin03	0.9329	5831.4
Basin04	0.5410	3489.4
Basin05	2.2137	14675.6
Basin06	1.3932	8601.1
Basin07	1.0554	6204.8
Basin08	0.7373	4535.5
Basin09	2.7658	15544.9
Basin10	0.9576	5376.9
Basin11	0.6580	4219.7
Basin12	0.9518	5923.6
Basin13	0.1297	2247.7
Basin14	0.1035	1793.6
Basin15	0.0602	1043.2
Junction-1	0.7373	4535.5
Junction-2	2.7547	18165
Reach-1	1.5729	10146.7
Reach-2	0.7373	4535.5
Reach-7	2.7547	18165
Sink-1	1.7927	10740.3
Sink-2	1.3932	8601.1
Sink-3	0.9576	5376.9
Sink-4	5.5205	33709.9
Sink-5	4.2056	25336.3
Sink-6	0.9329	5831.4
Sink-7	0.6580	4219.7
Sink-8	0.9518	5923.6
Sink-9	0.1297	2247.7
Sink-10	0.1035	1793.6
Sink-11	0.0602	1043.2

## 4.0 Life-of-Mine, Year 15 – Final Facility Drainage Configuration Model

The development and construction of Project facilities, which includes Tailings Storage Facilities (TSF), Mine Pits, Leach Pad, and Waste Rock Facility (WRF) and other related facilities, will alter the drainage pattern of several basins. In addition, surface runoff water that encounters Project process facilities is required to be retained on site. The configuration of drainage basins for planned mine facilities, including the Rosemont Pit as part of Basin 12, are shown in Appendix A, Figure 8.

One aspect of drainage pattern change is the creation of closed basins (areas where surface water runoff can accumulate), and the boundaries are shown in Appendix A, Figure 8. Some closed basins are created by open pits and others by facility structures.

The HEC-HMS final drainage schematics are in Appendix A, Figure 10, which is a complex network of basins, reaches, reservoirs, and Points of Concentration, where many discharge lines come together. These were grouped to obtain the total volume of contact water to be retained on Site.

### 4.1 Design Storm Model

The HEC-HMS parameters for the final drainage model are the same as the ones used for the baseline analysis, but with the Project facilities added in, which changes the Loss parameter associated with SCS CN areas. The addition of facilities has the effect of increasing disturbed soil areas and decreasing vegetated areas resulting in a hydrologic condition of low infiltration and soil Type D was selected as the design condition. Project facility areas overlain on a Hydrologic Soil Groups map are shown in Appendix A, Figure 9. The SCS CN values for the Project facilities configuration model are summarized in Table 7.

*Table 7 SCS curve numbers for project facilities*

Project facility	CN
PIT	91
WRF	91
TSF	91
HLF	91

Table 8 provides volume results for the final drainage configuration with contact water segregated for the 100-year, 24-hour Design Storm Model.

Table 8 Final configuration drainage results – 100-year, 24-hour design storm

Rosemont Copper World Project 2.1 simulation run: Final Contact Volumes for design event		
Basin model: LOM 15		
Meteorologic Model: 100yr-24hr		
Control specification: 24hr-5m		
Hydrologic Element	Drainage Area (mi <sup>2</sup> )	Peak flow (cfs)
Junction 04A	0.0567	175.6
Junction 05A	0.1295	263.1
Junction 07B	1.0840	1663.3
Junction 07C	0.6792	1313.7
Junction 08A	0.8354	1589.6
Junction 10B	0.2327	363.9
Junction 10B2	0.2327	363.9
Junction 12A	0.1874	682
Junction 12B	0.0398	110.1
Reach 04A	0.0567	175.6
Reach 05A	0.1295	263.1
Reach 07B	1.0840	1663.3
Reach 07C	0.6792	1313.7
Reach 08A	0.8354	1589.6
Reach 10B	0.2327	363.9
Reach 10B2	0.2327	363.9
Reach 12A	0.1874	682
Reach 12B	0.0398	110.1
Sink HLF	0.5517	562.6
Sink Platform	0.1524	182.2
Sink R02A	1.0536	1427.7
Sink R02B	0.5750	1152
Sink R04A-1	0.1705	319
Sink R05B	0.0518	161.8
Sink R05C	0.3880	1112.1
Sink R05D	0.6777	1449.1
Sink R05E	0.0105	38.6
Sink R05F	0.0349	126.2
Sink R05G	0.0468	166.5
Sink R09C	0.1053	240.2
Sink R09D-1	0.0995	356
Sink R12A-1	0.9566	1912.8
Sink TSF 1	1.4986	1258
Sink TSF 2	0.5562	815.5
Sink WRF1a	0.8191	2439.1
Sink WRF1b	0.4307	1298.3

Table 8 Final configuration drainage results – 100-year, 24-hour design storm (continued)

Rosemont Copper World Project 2.1 simulation run: Final Contact Volume design event		
Basin model: LOM 15		
Meteorologic Model: 100yr-24hr		
Control specification: 24hr-5m		
Hydrologic Element	Drainage Area	Peak flow (cfs)
Sink 01A	1.5618	1749.8
Sink 03A	0.8100	1129.4
Sink 06A	0.1845	320.5
Sink 07A	2.1658	2362
Sink 09A	2.0834	1195.1
Sink 10A	1.0574	600.6
Sink 11A	0.3741	772.7
Sink 13A	0.0400	133.8
Subbasin 01A	1.5618	1749.8
Subbasin 01B-1	1.4986	1258
Subbasin 02A	1.0536	1427.7
Subbasin 02B	0.5750	1152
Subbasin 02B-1	0.2010	606.9
Subbasin 03A	0.8100	1129.4
Subbasin 03A-1	0.1403	414.2
Subbasin 04A	0.0567	175.6
Subbasin 04A-1	0.1138	318.7
Subbasin 04B-1	0.1382	377.9
Subbasin 05A	0.1295	263.1
Subbasin 05B	0.0518	161.8
Subbasin 05B-1	0.2809	855.5
Subbasin 05C	0.3880	1112.1
Subbasin 05D	0.6777	1449.1
Subbasin 05E	0.0105	38.6
Subbasin 05F	0.0349	126.2
Subbasin 05F-1	0.0911	275.6
Subbasin 05G	0.0468	166.5
Subbasin 05G-1	0.0587	186.5
Subbasin 06A	0.1845	320.5
Subbasin 06B-1	0.1524	182.2
Subbasin 06C-1	0.5517	562.6
Subbasin 07A	0.2464	521.5
Subbasin 07B	0.4048	643
Subbasin 07C	0.6792	1313.7
Subbasin 07D-1	0.5562	815.5
Subbasin 08A	0.8354	1589.6



*Table 8 Final configuration drainage results – 100-year, 24-hour design storm (continued)*

Rosemont Copper World Project 2.1 simulation run: Final Contact Volume design event		
Basin model: LOM 15		
Meteorologic Model: 100yr-24hr		
Control specification: 24hr-5m		
Hydrologic Element	Drainage Area	Peak flow (cfs)
Subbasin 09A	2.0834	1195.1
Subbasin 09C	0.1053	240.2
Subbasin 09D-1	0.0995	356
Subbasin 10A	0.8247	316.2
Subbasin 10B	0.1032	150.1
Subbasin 11A	0.3741	772.7
Subbasin 11A-1	0.2205	656.5
Subbasin 11A-2	0.0839	264.7
Subbasin 11A-3	0.0352	130.5
Subbasin 12A	0.1874	682
Subbasin 12A-1	0.7294	1887.5
Subbasin 12B	0.0398	110.1
Subbasin 13A	0.04	44.2

Design Storm contact water peak flows to be conveyed on site are summarized in Table 9.

*Table 9 Project Facility contact water - design storm model*

Project Facility	Peak Flow (cfs)
Sink TSF 1	1258.0
Sink TSF 2	815.5
Sink WRF1a	2439.1
Sink WRF1b	1298.3
Sink HLF	562.6

Table 10 provides volume results for the final drainage configuration with contact water segregated for the 1000-year, 24-hour Design Storm Model.

Table 10 Final facility configuration drainage results – 1,000-year, 24-hour design storm

Rosemont Copper World Project 2.1 simulation run: Final Contact Volumes for design event		
Basin model: LOM 15		
Meteorologic Model: 1000yr-24hr		
Control specification: 24hr-5m		
Hydrologic Element	Drainage Area (mi <sup>2</sup> )	Peak flow (cfs)
Junction 04A	0.0567	247.8
Junction 05A	0.1295	388.2
Junction 07B	1.0840	2438.6
Junction 07C	0.6792	1926.4
Junction 08A	0.8354	2378.1
Junction 10B	0.2327	547.6
Junction 10B2	0.2327	547.6
Junction 12A	0.1874	956.9
Junction 12B	0.0398	185.9
Reach 04A	0.0567	247.8
Reach 05A	0.1295	388.2
Reach 07B	1.0840	2438.6
Reach 07C	0.6792	1926.4
Reach 08A	0.8354	2378.1
Reach 10B	0.2327	547.6
Reach 10B2	0.2327	547.6
Reach 12A	0.1874	956.9
Reach 12B	0.0398	185.9
Sink HLF	0.5517	851.4
Sink Platform	0.1524	278.6
Sink R02A	1.0536	2174.9
Sink R02B	0.5750	1685.4
Sink R04A-1	0.1705	469.9
Sink R05B	0.0518	228
Sink R05C	0.3880	1581
Sink R05D	0.6777	2113.6
Sink R05E	0.0105	54.3
Sink R05F	0.0349	178.1
Sink R05G	0.0468	234.5
Sink R09C	0.1053	348.9
Sink R09D-1	0.0995	496.4
Sink R12A-1	0.9566	2776.8
Sink TSF 1	1.4986	1967.7
Sink TSF 2	0.5562	1218
Sink WRF1a	0.8191	3419.6
Sink WRF1b	0.4307	1817.6

Table 10 Final facility configuration drainage – 1,000-year, 24-hour design storm (continued)

Rosemont Copper World Project 2.1 simulation run: Final Contact Volume design event		
Basin model: LOM 15		
Meteorologic Model: 1000yr-24hr		
Control specification: 24hr-5m		
Hydrologic Element	Drainage Area	Peak flow (cfs)
Sink 01A	1.5618	2752.9
Sink 03A	0.8100	1715.9
Sink 06A	0.1845	482.8
Sink 07A	2.1658	3754.7
Sink 09A	2.0834	1938.1
Sink 10A	1.0574	944.2
Sink 11A	0.3741	1134
Sink 13A	0.0400	189.2
Subbasin 01A	1.5618	2752.9
Subbasin 01B-1	1.4986	1967.7
Subbasin 02A	1.0536	2174.9
Subbasin 02B	0.5750	1685.4
Subbasin 02B-1	0.2010	851.7
Subbasin 03A	0.8100	1715.9
Subbasin 03A-1	0.1403	580.6
Subbasin 04A	0.0567	247.8
Subbasin 04A-1	0.1138	447
Subbasin 04B-1	0.1382	531.5
Subbasin 05A	0.1295	388.2
Subbasin 05B	0.0518	228
Subbasin 05B-1	0.2809	1197.7
Subbasin 05C	0.3880	1581
Subbasin 05D	0.6777	2113.6
Subbasin 05E	0.0105	54.3
Subbasin 05F	0.0349	178.1
Subbasin 05F-1	0.0911	386
Subbasin 05G	0.0468	234.5
Subbasin 05G-1	0.0587	261.5
Subbasin 06A	0.1845	482.8
Subbasin 06B-1	0.1524	278.6
Subbasin 06C-1	0.5517	851.4
Subbasin 07A	0.2464	772.1
Subbasin 07B	0.4048	971.4
Subbasin 07C	0.6792	1926.4
Subbasin 07D-1	0.5562	1218
Subbasin 08A	0.8354	2378.1

Table 10 Final configuration drainage – 1,000-year, 24-hour design storm (continued)

Rosemont Copper World Project 2.1 simulation run: Final Contact Volumes design event		
Basin model: LOM 15		
Meteorologic Model: 1000yr-24hr		
Control specification: 24hr-5m		
Hydrologic Element	Drainage Area	Peak flow (cfs)
Subbasin 09A	2.0834	1938.1
Subbasin 09C	0.1053	348.9
Subbasin 09D-1	0.0995	496.4
Subbasin 10A	0.8247	513.8
Subbasin 10B	0.1032	230.5
Subbasin 11A	0.3741	1134
Subbasin 11A-1	0.2205	920
Subbasin 11A-2	0.0839	370
Subbasin 11A-3	0.0352	182.3
Subbasin 12A	0.1874	956.9
Subbasin 12A-1	0.7294	2636.9
Subbasin 12B	0.0398	185.9
Subbasin 13A	0.0400	189.2

## 4.2 Continuous Flow Model

Table 11 Final facility configuration drainage –Contact water - Continuous flow

Rosemont Copper World Project 2.1 Simulation run: Final contact Volume		
Basin model: LOM 15		
Meteorologic Model: Met 2 – Hvetograph PE Nogales		
Control specification: Control 3 – 1925-1960 6h		
Hydrologic Element	Drainage Area (mi <sup>2</sup> )	Volume (ac-ft)
Junction 04A	0.0567	324
Junction 05A	0.1295	717.8
Junction 07B	1.084	6187.2
Junction 07C	0.6792	3914
Junction 08A	0.8354	4608.3
Junction 10B	0.2327	1303.5
Junction 10B2	0.2327	1303.5
Junction 12A	0.1874	1138.6
Junction 12B	0.0398	88.3
Reach 04A	0.0567	324
Reach 05A	0.1295	717.8
Reach 07B	1.084	6187.2
Reach 07C	0.6792	3914
Reach 08A	0.8354	4608.3
Reach 10B	0.2327	1303.5
Reach 10B2	0.2327	1303.5
Reach 12A	0.1874	1138.6
Reach 12B	0.0398	88.3
Sink HLF	0.5517	9181.3
Sink Platform	0.1524	2409.4
Sink R02A	1.0536	6059.3
Sink R02B	0.575	3354.2
Sink R04A-1	0.1705	2321.9
Sink R05B	0.0518	294.7
Sink R05C	0.388	2250.3
Sink R05D	0.6777	3804.6
Sink R05E	0.0105	62.4
Sink R05F	0.0349	196.8
Sink R05G	0.0468	271.2
Sink R09C	0.1053	615.6
Sink R09D-1	0.0995	1899.1
Sink R12A-1	0.9566	15148.7
Sink TSF 1	1.4986	23692.5
Sink TSF 2	0.5562	8942.5
Sink WRF1a	0.8191	13834.5
Sink WRF1b	0.4307	7360.5
Sink 01A	1.5618	8558.9

Table 11 Final facility configuration drainage –Contact water- Continuous flow (Continued)

Rosemont Copper World Project 2.1 Simulation run: Final contact Volume		
Basin model: LOM 15		
Meteorologic Model: Met 2 – Hvetograph PE Nogales		
Control specification: Control 3 – 1925-1960 6h		
Hydrologic Element	Drainage Area (mi <sup>2</sup> )	Volume (ac-ft)
Sink 03A	0.81	4531.9
Sink 06A	0.1845	985.5
Sink 07A	2.1658	12111.6
Sink 09A	2.0834	11740.6
Sink 10A	1.0574	5984.1
Sink 11A	0.3741	2007.5
Sink 13A	0.04	221
Subbasin 01A	1.5618	8558.9
Subbasin 01B-1	1.4986	23692.5
Subbasin 02A	1.0536	6059.3
Subbasin 02B	0.575	3354.2
Subbasin 02B-1	0.201	3374.5
Subbasin 03A	0.81	4531.9
Subbasin 03A-1	0.1403	2376.2
Subbasin 04A	0.0567	324
Subbasin 04A-1	0.1138	1997.9
Subbasin 04B-1	0.1382	2340.7
Subbasin 05A	0.1295	717.8
Subbasin 05B	0.0518	294.7
Subbasin 05B-1	0.2809	4757.6
Subbasin 05C	0.388	2250.3
Subbasin 05D	0.6777	3804.6
Subbasin 05E	0.0105	62.4
Subbasin 05F	0.0349	196.8
Subbasin 05F-1	0.0911	1556.8
Subbasin 05G	0.0468	271.2
Subbasin 05G-1	0.0587	985.5
Subbasin 06A	0.1845	985.5
Subbasin 06B-1	0.1524	2409.4
Subbasin 06C-1	0.5517	9181.3
Subbasin 07A	0.2464	1316.1
Subbasin 07B	0.4048	2273.1
Subbasin 07C	0.6792	3914
Subbasin 07D-1	0.5562	8942.5
Subbasin 08A	0.8354	4608.3

Table 11 Final facility configuration drainage – Contact water - Continuous flow (Continued)

Rosemont Copper World Project 2.1 Simulation run: Final contact Volume		
Basin model: LOM 15		
Meteorologic Model: Met 2 – Hvetograph PE Nogales		
Control specification: Control 3 – 1925-1960 6h		
Hydrologic Element	Drainage Area (mi <sup>2</sup> )	Volume (ac-ft)
Subbasin 09A	2.0834	11740.6
Subbasin 09C	0.1053	615.6
Subbasin 09D-1	0.0995	1899.1
Subbasin 10A	0.8247	4680.5
Subbasin 10B	0.1032	585.7
Subbasin 11A	0.3741	2007.5
Subbasin 11A-1	0.2205	3734.6
Subbasin 11A-2	0.0839	1473
Subbasin 11A-3	0.0352	596.2
Subbasin 12A	0.1874	1138.6
Subbasin 12A-1	0.7294	13921.9
Subbasin 12B	0.0398	88.3
Subbasin 13A	0.04	221
Subbasin 09A	2.0834	11740.6
Subbasin 09C	0.1053	615.6
Subbasin 09D-1	0.0995	1899.1
Subbasin 10A	0.8247	4680.5
Subbasin 10B	0.1032	585.7
Subbasin 11A	0.3741	2007.5
Subbasin 11A-1	0.2205	3734.6
Subbasin 11A-2	0.0839	1473
Subbasin 11A-3	0.0352	596.2
Subbasin 12A	0.1874	1138.6
Subbasin 12A-1	0.7294	13921.9
Subbasin 12B	0.0398	88.3
Subbasin 13A	0.04	221

A summary of contact water volumes for the Continuous Flow Model are shown in Table 12. Annual flow volume summaries for the specific mine facilities are presented in Appendix B.

*Table 12 Project facility contact water - Continuous flow*

Project Facility	Flow Volume (ac-ft)	Annual Ave. Flow (ac-ft)	Std. Dev. (ac-ft)
Sink HLF	9,181.3	353	165
Sink TSF 1	23,692.5	911	439
Sink TSF 2	8,942.5	344	164
Sink WRF1a	13,843.5	533	245
Sink WRF1b	7,360.5	283	130

### 4.3 Other Design Storm Events

Additional design storm event scenarios were modeled, which included the following:

- 100-year, 3-hour
- 1,000-year, 3-hour

The 100-year, 3-hour and 1,000-year, year, 3-hour event were simulated for the Year 15 Facility Configuration only. The 100-year, 3-hour design storm events models present the peak estimation regulated by Pima County Flood Control District and considered more representative of storms at the project Site. The 1,000-year, 3-hour storm is included as additional information for reference and comparison.

The 100-year, 3-hour storm distribution was used for the HEC-HMS model in the case where the time of concentration ( $T_c$ ) was equal to or less than three hours (Pima County Tech-018). A 100-year, 3-hour storm was selected since  $T_c$  is less than 3 hours for most of the sub-basins. For the 100-year, 3-hour event the upper 90 percent confidence interval for point rainfall depth upper 90% confidence interval value of 3.98 inches from the NOAA Atlas 14 Helvetia Santa Rita Range station was utilized for the model as required by Pima county

For the 1,000-year, 3-hour design storm event model a Hyetograph utilizing the 3-hour distribution was produced following the Pima County methodology described in Section 2.1. The rainfall depth for the 1,000- year, 3-hour was the mean value of 4.92 inches.

Results for the 100-year, 3-hour and 1,000-year, 3-hour event are in Appendix C.



Appendix A

Report Figures

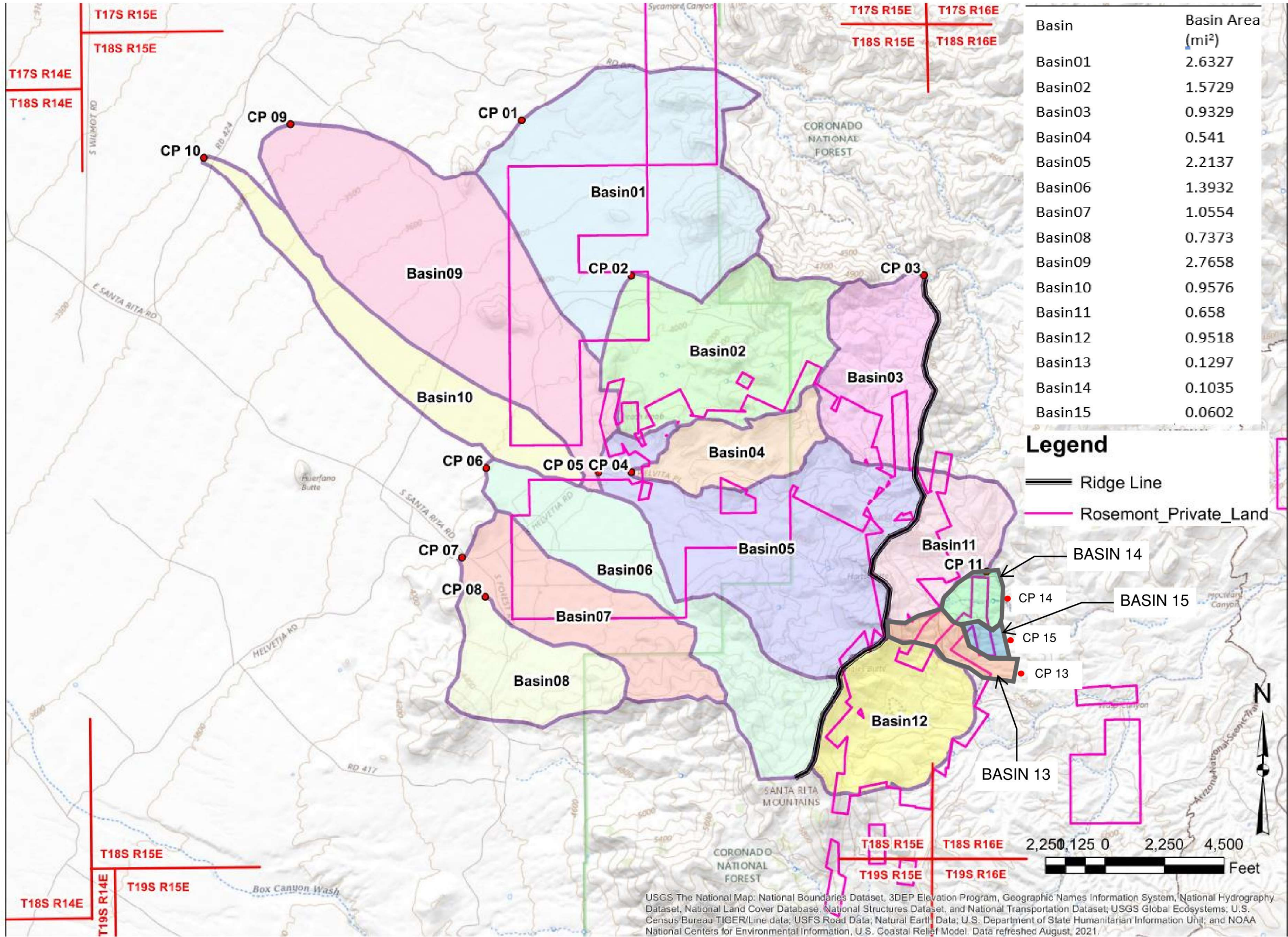


FIGURE 1 –DELINEATION OF DRAINAGE BASINS



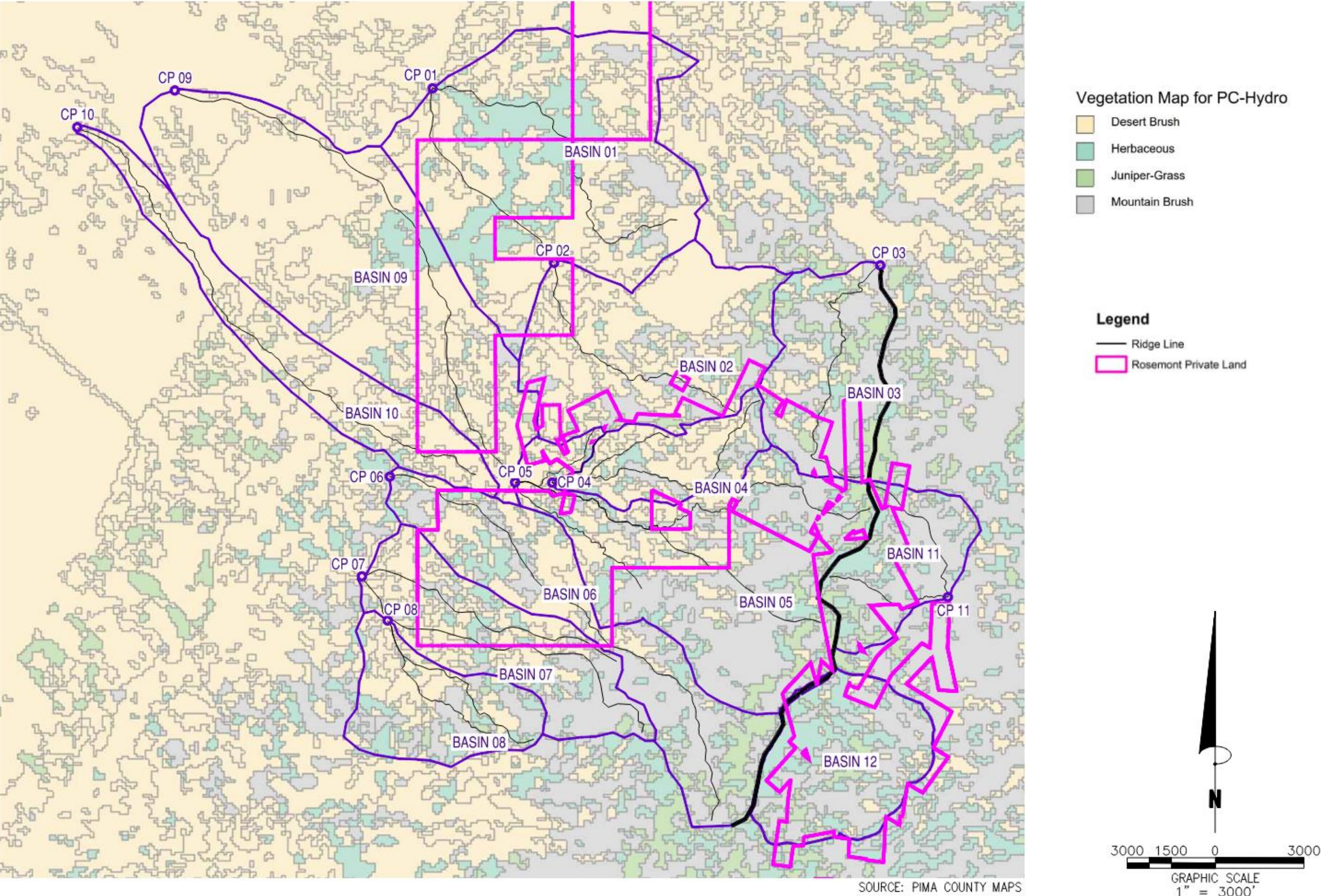


FIGURE 2 –SITE VEGETATION



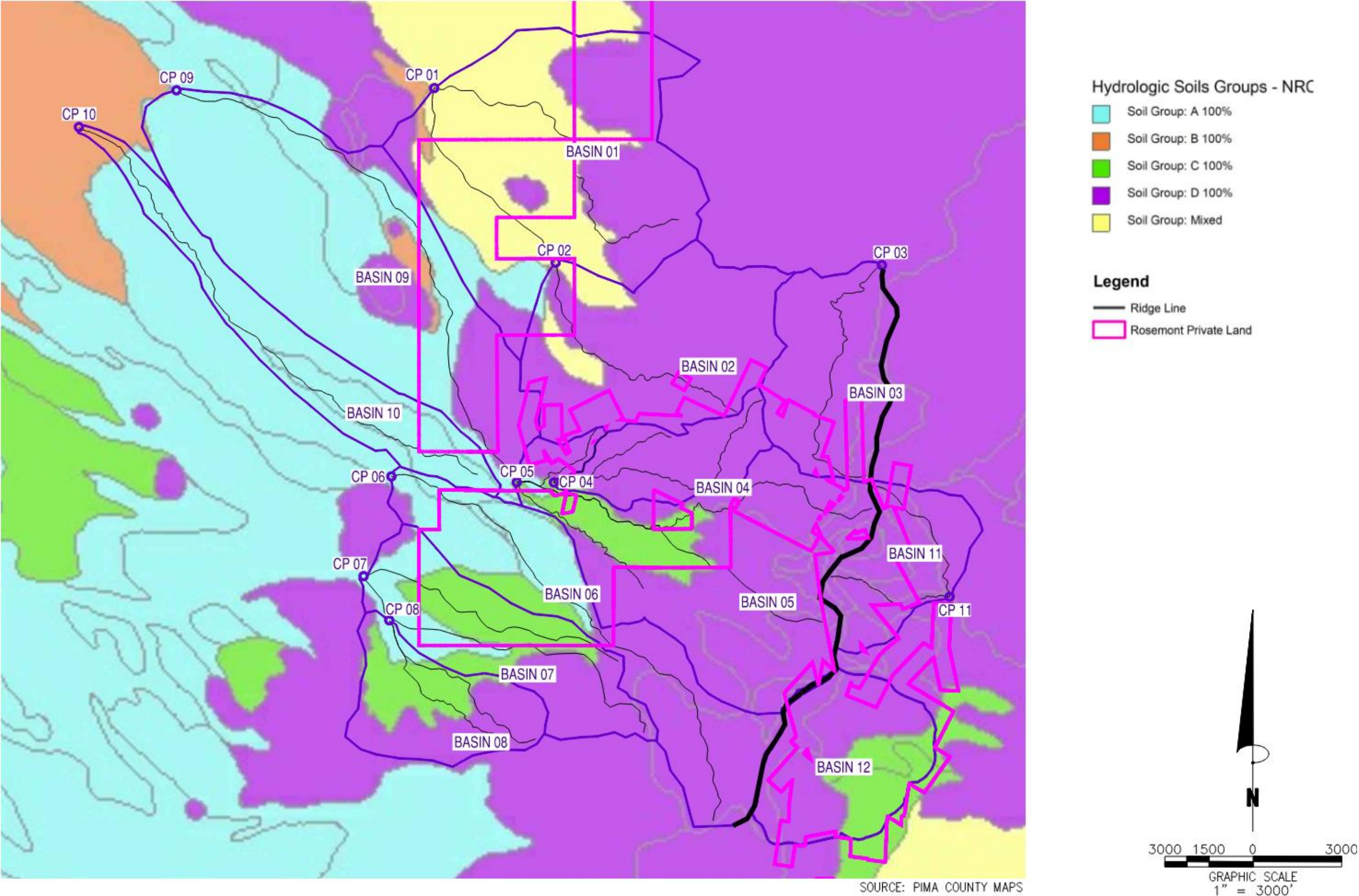


FIGURE 3 –SITE SOILS



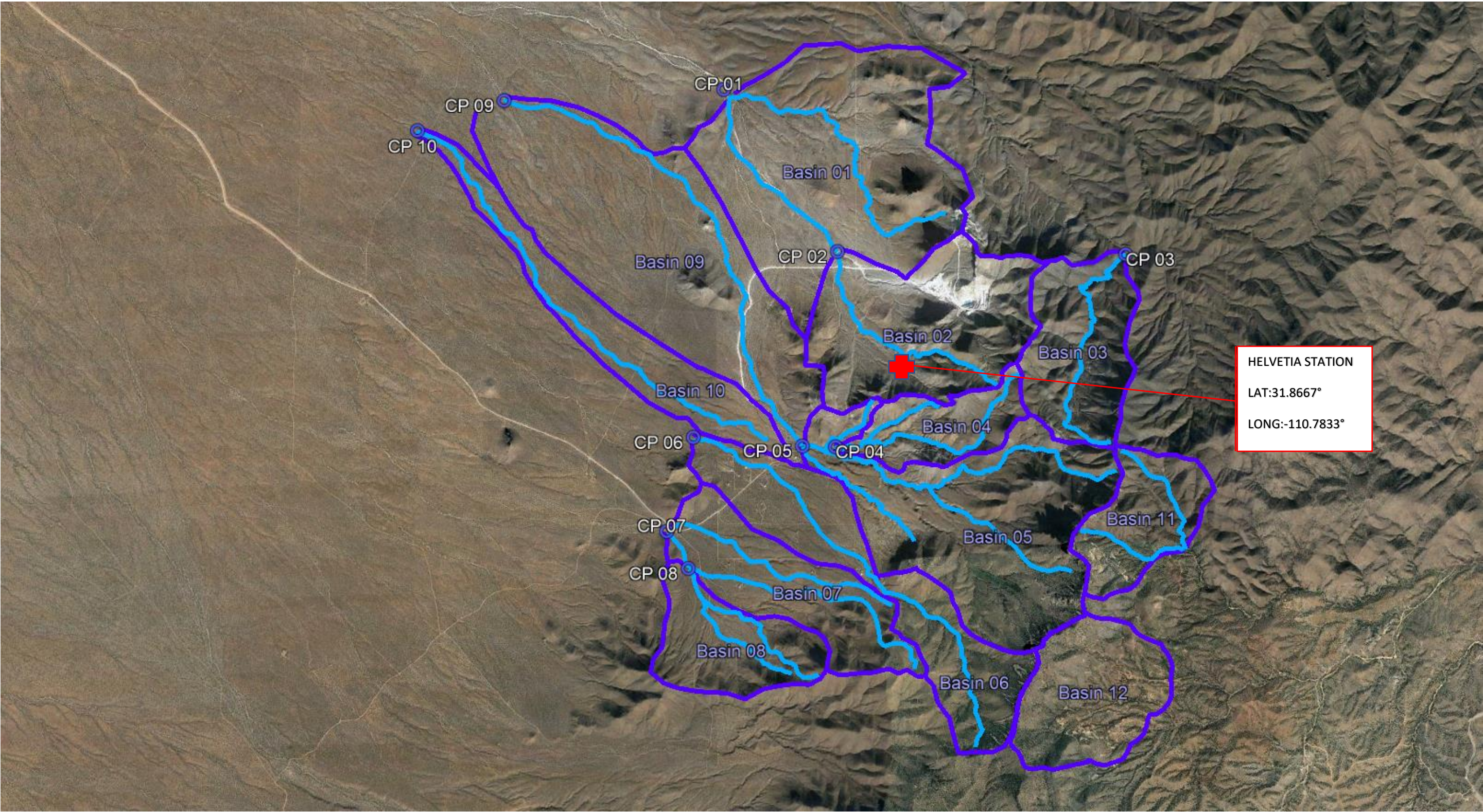


FIGURE 4 – AERIAL WITH MAJOR DRAINAGE OUTLINE



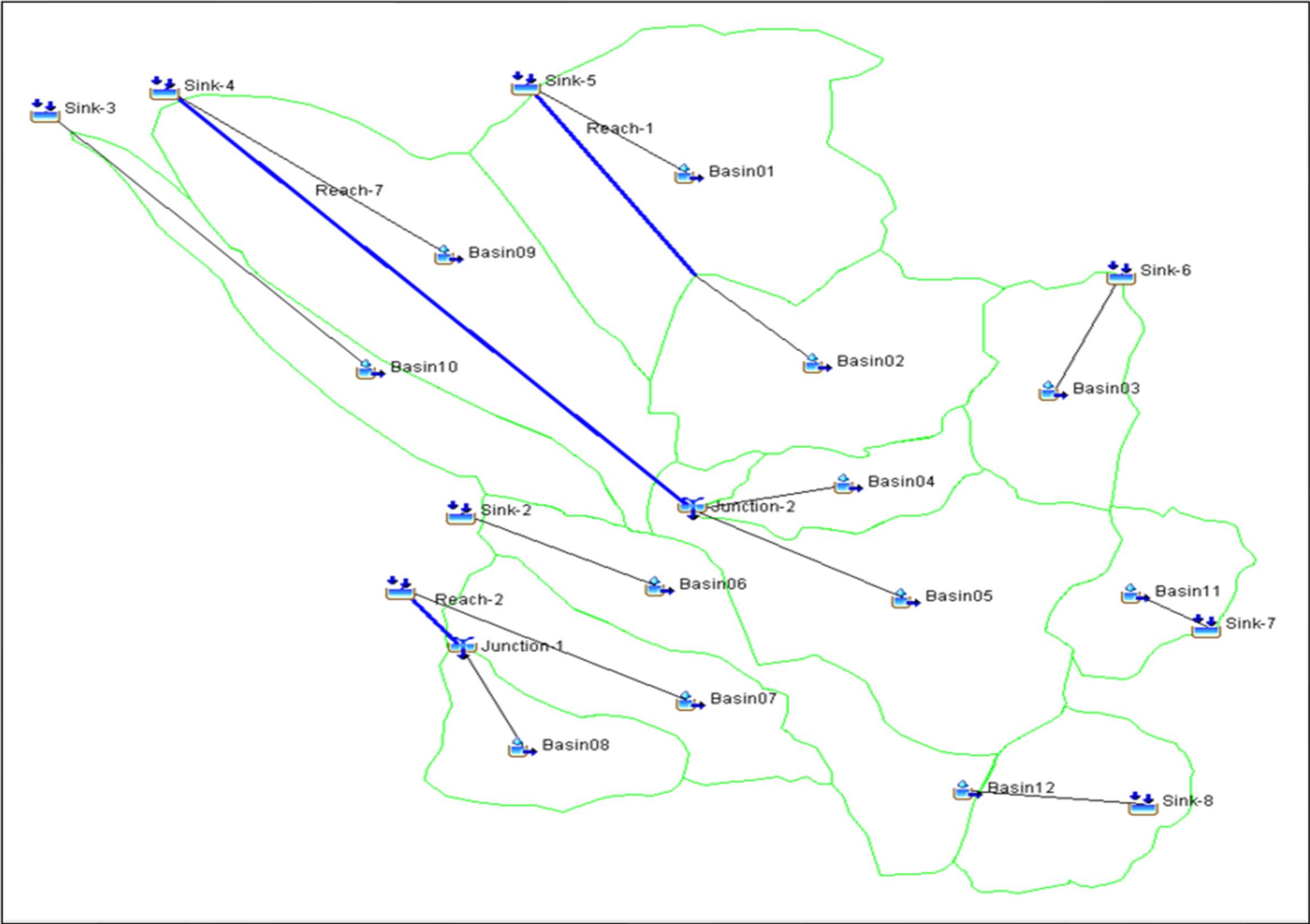


FIGURE 5 - HEC-HMS BASELINE MODEL SCHEMATICS



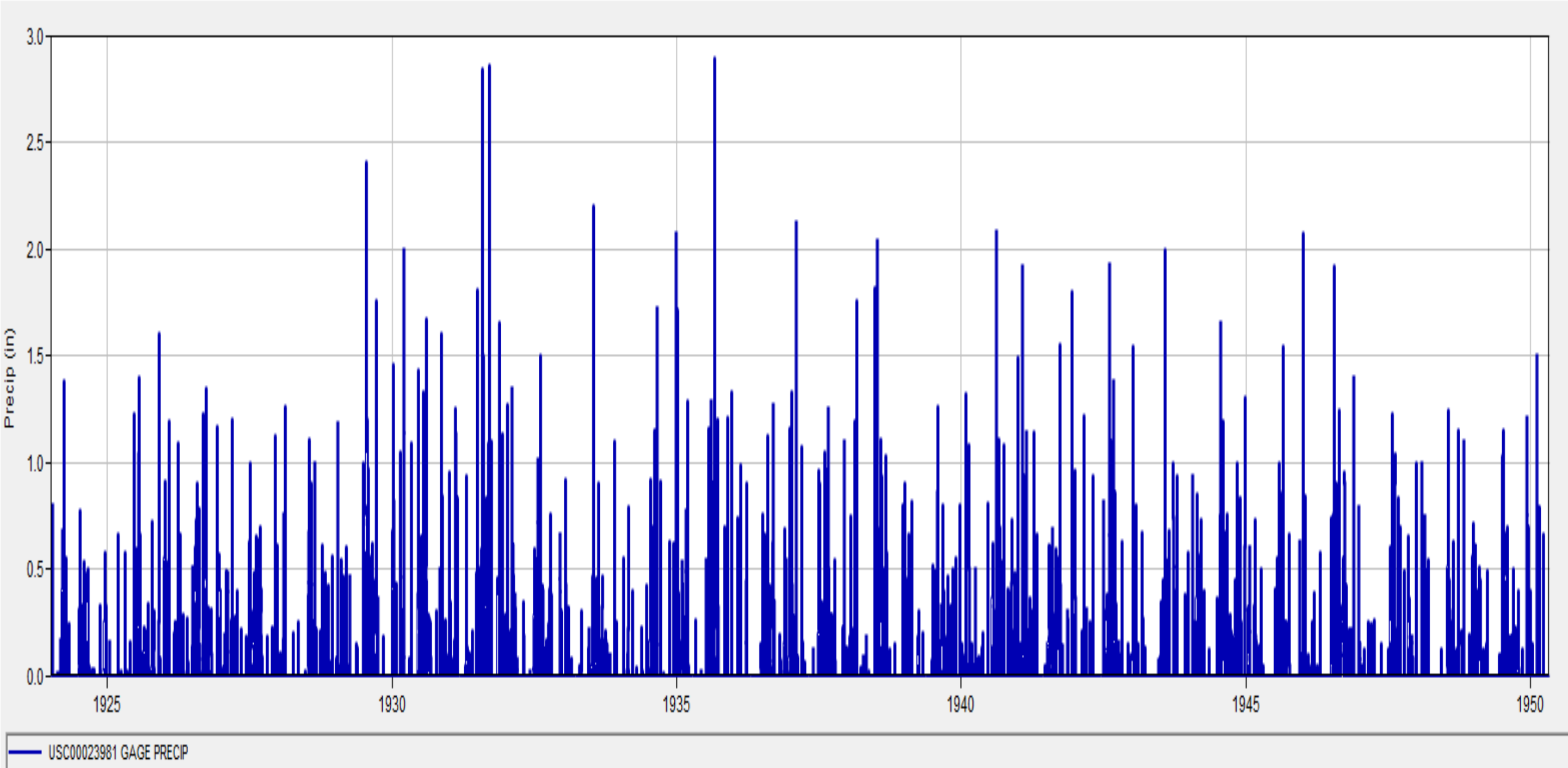


FIGURE 6 – HELVETIA WEATHER STATION – GAGE PRECIPITATION PLOT

NOAA Atlas 14, Volume 1, Version 5 HELVETIA  
SANTA RITA RANGE

Station ID: 02-3981

Location name: Vail, Arizona, USA\*

Latitude: 31.8667°, Longitude: -110.7833°

**Elevation:**

Elevation (station metadata): 4304 ft\*\*

\* source: ESRI Maps

\*\* source: USGS

### POINT PRECIPITATION FREQUENCY ESTIMATES

Sanja Perica, Sarah Dietz, Sarah Heim, Lillian Hiner, Kazungu Maitaria, Deborah Martin, Sandra Pavlovic, Ishani Roy, Carl Trypsakuk, Dale Unruh, Fenglin Yan, Michael Yekta, Tan Zhao, Geoffrey Bonnin, Daniel Brewer, Li-Chuan Chen, Tye Parzybok, John Yarchoan

NOAA, National Weather Service, Silver Spring, Maryland

[PF tabular](#) | [PF graphical](#) | [Maps & aerials](#)

### PF tabular

<b>Duration</b>	<b>Average recurrence interval (years)</b>									
	<b>1</b>	<b>2</b>	<b>5</b>	<b>10</b>	<b>25</b>	<b>50</b>	<b>100</b>	<b>200</b>	<b>500</b>	<b>1000</b>
<b>5-min</b>	<b>0.342</b> (0.309-0.383)	<b>0.440</b> (0.396-0.491)	<b>0.572</b> (0.512-0.636)	<b>0.668</b> (0.597-0.742)	<b>0.797</b> (0.704-0.884)	<b>0.891</b> (0.780-0.993)	<b>0.985</b> (0.853-1.10)	<b>1.08</b> (0.924-1.22)	<b>1.20</b> (1.01-1.37)	<b>1.29</b> (1.07-1.49)
<b>10-min</b>	<b>0.520</b> (0.470-0.583)	<b>0.669</b> (0.603-0.748)	<b>0.870</b> (0.780-0.969)	<b>1.02</b> (0.909-1.13)	<b>1.21</b> (1.07-1.35)	<b>1.36</b> (1.19-1.51)	<b>1.50</b> (1.30-1.68)	<b>1.64</b> (1.41-1.85)	<b>1.83</b> (1.53-2.08)	<b>1.97</b> (1.63-2.27)
<b>15-min</b>	<b>0.645</b> (0.582-0.722)	<b>0.830</b> (0.748-0.927)	<b>1.08</b> (0.967-1.20)	<b>1.26</b> (1.13-1.40)	<b>1.50</b> (1.33-1.67)	<b>1.68</b> (1.47-1.87)	<b>1.86</b> (1.61-2.08)	<b>2.03</b> (1.74-2.29)	<b>2.26</b> (1.90-2.58)	<b>2.44</b> (2.01-2.81)
<b>30-min</b>	<b>0.869</b> (0.784-0.972)	<b>1.12</b> (1.01-1.25)	<b>1.45</b> (1.30-1.62)	<b>1.70</b> (1.52-1.89)	<b>2.02</b> (1.79-2.25)	<b>2.26</b> (1.98-2.52)	<b>2.50</b> (2.17-2.80)	<b>2.74</b> (2.35-3.09)	<b>3.05</b> (2.56-3.47)	<b>3.29</b> (2.71-3.79)
<b>60-min</b>	<b>1.08</b> (0.971-1.20)	<b>1.38</b> (1.25-1.55)	<b>1.80</b> (1.61-2.00)	<b>2.10</b> (1.88-2.34)	<b>2.50</b> (2.22-2.78)	<b>2.80</b> (2.45-3.12)	<b>3.10</b> (2.68-3.47)	<b>3.39</b> (2.91-3.82)	<b>3.77</b> (3.16-4.30)	<b>4.07</b> (3.36-4.69)
<b>2-hr</b>	<b>1.19</b> (1.07-1.33)	<b>1.51</b> (1.37-1.69)	<b>1.94</b> (1.75-2.16)	<b>2.27</b> (2.03-2.53)	<b>2.73</b> (2.42-3.04)	<b>3.08</b> (2.71-3.44)	<b>3.45</b> (2.99-3.86)	<b>3.81</b> (3.26-4.29)	<b>4.31</b> (3.60-4.90)	<b>4.70</b> (3.86-5.40)
<b>3-hr</b>	<b>1.24</b> (1.12-1.38)	<b>1.56</b> (1.42-1.74)	<b>1.98</b> (1.79-2.21)	<b>2.32</b> (2.08-2.58)	<b>2.79</b> (2.48-3.10)	<b>3.16</b> (2.78-3.52)	<b>3.55</b> (3.07-3.98)	<b>3.95</b> (3.36-4.46)	<b>4.50</b> (3.74-5.13)	<b>4.93</b> (4.01-5.70)
<b>6-hr</b>	<b>1.43</b> (1.28-1.60)	<b>1.79</b> (1.60-2.01)	<b>2.24</b> (2.00-2.51)	<b>2.62</b> (2.33-2.93)	<b>3.15</b> (2.77-3.53)	<b>3.58</b> (3.11-4.02)	<b>4.03</b> (3.45-4.55)	<b>4.49</b> (3.78-5.11)	<b>5.14</b> (4.21-5.90)	<b>5.65</b> (4.55-6.57)
<b>12-hr</b>	<b>1.68</b> (1.51-1.87)	<b>2.10</b> (1.89-2.33)	<b>2.61</b> (2.34-2.91)	<b>3.03</b> (2.71-3.38)	<b>3.63</b> (3.21-4.04)	<b>4.10</b> (3.58-4.57)	<b>4.59</b> (3.96-5.16)	<b>5.10</b> (4.33-5.77)	<b>5.80</b> (4.81-6.64)	<b>6.35</b> (5.17-7.35)
<b>24-hr</b>	<b>1.73</b> (1.58-1.89)	<b>2.16</b> (1.98-2.36)	<b>2.68</b> (2.46-2.93)	<b>3.10</b> (2.83-3.40)	<b>3.67</b> (3.34-4.08)	<b>4.13</b> (3.71-4.62)	<b>4.64</b> (4.10-5.21)	<b>5.15</b> (4.48-5.83)	<b>5.86</b> (4.98-6.71)	<b>6.42</b> (5.36-7.42)
<b>2-day</b>	<b>1.94</b> (1.79-2.13)	<b>2.42</b> (2.22-2.65)	<b>2.99</b> (2.75-3.28)	<b>3.47</b> (3.18-3.80)	<b>4.13</b> (3.77-4.52)	<b>4.65</b> (4.21-5.10)	<b>5.19</b> (4.68-5.71)	<b>5.76</b> (5.15-6.38)	<b>6.53</b> (5.78-7.28)	<b>7.15</b> (6.24-7.99)
<b>3-day</b>	<b>2.13</b> (1.97-2.34)	<b>2.65</b> (2.44-2.91)	<b>3.29</b> (3.03-3.61)	<b>3.83</b> (3.51-4.19)	<b>4.57</b> (4.16-5.00)	<b>5.16</b> (4.66-5.65)	<b>5.78</b> (5.19-6.35)	<b>6.43</b> (5.73-7.10)	<b>7.33</b> (6.44-8.15)	<b>8.05</b> (6.98-8.98)
<b>4-day</b>	<b>2.32</b> (2.14-2.55)	<b>2.89</b> (2.66-3.17)	<b>3.60</b> (3.31-3.94)	<b>4.18</b> (3.83-4.58)	<b>5.01</b> (4.55-5.48)	<b>5.67</b> (5.11-6.21)	<b>6.37</b> (5.71-6.99)	<b>7.10</b> (6.31-7.83)	<b>8.13</b> (7.11-9.03)	<b>8.95</b> (7.72-9.97)
<b>7-day</b>	<b>2.78</b> (2.53-3.08)	<b>3.47</b> (3.15-3.84)	<b>4.33</b> (3.93-4.80)	<b>5.03</b> (4.55-5.58)	<b>5.99</b> (5.40-6.66)	<b>6.76</b> (6.05-7.52)	<b>7.55</b> (6.72-8.43)	<b>8.37</b> (7.38-9.35)	<b>9.49</b> (8.27-10.7)	<b>10.4</b> (8.95-11.7)
<b>10-day</b>	<b>3.22</b> (2.91-3.61)	<b>4.02</b> (3.63-4.50)	<b>4.98</b> (4.49-5.58)	<b>5.75</b> (5.17-6.43)	<b>6.79</b> (6.08-7.61)	<b>7.59</b> (6.75-8.50)	<b>8.40</b> (7.43-9.45)	<b>9.24</b> (8.10-10.4)	<b>10.4</b> (8.96-11.8)	<b>11.2</b> (9.64-12.8)
<b>20-day</b>	<b>4.39</b> (3.99-4.87)	<b>5.48</b> (4.99-6.09)	<b>6.74</b> (6.12-7.49)	<b>7.70</b> (6.97-8.56)	<b>8.96</b> (8.09-9.97)	<b>9.89</b> (8.90-11.0)	<b>10.8</b> (9.68-12.1)	<b>11.7</b> (10.4-13.1)	<b>12.9</b> (11.4-14.6)	<b>13.8</b> (12.1-15.6)
<b>30-day</b>	<b>5.55</b> (5.07-6.10)	<b>6.92</b> (6.33-7.61)	<b>8.43</b> (7.70-9.29)	<b>9.55</b> (8.71-10.5)	<b>11.0</b> (9.98-12.2)	<b>12.0</b> (10.9-13.3)	<b>13.0</b> (11.8-14.5)	<b>14.0</b> (12.6-15.5)	<b>15.2</b> (13.6-17.0)	<b>16.1</b> (14.3-18.0)
<b>45-day</b>	<b>6.92</b> (6.37-7.58)	<b>8.62</b> (7.92-9.44)	<b>10.4</b> (9.56-11.4)	<b>11.7</b> (10.7-12.8)	<b>13.3</b> (12.2-14.6)	<b>14.4</b> (13.1-15.9)	<b>15.5</b> (14.0-17.1)	<b>16.5</b> (14.9-18.2)	<b>17.7</b> (15.9-19.7)	<b>18.6</b> (16.6-20.7)
<b>60-day</b>	<b>8.20</b> (7.50-8.99)	<b>10.2</b> (9.32-11.2)	<b>12.3</b> (11.2-13.5)	<b>13.8</b> (12.5-15.1)	<b>15.6</b> (14.2-17.1)	<b>16.9</b> (15.3-18.6)	<b>18.1</b> (16.3-19.9)	<b>19.2</b> (17.3-21.2)	<b>20.5</b> (18.4-22.8)	<b>21.5</b> (19.2-24.0)

<sup>1</sup> Precipitation frequency (PF) estimates in this table are based on frequency analysis of partial duration series (PDS).

Numbers in parenthesis are PF estimates at lower and upper bounds of the 90% confidence interval. The probability that precipitation frequency estimates (for a given duration and average recurrence interval) will be greater than the upper bound (or less than the lower bound) is 5%. Estimates at upper bounds are not checked against probable maximum precipitation (PMP) estimates and may be higher than currently valid PMP values.

Please refer to NOAA Atlas 14 document for more information.

[Back to Top](#)

FIGURE 7 – HELVETIA PRECIPITATION – NOAA ATLAS 14



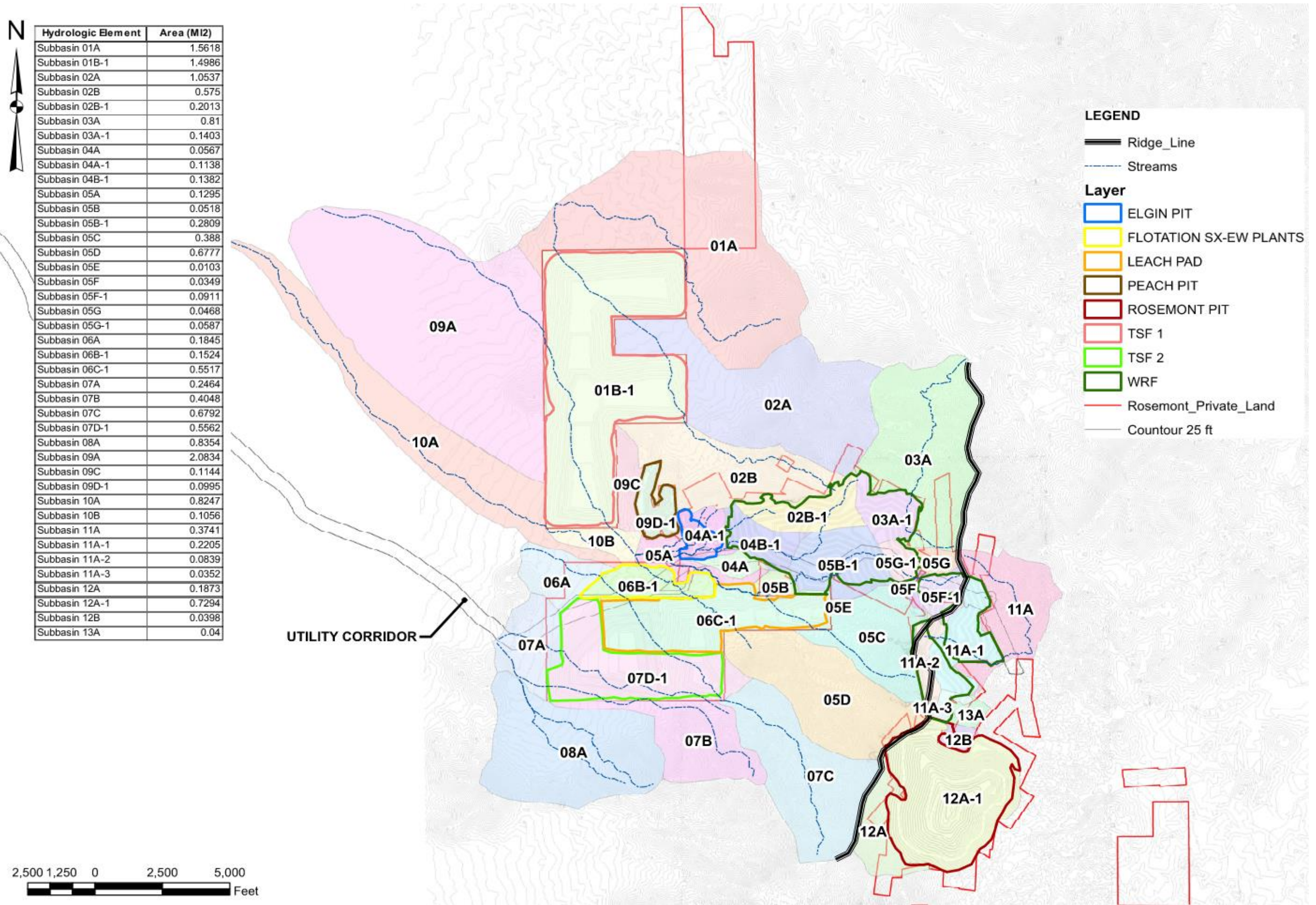
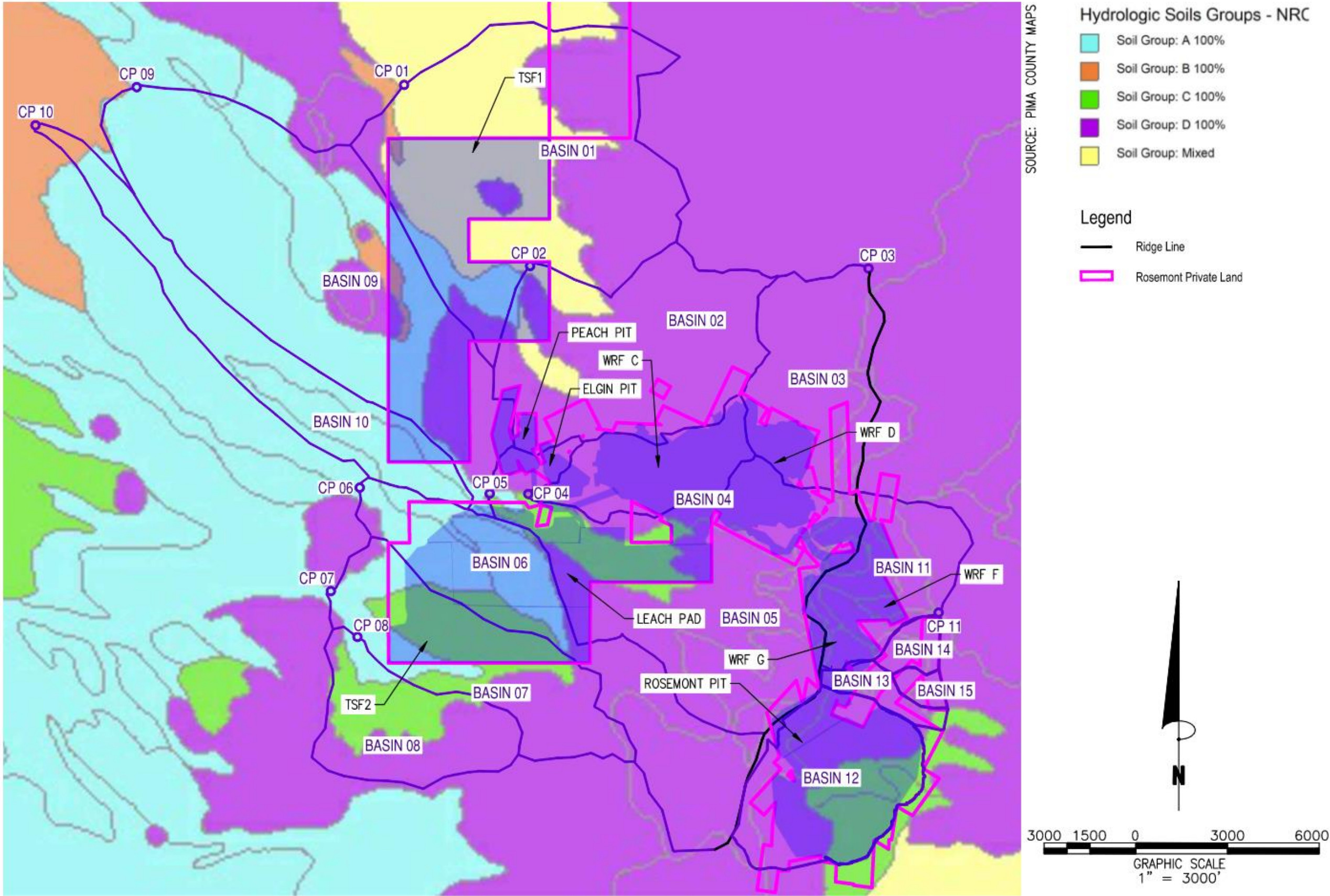


FIGURE 8 – BASIN DELINEATIONS FOR FINAL DRAINAGE CONFIGURATION WITH CONTACT WATER SEPARATION





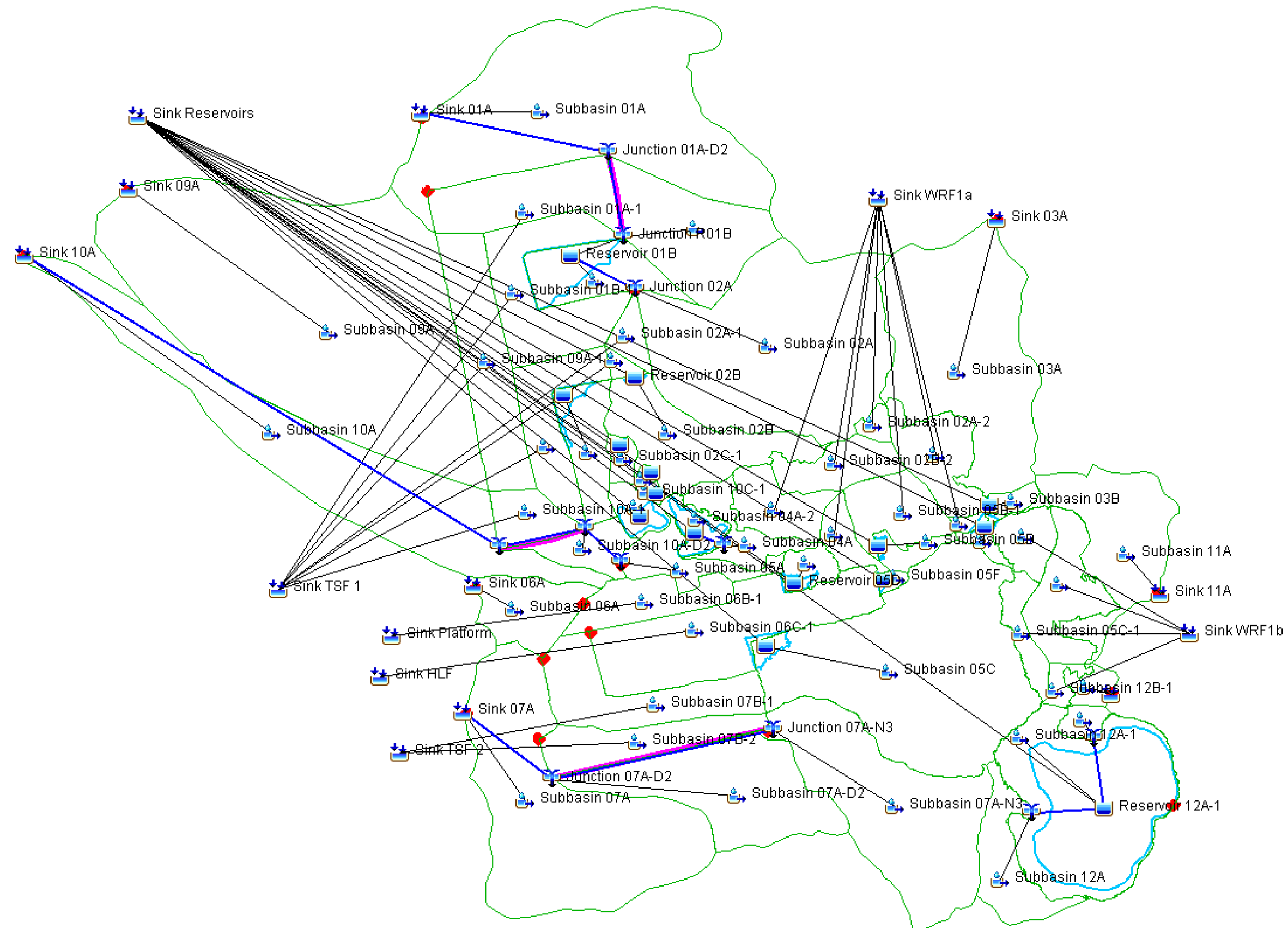


FIGURE 10-HEC HMS MODEL SCHEMATIC FOR FINAL DRAINAGE CONFIGURATION

## Appendix B

Annualized summaries for project facility final configuration - continuous mode



SINK HLF FLOW-CUMULATIVE		SINK TSF 1 FLOW-CUMULATIVE		SINK TSF 2 FLOW-CUMULATIVE		SINK WRF1A FLOW-CUMULATIVE		SINK WRF1B FLOW-CUMULATIVE	
RUN:PHASE II-Y15 CFLOW 6H NOGPE AC-FT INST-VAL		RUN:PHASE II-Y15 CFLOW 6H NOGPE AC-FT INST-VAL		RUN:PHASE II-Y15 CFLOW 6H NOGPE AC-FT INST-VAL		RUN:PHASE II-Y15 CFLOW 6H NOGPE AC-FT INST-VAL		RUN:PHASE II-Y15 CFLOW 6H NOGPE AC-FT INST-VAL	
FLOW PER YEAR									
31Dec1925 1800	42.3242	104.2155		39.8026		82.8664		36.1065	
31Dec1926 1800	480.1859	1245.0678		469.3435		721.9200		381.6506	
31Dec1927 1800	307.9711	780.0132		296.5267		465.9234		248.5137	
31Dec1928 1800	202.8777	511.6690		193.9850		308.4278		165.3381	
31Dec1929 1800	511.8059	1347.1401		504.6497		767.8206		406.9629	
31Dec1930 1800	573.8105	1511.5144		566.8637		860.1610		455.8561	
31Dec1931 1800	839.6495	2223.6897		832.2840		1256.0013		664.2475	
31Dec1932 1800	399.6149	1024.4028		387.7587		602.6771		320.8094	
31Dec1933 1800	244.6582	626.9828		237.3519		369.0104		196.3846	
31Dec1934 1800	297.4512	760.9859		288.2498		448.8319		239.3909	
31Dec1935 1800	572.4869	1500.6961		563.3718		858.6153		455.2287	
31Dec1936 1800	320.3346	828.2223		312.4825		482.0854		256.1367	
31Dec1937 1800	394.2946	1028.7424		387.0458		591.8919		313.8756	
31Dec1938 1800	393.1346	1020.8911		384.7135		590.8888		313.8662	
31Dec1939 1800	239.8094	593.4448		226.9403		366.1307		196.7703	
31Dec1940 1800	374.4212	960.6598		363.5217		564.5457		300.5122	
31Dec1941 1800	425.0491	1090.3496		412.2373		641.8733		341.9246	
31Dec1942 1800	262.8410	658.3530		251.0311		398.8832		213.3604	
31Dec1943 1800	346.5881	884.2725		335.1709		524.2343		279.7734	
31Dec1944 1800	336.6687	853.7203		323.8318		510.6559		272.9605	
31Dec1945 1800	313.3380	808.8351		305.4286		471.6940		250.8064	
31Dec1946 1800	436.6545	1128.9216		425.9719		657.6621		350.0839	
31Dec1947 1800	191.8303	492.8779		186.4182		289.1317		153.7970	
31Dec1948 1800	311.6483	799.5449		302.5621		469.9054		250.0291	
31Dec1949 1800	277.2258	702.2011		266.1426		420.2400		224.5027	
30Apr1950 0000	49.1142	119.3118		46.0264		75.0807		40.4498	

ANNUALIZED SUMMARIES FOR PROJECT FACILITY FINAL CONFIGURATION – CONTINUOUS MODE

## Appendix C

### Other Design Storm Events

## Final facility configuration drainage results – 100-year, 3-hour design storm

Rosemont Copper World Project 2.1 simulation run: Final Contact Volumes for design event		
Basin model: LOM 15		
Meteorologic Model: 100yr-3hr Hveto		
Control specification: 3hr-5m		
Hydrologic Element	Drainage Area (mi <sup>2</sup> )	Peak flow (cfs)
Junction 04A	0.0567	49.4
Junction 05A	0.1295	100.6
Junction 07B	1.0840	411.5
Junction 07C	0.6792	520.6
Junction 08A	0.8354	623.8
Junction 10B	0.2327	83.8
Junction 10B2	0.2327	9.4
Junction 12A	0.1874	164.7
Junction 12B	0.0398	32.4
Reach 04A	0.0567	38.1
Reach 05A	0.1295	24.2
Reach 07B	1.0840	55.1
Reach 07C	0.6792	146.6
Reach 08A	0.8354	143.2
Reach 10B	0.2327	9.4
Reach 10B2	0.2327	1.8
Reach 12A	0.1874	148.9
Reach 12B	0.0398	0.7
Sink HLF	0.5517	161.5
Sink Platform	0.1524	61.2
Sink R02A	1.0536	550.4
Sink R02B	0.5750	446
Sink R04A-1	0.1705	136.7
Sink R05B	0.0518	45.3
Sink R05C	0.3880	335.9
Sink R05D	0.6777	544.8
Sink R05E	0.0105	9.2
Sink R05F	0.0349	30.7
Sink R05G	0.0468	41.2
Sink R09C	0.1053	86.6
Sink R09D-1	0.0995	88
Sink R12A-1	0.9566	776.6
Sink TSF 1	1.4986	243.8
Sink TSF 2	0.5562	324
Sink WRF1a	0.8191	710.5
Sink WRF1b	0.4307	374.8

Final facility configuration drainage results – 100-year, 3-hour design storm (continued)

Rosemont Copper World Project 2.1 simulation run: Final Contact Volume design event		
Basin model: LOM 15		
Meteorologic Model: 100yr-3hr Hveto		
Control specification: 3hr-5m		
Hydrologic Element	Drainage Area	Peak flow (cfs)
Sink 01A	1.5618	538.6
Sink 03A	0.8100	445.2
Sink 06A	0.1845	127.7
Sink 07A	2.1658	393.8
Sink 09A	2.0834	109.2
Sink 10A	1.0574	14.4
Sink 11A	0.3741	293
Sink 13A	0.0400	34.9
Subbasin 01A	1.5618	538.6
Subbasin 01B-1	1.4986	243.8
Subbasin 02A	1.0536	550.4
Subbasin 02B	0.5750	446
Subbasin 02B-1	0.2010	175.6
Subbasin 03A	0.8100	445.2
Subbasin 03A-1	0.1403	121.2
Subbasin 04A	0.0567	49.4
Subbasin 04A-1	0.1138	98.6
Subbasin 04B-1	0.1382	118.6
Subbasin 05A	0.1295	100.6
Subbasin 05B	0.0518	45.3
Subbasin 05B-1	0.2809	243.4
Subbasin 05C	0.3880	335.9
Subbasin 05D	0.6777	544.8
Subbasin 05E	0.0105	9.2
Subbasin 05F	0.0349	30.7
Subbasin 05F-1	0.0911	79.5
Subbasin 05G	0.0468	41.2
Subbasin 05G-1	0.0587	51.7
Subbasin 06A	0.1845	127.7
Subbasin 06B-1	0.1524	61.2
Subbasin 06C-1	0.5517	161.5
Subbasin 07A	0.2464	195.5
Subbasin 07B	0.4048	264.9
Subbasin 07C	0.6792	520.6
Subbasin 07D-1	0.5562	324
Subbasin 08A	0.8354	623.8

Final facility configuration drainage results – 100-year, 3-hour design storm (continued)

Rosemont Copper World Project 2.1 simulation run: Final Contact Volumes design event		
Basin model: LOM 15		
Meteorologic Model: 100yr-3hr Hveto		
Control specification: 3hr-5m		
Hydrologic Element	Drainage Area	Peak flow (cfs)
Subbasin 09A	2.0834	109.2
Subbasin 09C	0.1053	86.6
Subbasin 09D-1	0.0995	88
Subbasin 10A	0.8247	12.6
Subbasin 10B	0.1032	59.6
Subbasin 11A	0.3741	293
Subbasin 11A-1	0.2205	190.6
Subbasin 11A-2	0.0839	73.7
Subbasin 11A-3	0.0352	31
Subbasin 12A	0.1874	164.7
Subbasin 12A-1	0.7294	627
Subbasin 12B	0.0398	32.4
Subbasin 13A	0.0400	34.9

## Final facility configuration drainage results – 1000-year, 3-hour design storm

Rosemont Copper World Project 2.1 simulation run: Final Contact Volumes for design event		
Basin model: LOM 15		
Meteorologic Model: 1000yr-3hr Hveto		
Control specification: 3hr-5m		
Hydrologic Element	Drainage Area (mi <sup>2</sup> )	Peak flow (cfs)
Junction 04A	0.0567	62.3
Junction 05A	0.1295	133.7
Junction 07B	1.0840	817.3
Junction 07C	0.6792	687.7
Junction 08A	0.8354	845
Junction 10B	0.2327	174.2
Junction 10B2	0.2327	34.4
Junction 12A	0.1874	206.5
Junction 12B	0.0398	42.8
Reach 04A	0.0567	56.6
Reach 05A	0.1295	84.3
Reach 07B	1.0840	179
Reach 07C	0.6792	440.3
Reach 08A	0.8354	488.9
Reach 10B	0.2327	34.4
Reach 10B2	0.2327	2.3
Reach 12A	0.1874	190.3
Reach 12B	0.0398	23.8
Sink HLF	0.5517	290.5
Sink Platform	0.1524	104.3
Sink R02A	1.0536	860.1
Sink R02B	0.5750	590
Sink R04A-1	0.1705	180.4
Sink R05B	0.0518	56.8
Sink R05C	0.3880	420.6
Sink R05D	0.6777	709.1
Sink R05E	0.0105	11.6
Sink R05F	0.0349	38.4
Sink R05G	0.0468	51.5
Sink R09C	0.1053	112
Sink R09D-1	0.0995	110
Sink R12A-1	0.9566	1001.6
Sink TSF 1	1.4986	491.6
Sink TSF 2	0.5562	483.6
Sink WRF1a	0.8191	895.7
Sink WRF1b	0.4307	472.2



Final facility configuration drainage results – 1,000-year, 3-hour design storm (continued)

Rosemont Copper World Project 2.1 simulation run: Final Contact Volume design event		
Basin model: LOM 15		
Meteorologic Model: 1000yr-3hr Hveto		
Control specification: 3hr-5m		
Hydrologic Element	Drainage Area	Peak flow (cfs)
Sink 01A	1.5618	990.2
Sink 03A	0.8100	680.6
Sink 06A	0.1845	179
Sink 07A	2.1658	925.2
Sink 09A	2.0834	238.1
Sink 10A	1.0574	28.3
Sink 11A	0.3741	388.2
Sink 13A	0.0400	44.2
Subbasin 01A	1.5618	990.2
Subbasin 01B-1	1.4986	491.6
Subbasin 02A	1.0536	860.1
Subbasin 02B	0.5750	590
Subbasin 02B-1	0.2010	220
Subbasin 03A	0.8100	680.6
Subbasin 03A-1	0.1403	153.2
Subbasin 04A	0.0567	62.3
Subbasin 04A-1	0.1138	123.8
Subbasin 04B-1	0.1382	150.3
Subbasin 05A	0.1295	133.7
Subbasin 05B	0.0518	56.8
Subbasin 05B-1	0.2809	307.5
Subbasin 05C	0.3880	420.6
Subbasin 05D	0.6777	709.1
Subbasin 05E	0.0105	11.6
Subbasin 05F	0.0349	38.4
Subbasin 05F-1	0.0911	99.9
Subbasin 05G	0.0468	51.5
Subbasin 05G-1	0.0587	64.7
Subbasin 06A	0.1845	179
Subbasin 06B-1	0.1524	104.3
Subbasin 06C-1	0.5517	290.5
Subbasin 07A	0.2464	257.2
Subbasin 07B	0.4048	377
Subbasin 07C	0.6792	687.7
Subbasin 07D-1	0.5562	483.6
Subbasin 08A	0.8354	845

Final facility configuration drainage results – 1,000-year, 3-hour design storm (continued)

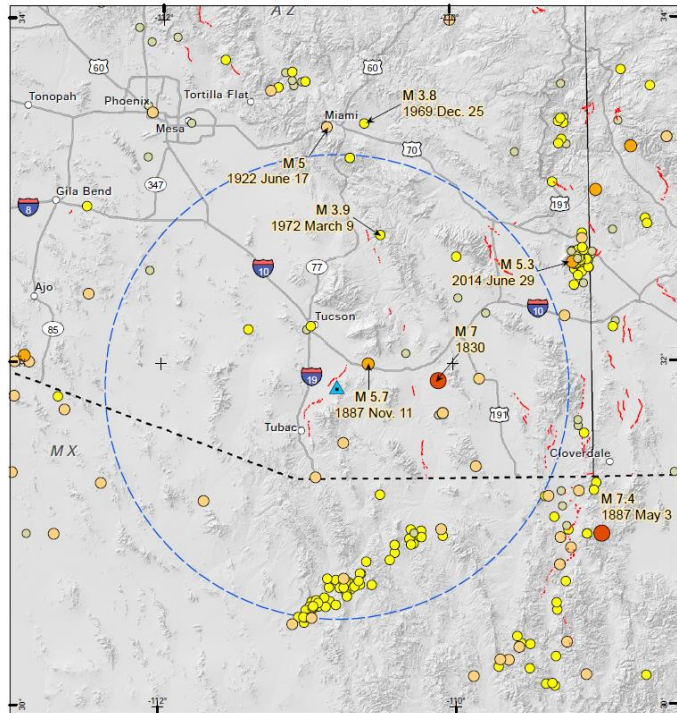
Rosemont Copper World Project 2.1 simulation run: Final Contact Volumes design event		
Basin model: LOM 15		
Meteorologic Model: 1000yr-3hr Hveto		
Control specification: 3hr-5m		
Hydrologic Element	Drainage Area	Peak flow (cfs)
Subbasin 09A	2.0834	238.1
Subbasin 09C	0.1053	112
Subbasin 09D-1	0.0995	110
Subbasin 10A	0.8247	26
Subbasin 10B	0.1032	89.9
Subbasin 11A	0.3741	388.2
Subbasin 11A-1	0.2205	241
Subbasin 11A-2	0.0839	92.3
Subbasin 11A-3	0.0352	39
Subbasin 12A	0.1874	206.5
Subbasin 12A-1	0.7294	787.5
Subbasin 12B	0.0398	42.8
Subbasin 13A	0.0400	44.2

**APPENDIX B.3**  
**SITE-SPECIFIC SEISMIC HAZARD ANALYSIS**

---

# Final Report

## Site-Specific Seismic Hazard Analyses and Development of Design Ground Motions for Rosemont Copper World Project, Arizona



Prepared for:

**WOOD ENVIRONMENT & INFRASTRUCTURE SOLUTIONS**  
4600 E. Washington St., Suite 600  
Phoenix, AZ 85034

Prepared by:

**LETTIS CONSULTANTS INTERNATIONAL, INC.**  
Qimin Wu and Ivan Wong  
1000 Burnett Ave., Suite 350  
Concord, CA 94520



10 January 2022

## TABLE OF CONTENTS

1.0	Introduction .....	1
1.1	Design Guidance .....	1
1.2	Scope of Work .....	2
2.0	PSHA Methodology .....	4
2.1	Seismic Source Characterization .....	5
2.1.1	Source Geometry .....	5
2.1.2	Recurrence .....	6
2.2	Ground Motion Characterization .....	7
3.0	Seismotectonic Setting and Historical Seismicity .....	8
3.1	Seismotectonic Setting .....	8
3.2	Historical Seismicity .....	9
3.2.1	Significant Earthquakes .....	10
3.2.2	Local Seismicity .....	11
4.0	Inputs to Analyses .....	12
4.1	Seismic Sources .....	12
4.1.1	Crustal Fault Sources .....	12
4.1.1.1	Santa Rita Fault Zone .....	14
4.1.1.2	Southern California Faults .....	15
4.1.2	Crustal Background Earthquakes .....	17
4.2	Site Characterization .....	19
4.3	Ground Motion Models .....	20
5.0	Seismic Hazard Results .....	22
5.1	PSHA Results .....	22
5.1.1	Hazard Sensitivities .....	23
5.2	Comparison with National Seismic Hazard Maps .....	23
5.3	DSHA Results .....	24
6.0	Design Earthquake Ground Motions .....	25
6.1	Conditional Mean Spectra .....	25
7.0	Development of Time Histories .....	27
8.0	References Cited .....	29

## LIST OF TABLES

Table 1. Completeness Estimates and Number of Earthquakes in Each Magnitude Interval .....	37
Table 2. Recurrence Parameters for the SBR Background Zone .....	37
Table 3. Summary of Probabilistic Ground Motions .....	38
Table 4. Magnitude and Distance Deaggregation.....	39
Table 5. Mean UHS, Enveloped Vs30.....	40
Table 6. Inputs for DSHA .....	41
Table 7. Median and 84th Percentile Deterministic Response Spectra .....	42
Table 8. CMS Conditioned at 0.2, 0.5, and 1.0 Sec for 10,000-Year Return Period .....	43
Table 9. Properties of Seed Time Histories .....	44
Table 10. Properties of Spectrally-Matched Time Histories .....	45

## LIST OF FIGURES

Figure 1. Site Location Map
Figure 2. Historical Seismicity in the Site Region, 1830 – November 2020
Figure 3. Quaternary Faults in the Site Region
Figure 4. Regional Quaternary Faults
Figure 5. Generalized Seismic Hazard Model Logic Tree
Figure 6. Seismotectonic Setting
Figure 7. Iseisismal Map of the 3 May 1887 <b>M</b> 7.4 Sonora, Mexico Earthquake
Figure 8. Iseisismal Map of the 17 June 1922 Miami, Arizona Earthquake
Figure 9. Did You Feel It Map for the 28 June 2014 <b>M</b> 5.2 Southeastern Arizona Earthquake
Figure 10. Local Historical Earthquakes, 1830 – November 2020
Figure 11. Independent Earthquakes, 1830 – November 2020, in the SBR Seismic Source Zone ( <b>M</b> ≥ 3.0)
Figure 12. Stepp Plot for the SBR Seismic Source Zone
Figure 13. Gridded Seismicity for the SBR Seismic Source Zone
Figure 14. Cumulative Magnitude-Recurrence Curves for the SBR Seismic Source Zone for $M_{MAX}$ 6.80
Figure 15. Shear-Wave Velocity Profiles
Figure 16. Seismic Hazard Curves for Peak Horizontal Acceleration for Vs30 1,200 m/sec



- Figure 17. Seismic Hazard Curves for 1.0 Sec Horizontal Spectral Acceleration for  $V_{s30}$  1,200 m/sec
- Figure 18. Seismic Source Contributions to Mean Peak Horizontal Acceleration Hazard for  $V_{s30}$  1,200 m/sec
- Figure 19. Seismic Source Fractional Contributions to Mean Peak Horizontal Acceleration Hazard for  $V_{s30}$  1,200 m/sec
- Figure 20. Seismic Source Contributions to Mean 1.0 Sec Horizontal Spectral Acceleration Hazard for  $V_{s30}$  1,200 m/sec
- Figure 21. Seismic Source Fractional Contributions to Mean 1.0 Sec Horizontal Spectral Acceleration Hazard for  $V_{s30}$  1,200 m/sec
- Figure 22. Magnitude and Distance Contributions to the Mean Peak Horizontal Acceleration Hazard at 475 and 2,475-Year Return Periods for  $V_{s30}$  1,200 m/sec
- Figure 23. Magnitude and Distance Contributions to the Mean Peak Horizontal Acceleration Hazard at 5,000 and 10,000-Year Return Periods for  $V_{s30}$  1,200 m/sec
- Figure 24. Magnitude and Distance Contributions to the Mean 1.0 Sec Horizontal Spectral Acceleration Hazard at 475 and 2,475-Year Return Periods for  $V_{s30}$  1,200 m/sec
- Figure 25. Magnitude and Distance Contributions to the Mean 1.0 Sec Horizontal Spectral Acceleration Hazard at 5,000 and 10,000-Year Return Periods for  $V_{s30}$  1,200 m/sec
- Figure 26. Sensitivity of Uniform Hazard Spectra to  $V_{s30}$  at 2,475 and 10,000-Year Return Periods
- Figure 27. Enveloped Uniform Hazard Spectra at 475, 975, 2,475, 5,000 and 10,000-Year Return Periods
- Figure 28. Sensitivity of Mean Peak Horizontal Acceleration Hazard to GMMs for  $V_{s30}$  1,200 m/sec
- Figure 29. Sensitivity of Mean 1.0 Sec Horizontal Spectral Acceleration Hazard to GMMs for  $V_{s30}$  1,200 m/sec
- Figure 30. Sensitivity of 84<sup>th</sup> Percentile Deterministic Spectrum for **M** 7.2 Santa Rita Fault Earthquake to GMMs
- Figure 31. Comparison of Deterministic Spectra and Uniform Hazard Spectra
- Figure 32. Uniform Hazard Spectrum at 10,000-Year Return Period and CMS Conditioned at 0.2, 0.5, and 1.0 Sec
- Figure 33. Response Spectra for Time History Spectrally Matched to 475-Year Return Period UHS - 1980 Irpinia, Italy-02 Earthquake - AUL270 Seed (RSN 295)
- Figure 34. Time History Spectrally Matched to 475-Year Return Period UHS - 1980 Irpinia, Italy-02 Earthquake - AUL270 Seed (RSN 295)
- Figure 35. Response Spectra for Time History Spectrally Matched to 975-Year Return Period

UHS - 1999 Chi-Chi, Taiwan-03 Earthquake - TCU120E Seed (RSN 2654)

Figure 36. Time History Spectrally Matched to 975-Year Return Period UHS - 1999 Chi-Chi, Taiwan-03 Earthquake - TCU120E Seed (RSN 2654)

Figure 37. Response Spectra for Time History Spectrally Matched to 2,475-Year Return Period UHS - 2009 L'Aquila, Italy Earthquake - GE146YLN Seed (RSN 4478)

Figure 38. Time History Spectrally Matched to 2,475-Year Return Period UHS - 2009 L'Aquila, Italy Earthquake - GE146YLN Seed (RSN 4478)

Figure 39. Response Spectra for Time History Spectrally Matched to 5,000-Year Return Period UHS - 2003 San Simeon, CA Earthquake - SLO090 Seed (RSN 4016)

Figure 40. Time History Spectrally Matched to 5,000-Year Return Period UHS - 2003 San Simeon, CA Earthquake - SLO090 Seed (RSN 4016)

Figure 41. Response Spectra for Time History Spectrally Matched to 10,000-Year Return Period UHS - 1979 Imperial Valley-06 Earthquake - H-E08140 Seed (RSN 183)

Figure 42. Time History Spectrally Matched to 5,000-Year Return Period UHS - 1979 Imperial Valley-06 Earthquake - H-E08140 Seed (RSN 183)

## 1.0 INTRODUCTION

This report presents the results of a site-specific probabilistic seismic hazard analysis (PSHA) and deterministic seismic hazard analysis (DSHA) for the Rosemont Copper World Project (Project) southeast of Sahuarita, Arizona (Figure 1). The objective of these seismic hazard analyses is to estimate the levels of ground motions that could be exceeded at specified annual frequencies (or return periods) at the Project site and compare the site-specific PSHA results with the results of a DSHA. The site is located in the Basin and Range Province of southern Arizona (Figure 1). Southern Arizona has a relatively low level of seismicity compared to the rest of the western U.S. (Figure 2). The Project is located about 5 km east of the nearest Quaternary active fault, the Santa Rita fault zone (Figure 3). Because of the low level of seismicity in southern Arizona, this study also assessed whether very active faults such as those in southern California, could contribute to the hazard at long periods at the site (Figure 4).

In this report, geological and seismological data were used to evaluate and characterize potential seismic sources, the likelihood of earthquakes of various magnitudes occurring on those sources, and the likelihood of the earthquakes producing ground motions over a specified level. The analyses presented in this report build upon Lettis Consultant's International's (LCI) numerous studies that have been performed for other mining facilities in central and southern Arizona.

The PSHA methodology is used in this report for assessing ground motion hazard. The evaluation of seismic hazard requires the explicit inclusion of the range of possible interpretations of components in the seismic hazard model, including seismic source characterization and ground motion estimation. These uncertainties, particularly in areas like Arizona, can be large for several reasons but primarily due to lack of comprehensive studies. Uncertainties in models and parameters are incorporated into the PSHA through the use of logic trees (Figure 5).

This report presents the seismic source characterization, the ground motion models (GMMs) used in the PSHA and DSHA, the probabilistic and deterministic ground motion hazard results, calculation of Uniform Hazard Spectra (UHS) and Conditional Mean Spectra (CMS), and development of time histories.

### 1.1 DESIGN GUIDANCE

As stated in Appendix E "Engineering Design Guidance" of the Arizona Mining BADCT Guidance Manual:

*The minimum design earthquake is the maximum probable earthquake (MPE). The MPE is defined as the maximum earthquake that is likely to occur during a 100-year interval (80% probability of not being exceeded in 100 years) and shall not be less than the maximum historical event. The design earthquake may apply to structures with a relatively short design life (e.g., 10 years) and minimum potential threat to human life or the environment.*

*Where human life is potentially threatened, the maximum credible earthquake (MCE) should be used. MCE is the maximum earthquake that appears capable of occurring under the presently known tectonic framework.*

- *Potential threat to human life or the environment*
- *Facility life*
- *Potential future property development downstream of the embankment or earth structure*
- *Seismic history in the area*

The MPE 80% probability of not being exceeded in 100 years has an equivalent return period of about 450 years. Based on the experience of LCI, more conservative criteria have been developed that have been accepted by the Arizona Department of Environmental Quality.

## 1.2 SCOPE OF WORK

Ground motions have been computed for a range of return periods up to 10,000 years. Both UHS and CMS have been computed. Comparison of these probabilistic and the deterministic ground motions are provided for use in selection of design ground motions for this Project. The following scope of work was performed.

### ***Task 1 – Evaluation of Historical and Contemporary Seismicity***

LCI employed the seismic source model developed for previous studies in southeastern Arizona. The historical and contemporary seismicity was evaluated in the site region based on an updated seismicity catalog. Historical ground shaking in the Project area from past earthquakes was evaluated. Recurrence rates of the historical seismicity for defined regional seismic source zones were updated for input into the PSHA.

### ***Task 2 – Site Characterization and Geophysical Survey***

All available geological, geophysical, and geotechnical information for the Project area were reviewed including shear-wave velocity ( $V_s$ ) data provided by Wood Environmental and Infrastructure Solutions (Wood). Based on these data, a  $V_{s30}$  (time-averaged  $V_s$  in the top 30 m) for the site was computed.  $V_{s30}$  is an input parameter into the GMMs. The hazard is defined at the top of rock so a site response analysis is not required.

### ***Task 3 – Probabilistic Seismic Hazard Analysis (PSHA)***

Based on LCI's seismic source model for the region and GMMs, site-specific probabilistic hazard was calculated for the site-specific  $V_{s30}$ . State-of-the-art GMMs were used in the PSHA, including the Pacific Earthquake Engineering Research (PEER) Center's Next Generation of Attenuation (NGA)-West2 models.

Hazard curves and horizontal UHS for the return periods of 475, 975, 2,475, 5,000, and 10,000 years at 5% damping were calculated. The horizontal hazard was deaggregated at selected return periods and spectral periods to characterize the controlling earthquakes. The probabilistic hazard was compared with the 2018 U.S. Geological Survey (USGS) National Seismic Hazard Maps, which are for a firm rock site condition ( $V_{s30}$  of 760 m/sec).

#### ***Task 4 – Deterministic Seismic Hazard Analysis (DSHA)***

A DSHA was performed for the most significant seismic sources affecting the site using the same GMMs selected for the PSHA. The site-specific  $V_{s30}$  was used. The ground motions from the controlling deterministic earthquakes were compared to the UHS from the PSHA.

#### ***Task 5 – Design Earthquake Ground Motions and CMS***

A preliminary horizontal Design Earthquake (DE) spectrum was proposed based on the results of the PSHA and DSHA and in consultation with Wood. Based on the preliminary DE, Conditional Mean Spectra (CMS) were computed based on the selected structural periods of interest and deaggregation results from the PSHA.

#### ***Task 6 – Development of Time Histories***

Five horizontal-component time histories were developed by spectral matching to the UHS for each of the five return periods.

## 2.0 PSHA METHODOLOGY

The PSHA approach used in this study is based on the model developed principally by Cornell (1968). The occurrence of earthquakes on a fault is assumed to be a Poisson process. The Poisson model is widely used and is a reasonable assumption in regions where data are sufficient to provide only an estimate of average recurrence rate (Cornell, 1968). When there are sufficient data to permit a real-time estimate of the occurrence of earthquakes, the probability of exceeding a given value can be modeled as an equivalent Poisson process in which a variable average recurrence rate is assumed. The occurrence of ground motions at the site in excess of a specified level is also a Poisson process, if (1) the occurrence of earthquakes is a Poisson process, and (2) the probability that any one event will result in ground motions at the site in excess of a specified level is independent of the occurrence of other events.

The probability that a ground motion parameter "Z" exceeds a specified value "z" in a time period "t" is given by:

$$p(Z > z) = 1 - e^{-\nu(z) \cdot t} \quad (1)$$

where  $\nu(z)$  is the annual mean number (or rate) of events in which Z exceeds z. It should be noted that the assumption of a Poisson process for the number of events is not critical. This is because the mean number of events in time t,  $\nu(z) \cdot t$ , can be shown to be a close upper bound on the probability  $p(Z > z)$  for small probabilities (less than 0.10) that generally are of interest for engineering applications. The annual mean number of events is obtained by summing the contributions from all sources, that is:

$$\nu_k(Z > z) = \sum_n \nu_{kn}(Z > z) \quad (2)$$

where  $\nu_{kn}(Z > z)$  is the annual mean number (or rate) of events on source n for which Z exceeds z at site k. The parameter  $\nu_{kn}(Z > z)$  is given by the expression:

$$\nu(Z > z) = \sum_n \alpha_n (M^0) \int_{M^0}^{M_n^u} f_n(M) \left[ \int_0^\infty f_{kn}(r|M) \cdot P_{kn}(Z > z|M, r) \cdot dr \right] \cdot dM \quad (3)$$

where  $\alpha_n (M^0)$  is the rate of all earthquakes on source n above a minimum magnitude,  $M^0$ ;  $f_n(M)$  is the probability density function of earthquake magnitude between  $M^0$  and a maximum earthquake that source n can produce,  $M_n^u$  (i.e., recurrence model);  $f_{kn}(r|M)$  is the conditional probability density function for distance from site k to an earthquake of magnitude M occurring on source n; and  $P_{kn}(Z > z|M, r)$  is the conditional probability that, given an earthquake of magnitude M at distance r from site k, the ground motion (Z) will exceed the specified level z. Distance r is calculated as the closest distance from the rupture to the site.

Calculations were made using the computer program APEX developed by LCI, which was developed and qualified under the LCI Quality Assurance (QA) program, and has been validated using the test cases in the PEER Center-sponsored PSHA Computer Program Validation Project (Hale *et al.*, 2018).



---

## 2.1 SEISMIC SOURCE CHARACTERIZATION

Two types of earthquake sources are characterized in this PSHA: (1) fault sources; and (2) areal source zones (Section 4.1). Fault sources are modeled as three-dimensional fault surfaces and details of their behavior are incorporated into the source characterization. Areal source zones to address the hazard from background earthquakes are regions where earthquakes are assumed to occur randomly. A gridded seismicity approach was also used to address background earthquakes (Section 4.1.2). Seismic sources are modeled in the hazard analysis in terms of geometry and earthquake recurrence.

The geometric source parameters for faults include fault location, segmentation model, dip, and thickness of the seismogenic zone. The recurrence parameters include recurrence model, recurrence rate (slip rate or average recurrence interval for the maximum event), slope of the recurrence curve ( $b$ -value), and maximum magnitude. Clearly, the geometry and recurrence are not totally independent. For example, if a fault is modeled with several small segments instead of large segments, the maximum magnitude is lower, and a given slip rate requires many more small earthquakes to accommodate a cumulative seismic moment. For areal source zones, only the areas, maximum magnitude, seismogenic thickness and recurrence parameters (based on the historical earthquake record) need to be defined.

Uncertainties in the seismic source parameters as described below, which were sometimes large, were incorporated into the PSHA using a logic tree approach (Figure 5). In this procedure, values of the source parameters are represented by the branches of logic trees with weights that define the distribution of values. A sample logic tree for a fault is shown on Figure 5. In general, three values for each parameter were weighted and used in the analysis. Statistical analyses by Keefer and Bodily (1983) indicate that a three-point distribution of 5<sup>th</sup>, 50<sup>th</sup>, and 95<sup>th</sup> percentiles weighted 0.185, 0.63, and 0.185 (rounded to 0.2, 0.6, and 0.2), respectively, is the best discrete approximation of a continuous distribution. Alternatively, they found that the 10<sup>th</sup>, 50<sup>th</sup>, and 90<sup>th</sup> percentiles weighted 0.3, 0.4, and 0.3, respectively, can be used when limited available data make it difficult to determine the extreme tails (i.e., the 5<sup>th</sup> and 95<sup>th</sup> percentiles) of a distribution. Note that the weights associated with the percentiles are not equivalent to probabilities for these values, but rather are weights assigned to define the distribution. These guidelines were generally applied in developing distributions for seismic source parameters with continuous distributions (e.g.,  $M_{max}$ , fault dip, slip rate or recurrence) unless the available data suggested otherwise. Estimating the 5<sup>th</sup>, 95<sup>th</sup>, or even 50<sup>th</sup> percentiles is typically challenging and involves subjective judgment given limited available data.

### 2.1.1 Source Geometry

In the PSHA, it is assumed that earthquakes of a certain magnitude may occur randomly along the length of a given fault or segment. The distance from an earthquake to the site is dependent on the source geometry, the size and shape of the rupture on the fault plane, and the likelihood of the earthquake occurring at different points along the fault length. The distance to the fault is defined to be consistent with the specific ground motion model used to calculate the ground

motions. The distance, therefore, is dependent on both the dip and depth of the fault plane, and a separate distance function is calculated for each geometry and each ground motion model. The size and shape of the rupture on the fault plane are dependent on the magnitude of the earthquake; larger events rupture longer and wider portions of the fault plane. The rupture dimensions were modeled following the magnitude-rupture area and rupture-width relationships of Wells and Coppersmith (1994).

### 2.1.2 Recurrence

The recurrence relationships for the seismic sources are modeled using the truncated-exponential Gutenberg-Richter, characteristic earthquake, and the maximum magnitude recurrence models. These models are weighted (Figure 5) to represent our judgment on their applicability to the sources, as discussed in Section 4.2.1. For the areal source zones, only a truncated exponential recurrence relationship is assumed to be appropriate.

The general approach of Molnar (1979) and Anderson (1979) was used to arrive at the recurrence for the truncated exponential model. The number of events exceeding a given magnitude,  $N(m)$ , for the truncated exponential relationship is

$$N(m) = \alpha(m^o) \frac{10^{-b(m-m^o)} - 10^{-b(m^u-m^o)}}{1 - 10^{-b(m^u-m^o)}} \quad (4)$$

where  $\alpha(m^o)$  is the annual frequency of occurrence of earthquakes greater than the minimum magnitude,  $m^o$ ;  $b$  is the Gutenberg-Richter parameter defining the slope of the recurrence curve; and  $m^u$  is the upper-bound magnitude event that can occur on the source. A  $m^o$  of **M** 5.0 was used for the hazard calculations because smaller events are not considered likely to produce ground motions with sufficient energy to damage well-designed structures.

Fault rupture was modeled with a "characteristic" magnitude on specific segments; this model is described by Aki (1983) and Schwartz and Coppersmith (1984). For the characteristic model, the numerical model of Youngs and Coppersmith (1985) was used. In the characteristic model, the number of events exceeding a given magnitude is the sum of the characteristic events and the non-characteristic events. The characteristic events are distributed uniformly over a  $\pm 0.25$  magnitude unit around the characteristic magnitude, and the remainder of the moment rate is distributed exponentially using Equation (4) with a maximum magnitude 0.25 unit lower than the characteristic magnitude (Youngs and Coppersmith, 1985). The maximum magnitude model can be regarded as an extreme version of the characteristic model. We adopted the model proposed by Wesnousky (1986). In the maximum magnitude model, there is no exponential portion of the recurrence curve, i.e., no events can occur between the minimum magnitude of **M** 5.0 and the distribution about the maximum magnitude.

The recurrence rates for the fault sources are defined by either the slip rate or the average recurrence interval for the maximum or characteristic event and the recurrence  $b$ -value. Slip rate can be used to compute the activity rate by balancing the long-term accumulation of seismic

moment with the long-term release of seismic moment in earthquakes. The slip rate is used to calculate the moment rate on the fault using the following equation defining the seismic moment:

$$M_o = \mu A D \quad (5)$$

where  $M_o$  is the seismic moment,  $\mu$  is the shear modulus,  $A$  is the area of the rupture plane, and  $D$  is the slip on the plane. Differentiating with respect to time results in the moment rate as a function of slip rate:

$$\dot{M}_o = \mu A S \quad (6)$$

where  $\dot{M}_o$  is the moment rate and  $S$  is the slip rate. Equation (6) defines the annual rate of buildup of seismic moment. The long-term rate of seismic moment release is a function of the seismic moment released during an earthquake of a given magnitude and the distribution of magnitudes of earthquakes that occur.  $M_o$  has been related to moment magnitude,  $M$ , by Hanks and Kanamori (1979):

$$M = 2/3 \log M_o - 10.7 \quad (7)$$

Using this relationship and the relative frequency of different magnitude events from the recurrence model, the slip rate can be used to estimate the absolute frequency of different magnitude events.

## 2.2 GROUND MOTION CHARACTERIZATION

To characterize the ground motions at a specified site as a result of the seismic sources considered in the PSHA and DSHA, empirical GMMs for spectral accelerations were used. The models used in this study were selected on the basis of the appropriateness of the site conditions and tectonic environment for which they were developed (Figure 5; Section 4.3).

Ground motions are generally assumed to be lognormally distributed. However, recent studies (e.g., GeoPentech, 2015) have demonstrated that ground motions deviate from the generally assumed lognormal distribution at epsilon ( $\epsilon$ ) values greater than about 2.5, where  $\epsilon$  is the number of standard deviations above or below the median ground motion intensity. As part of the Southwestern United States Ground Motion Characterization SSHAC Level 3 study (GeoPentech, 2015), residuals for the NGA-West2 models were examined at various epsilon values, and it was determined that the within-event residuals had “fat tails” in that there was a higher probability of extremes (at both high and low epsilon) than predicted by a lognormal distribution. To adequately model these fat tails, a mixture model was developed, which consists of two equally weighted lognormal distributions: one model having a mean of zero and log standard deviation of 0.8 times sigma (from the individual GMMs) and the second model having a mean of zero and log standard deviation of 0.2 times sigma. The mixture model was implemented for this study. Five standard deviations about the median value were included in the analysis.

### 3.0 SEISMOTECTONIC SETTING AND HISTORICAL SEISMICITY

The seismotectonic setting and historical seismicity of the Rosemont Project area are discussed below.

#### 3.1 SEISMOTECTONIC SETTING

The Rosemont Copper World Project is located in southeastern Arizona, southeast of Tucson (Figures 1 and 2). Arizona is divided into three physiographic and seismotectonic provinces: the Colorado Plateau in the northeast, the Southern Basin and Range (SBR) in the south and southwest, and the intervening Transition Zone that is roughly 40 to 100-km-wide and northwest-southeast trending (Figure 6). All three provinces are characterized by relatively few late Quaternary faults and low rates of seismicity. These regions are bounded to the east by the Rio Grande Rift, and to the west by the Salton Trough Province (Figure 6). The Project is located in the SBR near the southern US border.

The SBR Province is a block-faulted terrain of alternating mountain ranges and intervening valleys, bounded by moderately to steeply dipping normal faults. The mountains comprise igneous, metamorphic, and indurated sedimentary rocks of Precambrian through Tertiary age; the valleys are filled with undeformed sequences of fluvial and lacustrine sediments of Oligocene to Pleistocene age. There are differing estimates on the timing of initiation of Basin and Range extension; McQuarrie and Wernicke (2005) suggest that deformation began at 25 Ma, whereas Menges and Pearthree (1989) indicate that deformation may have commenced during the Miocene at 15 Ma. However, there is general consensus that major extension ceased at some time in the late Miocene or Pliocene, and the modern landscape is dominated by geomorphological landforms that indicate tectonic inactivity (Menges and McFadden, 1981). Relative tectonic quiescence in southern Arizona is also reflected by the low levels of historical seismicity and sparse evidence for Quaternary faulting. The SBR Province is dominated by northwest-southeast-striking normal faults; however, the site region encompasses the transition from this northwest-southeast structural grain to a more north-south orientation as the province extends into northern Mexico.

The Transition Zone represents a tectonic transition from the relatively thin (~15 to 20 km) extended crust of the SBR to the thick (~40 km) crust of the Colorado Plateau. Bedrock in the region consists primarily of Precambrian metamorphic and granitic plutonic rocks and Paleozoic sediments. The composition of late Cenozoic basin-fill sediments reflects widespread Tertiary volcanism in the region. The Transition Zone is characterized by north- to northwest-trending mountain ranges and intervening basins related mainly to Miocene and younger normal faulting (Menges and McFadden, 1981; Mack *et al.*, 2003). The topography of the Transition Zone is more subdued than that of the SBR Province to the south: the ranges are less pronounced and the basins are smaller and less well-defined. The relatively subdued landforms, low to moderate levels of seismicity (Brumbaugh, 1987; Bausch and Brumbaugh, 1997), and relative lack of significant late Quaternary faulting (Pearthree *et al.*, 1983) have been interpreted to indicate geologically recent tectonic cessation of major extension in the region (Menges and McFadden,

1981). The few Quaternary normal faults that are mapped in the region generally trend northwest-southeast and are likely reactivated faults that originated during Basin and Range extension (Lockridge *et al.*, 2012) (Figure 3). Based on reconnaissance mapping and limited paleoseismic studies, these faults have average recurrence intervals of tens to hundreds of thousands of years (Pearthree, 1998; Piety and Anderson, 1991).

The Colorado Plateau in northern Arizona is part of a large region that extends across southeastern Utah, northwestern New Mexico, and western Colorado. Physiographically and geologically distinct from the highly deformed Rocky Mountains to the north and east and the Basin and Range region to the south and west, the Colorado Plateau is characterized by relative tectonic stability and elevated topography dissected by rivers. Whereas major crustal deformation of the Colorado Plateau ceased at the end of Laramide orogeny (40 Ma), the region has been subject to about 2 km of epeirogenic uplift during the Cenozoic Era (Morgan and Swanberg, 1985). During uplift, the plateau acted as a coherent block, with only minor differential movements creating northerly-trending monoclines and associated structural basins. Contemporary seismicity in the Colorado Plateau Province is low to moderate, with widespread, generally small events that cannot be correlated with surface geological features (Wong and Humphrey, 1989).

The Salton Trough to the west of the Basin and Range marks the transition between ocean-floor spreading in the Gulf of California and right-lateral strike-slip faulting along the San Andreas fault zone. This region is one of the most seismically active areas in the western United States, characterized by right-lateral strike-slip faulting and elevated levels of contemporary seismicity with repeated events of **M** 6 to 7 during the period of historical record (Figure 4). Slip rates on faults in this region are as high as 30 mm/yr (Working Group on California Earthquake Probabilities, 2008).

### 3.2 HISTORICAL SEISMICITY

A historical seismicity catalog compiled as part of previous analyses of mines in an area that encompassed over 150 km around the Project site, extending from a latitude of approximately 30°N to 36.3°N and a longitude of approximately 115°W to 107.5°W was used in this evaluation (Figure 2). The catalog was updated for this study to cover the time period from 1830 to November 2020. All magnitudes were converted to or assumed to be equivalent to moment magnitude. Primary data sources used in the compilation include the Northern Arizona University regional catalog (1830 through 2005), the Advanced National Seismic Service (ANSS), Sawires *et al.* (2019), and the National Autonomous University of Mexico (UNAM) (Figure 2). As in most of the western U.S., the historical record extends back less than 200 years, which is a relatively short period compared to the recurrence intervals of most active crustal faults.

The Project area is located in a region of relatively low historical seismicity (Figure 2). This area, however, has had poor seismographic coverage (Thomas *et al.*, 2015). In addition to the SBR, the catalog includes seismicity to the north in the area of the Transition Zone physiographic province as well as the southern Colorado Plateau (Section 3.1). The catalog includes 26 events

of **M** 5 to 5.9, three events of **M** 6 to 6.9, and three events of **M** 7 and greater (Figure 2). One of the **M** 7 events is documented as having occurred in 1830, though it is based on a single report made in the mid-1850's and is therefore considered suspect and poorly constrained and documented (DuBois *et al.*, 1982). Wong *et al.* (2013) noted that this event continues to be included in some catalogs but has been removed from the Arizona Geological Survey catalog because it is poorly dated, dubious, and because no physical evidence has been found to corroborate such a reportedly high intensity and relatively young event (Phil Pearthree, Arizona Geological Survey written communication to I. Wong, 2013). The event appears on Figure 2, but it was excluded from the earthquake recurrence calculations.

### 3.2.1 Significant Earthquakes

This section describes three significant historical earthquakes that have occurred in or near the site region whose effects were likely felt at the location of the Project area.

#### 1887 Sonora Earthquake

The largest event in the catalog and the largest historical earthquake to impact the southwestern U.S. was an earthquake of **M** 7.4 that occurred on 3 May 1887 in northern Sonora, Mexico, approximately 180 km southeast of the Project area (DuBois *et al.*, 1982; Suter and Contreras, 2002) (Figure 7). The earthquake ruptured three major normal faults (Otates, Teras, and Pitáycachi faults) and was felt throughout Arizona and New Mexico and as far south as Mexico City (DuBois *et al.*, 1982; Suter and Contreras, 2002). The maximum felt intensity was between Modified Mercalli intensity (MMI) XI and XII and intensity MMI VII would have been observed at the Project site (Figure 7; DuBois *et al.*, 1982).

#### 1887 **M** 5.7 Earthquake

The closest known earthquake to the Project site was a MM intensity VII event ( $\approx$  **M** 5.7) that occurred on 11 November 1887 and was located about 25 km northeast of the site; however, the location and size of this pre-instrumental event are highly uncertain. The earthquake reportedly cracked the depot buildings in the town of Pantano in Pima County, which were constructed of wood.

#### 1922 Miami Earthquake

A **M** 5.0 event occurred on 17 June 1922 in the vicinity of Miami, Arizona, approximately 160 km north of the site (DuBois *et al.*, 1982) (Figure 2). The felt intensity at the Project area was not included by DuBois *et al.* (1982), the felt intensity likely would have been very low based on the proximity to the MMI V contour (Figure 8). Although the event was felt throughout the town of Miami, no structural damage was reported (DuBois *et al.*, 1982). Wong *et al.* (2008) noted that this event was recorded on a seismograph in Tucson and that the location and size of the event are highly uncertain.



---

### *2014 Southeastern Arizona Earthquake*

A more recent **M** 5.3 event occurred on 29 June 2014 approximately 180 km southeast of the Project area, near the town of Duncan, Arizona and near the Arizona-New Mexico border (Figure 2). This event was recorded on the USGS “Did You Feel It?” (DYFI) website (<http://earthquake.usgs.gov/earthquakes/eventpage/usc000rnfe#dyfi>). The maximum reported intensity of MMI V was reported near the epicenter (Figure 9). Based on reported intensities surrounding the site, an intensity between MMI II and III would have been observed at the Project area (Figure 9). The earthquake occurred at a depth of 6.4 km and the moment tensor solution reported by the USGS shows that the event is consistent with northeast-striking oblique-normal faulting. Subsequent to this event, there have been over 40 likely aftershocks ranging in magnitude from **M** 2.0 to 4.0. Although this earthquake was relatively distant from the site, it represents a good example of a background earthquake with no apparent association with a Quaternary fault (Section 4.1.2).

#### **3.2.2 Local Seismicity**

Historical seismicity in the site region is sparse with only five events within 50 km of the Project site (Figure 10). The largest and closest event to the Project area was the 11 November 1887 **M** 5.7 earthquake (Figure 10). In 1927, a **M** 4.3 earthquake occurred about 40 km to the south of the Project site (Figure 10).

## 4.0 INPUTS TO ANALYSES

The following section discusses the characterization of the seismic sources and the GMMs selected and used in the PSHA and DSHA. Also included in this section is a description of the site geology and  $V_{s30}$  used in the hazard analyses.

### 4.1 SEISMIC SOURCES

Seismic source characterization is concerned with three fundamental elements: (1) the identification, location and geometry of significant sources of earthquakes; (2) the maximum size of the earthquakes associated with these sources; and (3) the rate at which the earthquakes occur. The seismic source model includes crustal faults capable of generating large surface-faulting earthquakes (Section 4.1.1), and an areal source zone, which accounts for background crustal seismicity that cannot be attributed to identified faults explicitly included in the seismic source model (Section 4.1.2). A gridded seismicity approach was also used in the PSHA to account for the background earthquake hazard.

#### 4.1.1 Crustal Fault Sources

Fault parameters required in the PSHA include: (1) rupture model (including independent single plane and potentially linked models); (2) probability of activity; (3) fault geometry including rupture length, rupture width, fault orientation, and sense of slip; (4) maximum or characteristic magnitude [ $M_{max}$ ]; and (5) earthquake recurrence including both recurrence model and rates. These parameters are generally discussed further below. Selected faults that contribute the most to the hazard are specifically discussed in subsequent sections. Uncertainties in each parameter were explicitly incorporated through the use of logic trees, as exemplified in Figure 5.

All known active or potentially active faults were included in the analyses within 150 km of the site (Figure 3). We included known faults showing evidence for late Quaternary ( $\leq 130,000$  years) activity or repeated Quaternary ( $\leq 1.6$  million years) activity. We also included longer, more active faults in southern California and Baja California, such as the southern San Andreas fault, because from previous analyses in the region (e.g., Wong *et al.*, 2017), we know that these major fault sources can be significant contributors to the long-period hazard ( $> 1$  sec) despite their great distances (Figure 4). The Pitaycachi fault, source of the 1887 Sonora earthquake, was also included in the hazard analysis because although it is distant (around 180 km away) and its slip rate is low ( $< \sim 0.1$  mm/yr). It is the source of the largest earthquake in the region (Figure 2).

Faults are generally modeled as single, independent, planar sources, simplified from the complex zones shown on Figure 3. Our fault characterization is based on the model developed from our previous PSHAs in Arizona, and from data compiled in the USGS Quaternary Fault and Fold Database (<http://earthquake.usgs.gov/hazards/qfaults/>).

Maximum magnitudes were estimated for the local faults using the empirical relationships of: (1) Wells and Coppersmith (1994) for all fault types; (2) the Stirling *et al.* (2002) censored relationship for all fault types; and (3) Wesnousky (2008) for all fault types. None of the local faults are blind,

and minimum seismogenic depths were assumed to be 0 km. Maximum seismogenic depths of 12 km (weighted 0.3), 15 km (weighted 0.5), and 17 km (weighted 0.2) were assumed, primarily based on the maximum depth of historical seismicity in the region (e.g., Lockridge *et al.*, 2012).

Fault dips are averages over the entire seismogenic crust. Although near-surface fault dip data are available for many of the faults, crustal dip data are lacking. Default dips of  $50^{\circ}$  (weighted 0.6)  $\pm 15^{\circ}$  (weighted 0.2) were assumed for all the local faults, which all show dominantly normal slip. This default fault dip distribution is after recommendations made by the Basin and Range Province Earthquake Working Group II (BRPEWGII; Lund, 2012; see Issue G4) to the USGS regarding crustal-scale dips for typical range-bounding normal faults in the Basin and Range Province used in the 2014 update of the National Seismic Hazard Maps. This distribution was based on focal plane and aftershock data for historical surface-rupturing earthquakes in the Basin and Range Province, as well as normal faults worldwide (WGEUP, 2016).

It has been proposed that the recent 2020 **M** 5.7 Magna, Utah earthquake occurred on a listric Wasatch fault (Pang *et al.*, 2020), and this has hazard implications for all normal faults in the Basin and Range (Wong *et al.*, 2021a). According to Pang *et al.* (2020), the 2020 **M** 5.7 Magna, Utah earthquake occurred on a low-angle normal fault (approximate 35-degree dip) that they believe is the Salt Lake City segment of the Wasatch fault. The Wasatch fault is believed to be typical of Basin and Range faults which have been characterized as moderately dipping with dips of  $50 \pm 15$  degrees (WGEUP, 2016). Hence the observation that the Wasatch fault is possibly listric is contrary to this long-held belief and not only poses a challenge to the seismic source characterization and hazard characterization in Utah but also to the Basin and Range Province in general (Wong *et al.*, 2021c).

Recurrence models can significantly impact hazard calculations. The truncated exponential, maximum magnitude, and characteristic recurrence models were considered for this analysis. Observations of historical seismicity and paleoseismic investigations suggest that characteristic behavior is more likely for individual faults, whereas seismicity in areal zones best fits a truncated exponential model (Schwartz and Coppersmith, 1984; Youngs and Coppersmith, 1985). The maximum magnitude model is an extreme version of the characteristic model (Wesnousky, 1986). The characteristic model for all local fault sources was favored (weighted 0.7) and the remaining weight of 0.3 was assigned to the maximum magnitude model.

It has been argued that the exponential model may not be applicable to faults (e.g., Hecker *et al.*, 2013). However, fault zones consisting of multiple parallel faults observed in the Basin and Range Province have been characterized as small areal sources rather than single planar faults. Such zones would then be characterized by a truncated exponential recurrence model.

In assigning probabilities of activity for local fault sources, both the likelihood that the fault is structurally capable of independently generating earthquakes, and the likelihood that it is still active within the modern stress field were considered. We incorporated many factors in assessing these likelihoods, such as: orientation in the modern stress field, fault geometry (length, continuity,

and dip), relation to other faults, age of youngest movement, rates of activity, geomorphic expression, amount of cumulative offset, and any evidence for a non-tectonic origin. Faults with definitive evidence for repeated Quaternary activity were generally assigned probabilities of being active (seismogenic) of 1.0. The probability of activity for faults that do not show definitive evidence for repeated Quaternary activity was individually judged based on available data and the criteria explained above. Resulting values range from 0.5 to 1.0.

As recurrence interval data are generally lacking for local faults, slip rates were used to characterize rates of fault activity. All available long- ( $\leq 1.6$  Ma) and short-term ( $\leq 130$  ka) data were considered in developing slip rate distributions, but short-term data were used whenever possible. In addition to the time period, the type and quality of data were also considered in determining rates. Preferred slip rates (generally weighted 0.6) are generally based on data in the USGS Quaternary Fault and Fold database (USGS and AZGS, 2019). Maximum and minimum values (each generally weighted 0.2) are typically selected to represent 95<sup>th</sup> and 5<sup>th</sup> percentile values as previously discussed in Section 2, unless the available data suggest otherwise.

The Santa Rita fault zone is the closest Quaternary fault to the site, so it is discussed below (Figure 3). The southern Cerro Prieto and southern San Andreas faults are significant fault sources to the hazard at the site, and so they are also discussed below (Figure 4).

#### 4.1.1.1 Santa Rita Fault Zone

At its closest approach, the Santa Rita fault is 4.9 km northwest of the Project area (Figure 3). Thomas *et al.* (2015) described the Santa Rita fault as a 52-km-long north-south-striking fault. The fault is expressed as a roughly north-south-trending alignment of discontinuous faults scarps several meters high representing displacement of mid to late Pleistocene alluvial fan deposits sourced from the Santa Rita Mountains to the east. Work by Pearthree *et al.* (1983) and Pearthree and Calvo (1987) documents two surface-rupturing earthquakes, with the most recent event likely occurring between 50 and 100 ka. Based on 4 to 5 m of vertical displacement in the last 200 to 300 ka and 2 to 3 m of vertical displacement in the last 60 to 130 ka, Thomas *et al.* (2015) assigned a preferred slip rate of 0.025 mm/yr, with maximum and minimum values of 0.08 and 0.008 mm/yr, respectively. Given that the close proximity of the fault to the Rosemont Project site, calculated hazard is highly sensitive to the dip of the fault. In their model, Thomas *et al.* (2015) assigned dips of 30°, 50°, and 65° for minimum, preferred, and maximum values, with a weighted mean dip of 49°. Fault length was modeled as a single independent (full length) 52 km rupture with an  $M_{\max}$  of  $7.1 \pm 0.3$ .

In a recent study, LCI completed a review of the Thomas *et al.* (2015) seismic source model with a focus on re-evaluating the Santa Rita fault in the context of newly available LiDAR data, the occurrence of the 2020 Magna earthquake, and a shift away from more traditional segmented fault models used in previous generations of source characterizations (Wong *et al.*, 2021c). This review consisted of a literature search and review, communication with experts on the Santa Rita fault, review of Google Earth satellite imagery, and processing and review of LiDAR-based high

resolution topography data along the Santa Rita fault downloaded from the USGS 3D Elevation Program website. LCI's updated seismic source model for Santa Rita fault includes two equally weighted epistemic alternatives in the rupture model. One branch represents a 40-km floating rupture (no segment boundaries) which is roughly equal to the length of the southern section of the fault. The other alternative utilizes a full-length rupture of the updated (59-km) source. Together with updates to epistemic source lengths, updated  $M_{\max}$  values were calculated using the Working Group on Utah Earthquake Probabilities (WGUEP, 2016) methodology to calculate magnitudes for faults with limited paleoseismic data. The updated  $M_{\max}$  values for the 40- and 59-km scenarios are  $7.0 \pm 0.3$  and  $7.2 \pm 0.3$ , respectively. In addition, given the equivocal arguments regarding the capability of low-angle normal faults to accommodate contemporary deformation, the dip distribution of the Santa Rita fault was updated to reflect a low-angle ( $20^\circ$ ) alternative. The updated dip distribution is  $20^\circ$  (0.2),  $35^\circ$  (0.2),  $50^\circ$  (0.4), and  $65^\circ$  (0.2), with a weighted mean of  $44^\circ$ , or  $5^\circ$  shallower than the  $49^\circ$  weighted mean of the Thomas *et al.* (2015) model.

#### 4.1.1.2 Southern California Faults

LCI's characterization of southern California faults was modified from a recent hazard analysis in the region (Wong *et al.*, 2017). The San Andreas, San Jacinto, and Cerro Prieto faults were included. These plate- boundary structures are all long, complex, and highly-active fault zones or systems that have been extensively studied. They are included in the PSHA because of their potential to generate very large (up to  $M$  8 or larger) and relatively frequent events compared to the local faults (Figure 4). The source characterization of these faults that follows was used by the USGS in the 2008 National Hazard Maps (Petersen *et al.*, 2008). This seismic source model is referred to as the Uniform California Earthquake Rupture Forecast, Version 2 (or UCERF2), which was developed by the Working Group on California Earthquake Probabilities and was documented by Wills *et al.* (2008) and Field *et al.* (2008). The UCERF2 model did not include the Cerro Prieto fault, but it was added here because it is a major transform structure south of the U.S.-Mexico border that appears to be accommodating significant slip comparable to the Imperial fault and is included in the UCERF3 model (Figure 4).

#### **Cerro Prieto Fault**

LCI's characterization of the Cerro Prieto fault is taken from Thomas *et al.* (2015). Although it is not included in either the USGS Quaternary Fault and Fold Database, or the California Geological Survey 2010 Fault Activity Map (<http://www.quake.ca.gov/gmaps/FAM/faultactivitymap.html>), the Cerro Prieto fault was included in Jennings' (1994) earlier Fault Activity Map of California and Adjacent Areas after original mapping by Gastil *et al.* (1975). It is now included in the UCERF3 model, which is the basis for the 2014 USGS National Seismic Hazard Maps. The Cerro Prieto fault is a northwest-striking dextral-slip transform fault that extends for over 115 km and is part of where the East Pacific Rise comes onshore (Figure 4). It extends from the Wagner Basin spreading center in the Gulf of California to at least the Cerro Prieto spreading center (and volcano and geothermal field), near Mexicali, Mexico. It is approximately 300 km west of the site. It has not been mapped or studied paleoseismically in any detail and the Southern California

Earthquake Data Center lists the slip rate as uncertain with the fault being “difficult to trace in alluvium of the Colorado River delta” (<http://www.data.scec.org/significant/cerroprieto.html>).

The Cerro Prieto fault does have linear trends of associated microseismicity that extend northwest of the fault as mapped by Jennings (1994), well beyond the Cerro Prieto volcano, prompting Magistrale (2002) to suggest the fault extends another 35 km to the northwest into southern California. Based on this, the model includes two scenarios for the northern end of the fault: Scenario A, at the Cerro Prieto Volcano (weighted 0.6); and, Scenario B, extending into southern California after the microseismicity trend defined by Magistrale (weighted 0.4).

There is suggestion that multiple large historical surface ruptures (about **M** 7.1) have occurred on the southern Cerro Prieto fault, including one in 1915 and 1934, but they are not as well-documented (Biehler *et al.*, 1964; Merriam, 1965; Allen *et al.*, 1965). Due to lack of other published information on previous ruptures and the large uncertainties on rupture behavior, the model assumes a floating rupture model for the Cerro Prieto fault with a preferred characteristic magnitude of **M** 7.1, but included a broad distribution (+0.5 and -0.3) due to the large uncertainties. The upper bound of **M** 7.6 allows the entire fault to rupture.

Rates are unknown for the Cerro Prieto fault. Several investigators have postulated that it is a principal plate-bounding structure, with slip from the San Jacinto fault being transferred to the Cerro Prieto fault via the Imperial fault (Magistrale, 2002; Suarez-Vidal *et al.*, 2007; T. Rockwell, San Diego State University, written communication, cited in Table B-1 of Field *et al.*, 2013). The Imperial fault has an estimated rate of 15 to 40 mm/yr, with paleoseismic trench data indicating 5 m of slip occurred between the 1940 and 1690 fault ruptures (Thomas and Rockwell, 1996). The UCERF3 model uses an input range of  $35 \pm 5$  mm/yr for the Cerro Prieto fault, which is geodetically based, whereas the modeled mean rates are lower, ranging from 11 to 15 mm/yr (Field *et al.*, 2013). Given the very large uncertainty, this study uses a broad slip rate distribution of: 15 mm/yr (weighted 0.25), 20 mm/yr (weighted 0.35), 35 mm/yr (weighted 0.25), 40 mm/yr (weighted 0.15).

### Southern San Andreas Fault Zone

The right-lateral strike-slip San Andreas fault zone is the most significant structure accommodating North American-Pacific plate motion, accounting for up to 70% of the relative plate motion along most of its length. The southern San Andreas fault zone includes the section of the fault south of the creeping segment in central California (Figure 4). This part of the fault has generated two large historical earthquakes, the 1857 **M** 7.8 to 8 Ft. Tejon earthquake that ruptured the Parkfield through Mojave South sections, and an **M** ~7.5 earthquake in 1812 that ruptured the North San Bernardino and Mojave South and possibly Mojave North sections. In addition, the northernmost Parkfield section has experienced numerous moderate earthquakes (**M** ~6) in the historical period, the most recent of which occurred in 2004.



The Working Group on California Earthquake Probabilities (WGCEP) (Field *et al.*, 2008) developed a new characterization of the San Andreas fault as part of UCERF2 that differs considerably from that of previous working groups (e.g., WGCEP, 1988; 1995; Cao *et al.*, 2003). A simplified version of their fault characterization and earthquake recurrence models was used to model the southern San Andreas fault. They include three alternative deformation models to describe how slip is distributed between the southern San Andreas and other faults in the area including the San Jacinto fault; LCI uses only their preferred model. UCERF3 was released in 2013 by Field *et al.* (2013) but LCI has not adopted this model because of issues regarding fault segmentation and multi-segment ruptures. LCI finds the earthquake scenarios in the model are not supported by paleoseismic data.

The San Andreas fault zone has the highest slip rate of any faults in California. On the Parkfield, Cholame, Carrizo and Big Bend sections, the average late Holocene slip rate is about 34 to 35 mm/yr, consistent with previous estimates (Sieh and Jahns, 1984; Sims, 1994). The slip rate decreases southward as more slip is transferred to other structures of the San Andreas fault system, especially the San Jacinto fault. As a consequence, the average slip rate on the southern sections of the fault decreases from about  $27 \pm 7$  mm/yr in the Mojave North section to about  $20 \pm 6$  mm/yr on the southernmost Coachella Valley section.

Field *et al.* (2008) used the recurrence interval data determined from paleoseismic studies and a method of assessing the probability that a specific rupture scenario is consistent with the paleoseismic record to determine a rupture recurrence rate for each of the ten sections. They used slip rates to moment balance the *a priori* recurrence rates to develop final moment-balanced rupture rates for all possible rupture scenarios. These rates have been adopted for use in the model in the analyses described in this report.

#### 4.1.2 Crustal Background Earthquakes

LCI's treatment of background seismicity in the PSHA was adopted from Wong *et al.* (2020). The following discusses that evaluation. In state-of-the-practice seismic hazard evaluations, the hazard from background earthquakes is addressed. Background earthquakes are those events that do not appear to be associated with known geologic structures. They occur on crustal faults that exhibit no surficial expression (buried faults) or are unmapped due to inadequate studies. In this source characterization, the hazard from background earthquakes was addressed through: (1) a gridded seismicity model, where locations of past seismicity appear to be likely locations of future seismicity (stationarity); and (2) the use of a regional seismic source zone for the SBR, where earthquakes are assumed to occur randomly (Figure 11). For both approaches, the background earthquakes are assumed to occur uniformly from 2 km to the bottom of the seismogenic crust. The maximum depths of the seismogenic crust follow the same distribution used for the crustal faults (Section 4.1.1).

Earthquake recurrence estimates in the site region are required in order to assess the hazard from background earthquakes. A declustered SBR background zone catalog was developed by

Thomas *et al.* (2015) and updated for this report (Section 3.2; Figure 11). The SBR zone, as defined in this report, incorporates seismicity from the SBR and the Transition Zone (as defined by Peirce [1984]), because the number of earthquakes in each of these two zones was deemed insufficient to independently determine earthquake recurrence parameters. The recurrence parameters for the SBR were developed using the historical seismicity record for the period of 1830 to 2020.

Completeness intervals are from Wong *et al.* (2020) and were developed from Stepp (1972) plots using the updated earthquake catalog. These plots were developed by calculating the average annual number of independently occurring events in each half-magnitude increment for the SBR catalog (Figure 12). Completeness estimates and number of earthquakes within each interval used in the recurrence calculations are listed in Table 1.

In the western U.S., the conventional approach has been to assume that the minimum threshold for surface faulting represents the upper size limit for background earthquakes. In the Basin and Range Province, this threshold ranges from **M** 6 to 6.75 (e.g., dePolo, 1994). It is believed that larger earthquakes will be accompanied by surface rupture, and repeated events of this size will produce recognizable fault-related geomorphic features. LCI adopted a maximum magnitude distribution of **M** 6.2 [0.101], **M** 6.35 [0.244], **M** 6.5 [0.310], **M** 6.65 [0.244], and **M** 6.8 [0.101] for the SBR. This distribution is consistent with previous site-specific PSHAs completed in central and southern Arizona where all known Quaternary faults within the region are modeled (e.g., Wong *et al.*, 2008; Thomas *et al.*, 2015; Wong *et al.*, 2020). Note that the USGS National Seismic Hazard Map distribution of maximum magnitude extends to larger magnitudes, but is designed in part to account for the fact that the USGS model only includes faults for which sufficient paleoseismic history has been established. LCI's range of background maximum magnitudes in the Basin and Range Province is similar to what is used in other areas of the western U.S. that possess a moderate to high level of heat flow and hence moderate to high crustal temperatures that constrain the thickness of the seismogenic crust to less than 15 to 20 km (e.g., Wong and Chapman, 1990).

LCI estimated recurrence for the background earthquakes for both the gridded seismicity and uniform source zone. In both cases, recurrence parameters (*b*-values and rates) were calculated using a modified version of the program ABSMOOTH (EPRI/DOE/NRC, 2012). For the gridded seismicity, the program divides the source zone into cells of a selected size (0.2-degree cells in this report) and calculates the *b*-value and rate in each cell using the likelihood function of the data in that cell along with penalty functions. These penalty functions smooth the cell-to-cell variation in the rate and/or the *b*-value, therefore optimizing these values. The program outputs both mean values and eight alternative sets ("realizations") of the recurrence parameters in order to characterize epistemic uncertainty in the rates and *b*-values (EPRI/DOE/NRC, 2012). The uniform source zone recurrence parameters were computed for the entire area as one cell.

Figure 13 shows the gridded seismicity results generated from ABSMOOTH for the SBR. Recurrence parameters for the uniform seismic source zone were adopted from the eight

realizations generated for the gridded seismicity, such that the total rates generated for each realization were assumed to apply uniformly across the SBR zone (Figure 5).

In general, earthquake recurrence for the SBR zone is not well constrained. There are too few earthquakes (163 independent events; Table 1) even at magnitudes less than **M** 4.0 and the historical record is short (< 200 years). Because of the limited seismographic coverage of the SBR, the recurrence is highly uncertain. To incorporate uncertainty into the hazard analysis, LCI implemented the eight realizations (which include eight *b*-values and rates) generated by ABSMOOTH, with equal weight applied to each realization (Figure 5). Table 2 provides the rates of events for **M** 5 and above for the corresponding *b*-values for use in the PSHA. Figure 14 shows the resulting recurrence curves for **M**  $\geq$  5.0 and the range of *b*-values compared to the historical seismicity. Although spanning a broad range, the eight realizations do not always envelope the historical seismicity; this is likely due to the paucity of events in the catalog and their large uncertainties.

An inspection of the resulting recurrence intervals for **M** 5 and 6 events was performed to check the reasonableness of the eight *b*-values and rates for the SBR (Figure 14). To do this, using the mean maximum magnitude and the mean of the eight realizations of the recurrence parameters, the resulting recurrence intervals were evaluated. The mean rate at **M** 5.0 was 0.0974, or a recurrence interval of 10 years, and the mean rate at **M** 6.0 was 0.0131, or a recurrence interval of 76 years. The average *b*-value of the eight realizations was 0.77.

The uniform and gridded seismic source zones were weighted equally at 0.5 and 0.5, respectively (Figure 5). Recent seismicity may be considered more likely representative of seismicity occurring in the next 100 years. However, given the short 190-year long and incomplete historical record the possibility exists that the catalog is not representative of the long-term record of seismicity and thus the two approaches were implemented with equal weight.

## 4.2 SITE CHARACTERIZATION

The near-surface geology in the area of the Project site is highly variable. The western portion of the site consists of relatively flat, low-lying hills comprised of alluvial surficial deposits and low desert vegetation. The eastern portion of the site is mountainous terrain of the Santa Rita Mountains and is comprised of a variety of rock types that vary greatly in age. One of the primary inputs required in the GMMs is  $V_{s30}$  (Section 4.3). Since the seismic hazard is defined at the top of competent rock,  $V_s$  of the of competent rock layer is required.  $V_s$  profiles obtained from previous seismic refraction and ReMi surveys along 15 survey lines near the site were provided by Wood. Figure 15 shows the 15  $V_s$  profiles used to calculate  $V_{s30}$ . In each profile,  $V_s$  indicative of competent rock was encountered at depths of 14 to 89 ft. Based on the 15  $V_s$  profiles, LCI calculated the best-estimate median  $V_{s30}$  of 1,372 m/sec with  $\pm 1$  sigma being 1,188 and 1,770 m/sec. So  $V_{s30}$  values of 1,200, 1,400, and 1,800 m/sec were considered to capture the variability in site conditions. Since  $V_{s30}$  1,800 m/sec is associated with hard rock site condition that results in lower hazard, only  $V_{s30}$  values of 1,200 and 1,400 m/sec were used in hazard calculations.

### 4.3 GROUND MOTION MODELS

To estimate the ground motions for crustal earthquakes in the PSHA and DSHA, GMMs appropriate for tectonically active crustal regions were used following the recommendations made by Wong *et al.* (2021b) based on ground motion characterization for tailings facilities in Colorado. These recommendations are also appropriate for the Project area. The crustal GMMs, developed as part of the NGA-West2 Project sponsored by PEER Center Lifelines Program, were used in this study. In addition, the GMM of Akkar *et al.* (2014) developed for Europe, which is based on datasets that contain more normal-faulting events was used.

The NGA-West2 GMMs were developed based on an expanded strong motion database compared to the initial NGA database. A number of more recent well-recorded earthquakes were added to the NGA-West2 database including the Wenchuan, China, event, numerous moderate magnitude California events down to  $M$  3.0, and several Japanese, New Zealand, and Italian earthquakes. Four of the NGA-West2 GMMs, Chiou and Youngs (2014), Campbell and Bozorgnia (2014), Abrahamson *et al.* (2014), and Boore *et al.* (2014) were used along with the Akkar *et al.* (2014) GMM in the PSHA and DSHA. The five models were weighted equally in the hazard analyses (Figure 5). The model of Idriss (2014) of NGA-West2 was not included due to its lack of applicability for distances greater than 150 km and its lack of a hanging wall model. The four NGA-West2 GMMs used all list distance applicability of 300 to 400 km. Sensitivity tests indicated these models are stable out to the distances of the major faults in Southern California, while the Idriss (2014) model does not extrapolate well to these large distances. The four NGA-West2 GMMs model the effects of larger ground motions on the hanging-wall side of a dipping fault using various distance metrics. The Akkar *et al.* (2014) GMM was found applicable to the Rosemont Project region with local faults showing dominantly normal slip.

As noted by Al Atik and Youngs (2014), the development of the NGA-West2 GMMs was a collaborative effort with many interactions and exchanges of ideas among the developers and the developers indicated that an additional epistemic uncertainty needs to be incorporated into the median ground motions in order to more fully represent an appropriate level of epistemic uncertainty. Hence, for each of the four NGA-West2 GMMs, an additional epistemic uncertainty on the median was included (Figure 5). The three-point distribution and model of Al Atik and Youngs (2014) was applied which weights the median GMMs 0.6 and  $\pm$  additional epistemic uncertainty of  $1.645 \cdot \sigma_{in}$  weighted 0.2 each. The model is a function of magnitude, style of faulting and spectral period. For the Akkar *et al.* (2014) GMM, the sigma model was found not applicable to large magnitudes, and was recommended to be replaced with the sigma model from Abrahamson *et al.* (2014) (Wong *et al.*, 2021b)

As noted above, a range of  $V_{s30}$  (1,200 and 1,400 m/sec) was used in the GMMs based on the site conditions (see Section 4.2). Other input parameters include  $Z_{2.5}$ , the depth to the  $V_s$  of 2.5 km/sec (a proxy for basin effects), which is only used in one model, Campbell and Bozorgnia (2014). In addition, Abrahamson *et al.* (2014), Boore *et al.* (2014) and Chiou and Youngs (2014) use  $Z_{1.0}$ , the depth to the  $V_s$  of 1.0 km/sec. Default values of  $Z_{1.0}$  and  $Z_{2.5}$  were estimated from equations from the developers based on  $V_{s30}$ . Other parameters such as depth to the top of



rupture (zero for all faults with surficial expressions unless specified otherwise), dip angle, rupture width and aspect ratio were specified for each fault or calculated within the PSHA code.

## 5.0 SEISMIC HAZARD RESULTS

The hazard results for ground motions are described below and shown in Figures 16 to 31.

### 5.1 PSHA RESULTS

The results of the PSHA are presented in terms of ground motion as a function of annual exceedance frequency (AEF). AEF is the reciprocal of the average return period. The results for a  $V_{s30}$  of 1,200 m/sec are presented. Results for  $V_{s30}$  of 1,400 m/sec are similar, but slightly lower. Figure 16 shows the mean, median (50<sup>th</sup> percentile), 5<sup>th</sup>, 15<sup>th</sup>, 85<sup>th</sup>, and 95<sup>th</sup> percentile hazard curves for peak horizontal ground acceleration (PGA). The range of uncertainty between the 5<sup>th</sup> and 95<sup>th</sup> percentile (fractiles) is about a factor of 3.7 at a return period of 10,000 years (Table 3). These fractiles indicate the range of epistemic uncertainty about the mean hazard. The 1.0 sec horizontal spectral acceleration (SA) hazard is shown on Figure 17. At the return periods of 475, 975, 2,475, 5,000, and 10,000 years, selected mean spectral values and their uncertainties are summarized in Table 3. The hazard can be characterized as low to moderate even at a long return period of 10,000 years.

The contributions of the various seismic sources to the mean PGA and 1.0 sec SA hazard are shown on Figures 18 to 21. For PGA, the contribution from the SBR background earthquakes dominates the hazard, while at longer return periods, the Santa Rita fault shows increasing level of contributions up to 40% at 100,000-year return period (Figures 18 and 19). At 1.0 sec SA, the background seismicity controls the hazard for return periods greater than 1,500 years. At shorter return periods, the relatively distant Cerro Prieta fault controls the hazard due to the absence of active local faults (Figures 20 and 21). At 1.0 sec SA, the distant Cerro Prieta and San Andreas faults also contribute to the long-period hazard at short return periods due to their high activity rates and potential large earthquakes (Figure 20). At the 10,000-year return period level, the hazard is 20% from the Santa Rita fault, 34% from background seismicity and 46% from the distant California and Mexico faults with the Cerro Prieta fault contributing about 20% (Figure 21).

The hazard can also be deaggregated in terms of the joint magnitude-distance-epsilon probability conditional on the ground motion parameter (PGA or SA exceeding a specific value). Epsilon is the difference between the logarithm of the ground motion amplitude and the mean logarithm of ground motion (for that  $M$  and  $R$ ) measured in units of standard deviation ( $\epsilon$ ). Thus, positive epsilons indicate larger than average ground motions. By deaggregating the PGA and 1.0 sec SA hazard by magnitude, distance and epsilon bins, we can illustrate the contributions by events at various periods. Figures 22 to 25 illustrate the contributions by events for return periods of 475, 2,475, 5,000 and 10,000 years. At PGA and all return periods, background earthquakes within 100 km of the Project site dominate the hazard (Figures 22 and 23). At 1.0 sec SA, in addition to moderate events ( $M$  6.5 to 7.5) on the Santa Rita fault as well as background earthquakes, the contributions from the more distant faults, Cerro Prieta and San Andreas, are shown in Figures 24 and 25.

Based on the magnitude and distance bins (Figures 22 to 25), the controlling earthquakes as defined by the mean magnitude ( $M\text{-bar}$ ) and modal magnitude ( $M^*$ ) and mean distance ( $D\text{-bar}$ ) and modal distance ( $D^*$ ) can be calculated. Table 4 lists the  $M\text{-bar}$ ,  $M^*$ ,  $D\text{-bar}$ , and  $D^*$  for the five return periods (475, 975, 2,475, 5,000, and 10,000 years) and for PGA and 1.0 sec horizontal SA.

In Figure 26, the UHS are shown for the two values of  $V_{s30}$  (1,200 and 1,400 m/sec) and return periods of 2,475 and 10,000 years. A UHS depicts the ground motions at all spectral periods with the same annual exceedance frequency or return period. The UHS at both  $V_{s30}$  are enveloped to account for spatial variability beneath the Project footprint. Figure 27 shows the UHS at all five return periods and they are tabulated in Table 5.

### 5.1.1 Hazard Sensitivities

In this section, sensitivities to the hazard due to the GMMs and major components of the seismic source model are examined. Sensitivities were performed for a  $V_{s30}$  of 1,200 m/sec, but the relative results are applicable to all site conditions.

Sensitivities of the hazard to the GMMs and the most significant portions of the seismic source model were performed. In these sensitivity analyses, the total mean hazard curves are conditioned on specific nodes in the logic tree having a full weight of 1.0. Figures 28 and 29 illustrate the sensitivity of the mean PGA and 1.0 sec horizontal SA hazard to the choice of GMMs. At the 10,000-year return period, there is a factor of approximately 2.5 difference between the models giving the largest and smallest ground motion. This is a typical value for current GMMs in tectonically active regions and is a significant source of uncertainty in the hazard. The Akkar *et al.* (2014) GMM developed using ground motion data recorded in Europe and the Middle East is similar to the NGA-West2 GMMs at PGA but gives higher hazard at 1.0 sec SA (Figures 28 and 29).

### 5.2 COMPARISON WITH NATIONAL SEISMIC HAZARD MAPS

In 1996, the USGS released a "landmark" set of National Hazard Maps for earthquake ground shaking, which was a significant improvement from their previous maps they had developed (Frankel *et al.*, 1996). These maps have been revised and updated, and the most current version was released in 2018 (Petersen *et al.*, 2019). These maps were the result of the most comprehensive analyses of seismic sources and ground motion prediction ever undertaken on a national scale and they made use of the five NGA-West2 relationships. The 2014 maps are the basis for the current International Building Code. The 2018 maps are for NEHRP site class B/C (firm rock, or  $V_{s30}$  760m/sec) and site class D (stiff soil, or  $V_{s30}$  260 m/sec).

For a 2,475-year return period, the 2018 USGS National Seismic Hazard Maps indicate a firm rock ( $V_{s30}$  760 m/sec) PGA and 1.0 sec SA of 0.11 and 0.064 g, respectively, for the Project area compared to the site-specific values of 0.088 and 0.067 g for a  $V_{s30}$  of 760 m/sec. The results are similar, particularly at 1.0 sec, given the differences in the seismic source model. Our lower hazard for PGA is due mainly to the difference in the treatment of the hazard from the background

seismicity. The USGS uses a minimum rate or floor for the region covered by the SBR based on uniform smoothing of seismicity. The region for which the background rates are computed is much larger and includes higher seismicity regions to the north. In addition, the USGS uses a higher maximum magnitude (**M** 7.45) and a large smoothing kernel (50 km) in their Gaussian smoothing approach.

### 5.3 DSHA RESULTS

The most significant seismic source to the Project area in a deterministic sense is the Santa Rita fault, the closest known active fault (Figure 3). The source-to-site distance (Rrup) is 4.9 km and the characteristic magnitude is **M** 7.2 based on our updated source characterization (Section 4). The same GMMs and  $V_{s30}$  used in the PSHA were used to calculate deterministic spectra. Figure 30 shows the median and 84<sup>th</sup> percentile 5%-damped horizontal acceleration response spectra and the individual spectra from each of the GMMs for the 84<sup>th</sup> percentile. Tables 6 and 7 provide the inputs and results of the DSHA, respectively.

Figure 31 shows comparisons of the horizontal deterministic spectra with UHS for a range of return periods. Both the 84<sup>th</sup> percentile and the median spectra are significantly higher than the UHS. This exceedance is due to the low slip rate of the Santa Rita fault and the very low activity rate of the background seismicity.



## 6.0 DESIGN EARTHQUAKE GROUND MOTIONS

Preliminary DE ground motions have been developed for the 10,000-year return period. CMS were developed at 10,000 years conditioned at 0.2, 0.5, and 1.0 sec SA for comparison with the UHS (Section 6.1).

### 6.1 CONDITIONAL MEAN SPECTRA

The UHS represents the spectral accelerations at each period based on the rates of occurrence of all nearby sources, the ground motion models, and the uncertainties in these models. It is generally a broader spectrum than is expected for any single event. As in the case of the controlling earthquake spectra approach, this uniform hazard can be represented by a suite of spectra that individually more closely represent the spectral shape of expected events contributing to the UHS. At a given period, a spectrum can be computed based on the deaggregated magnitude, distance and epsilon at that period. Depending on the epsilon required to match the spectrum to the UHS, the expected shape of this spectrum is not necessarily the median predicted spectral shape, i.e., the controlling earthquake spectrum. Given the epsilon at a target period, epsilon at all other periods can be determined using a correlation function. Thus, a CMS represents a more realistic shape of an event likely to cause the target spectral acceleration at the target period (Baker, 2011).

The CMS approach is described in Baker (2011) and is summarized here. The steps in the process are:

#### ***Step 1: Determine the Target $S_a$ at a Given Period, and the Associated $M$ , $R$ and $\epsilon$***

For a specified return period, determine the target  $S_a$  from the mean hazard curve for  $S_a$  for the fundamental period of the structure to be analyzed. This period is denoted  $T^*$ . For this ground motion, obtain the mean magnitude ( $M$ ), distance ( $R$ ), and  $\epsilon$  from the PSHA deaggregation results. Depending upon the response characteristics of the structure or structures to be analyzed, CMS should be developed for several values of  $T^*$ .

#### ***Step 2: Compute the Mean and Standard Deviation of the Response Spectrum, Given $M$ and $R$***

For the mean  $M$  and  $R$  determined in Step 1, compute the mean and standard deviation of logarithmic spectral acceleration at all periods for the mean magnitude and distance. These are provided by standard ground motion prediction models. The predicted mean and standard deviation, given magnitude, distance, period, etc., are denoted  $\overline{\ln S_a}(M, R, T)$  and  $\sigma_{\ln S_a}(T)$ , respectively. The mean and standard deviation of the log spectral acceleration can be computed using the GMMs that were used in the PSHA itself. Since multiple GMMs were used in the PSHA, a weighted estimate of the mean log  $S_a$  and the standard deviation can be used. For this project, CMS for each GMM were computed and combined using deaggregation weights. Deaggregation

weights are the fractional contribution of each GMM to the total hazard for a given period and hazard level, as described in Lin *et al.* (2013).

**Step 3: Compute  $\varepsilon$  at Other Periods, Given  $\varepsilon(T^*)$**

Compute the “conditional mean”  $\varepsilon$  at other periods. The conditional mean  $\varepsilon$  at  $\varepsilon(T^*)$  was determined in Step 1. The conditional mean at other periods,  $T_i$ , is determined by,

$$\mu_{\varepsilon(T_i)|\varepsilon(T^*)} = \rho(T_i, T^*)\varepsilon(T^*) \quad (8)$$

where  $\rho(T_i, T^*)$  is the correlation coefficient between  $\varepsilon$  for periods  $T_i$  and  $T^*$ . The correlation coefficients of Baker and Jayaram (2008), which are developed using the NGA West database and are applicable in the range 0.01 to 10 sec are used to compute the conditional mean  $\varepsilon$  at other periods.

**Step 4: Compute the Conditional Mean Spectrum**

The CMS is computed using the estimated log mean and standard deviation from Step 2 and the conditional mean  $\varepsilon(T_i)$  values determined in Step 3. The CMS is estimated according to:

$$\mu_{\ln S_a(T_i)|\ln S_a(T^*)} = \mu_{\ln S_a}(M, R, T_i) + \rho(T_i, T^*)\varepsilon(T^*)\sigma_{\ln S_a}(T_i) \quad (9)$$

The CMS is,

$$S_{a,CMS}(T) = \exp(\mu_{\ln S_a(T_i)|\ln S_a(T^*)}) \quad (10)$$

The standard deviation of  $\ln S_a(T_i)$  is

$$\sigma_{\ln S_a(T_i)|\ln S_a(T^*)} = \sigma_{\ln S_a(T_i)} \sqrt{1 - \rho^2(T_i, T^*)} \quad (11)$$

For this project, horizontal CMS were developed corresponding to the 10,000-year UHS as an alternative to using the UHS. Conditioning periods of 0.2, 0.5, and 1.0 sec were selected for the CMS. These periods span the possible range of fundamental periods of the mining facilities.

The horizontal CMS and the UHS for 10,000-year return period are shown in Figure 32 and listed in Table 8.

## 7.0 DEVELOPMENT OF TIME HISTORIES

Five horizontal-component time histories were developed with one for each of UHS for the five return periods (475, 975, 2,475, 5,000 and 10,000-year return periods) (Table 9; Figures 33 to 42). Because the response spectrum of a time history has peaks and valleys that deviate from the design response spectrum (target spectrum), it is necessary to modify the motion to improve its response spectrum compatibility. The procedure proposed by Lilhanand and Tseng (1988), as modified by Al Atik and Abrahamson (2010) and contained in their computer code RSPMatch09, was used to develop the acceleration time histories through spectral matching to the target (seed) spectrum. This time-domain procedure has been shown to be superior to previous frequency-domain approaches because the adjustments to the time history are only done at the time at which the spectral response occurs, resulting in only localized perturbations on both the time history and the spectra (Lilhanand and Tseng, 1988).

To match the target spectrum, seed time histories should be selected from events of similar magnitude, distance (for duration), to a lesser extent site condition, and most importantly, spectral shape as the earthquake dominating the spectrum. The site condition is a secondary criterion that may be used to favor some seeds over others if the main criteria are similar. The main goal of matching is to modify the seed to match its response spectrum to the target. For this purpose, seeds with spectral shapes closer to the target undergo less distortion to match the target. The seed time histories selected and their properties are listed in Table 9.

To ensure that the matched time histories have similar energy release time and damage potential as the seed time histories, the duration and Arias intensity of the ground motions before and after matching are calculated and compared. Duration and Arias intensity parameters are described below.

Arias intensity is a ground motion parameter defined by Arias (1970) as the integral of the square of acceleration over the duration of a time series record, as follows:

$$I_a = \frac{\pi}{2g} \int_0^{\infty} a(t)^2 dt \quad (9)$$

where  $I_a$  is Arias intensity,  $a(t)$  is acceleration, and  $g$  is the acceleration of gravity. Recent studies show that  $I_a$  correlates well with the damage potential of earthquakes (e.g., Travarasou *et al.*, 2003). The target  $I_a$  for the horizontal time histories at the 475-year return period level, computed using the models of Watson-Lamprey and Abrahamson (2006) and Abrahamson *et al.* (2016) for the target horizontal spectrum, is 0.007 m/sec, with a  $\pm$  one sigma range of 0.005 to 0.01 m/sec based on the mean magnitude and distance contributing to the 1.0 sec SA hazard (**M** 6.0 at 60 km). The deaggregated magnitude and distance at 0.5 sec SA and at distances less than 300 km was selected. At the 975-year return period level, the resulting target  $I_a$  is 0.016 m/sec, with a  $\pm$  one sigma range of 0.011 to 0.022 m/sec based on the deaggregated mean magnitude and distance of **M** 6.0 at 47 km. At the 2,475-year return period level, the resulting target  $I_a$  is 0.04 m/sec, with a  $\pm$  one sigma range of 0.03 to 0.06 m/sec based on the deaggregated mean

magnitude and distance of **M** 6.0 at 33 km. At the 5,000-year return period level, the resulting target  $I_a$  is 0.09 m/sec, with a  $\pm$  one sigma range of 0.06 to 0.13 m/sec based on the deaggregated mean magnitude and distance of **M** 6.1 at 25 km. At the 10,000-year return period level, the resulting target  $I_a$  is 0.18 m/sec, with a  $\pm$  one sigma range of 0.13 to 0.26 m/sec based on the deaggregated mean magnitude and distance of **M** 6.1 at 19 km. Note that these relationships provide targets for geometric mean  $I_a$ .

Duration of a strong ground motion is related to the time required for release of accumulated strain energy by rupture along the fault and generally increases with magnitude of the earthquake. Trifunac and Brady (1975) defined significant duration as the time interval between the points at which 5% and 95% of the total energy ( $I_a$ ) has been recorded. The target durations for the 475, 975, 2,475, 5,000, and 10,000-year time histories were calculated using the model of Silva *et al.* (1997) and Kempton and Stewart (2006). The target 5 to 95% duration for the 475-year return period time histories is 12.7 sec with a  $\pm$  one sigma range of 8.0 to 20.3 sec using the models of Silva *et al.* (1997) and Kempton and Stewart (2006). The calculated target 5 to 95% duration for the 975-year return period time histories is 10.8 sec with a  $\pm$  one sigma range of 6.8 to 17.2 sec. The target 5 to 95% durations are 8.7 sec ( $\pm$  one sigma range 5.5 – 13.9 sec), 8.5 sec ( $\pm$  one sigma range 5.3 – 13.6 sec), and 7.1 sec ( $\pm$  one sigma range 4.5 – 11.4 sec) for 2,475, 5,000, and 10,000-year return period time histories, respectively.

The spectral matches (up to 4 sec) and the resulting acceleration, velocity, and displacement time histories are shown in Figures 33 to 42. Also shown with the spectral matches are the response spectra calculated from the scaled seed time histories (Figures 33, 35, 37, 39, and 41). Acceleration, velocity, and displacement time histories were developed (Figures 34, 36, 38, 40, and 42). Husid plots at the bottom of each of these figures illustrate the increase in energy (normalized Arias intensity) with time.

Table 10 lists the properties of the matched time histories that include peak acceleration, velocity, and displacement, as well as Arias intensities and 5–95% durations. The Arias intensities and 5–95% durations of the spectrally-matched horizontal time histories generally lie within the  $\pm$  one sigma ranges of the target for each return period (Table 10).



## 8.0 REFERENCES CITED

- Abrahamson, N.A. and Silva, W.J., and Kamai, R., 2014, Summary of the ASK14 ground-motion relation for active crustal regions: *Earthquake Spectra*, v. 30, p. 1025-1055.
- Abrahamson, C., Hao-Jun, M.S. and Yang, B., 2016, Ground-motion prediction equations for arias intensity consistent with the NGA-West2 ground-motion Models: PEER Report No. 2016/05, Pacific Earthquake Engineering Research Center, University of California, Berkeley, 42 p.
- Aki, K., 1983, Seismological evidence in support of the existence of "Characteristic Earthquakes": *Earthquake Notes*, v. 54, p. 60-61.
- Akkar, S., Sandikkaya, M.A., and Bommer, J.J., 2014, Empirical ground-motion models for point- and extended-source crustal earthquake scenarios in Europe and the Middle East: *Bulletin of Earthquake Engineering*, v. 12, p. 359-388.
- Al Atik, L. and Abrahamson, N., 2010, An improved method for nonstationary spectral matching: *Earthquake Spectra*: v. 26, p. 601-617.
- Al Atik, L. and Youngs, R., 2014, Epistemic uncertainty for NGA-West2 models: *Earthquake Spectra*: v. 30, p. 1301-1318.
- Allen, C.R., St. Armand, P., Richter, C.F., and Nordquist, J.M., 1965, Relationship between seismicity and geologic structure in the southern California region: *Bulletin of the Seismological Society of America*, v. 55, p. 753-797.
- Anderson, J.G., 1979, Estimating the seismicity from geological structure for seismic risk studies: *Bulletin of the Seismological Society of America*, v. 69, p. 135-158.
- Arias, A., 1970, A measure of earthquake intensity: *Seismic Design for Nuclear Power Plants*, R.J. Hansen, ed., MIT Press, Cambridge, Massachusetts, pp.438-483.
- Baker, J.W., 2011, The conditional mean spectrum: A tool for ground motion selection," *American Society of Civil Engineers, Journal of Structural Engineering*, v. 137, p. 322-331.
- Baker, J. W., and Jayaram, N., 2008, Correlation of spectral acceleration values from NGA ground motion models, *Earthquake Spectra*, v. 24, p. 299-317.
- Bausch, D. and Brumbaugh, D.A., 1997, Relocation study of early Arizona earthquakes: Events of 1906, 1910, and 1912: unpublished report prepared for Arizona Division of Emergency Management, Earthquake Program, 65 p. + Appendices.
- Biehler, S., Kovach, R.L., and Allen, C., 1964, Geophysical framework of northern end of Gulf of California structural province, in *Marine Geology of the Gulf of California*, H. Tjeerd van Andel, and G.G. Shore (eds): *American Association of Petroleum Geologists Memoir 3*, p. 126-142.
- Boore, D.M., Stewart, J.P., Seyhan, E., Atkinson, G.M., 2014, NGA-West2 equations for predicting PGA, PGV, and 5%-damped PSA for shallow crustal earthquakes: *Earthquake Spectra*, v. 32, p. 979-1004.
- Brumbaugh, D. S., 1987, A tectonic boundary for the Southern Colorado Plateau: *Tectonophysics*, v. 136, p. 125-136.

- Campbell, K.W. and Bozorgnia, Y., 2014, NGA-West2 ground motion model for the average horizontal components of PGA, PGV, and 5%-damped linear acceleration response spectra: *Earthquake Spectra*, v. 30, p. 1087-1115.
- Cao, T.C., Bryant, W.A., Rowshandel, B., Branum, D., and Wills, C.J., 2003, The revised 2002 California probabilistic seismic hazard maps, June 2003: California Geological Survey website.
- Chiou, B-S.J. and Youngs, R.R., 2014, Update of the Chiou and Youngs NGA ground motion model for average horizontal component of peak ground motion and response spectra: *Earthquake Spectra*, v. 30, p. 1117-1153.
- Cornell, C.A., 1968, Engineering seismic risk analysis: *Bulletin of the Seismological Society of America*, v. 58, p. 1583-1606.
- dePolo, C.M., 1994, The maximum background earthquake for the Basin and Range Province, western North America: *Bulletin of the Seismological Society of America*, v. 84, p. 466-472.
- DuBois, S.M., Smith, A.W., Nye, N.K., and Nowak, T.A., 1982, Arizona earthquakes, 1776- 1980: Arizona Bureau of Geology and Mineral Technology Bulletin, v. 192, 456 p.
- EPRI/DOE/NRC, 2012, Technical Report: Central and Eastern United States Seismic Source Characterization for Nuclear Facilities. EPRI, Palo Alto, CA, U.S. DOE, and U.S. NRC: 2012.
- Field, E., Dawson, T., Ellsworth, W., Felzer, V., Frankel, A., Gupta, V., Jordan, T., Parsons, T., Petersen, M., Stein, R., Weldon, R., and Wills, C., 2008, The Uniform California Earthquake Rupture Forecast, Version 2 (UCERF 2): U.S. Geological Survey Open-File Report and California Geological Survey Special Report 203, 97 p.
- Field, E.H., Biasi, G.P., Bird, P., Dawson, T.E., Felzer, K.R., Jackson, D.D., Johnson, K.M., Jordan, T.H., Madden, C., Michael, A.J., Milner, K.R., Page, M.T., Parsons, T., Powers, P.M., Shaw, B.E., Thatcher, W.R., Weldon, R.J., II, and Zeng, Y., 2013, Uniform California Earthquake Rupture Forecast, Version 3 (UCERF3) – The Time-Independent Model: U.S. Geological Survey Open-File Report 2013-1165, California Geological Survey Special Report 228, and Southern California Earthquake Center Publication 1792.
- Frankel, A., Mueller, C., Barnhard, T., Perkins, D., Leyendecker, E.V., Dickman, N., Hanson, S., and Hopper, M., 1996, National Seismic Hazard Maps; documentation: U.S. Geological Survey Open-File Report 96-532, 110 p.
- Gastil, R.G., Phillips, R.P., and Allison, E.C., 1975, Reconnaissance geology of the State of Baja California: Geological Society of America Memoir 140, 170 p. Plate 1-A, scale 1:350,000 and Plate 3 (fault map of the State of Baja California).
- GeoPentech, 2015, Southwestern United States Ground Motion Characterization SSHAC Level 3 – Technical Report Rev. 2, March 2015.
- Hale, C., Abrahamson, N. and Bozorgnia, Y., 2018, Probabilistic seismic hazard analysis code verification: Pacific Earthquake Engineering Research Center, PEER Report 2018/03, 105 p.
- Hanks, T.C. and Kanamori, H. 1979, A moment magnitude scale: *Journal of Geophysical Research*, v. 84, p. 2348-2350.a

- Hecker, N., Abrahamson, A., and Wooddell, K.E., 2013, Variability of displacement at a point: implications for earthquake-size distribution and rupture hazard on faults: *Bulletin of the Seismological Society of America*, v. 103, p. 651-674.
- Idriss, I.M., 2014, An NGA-West2 empirical model estimating the horizontal spectral values generated by shallow crustal earthquakes: *Earthquake Spectra*, v. 30, p. 1155-1177.
- Jennings, C.W., 1994, Fault activity map of California and adjacent areas: California Division of Mines and Geology, California Geologic Data Map Series, Map No. 6. 1:750,000 scale.
- Keefer, D.I. and Bodily, S.E., 1983, Three-point approximations for continuous random variables: *Management Science*, v. 26, p. 595-609.
- Kempton, J.J, and Stewart, J.P., 2006, Prediction equations for significant duration of earthquake ground motions considering site and near-source effects: *Earthquake Spectra*, v. 22, p. 985 -1013.
- Lilhanand, K. and Tseng, W. S., 1988, Development and application of realistic earthquake time histories compatible with multiple-damping design spectra. 9th World Conference on Earthquake Engineering, Tokyo, Japan.
- Lin, T., Harmsen, S.C., Baker, J.W. and Luco, N., 2013. Conditional spectrum computation incorporating multiple causal earthquakes and ground-motion prediction models, *Bulletin of the Seismological Society of America*, v. 103, p.1103-1116.
- Lockridge, J.S., Fouch, M.J., and Arrowsmith, J.R., 2012, Seismicity within Arizona during the deployment of the EarthScope USArray Transportable Array: *Bulletin of the Seismological Society of America*, v. 102, p. 1850-1863.
- Lund, W.R., 2012, Basin and Range Province Earthquake Working Group II Recommendations to the U.S. Geological Survey National Seismic Hazard Mapping Program for the 2014 Update of the National Seismic Hazard Maps: Utah Geological Survey Open-File Report 591, 17 p.
- Mack, G.H., Seager, W.R., and Leeder, M.R., 2003, Synclinal-horst basins: examples from the southern Rio Grande rift and southern transition zone of southwestern New Mexico: *Basin Research*, v. 15, p. 365-377.
- Magistrale, H., 2002, The relation of the southern San Jacinto fault zone to the Imperial and Cerro Prieto faults in contributions to crustal evolution of the southwestern United States: *GSA Special Paper* 365, p. 271-278.
- McQuarrie, N., and Wernicke, B.P., 2005, An animated tectonic reconstruction of southwestern North America since 36 Ma: *Geosphere*, v. 1, p. 147–172.
- Menges, C.M. and McFadden, L.D., 1981, Evidence for the latest-Miocene to Pliocene transition from Basin-Range tectonic to post-tectonic landscape evolution in southeastern Arizona: *Arizona Geological Society Digest*, v. 13, p. 151-160.
- Menges, C.M. and Pearthree, P.A., 1989, Late Cenozoic tectonism in Arizona and its impact on regional landscape evolution: *in* *Geologic Evolution of Arizona*, Arizona Geological Society Digest No. 17, p. 649–680.

- Merriam, R., 1965, San Jacinto fault in northwestern Sonora, Mexico: Geological Society of America Bulletin, v. 76, p. 1051-1054.
- Molnar, P., 1979, Earthquake recurrence intervals and plate tectonics: Bulletin of the Seismological Society of America, v. 69, p. 115-133.
- Morgan, P., and Swanberg, C.A., 1985, on the Cenozoic uplift and tectonic stability of the Colorado Plateau: Journal of Geodynamics, v. 3, p. 39-63.
- Pang, G., Koper, K.D., Mesimeri, M., Pankow, K.L., Baker, B., Farrell, J., Holt, J., Hale, J.M., Roberson, P., Burlacu, R., Pechmann, J.C., Whidden, K., Holt, M., Allam, A., and DuRoss, C., 2020, Seismic analysis of the 2020 Magna, Utah, earthquake sequence: Evidence for a listric Wasatch fault: Geophysical Research Letters, v. 47, p. 1-10.
- Pearthree, P.A., 1998, Quaternary Fault Data and Map for Arizona: Arizona Geological Survey Open-File Report OFR-98-24, 122 p., with 1 plate, 1:750,000 scale.
- Pearthree, P.A., and Calvo, S.S., 1987, The Santa Rita fault zone--Evidence for large magnitude earthquakes with very long recurrence intervals, Basin and Range province of southeastern Arizona: Bulletin of the Seismological Society of America, v. 77, p. 97-116.
- Pearthree, P.A., Menges, C.M., and Mayer, L., 1983, Distribution, recurrence, and possible tectonic implications of late Quaternary faulting in Arizona: Arizona Bureau of Geologic Mineral Technical Open-File Report 83-20, 51 p.
- Peirce, H.W., 1984, The Mogollon escarpment: Arizona Bureau of Geology and Mineral Technology Fieldnotes, v. 4, p. 8-11.
- Petersen, M.D., Frankel, A.D., Harmsen, S.C., Mueller, C.S., Haller, K.M., Wheeler, R.L., Wesson, R.L., Zeng, Y., Boyd, O.S., Perkins, D.M., Luco, N., Field, E.H., Wills, C.J., and Rukstales, K.S., 2008, Documentation for the 2008 update of the United States National Seismic Hazard Maps: U.S. Geological Survey Open-File Report 2008-1128, 61 p.
- Petersen, M.D., Shumway, A.M., Powers, P.M., Mueller, C.S., Moschetti, M.P., Frankel, A.D., Rezaeian, S., McNamara, D.E., Luco, N., Boyd, O.S., Rukstales, K.S., Jaiswal, K.S., Thompson, E.M., Hoover, S.M., Clayton, B.S., Field, E.H., and Zeng, Y., 2019, 2018 Update of the U.S. National Seismic Hazard Model: Overview of Model and Implications, Earthquake Spectra, v. 36, p. 5-41.
- Piety, L.A. and Anderson, L.W., 1991, The Horseshoe fault--Evidence for prehistoric surface- rupturing earthquakes in central Arizona: Arizona Geology, v. 21, p. 1, 4-8.
- Sawires, R., Santoyo, M.A., Peláez, J.A. and Fernández, R.D.C., 2019, An updated and unified earthquake catalog from 1787 to 2018 for seismic hazard assessment studies in Mexico: Scientific Data, v. 6, p.1-14.
- Schwartz, D.P. and Coppersmith, K.J., 1984, Fault behavior and characteristic earthquakes-- examples from the Wasatch and San Andreas fault zones: Journal of Geophysical Research, v. 89, p. 5681-5698.
- Sieh, K.E. and Jahns, R.H., 1984, Holocene activity of the San Andreas fault at Wallace Creek, California: Geological Society of America Bulletin, v. 95, p. 883-896.



- Silva, W.J., Abrahamson, N., Toro, G., and Costantino, C, 1997, Description and Validation of the Stochastic Ground Motion Model: unpublished report prepared for Brookhaven National Laboratory by Pacific Engineering and Analysis.
- Sims, J.D., 1994, Stream channel offset and abandonment and a 200-year average recurrence interval of earthquakes on the San Andreas fault at Phelan Creek, Carrizo Plain, California, *in* Prentice, C.S., Schwartz, D.P., and Yeats, R.S. (eds.), *Proceedings of the workshop on paleoseismology*: U.S. Geological Survey Open-File Report 94-568, p. 170-172.
- Stepp, J.C., 1972, Analysis of completeness of the earthquake sample in the Puget Sound area and its effect on statistical estimates of earthquake hazard: *Proceedings of the International Conference on Microzonation*, v. 2, 897-910.
- Stirling, M., Rhoades, D., and Berryman, K., 2002, Comparison of earthquake scaling relations derived from data of the instrumental and preinstrumental era: *Bulletin of the Seismological Society of America*, v. 92, p. 812-830.
- Suarez-Vidal, F., Munguia-Orozco, L., Gonzalez-Escobar, M., Gonzakez-Garcia, J., and Glowaka, E., 2007, Surface rupture of the Morelia fault near the Cerro Prieto geothermal field, Mexicali, Baja California, Mexico, during the Mw 5.4 earthquake of 24 May 2006: *Seismological Research Letters*, v. 78, p. 394-399.
- Suter, M. and Contreras, J., 2002, Active tectonics of northeastern Sonora, Mexico (southern Basin and Range Province) and the 3 May 1887 Mw 7.4 earthquake: *Bulletin of the Seismological Society of America*, v. 92, p. 581-589.
- Thomas, A.P. and Rockwell, T.R., 1996, A 300- to 550-year history of slip on the Imperial fault near the U.S.-Mexico border-Missing slip at the Imperial fault bottleneck: *Journal of Geophysical Research*, v. 101, p. 5987-5997.
- Thomas, P., Wong, I., Zachariasen, J., Olig, S., and Terra, F., 2015, Updated site-specific probabilistic and deterministic seismic hazard analyses, Sierrita Tailings Dam, Green Valley, Arizona: unpublished report prepared for Freeport-McMoran Copper & Gold, Inc. by URS Corporation.
- Travasarou, T., Bray, J.D., and Abrahamson, N.A., 2003, Empirical attenuation relationship for Arias intensity: *Earthquake Engineering and Structural Dynamics*, v. 32, p. 1133-1155.
- Trifunac, M. D. and Brady, A.G., 1975, On the correlation of seismic intensity scales with the peaks of recorded strong ground motion: *Bulletin of the Seismological Society of America*, v. 65, p. 139-162.
- U.S. Geological Survey and Arizona Geological Survey (USGS and AZGS), 2019, Quaternary Fault and Fold Database for the United States, accessed 16 April 2019, from USGS website: <https://earthquake.usgs.gov/hazards/qfaults>.
- Watson-Lamprey, J. and Abrahamson, N., 2006, Selection of ground motion time series and limits on scaling: *Soil Dynamics and Earthquake Engineering*, v. 26, p. 477-482.
- Wells, D.L. and Coppersmith, K.J., 1994, New empirical relationships among magnitude, rupture length, rupture width, rupture area, and surface displacement: *Bulletin of the Seismological Society of America*, v. 84, p. 974-1002.

- Wesnousky, S.G., 1986, Earthquakes, Quaternary faults, and seismic hazard in California: *Journal Geophysical Research*, v. 91, p. 12,587-12,631.
- Wesnousky, S.G., 2008, Displacement and geometrical characteristics of earthquake surface ruptures-issues and implications for seismic-hazard analysis and the process of earthquake rupture; *Bulletin of the Seismological Society of America*, v. 98, p. 1609-1632.
- WGCEP (Working Group on California Earthquake Probabilities), 1988, Probabilities of large earthquakes occurring in California on the San Andreas fault: U.S. Geological Survey Open- File Report 88-398, 62 p.
- WGCEP (Working Group on California Earthquake Probabilities, 1995, Seismic hazards in southern California: probable earthquakes, 1994 to 2024: *Bulletin of the Seismological Society of America*, v. 95, p. 379-439.
- WGCEP (Working Group on California Earthquake Probabilities), 2008, The Uniform California Earthquake Rupture Forecast, Version 2 (UCERF2), U.S. Geological Survey Open-File Report 2007-1437.
- WGUEP (Working Group on Utah Earthquake Probabilities), 2016, Earthquake probabilities for the Wasatch Front region in Utah, Idaho, and Wyoming: *Utah Geological Survey Miscellaneous Publication 16-3*, 164 p., 5 appendices.
- Wills, C.J., Weldon, R.J. III, and Bryant, W.A., 2008, Appendix A: California fault parameters for the National Seismic Hazard Maps and Working Group on California Earthquake Probabilities 2007: USGS Open-File Report 2007-1437A; also published as CGS Special Report 203A and SCEC Contribution 1138A.
- Wong, I.G. and Chapman, D.S., 1990, Deep intraplate earthquakes in the western U.S. and their relationship to lithospheric temperatures: *Bulletin of the Seismological Society of America*, v. 80, p. 589-599.
- Wong, I., Gray, B., Zandieh, A., and Lewandowski, N., 2021b, Regional seismic source and ground motion characterization models for the Freeport-McMoran Colorado facilities: unpublished report prepared for Freeport-McMoran Inc. by Lettis Consultants International.
- Wong, I.G. and Humphrey, J.R., 1989, Contemporary seismicity, faulting, and the state of stress in the Colorado Plateau: *Geological Society of America Bulletin*, v. 101, p. 1127-1146.
- Wong, I., Nemser, E., Dober, M., Olig, S., Bott, J., and Terra, F., Darragh, R., and Silva, W., 2013, Site-specific seismic hazard analyses for the Resolution Mining Company tailings storage facilities options, Southern Arizona: unpublished report prepared for Resolution Copper Mining.
- Wong, I., Pezzopane, S., and Dober, M., 2008, Site-specific seismic hazard analyses for Miami Tailing Dams, Claypool, Arizona: unpublished report prepared for Freeport-McMoran Copper and Gold Miami Operations.
- Wong, I., Thomas, P., Hartleb, R., Lewandowski, N., 2020, Site-specific seismic hazard analyses and development of design ground motions for the Asarco LLC Hayden Complex, Hayden, Arizona: unpublished report prepared for Wood Environment & Infrastructure Solutions.
- Wong, I., Thomas, P., Lewandowski, N., Lindvall, S. and Seifried, A., 2017, Updated site-specific seismic hazard and development of time histories for the Resolution Copper's Near West site, Southern Arizona: unpublished report prepared for Resolution Copper.

Wong, I., Wu, Q., Gray, B., and Smith, S., 2021, Updated site-specific seismic hazard of the Sierrita tailings dam Green Valley, Arizona: unpublished report prepared for AECOM.

Wong, I., Wu, Q. and Pechmann, J., 2021a, The 18 March 2020 M 5.7 Magna, Utah earthquake: Strong motion data and implications for seismic hazard in Salt Lake Valley: Seismological Research Letters, v. 92, p. 273-286.

Wong, I., Wu, Q., Gray, B., Smith, S., and Darragh, B., 2021c, Updated site-specific seismic hazard of the Sierrita tailings dam, Green Valley, Arizona: unpublished report prepared for Freeport-McMoran Inc.

Youngs, R.R. and Coppersmith, K.J., 1985, Implications of fault slip rates and earthquake recurrence models to probabilistic seismic hazard estimates: Bulletin of the Seismological Society of America, v. 75, p. 939-964.

# Tables

**Table 1. Completeness Estimates and Number of Earthquakes in Each Magnitude Interval**

MAGNITUDE RANGE (M)	EQUIVALENT TIME OF COMPLETENESS (yr)	NUMBER OF EARTHQUAKES
3.0 – 3.5	39	46
> 3.5 – 4.0	60	60
> 4.0 – 4.5	80	20
> 4.5 – 5.0	80	24
> 5.0 – 5.5	140	11
> 5.5	140	2

**Table 2. Recurrence Parameters for the SBR Background Zone**

REALIZATION	b-VALUE	N (M ≥ 5)	WEIGHT
1	0.68	0.1223	0.125
2	0.89	0.0612	0.125
3	0.78	0.0968	0.125
4	0.76	0.1013	0.125
5	0.75	0.1029	0.125
6	0.70	0.1215	0.125
7	0.83	0.0698	0.125
8	0.80	0.0924	0.125



**Table 3. Summary of Probabilistic Ground Motions**

<b>RETURN PERIOD (YEARS)</b>	<b>PGA (G's) MEAN [5<sup>TH</sup>, 95<sup>TH</sup> PERCENTILE]</b>	<b>1.0 SEC SA (G's) MEAN [5<sup>TH</sup>, 95<sup>TH</sup> PERCENTILE]</b>
475	0.024 [0.013, 0.038]	0.022 [0.010, 0.042]
975	0.039 [0.020, 0.065]	0.032 [0.014, 0.056]
2,475	0.073 [0.034, 0.122]	0.048 [0.022, 0.079]
5,000	0.115 [0.050, 0.186]	0.065 [0.030, 0.102]
10,000	0.173 [0.073, 0.267]	0.087 [0.040, 0.131]

**Table 4. Magnitude and Distance Deaggregation**

DISTANCE (km)	PGA				1.0 SEC SA			
	M* <sup>1</sup>	D* <sup>1</sup>	M-BAR <sup>2</sup>	D-BAR <sup>2</sup>	M* <sup>1</sup>	D* <sup>1</sup>	M-BAR <sup>2</sup>	D-BAR <sup>2</sup>
475-Year Return Period								
All	5.1	30	-	-	7.3	330	-	-
< 300	-	-	5.8	52	-	-	6.1	62
> 300	-	-	-	-	-	-	7.4	416
975-Year Return Period								
All	5.1	10	-	-	7.3	330	-	-
< 300	-	-	5.8	38	-	-	6.2	50
> 300	-	-	-	-	-	-	7.4	422
2,475-Year Return Period								
All	5.1	10	-	-	7.3	330	-	-
< 300	-	-	5.8	25	-	-	6.2	36
> 300	-	-	-	-	-	-	7.5	429
5,000-Year Return Period								
All	5.5	10	-	-	8.1	490	-	-
< 300	-	-	5.9	19	-	-	6.3	28
> 300	-	-	-	-	-	-	7.6	433
10,000-Year Return Period								
All	5.5	10	-	-	6.1	10	-	-
< 300	-	-	6.0	15	-	-	6.4	22
> 300	-	-	-	-	-	-	7.6	437

<sup>1</sup> Modal magnitude and distance are based on full hazard results for all magnitudes and distances.

<sup>2</sup> Mean magnitudes and distances are computed for 1.0 sec SA hazard from events at distances less than and greater than 300 km due to the bimodal nature of the hazard. Hazard from events at less than 300 km are from background seismicity and local faults. Hazard from events greater than 300 km are from faults in Southern California and Northern Mexico.

**Table 5. Mean UHS, Enveloped Vs30**

PERIOD (SEC)	SPECTRAL ACCELERATION (g)				
	475-YEAR RETURN PERIOD	975-YEAR RETURN PERIOD	2,475-YEAR RETURN PERIOD	5,000-YEAR RETURN PERIOD	10,000-YEAR RETURN PERIOD
0.01 (PGA)	0.024	0.039	0.073	0.115	0.173
0.02	0.024	0.040	0.076	0.119	0.179
0.03	0.027	0.045	0.086	0.136	0.206
0.05	0.034	0.059	0.116	0.185	0.283
0.075	0.042	0.075	0.149	0.240	0.367
0.1	0.046	0.082	0.163	0.262	0.400
0.15	0.048	0.083	0.163	0.260	0.396
0.2	0.045	0.075	0.144	0.228	0.346
0.3	0.038	0.059	0.107	0.166	0.250
0.4	0.034	0.051	0.085	0.127	0.189
0.5	0.031	0.045	0.073	0.105	0.153
0.75	0.027	0.038	0.057	0.078	0.107
1	0.022	0.032	0.048	0.065	0.087
1.5	0.018	0.025	0.038	0.050	0.066
2	0.014	0.020	0.031	0.041	0.054
3	0.009	0.013	0.020	0.026	0.034
4	0.008	0.011	0.016	0.022	0.028
5	0.004	0.006	0.009	0.011	0.015
7.5	0.003	0.005	0.007	0.009	0.012
10	0.002	0.004	0.006	0.008	0.010

**Table 6. Inputs for DSHA**

INPUT PARAMETER	INPUT PARAMETER DEFINITION	SANTA RITA FAULT
<b><math>M</math></b>	Moment magnitude	7.2
<b><math>R_{RUP}</math></b>	Closest distance to coseismic rupture (km)	4.9
<b><math>R_{JB}</math></b>	Closest distance to surface projection of coseismic rupture (km)	4.9
<b><math>R_X</math></b>	Horizontal distance from top of rupture measured perpendicular to fault strike (km)	-4.9
<b><math>R_{y0}</math></b>	The horizontal distance off the end of the rupture measured parallel to strike (km)	0
<b><math>U</math></b>	Unspecified-mechanism factor: 1 for unspecified; 0 otherwise	0
<b><math>F_{RV}</math></b>	Reverse-faulting factor: 0 for strike slip, normal, normal-oblique; 1 for reverse, reverse-oblique and thrust	0
<b><math>F_N</math></b>	Normal-faulting factor: 0 for strike slip, reverse, reverse-oblique, thrust and normal-oblique; 1 for normal	1
<b><math>F_{HW}</math></b>	Hanging-wall factor: 1 for site on down-dip side of top of rupture; 0 otherwise	0
<b><math>Z_{TOR}</math></b>	Depth to top of coseismic rupture (km)	0.0
<b><math>Dip</math></b>	Average dip of rupture plane (degrees)	45
<b><math>V_{S30}</math></b>	The average shear-wave velocity (m/s) over a subsurface depth of 30 m	1,200; 1,400
<b><math>F_{Measured}</math></b>		1
<b><math>Z_{HYP}</math></b>	Hypocentral depth from the earthquake	10.2
<b><math>Z_{1.0}</math></b>	Depth to $V_s=1$ km/sec	Default
<b><math>Z_{2.5}</math></b>	Depth to $V_s=2.5$ km/sec	Default
<b><math>W</math></b>	Fault rupture width (km)	15
<b><math>Region</math></b>	Specific Regions considered in the models	Global

---

**Table 7. Median and 84th Percentile Deterministic Response Spectra**

	<b>M 7.2 SANTA RITA FAULT</b>	
<b>PERIOD (SEC)</b>	<b>MEDIAN (g)</b>	<b>84<sup>TH</sup> PERCENTILE (g)</b>
0.01	0.309	0.561
0.02	0.321	0.583
0.03	0.363	0.661
0.05	0.479	0.880
0.075	0.605	1.139
0.1	0.664	1.275
0.15	0.694	1.339
0.2	0.637	1.212
0.3	0.498	0.936
0.4	0.402	0.756
0.5	0.335	0.635
0.75	0.224	0.430
1	0.163	0.320
1.5	0.107	0.213
2	0.080	0.160
3	0.053	0.105
4	0.038	0.077
5	0.031	0.061
7.5	0.015	0.031
10	0.010	0.019



---

**Table 8. CMS Conditioned at 0.2, 0.5, and 1.0 Sec for 10,000-Year Return Period**

PERIOD (SEC)	CMS (g)		
	T = 0.2 SEC	T = 0.5 SEC	T = 1.0 SEC
0.01	0.148	0.119	0.113
0.02	0.152	0.122	0.116
0.03	0.172	0.137	0.126
0.05	0.226	0.176	0.155
0.075	0.287	0.215	0.185
0.1	0.315	0.231	0.195
0.15	0.354	0.258	0.221
0.2	0.346	0.252	0.218
0.3	0.230	0.212	0.191
0.4	0.164	0.178	0.168
0.5	0.125	0.153	0.149
0.75	0.070	0.087	0.107
1	0.044	0.055	0.087
1.5	0.023	0.030	0.056
2	0.015	0.019	0.038
3	0.008	0.010	0.019
4	0.005	0.006	0.013
5	0.003	0.004	0.007
7.5	0.001	0.002	0.003
10	0.001	0.001	0.002

Table 9. Properties of Seed Time Histories

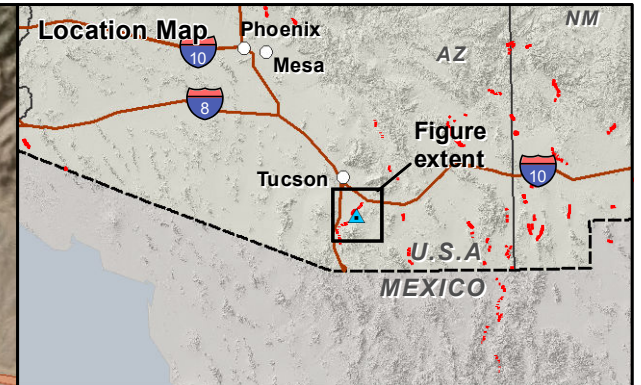
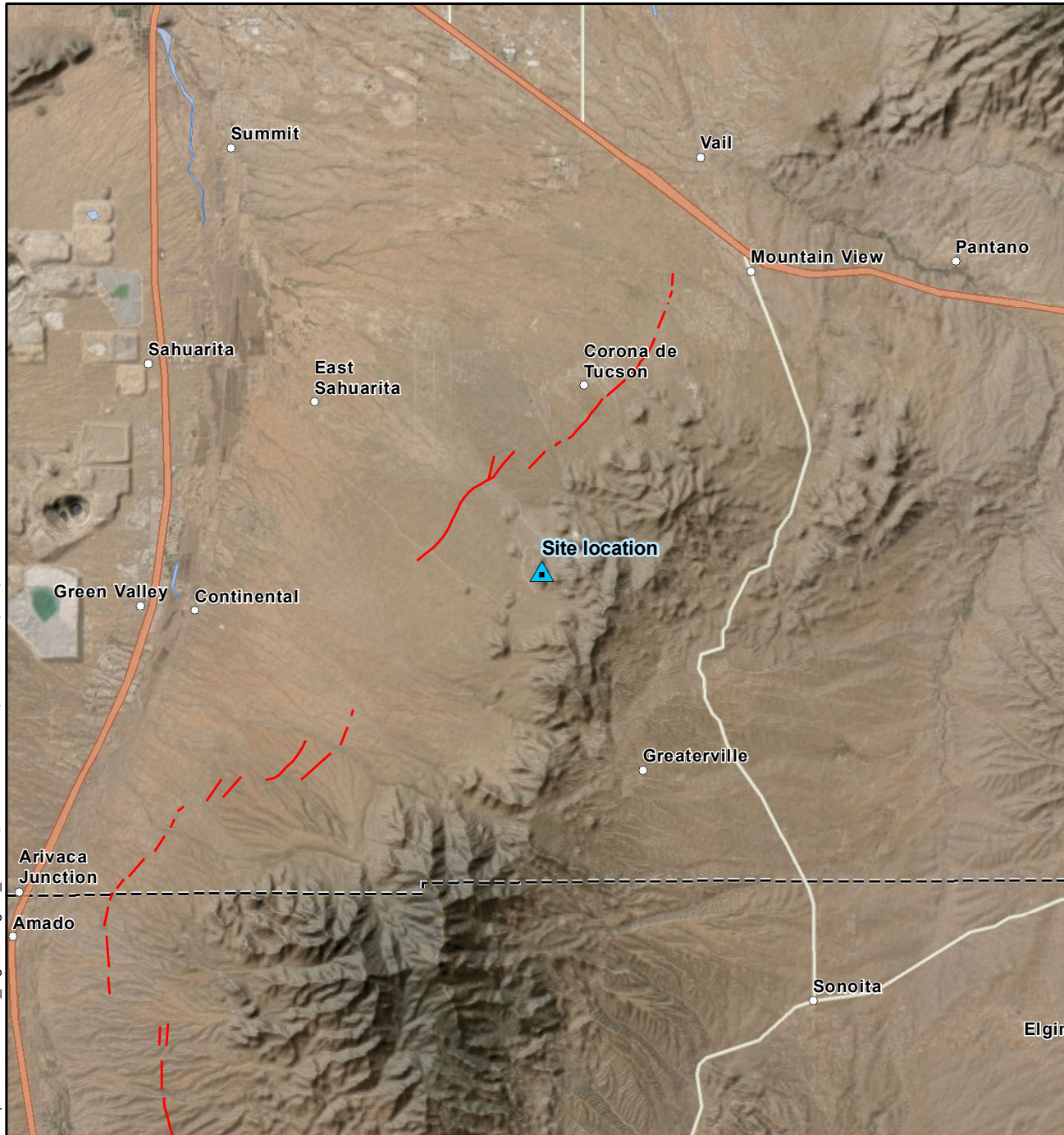
RSN	YEAR	Earthquake Name	Station Name	Mag	C1stD (km)	Vs30 (m/s)	PGA (g)	PGV (cm/sec)	PGD (cm)	AI (m/sec)	5-95% Duration (sec)	Scale Factor
<b>475-Year Return Period UHS</b>												
295	1980	Irpinia, Italy-02	Auletta	6.2	29.9	477	0.03	3.05	1.72	0.01	17.79	0.89
<b>975-Year Return Period UHS</b>												
2654	1999	Chi-Chi, Taiwan-03	TCU120	6.2	23.9	459	0.10	14.65	9.43	0.12	13.43	0.32
<b>2,475-Year Return Period UHS</b>												
4478	2009	L'Aquila, Italy	Lab.Gran Sasso	6.3	11.2	547	0.03	3.39	2.90	0.01	9.28	2.21
<b>5,000-Year Return Period UHS</b>												
4016	2003	San Simeon, CA	San Luis Obispo	6.5	31.4	494	0.16	13.39	9.53	0.21	10.72	0.68
<b>10,000-Year Return Period UHS</b>												
183	1979	Imperial Valley-06	El Centro Array #8	3.9	206	672	0.61	54.60	42.74	1.65	6.82	0.26

Table 10. Properties of Spectrally-Matched Time Histories



RSN	YEAR	Earthquake Name	Station Name	Mag	C1stD (km)	Vs30 (m/s)	PGA (g)	PGV (cm/sec)	PGD (cm)	AI (m/sec)	5-95% Duration (sec)
<b>475-Year Return Period UHS</b>											
295	1980	Irpinia, Italy-02	Auletta	6.2	29.9	477	0.02	2.24	1.60	0.01	21.50
<b>975-Year Return Period UHS</b>											
2654	1999	Chi-Chi, Taiwan-03	TCU120	6.2	23.9	459	0.03	2.99	2.27	0.01	14.28
<b>2,475-Year Return Period UHS</b>											
4478	2009	L'Aquila, Italy	Lab.Gran Sasso	6.3	11.2	547	0.07	6.59	6.34	0.04	10.29
<b>5,000-Year Return Period UHS</b>											
4016	2003	San Simeon, CA	San Luis Obispo	6.5	31.4	494	0.11	10.03	6.40	0.09	10.59
<b>10,000-Year Return Period UHS</b>											
183	1979	Imperial Valley-06	El Centro Array #8	3.9	206	672	0.17	13.30	11.71	0.13	6.75

# Figures

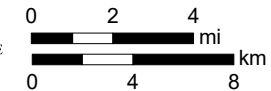
File path: S:\2138\00\_Figures\Figure\_01.mxd; Date: 11/09/2021; User: Javier, LCI; Rev.1



#### EXPLANATION

-  Site location
-  USGS fault; solid where certain, dashed where approximate, dotted where concealed (USGS, 2010)

Source:  
Aerial imagery from ESRI



Map projection and scale: NAD 1983 UTM Zone 12N, 1:300,000

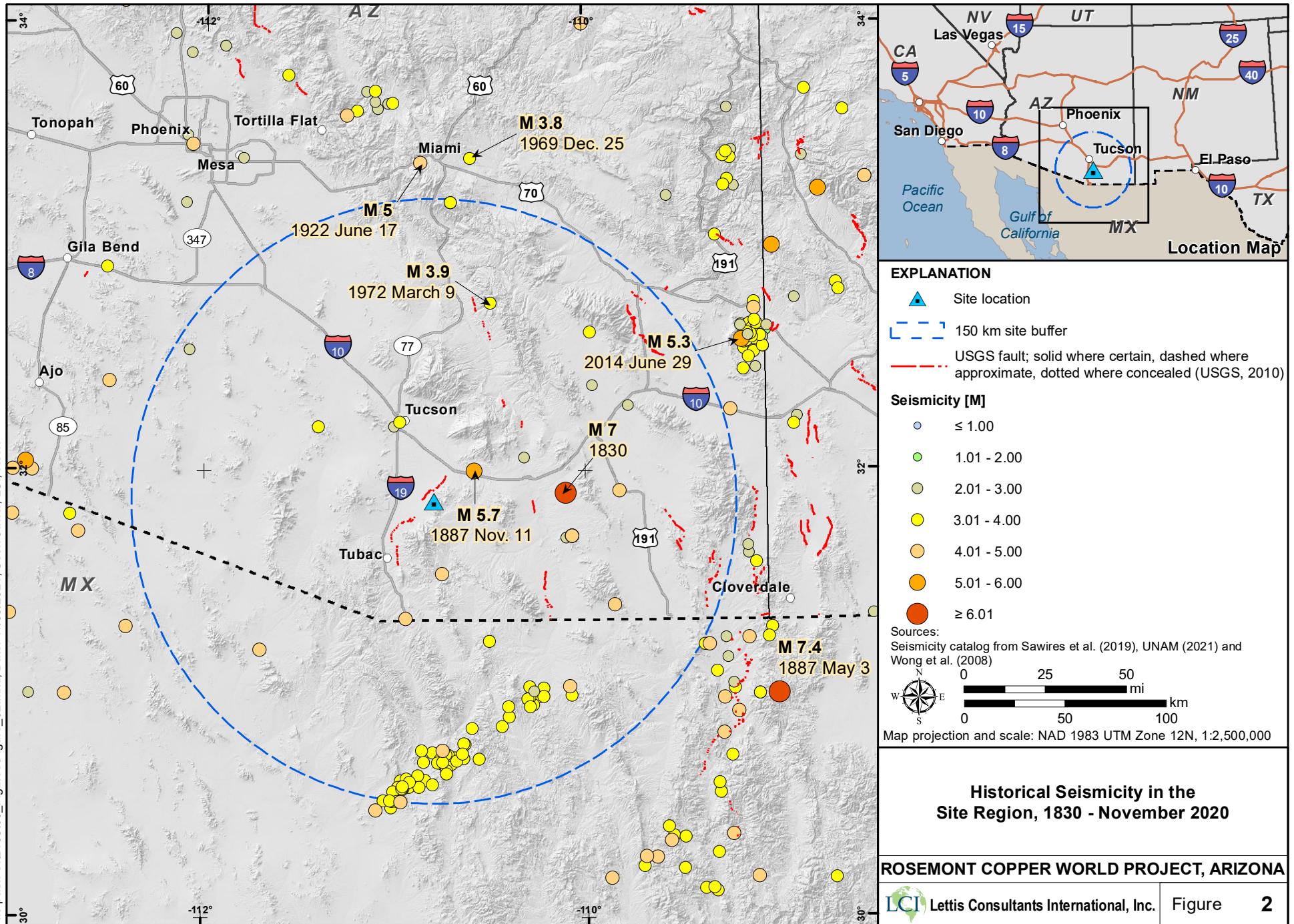
#### Site Location Map

#### ROSEMONT COPPER WORLD PROJECT, ARIZONA

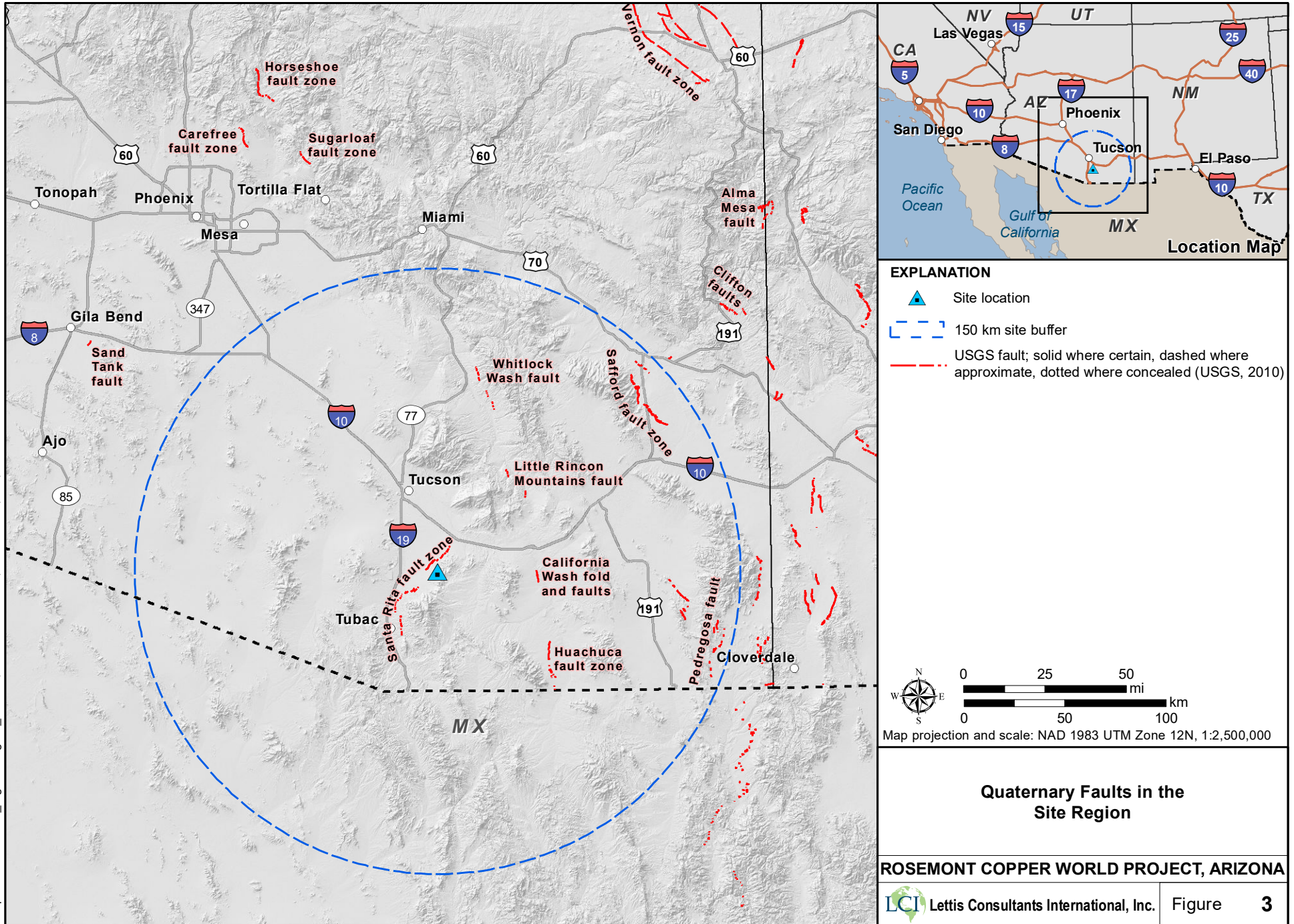
 Lettis Consultants International, Inc.

Figure **1**

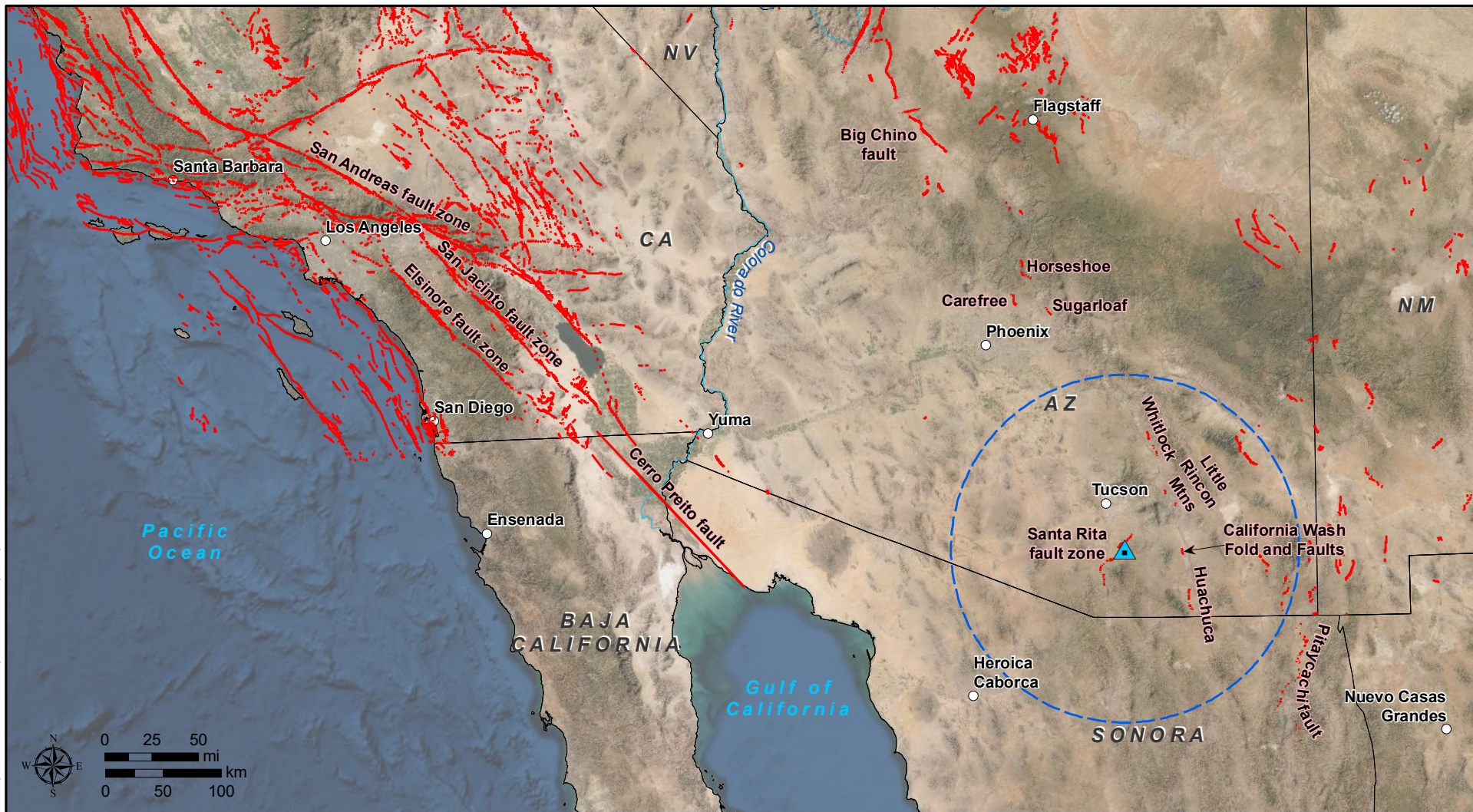












#### EXPLANATION

- Site location
- 150 km site buffer
- USGS fault; solid where certain, dashed where approximate, dotted where concealed (USGS, 2010)

Note:  
 - USGS fault data does not extend south of the US border  
 Sources:  
 - Cerro Prieto trace from UCER3 (Field et al., 2013)  
 - Aerial imagery from ESRI

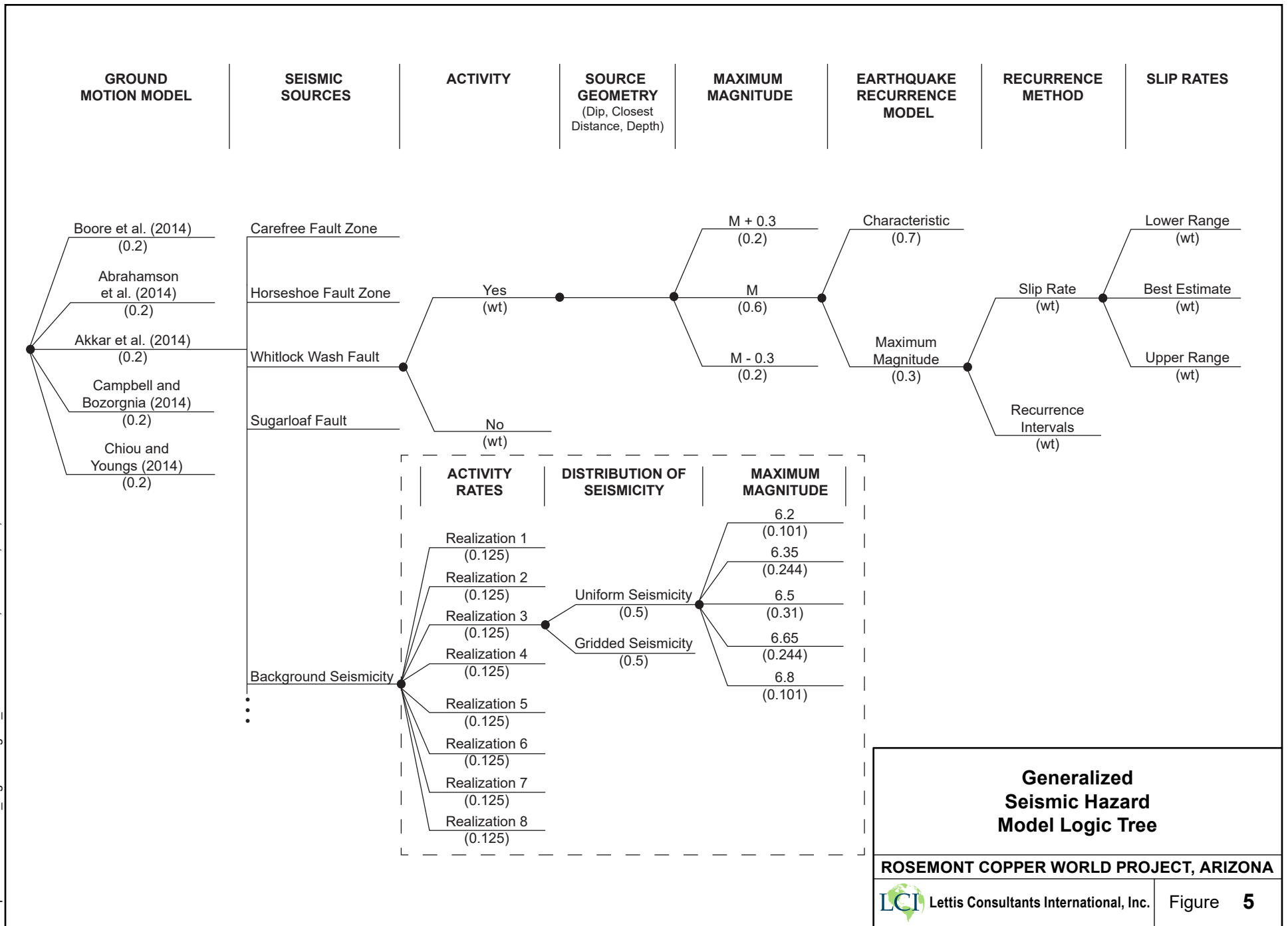
Map projection and scale: NAD 1983 UTM Zone 12N, 1:5,000,000

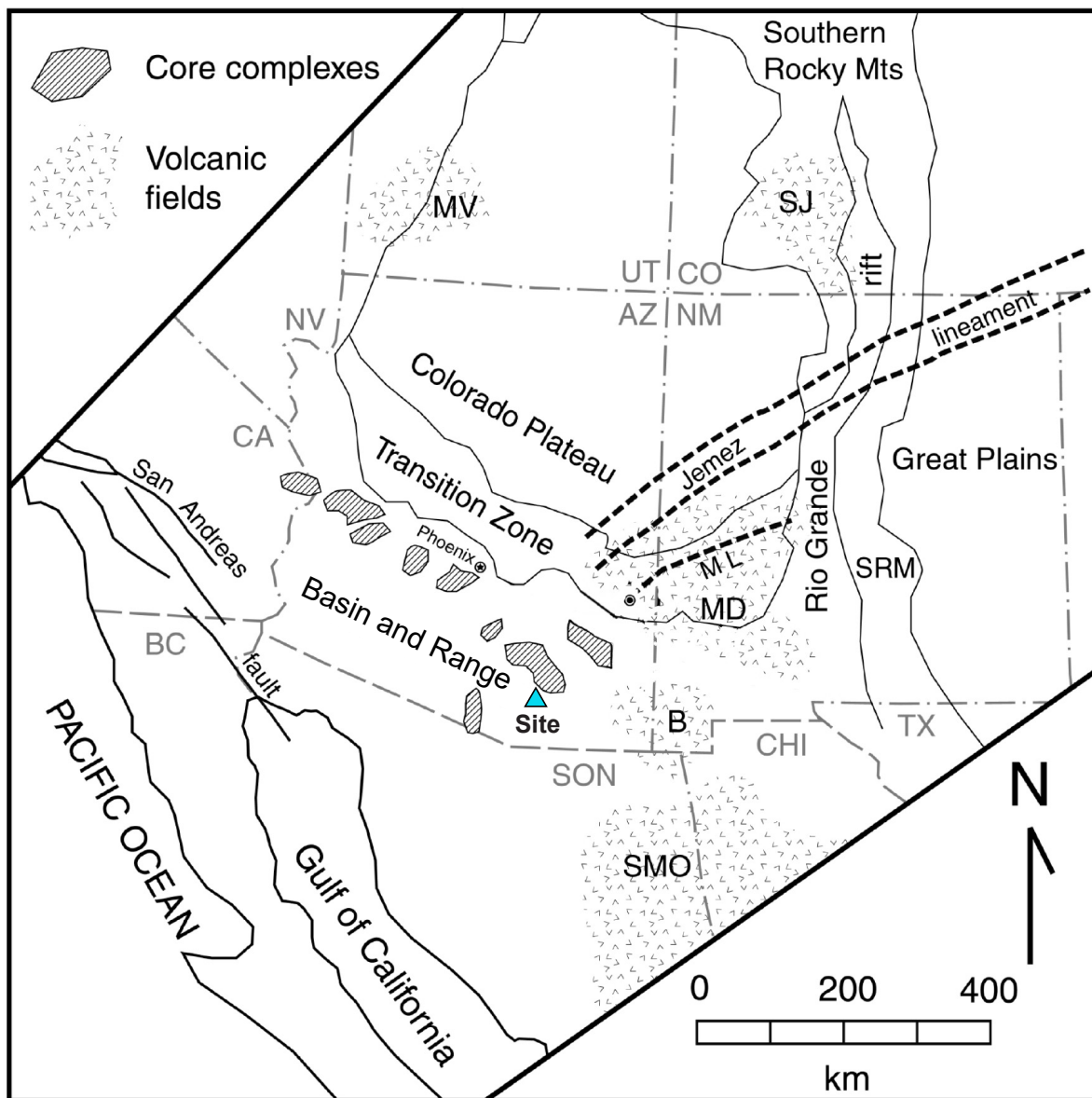
#### Regional Quaternary Faults

#### ROSEMONT COPPER WORLD PROJECT, ARIZONA

Lettis Consultants International, Inc.

Figure **4**





#### EXPLANATION

- ▲ Site location

Source: Figure modified from Drewes et al. (1985) and Wong et al. (2013)

#### Seismotectonic Setting

##### ROSEMONT COPPER WORLD PROJECT, ARIZONA

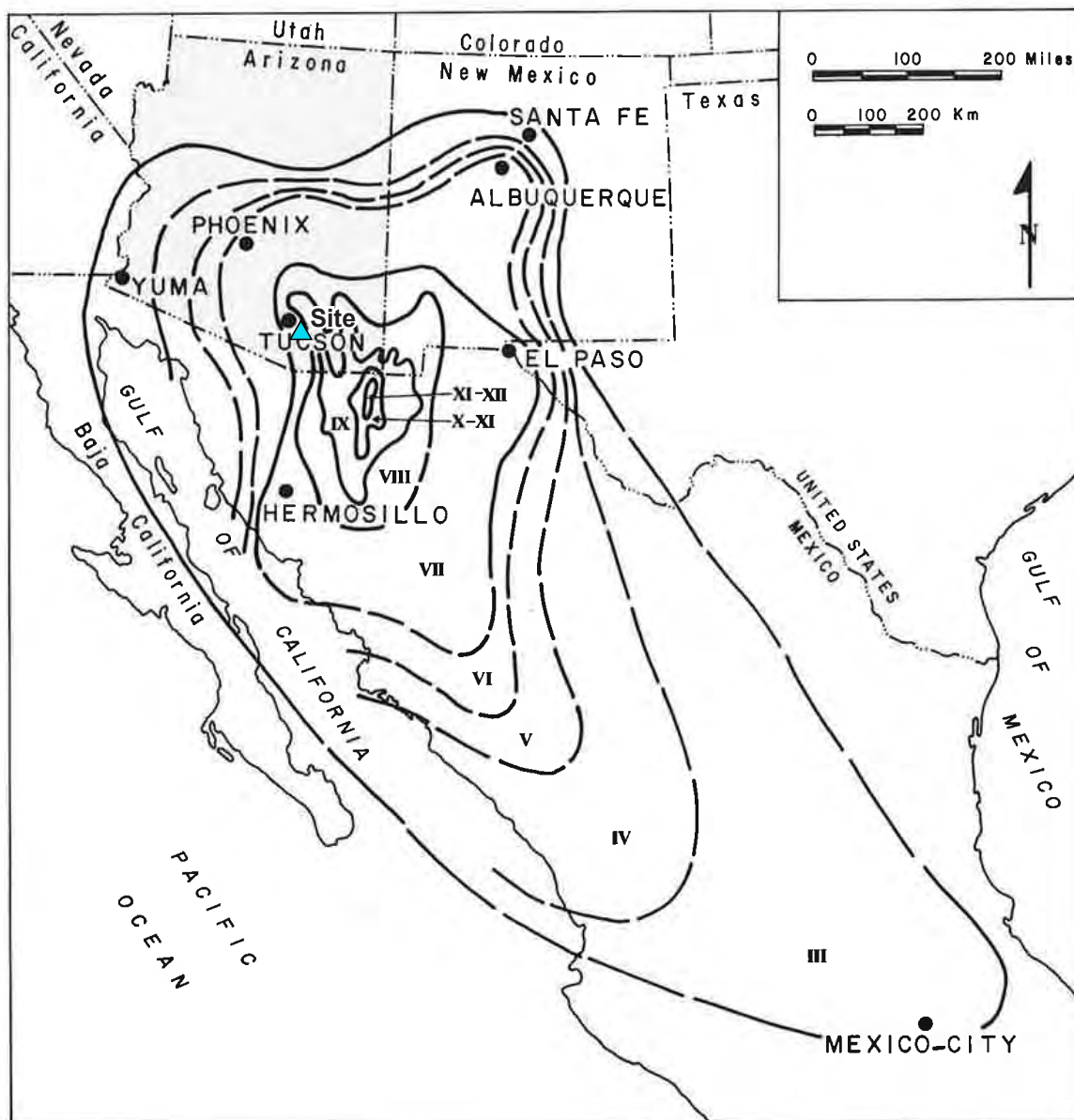


Lettis Consultants International, Inc.

Figure

6





#### EXPLANATION

▲ Site location

#### Isoseismal Map of 3 May 1887 M 7.4 Sonora, Mexico Earthquake

ROSEMONT COPPER WORLD PROJECT, ARIZONA

Source: Figure modified from DuBois et al. (1982)

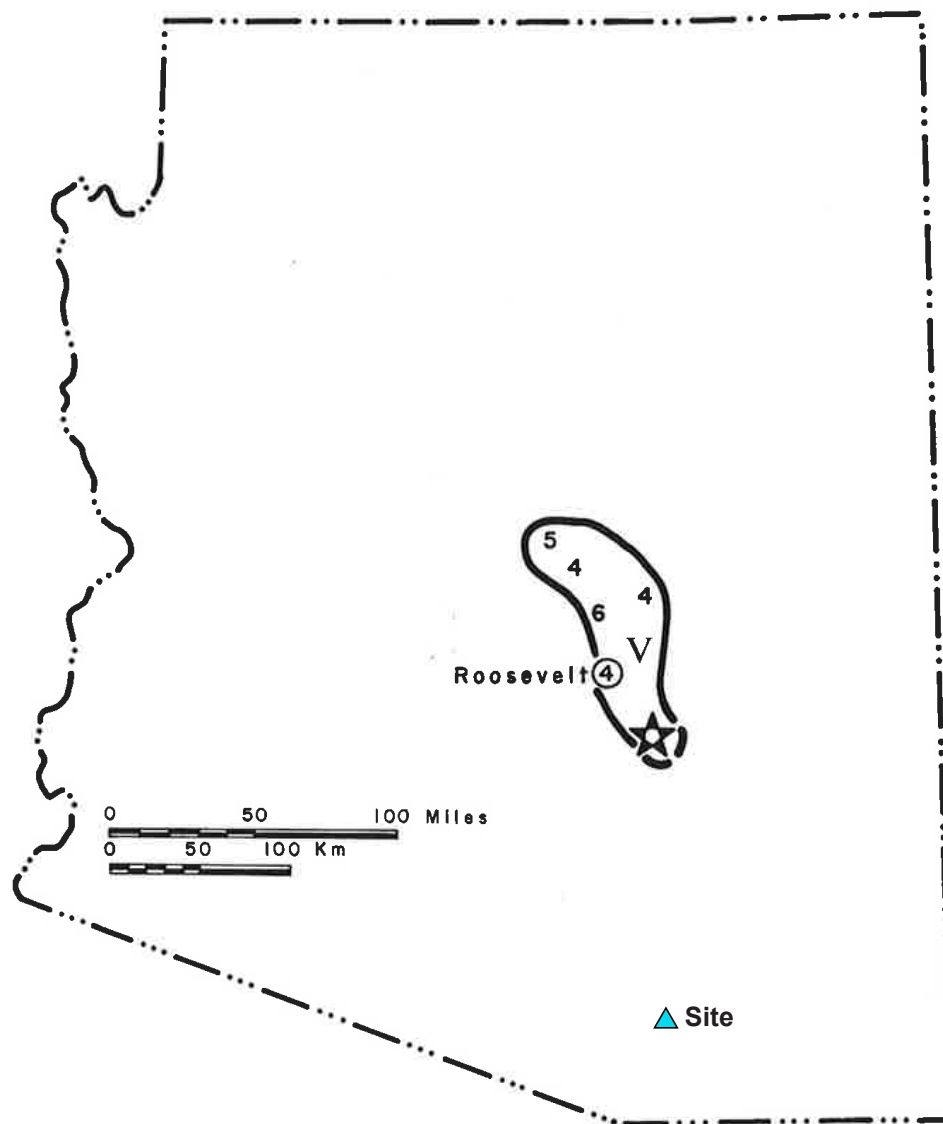


Lettis Consultants International, Inc.

Figure

7

File path:S:\2138\00\_Figures\Figure\_08.ai: 10/14/2021; User: JCh, LCI.



#### EXPLANATION

▲ Site location

Source: Figure modified from DuBois et al. (1982)

#### Isoseismal Map of the 17 June 1922 Miami, Arizona, Earthquake

ROSEMONT COPPER WORLD PROJECT, ARIZONA



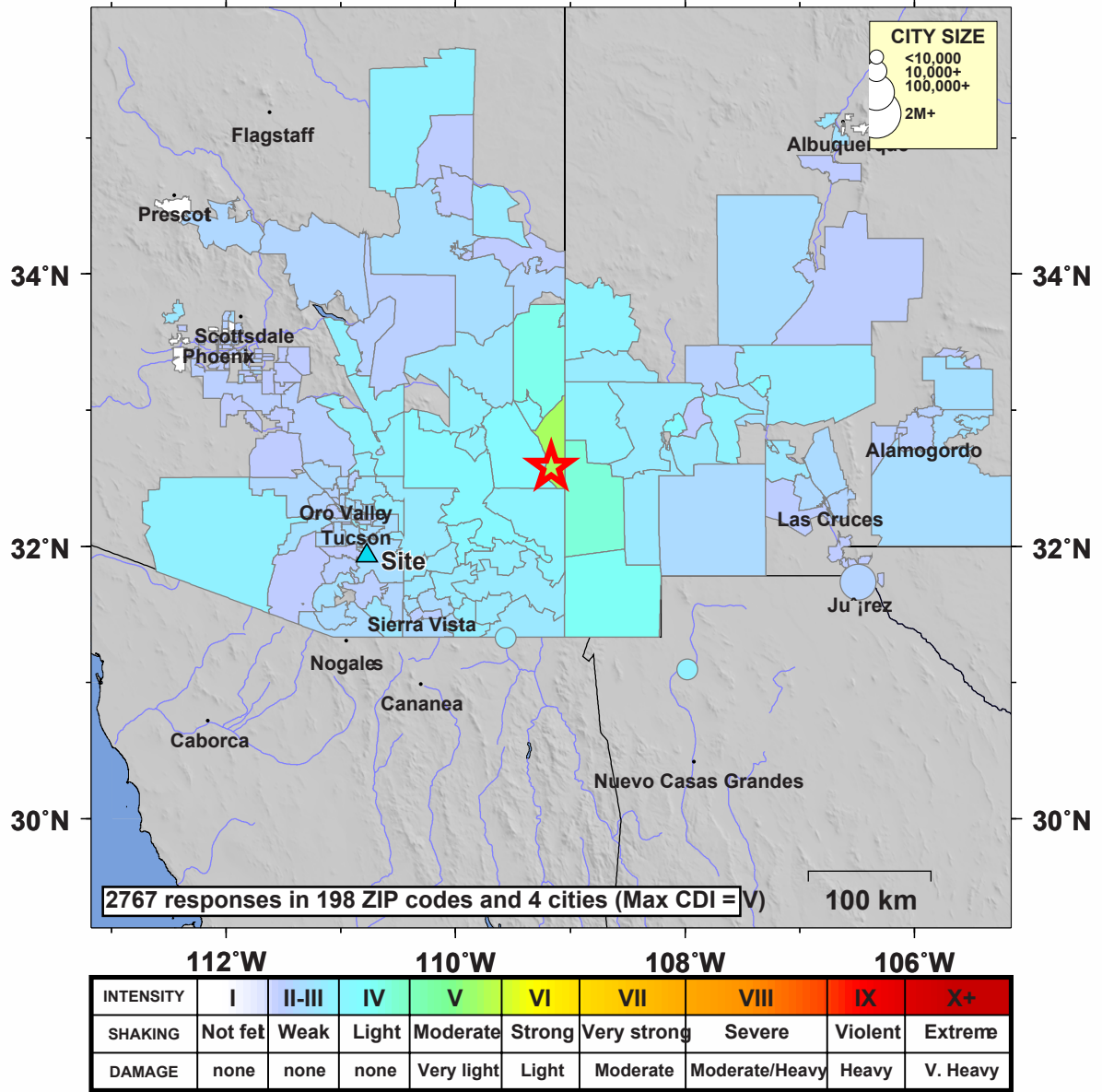
Lettis Consultants International, Inc.

Figure

8

# USGS Community Internet Intensity Map ARIZONA

Jun 28 2014 09:59:35 PM local 32.5822N 109.1682W M5.3 Depth: 6 km ID:usc000rnfe



## EXPLANATION

- Site location
- Earthquake epicenter

**Did You Feel It Map for the 28 June 2014  
M 5.2 Southeastern Arizona  
Earthquake**

**ROSEMONT COPPER WORLD PROJECT, ARIZONA**



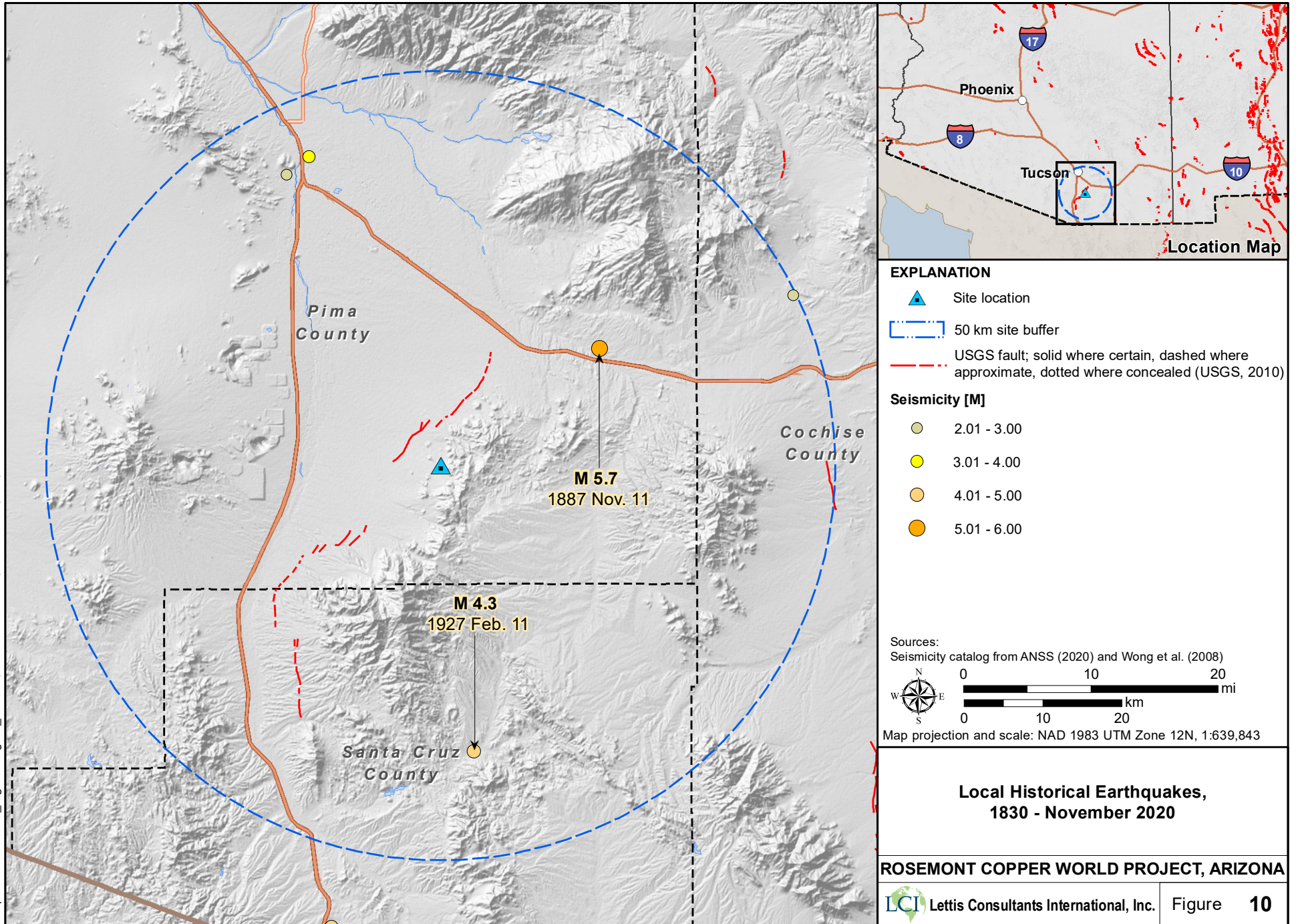
Lettis Consultants International, Inc.

Figure

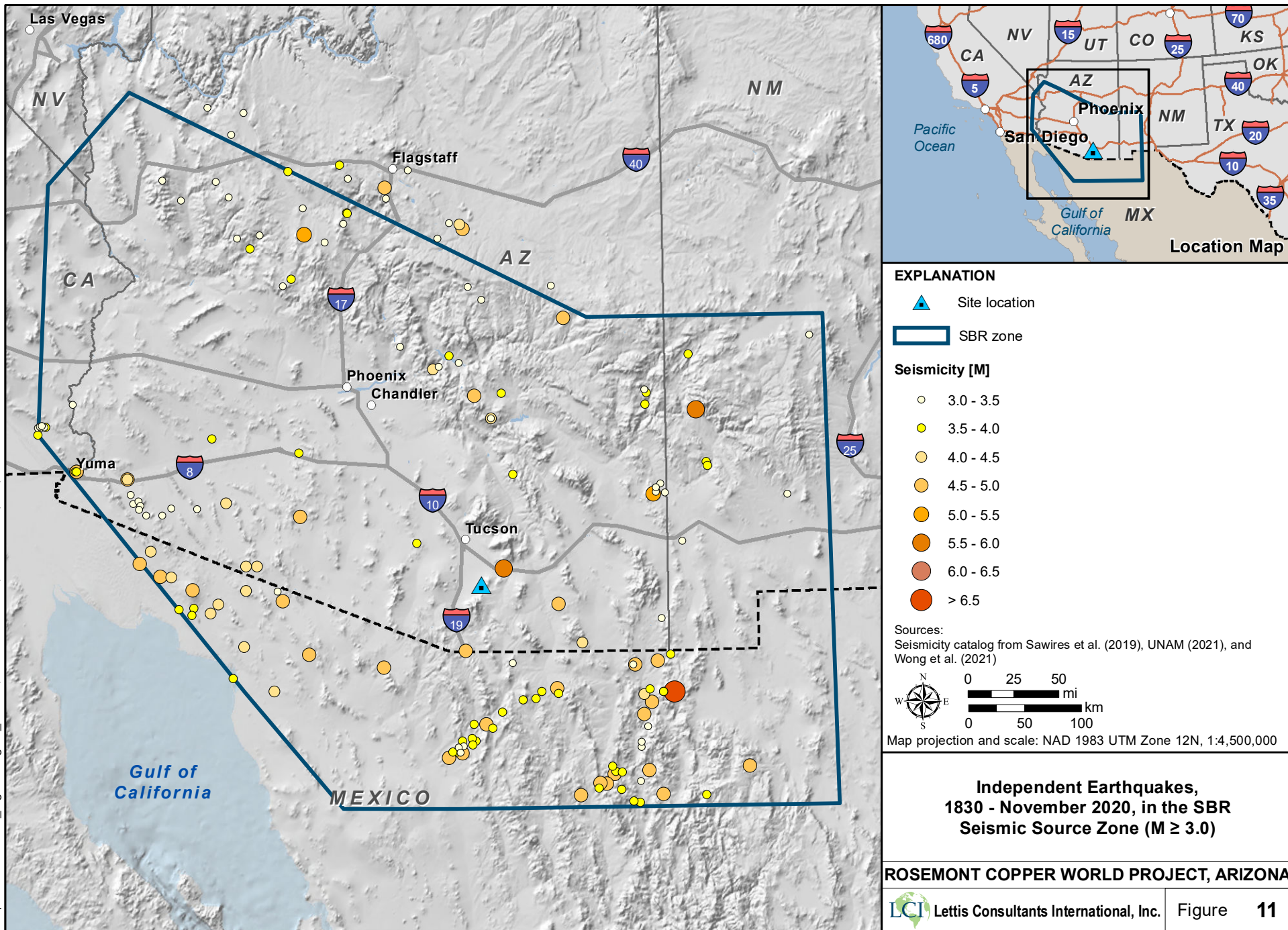
**9**

Source: Figure modified from USGS (2014)













#### EXPLANATION

##### Magnitude bin:

- 3.0 - 3.5
- 3.5 - 4.0
- 4.0 - 4.5
- 4.5 - 5.0
- 5.0 - 5.5
- 5.5 - 6.0
- 6.0 - 6.5
- 6.5 - 7.0

##### Completeness:

- - - 3.0 - 3.5
- - - 3.5 - 4.0
- - - 4.0 - 5.0
- - - ≥ 5.0

### Stepp Plot for the SBR Seismic Source Zone

ROSEMONT COPPER WORLD PROJECT, ARIZONA

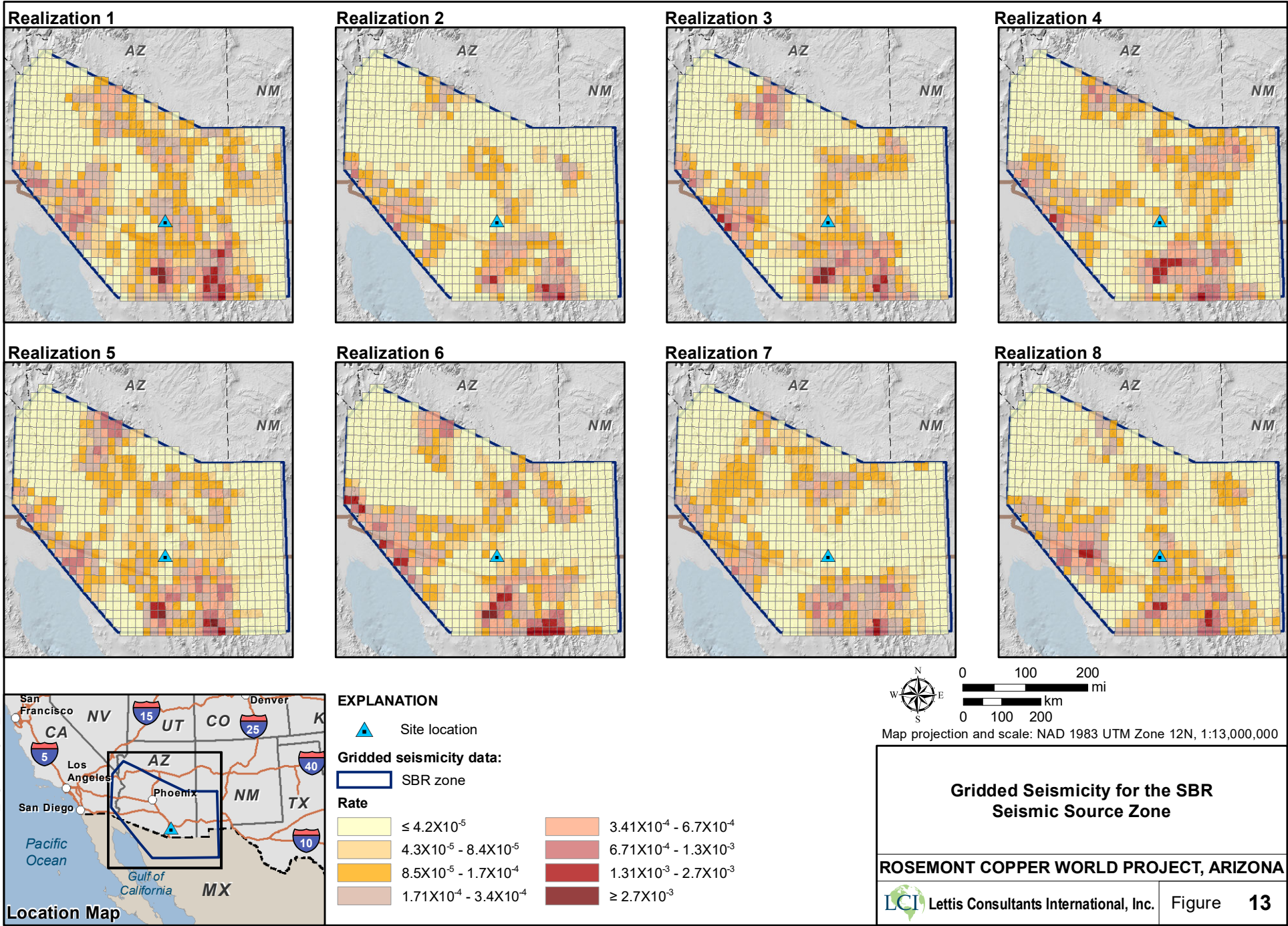


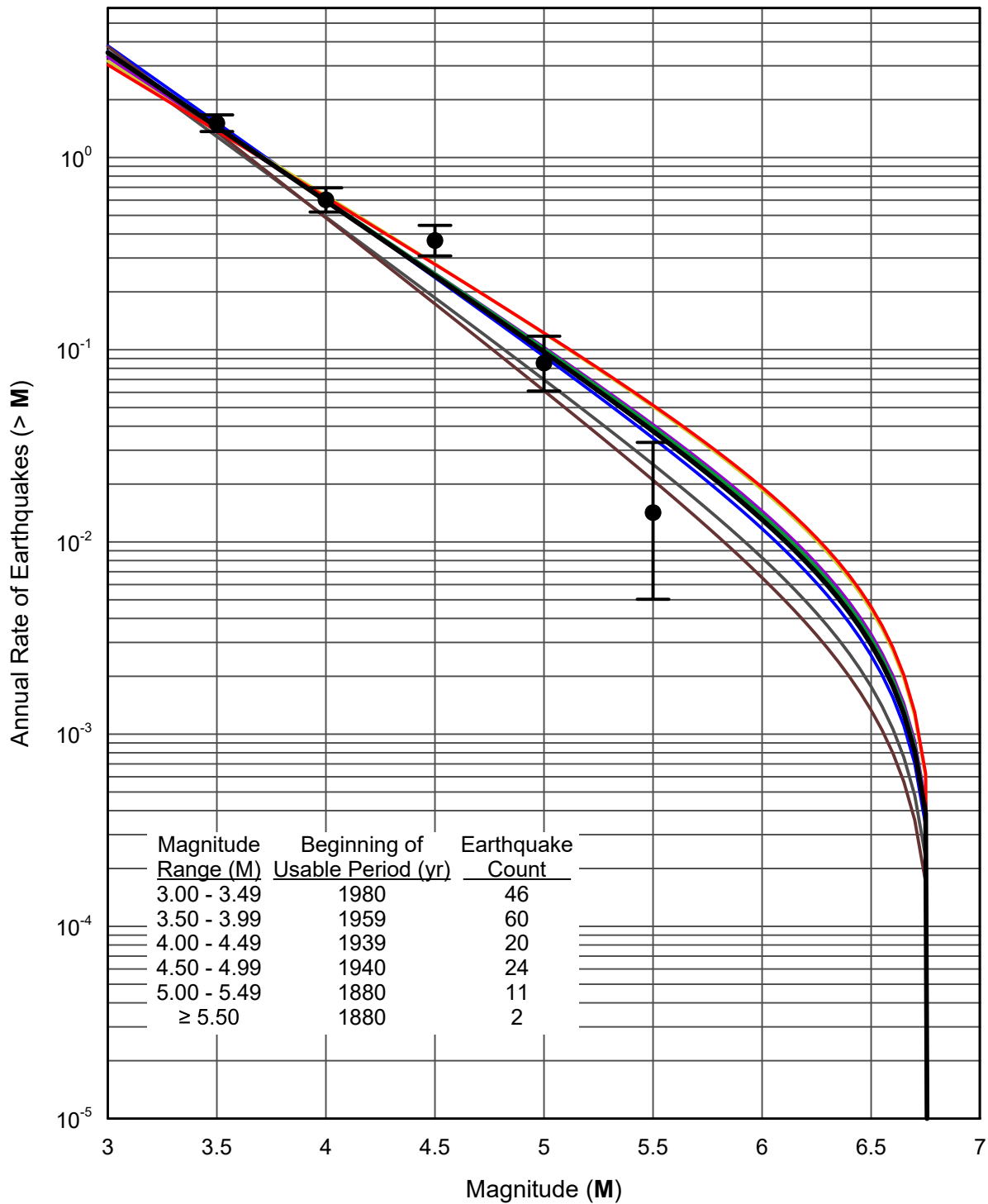
Lettis Consultants International, Inc.

Figure

12

File path: S:\2138\00\_Figures\Figure\_13.mxd; Date: 11/09/2021; User: Javier, LCI; Rev.1





#### EXPLANATION

● Cumulative earthquake rate

ABSMOOTH Realization



Note: Error bars on cumulative earthquake rate represent two standard deviations.

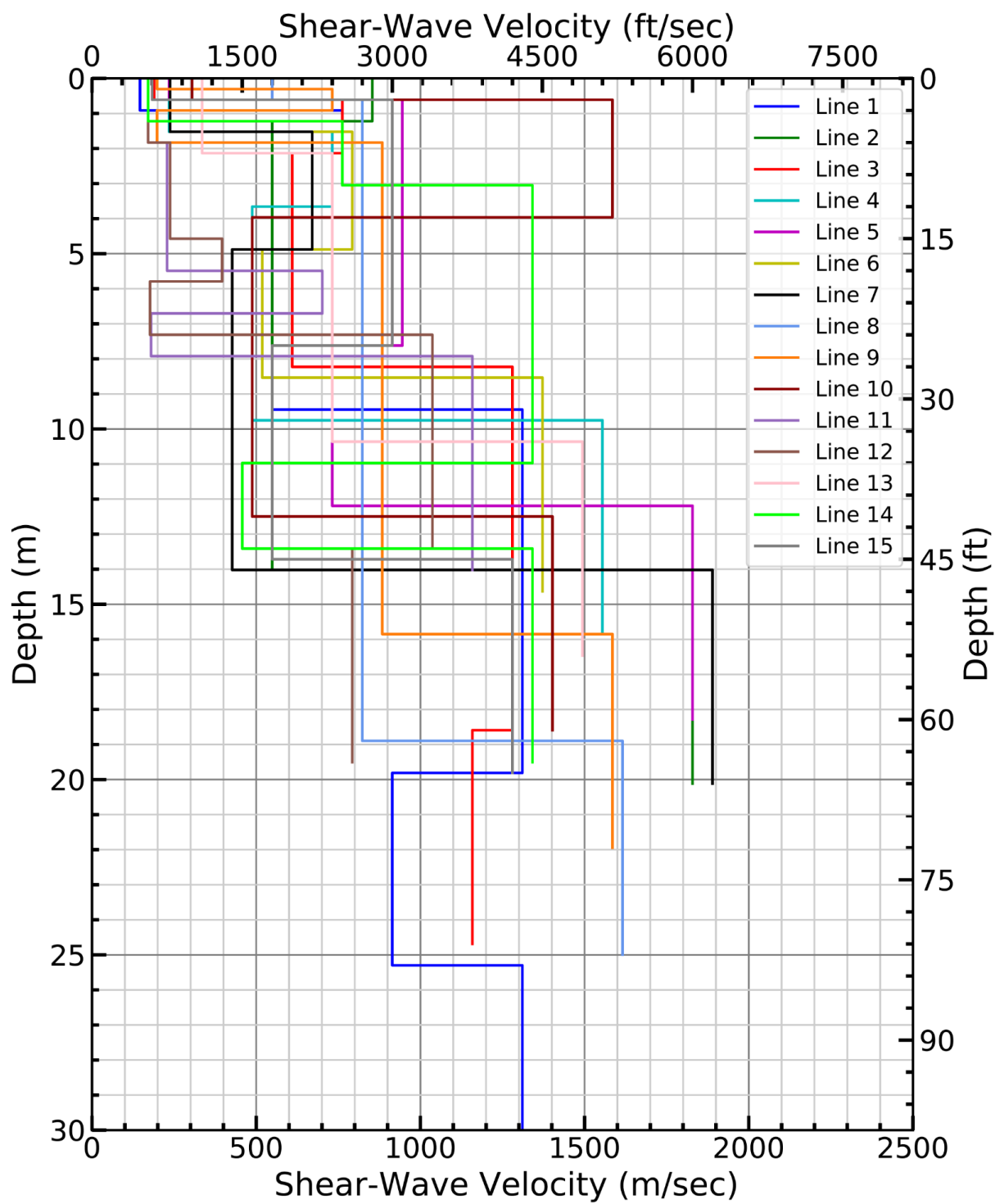
**Cumulative Magnitude-Recurrence  
Curves for the SBR Seismic  
Source Zone for  $M_{MAX}$  6.80**

**ROSEMONT COPPER WORLD PROJECT, ARIZONA**



Lettis Consultants International, Inc.

Figure 14



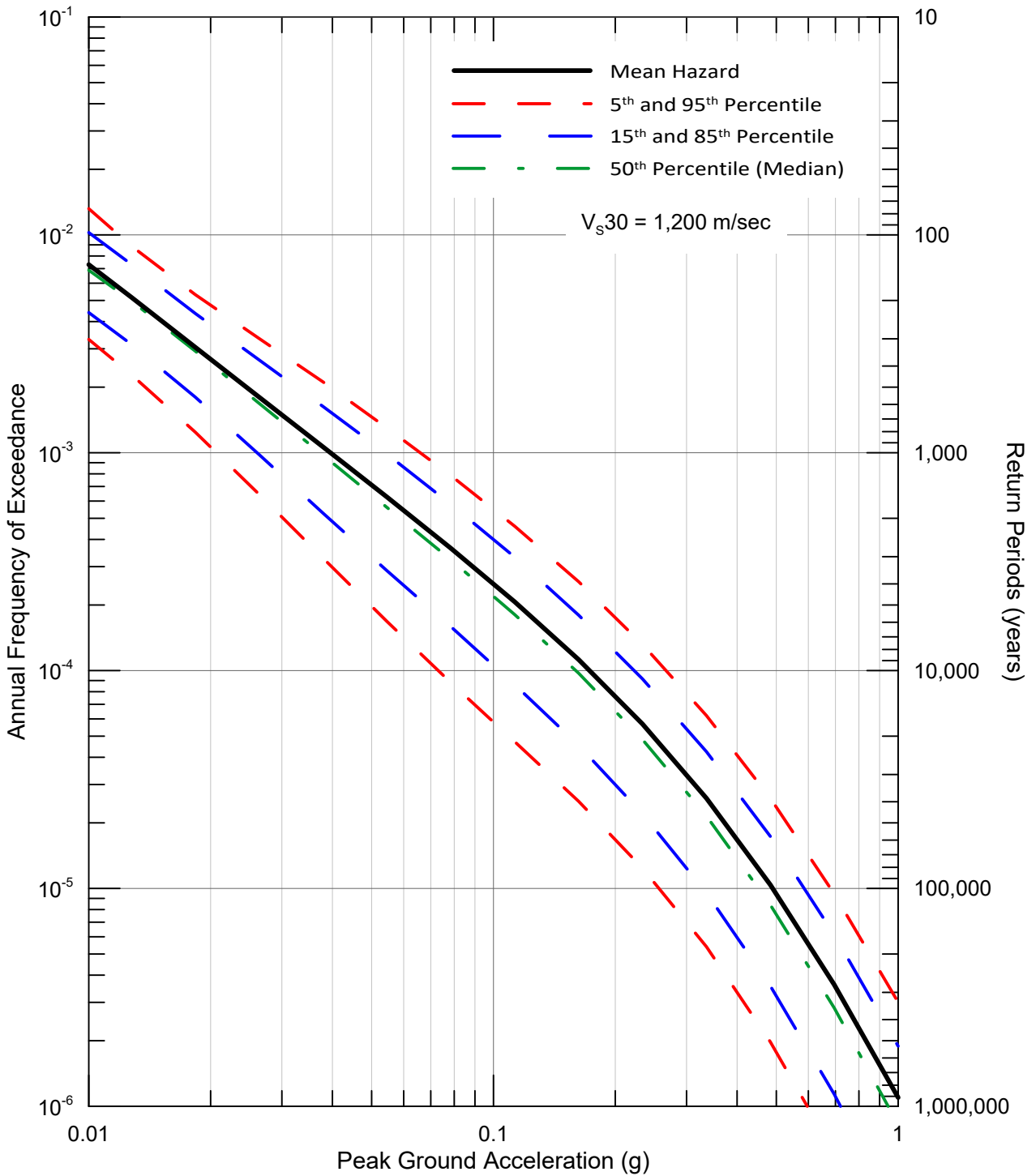
**Shear-Wave Velocity Profiles**

---

**ROSEMONT COPPER WORLD PROJECT, ARIZONA**

Lettis Consultants International, Inc.

Figure **15**



**Seismic Hazard Curves for Peak Horizontal  
Acceleration for  $V_{s30}$  1,200 m/sec**

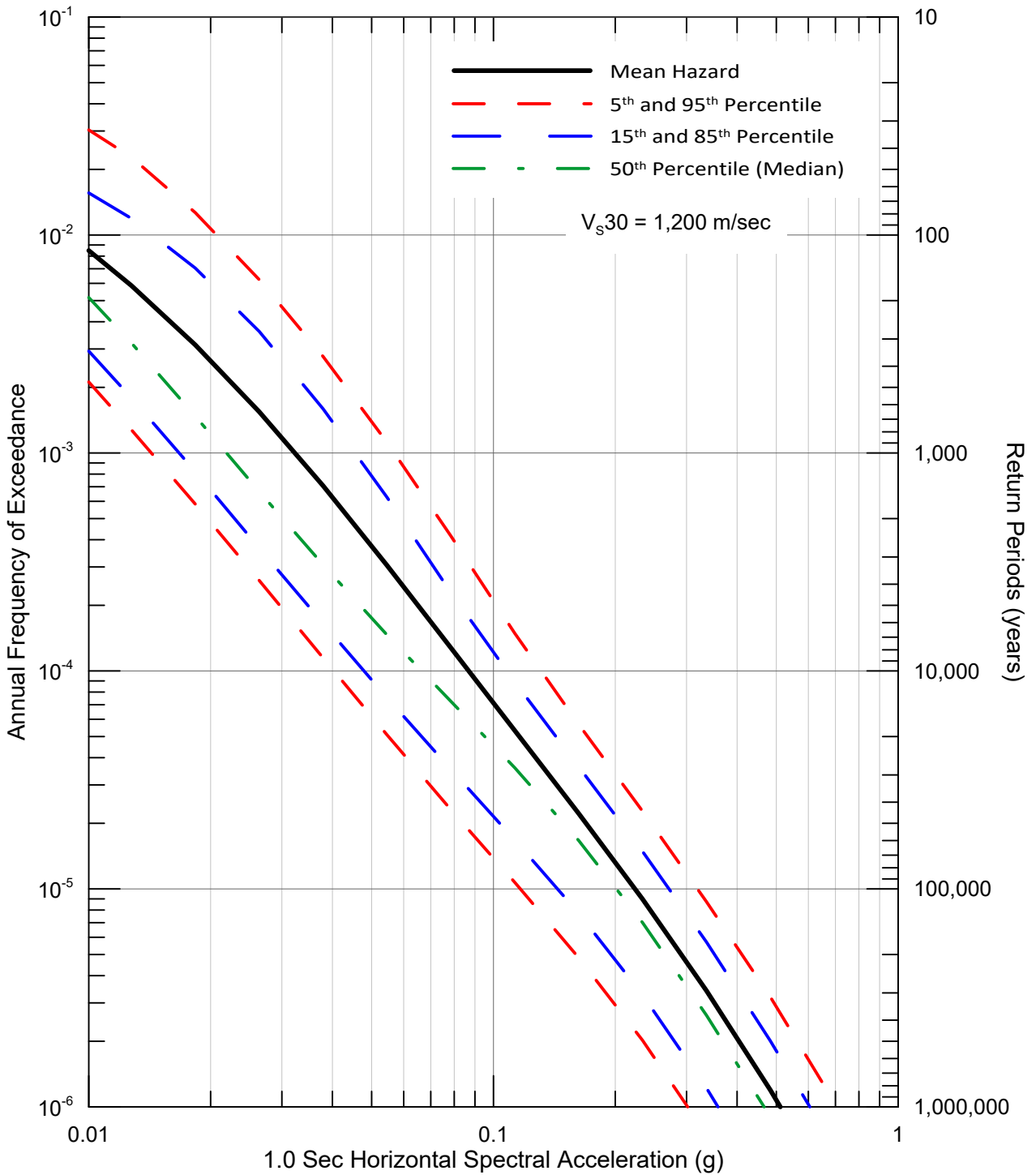
**ROSEMONT COPPER WORLD PROJECT, ARIZONA**



Lettis Consultants International, Inc.

Figure **16**





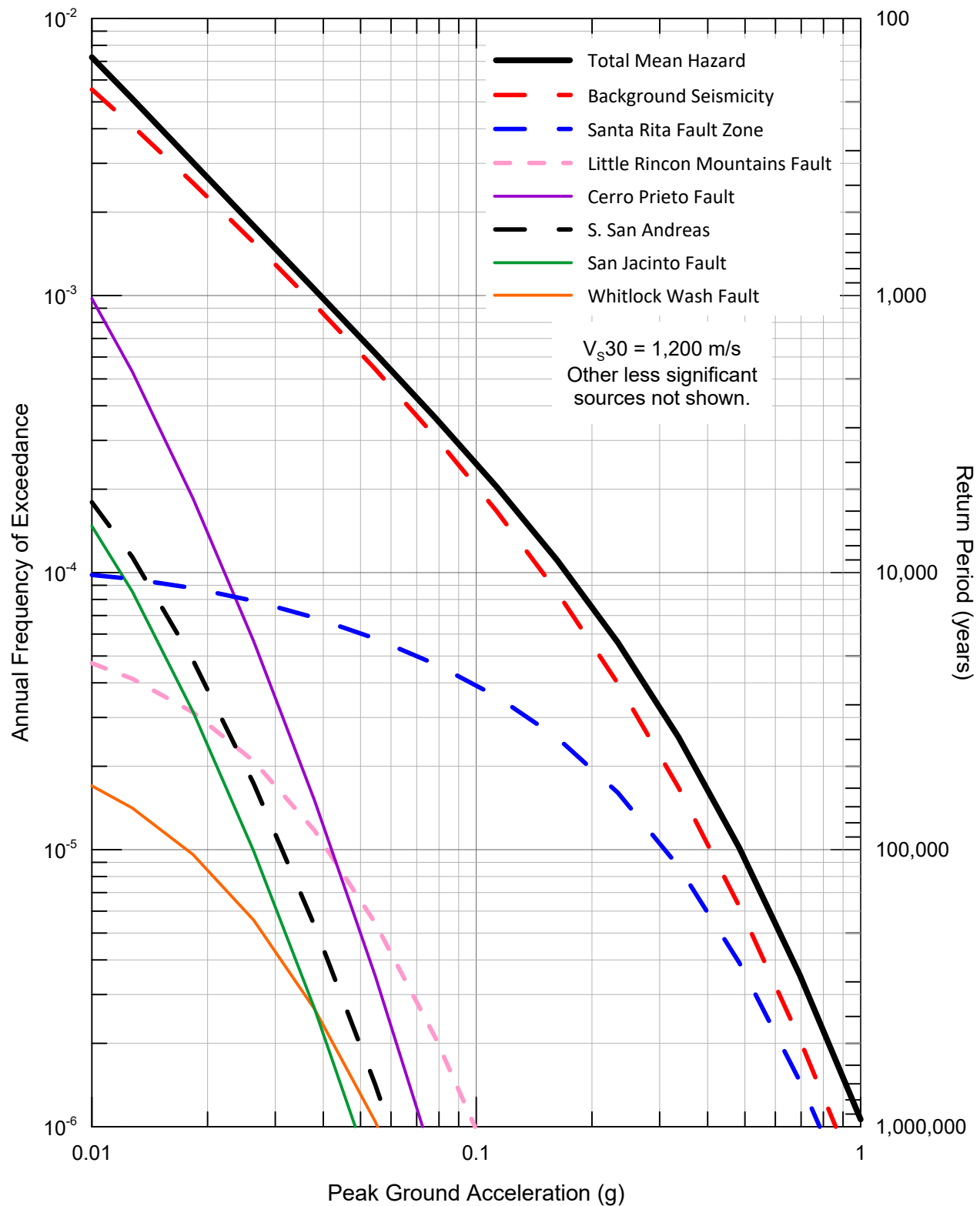
**Seismic Hazard Curves for 1.0 Sec  
Horizontal Spectral Acceleration  
for  $V_{s30}$  1,200 m/sec**

**ROSEMONT COPPER WORLD PROJECT, ARIZONA**



Lettis Consultants International, Inc.

Figure 17



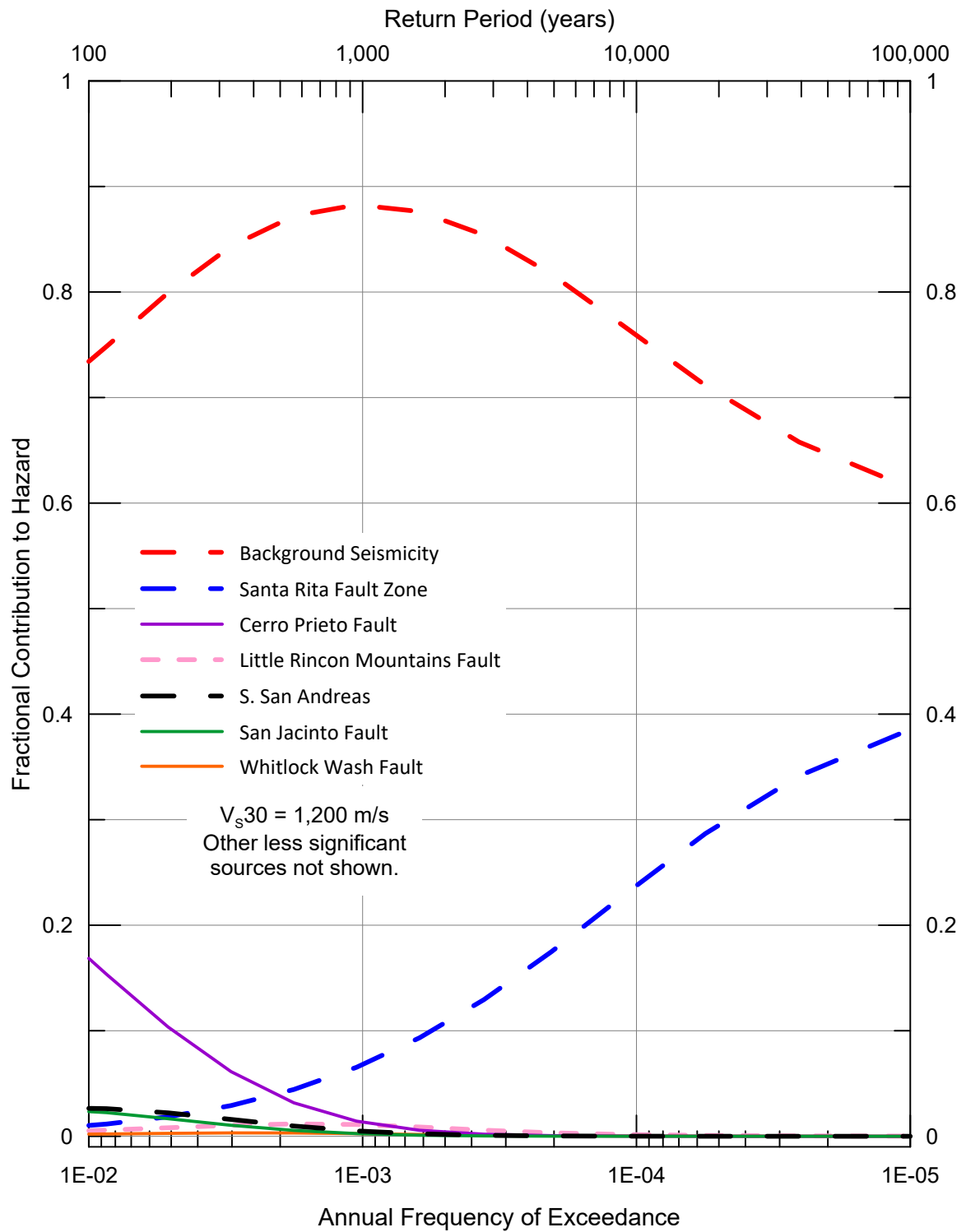
Seismic Source Contributions to Mean  
Peak Horizontal Acceleration Hazard  
for  $V_{s30}$  1,200 m/sec

ROSEMONT COPPER WORLD PROJECT, ARIZONA



Lettis Consultants International, Inc.

Figure 18



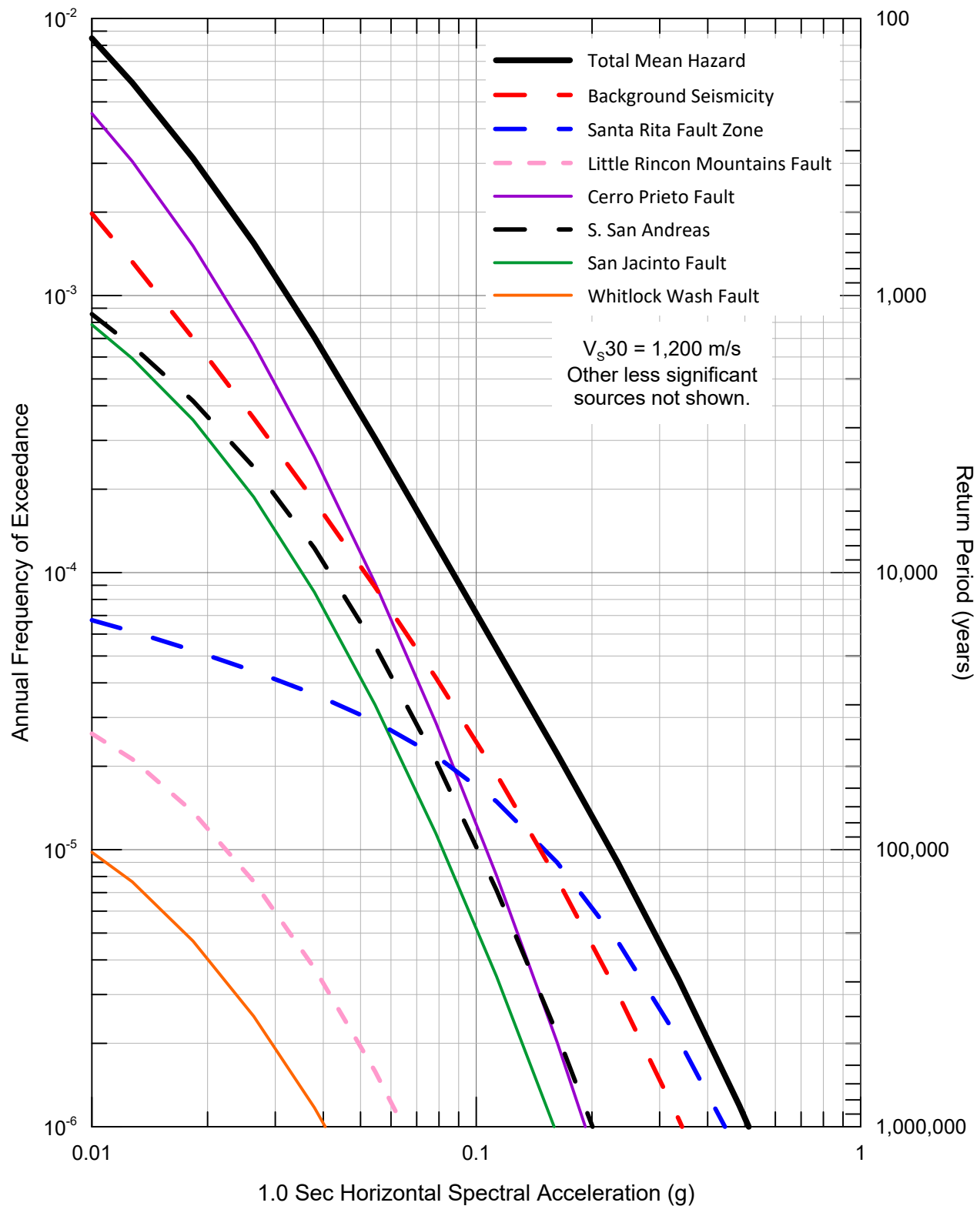
**Seismic Source Fractional Contributions to  
Mean Peak Horizontal Acceleration Hazard  
for  $V_{s30}$  1,200 m/sec**

**ROSEMONT COPPER WORLD PROJECT, ARIZONA**



Lettis Consultants International, Inc.

Figure 19



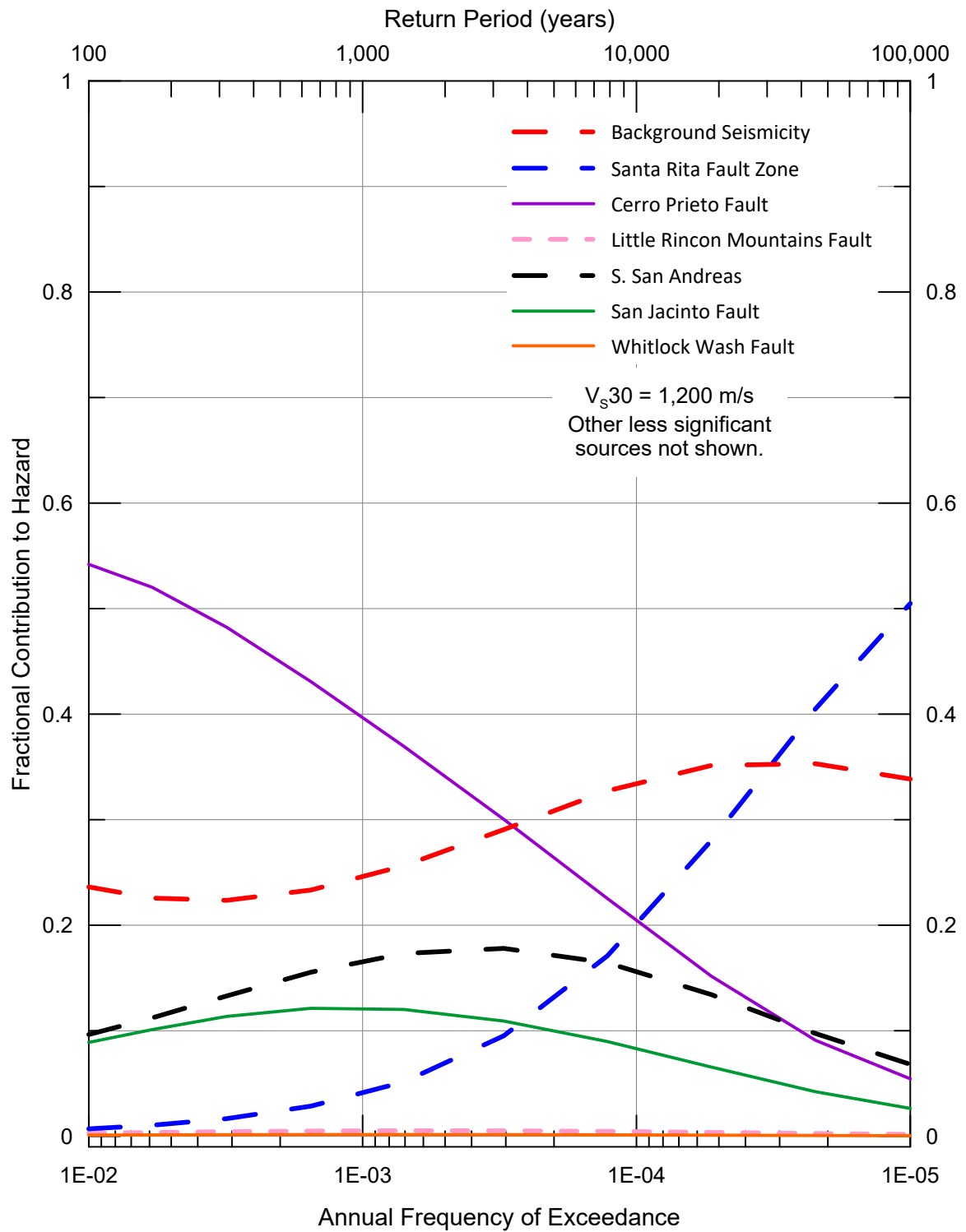
Seismic Source Contributions to Mean  
1.0 Sec Horizontal Spectral Acceleration  
Hazard for  $V_{s30}$  1,200 m/sec

ROSEMONT COPPER WORLD PROJECT, ARIZONA



Lettis Consultants International, Inc.

Figure 20



**Seismic Source Fractional Contributions to  
Mean 1.0 Sec Horizontal Spectral Acceleration  
Hazard for  $V_{s30}$  1,200 m/sec**

**ROSEMONT COPPER WORLD PROJECT, ARIZONA**



Lettis Consultants International, Inc.

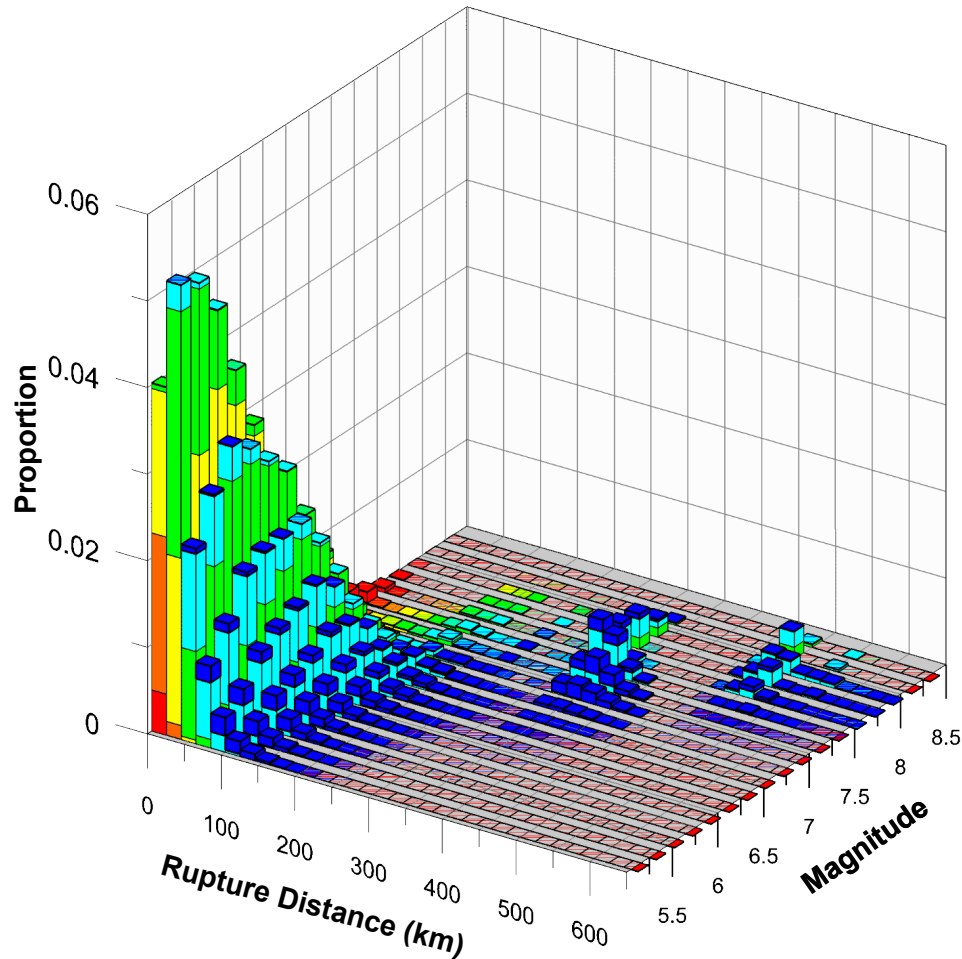
Figure 21



### 475-Year Return Period, PGA

Modal **M**, Rrup: 5.10, 30 km

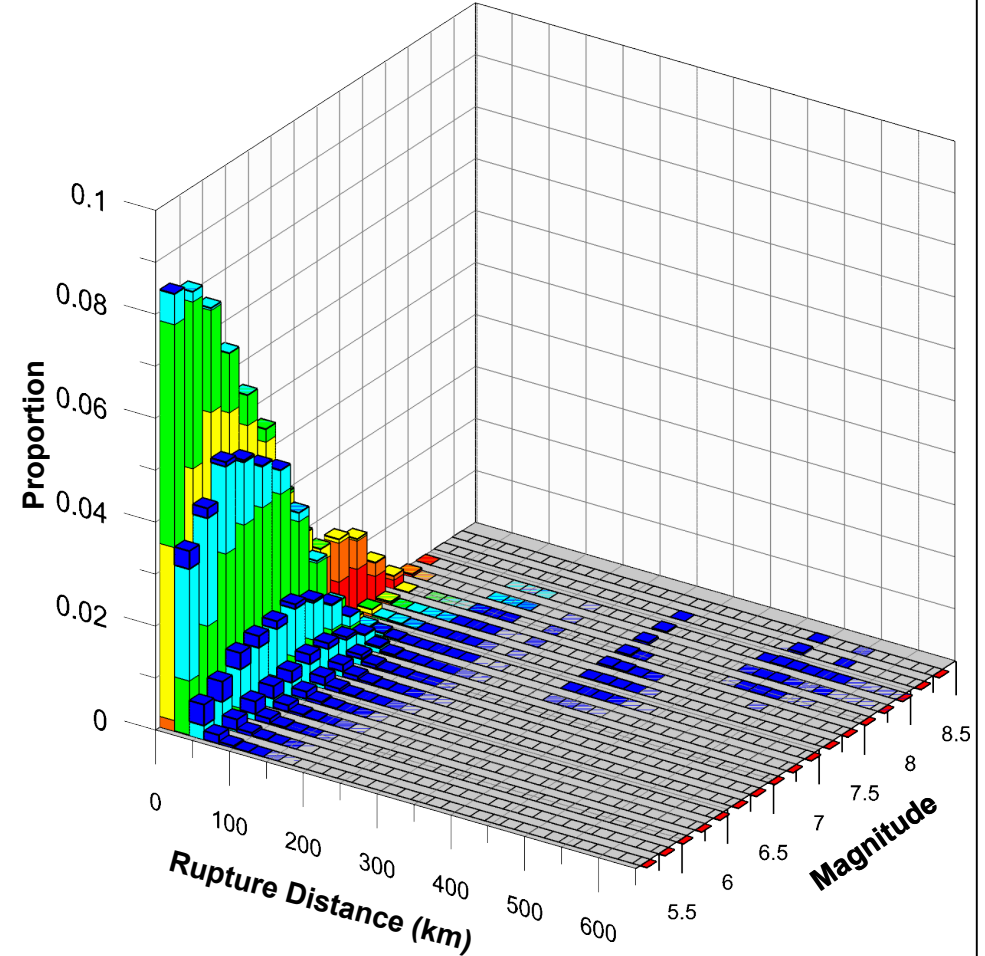
Mean **M**, Rrup: 5.83, 71 km



### 2,475-Year Return Period, PGA

Modal **M**, Rrup: 5.10, 10 km

Mean **M**, Rrup: 5.78, 26 km



#### Epsilon

- > 2
- 1 to 2
- 0 to 1
- 1 to 0
- 2 to -1
- < -2

$V_{s30} = 1,200$  m/s

Magnitude and Distance Contributions to  
the Mean Peak Horizontal Acceleration Hazard  
at 475 and 2,475-Year Return Periods  
for  $V_{s30}$  1,200 m/sec

ROSEMONT COPPER WORLD PROJECT, ARIZONA



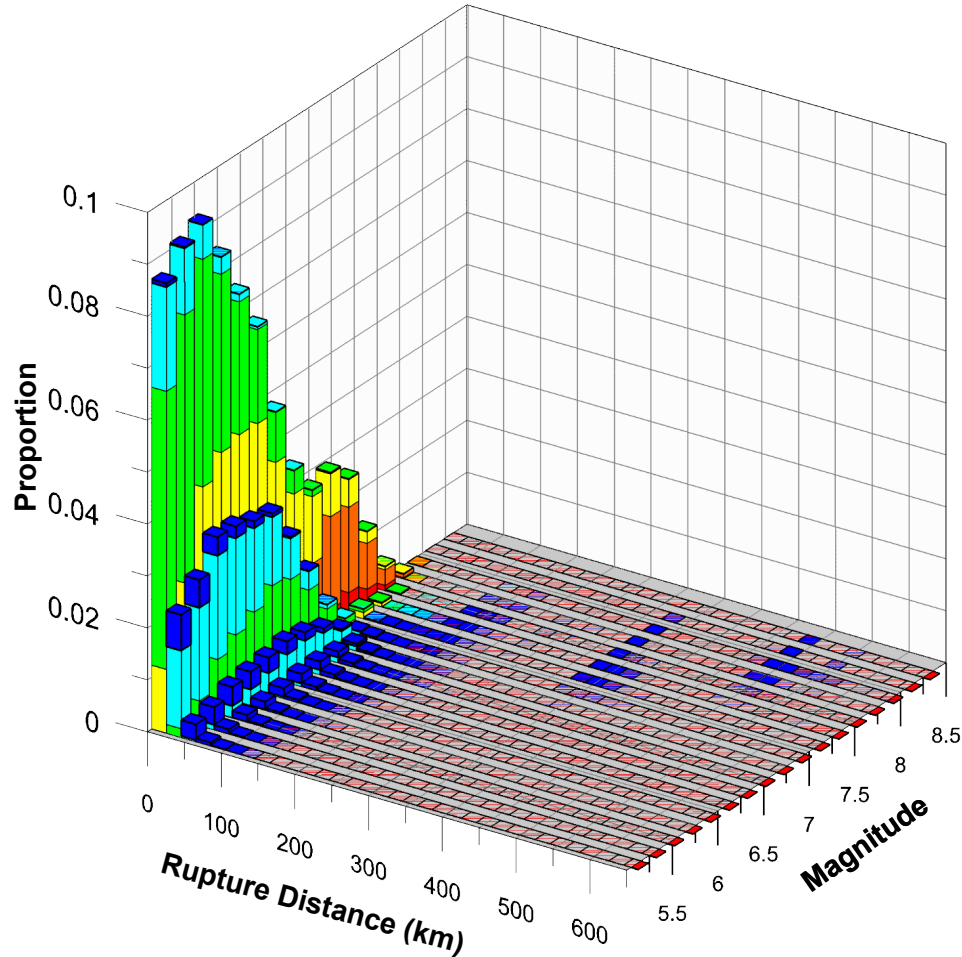
Lettis Consultants International, Inc.

Figure 22

### 5,000-Year Return Period, PGA

Modal **M**, Rrup: 5.50, 10 km

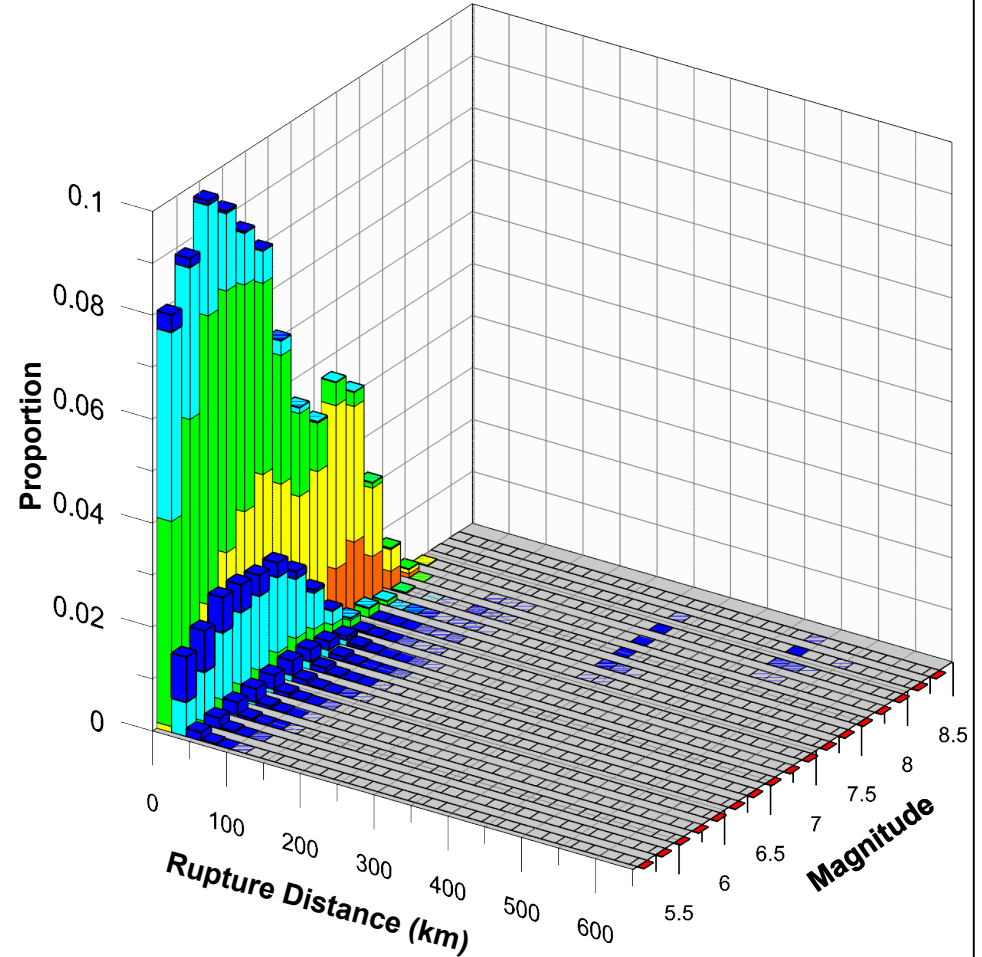
Mean **M**, Rrup: 5.85, 19 km



### 10,000-Year Return Period, PGA

Modal **M**, Rrup: 5.50, 10 km

Mean **M**, Rrup: 5.93, 14 km



#### Epsilon



$V_{s30} = 1,200$  m/s

Magnitude and Distance Contributions to  
the Mean Peak Horizontal Acceleration Hazard  
at 5,000 and 10,000-Year Return Periods  
for  $V_{s30}$  1,200 m/sec

ROSEMONT COPPER WORLD PROJECT, ARIZONA



Lettis Consultants International, Inc.

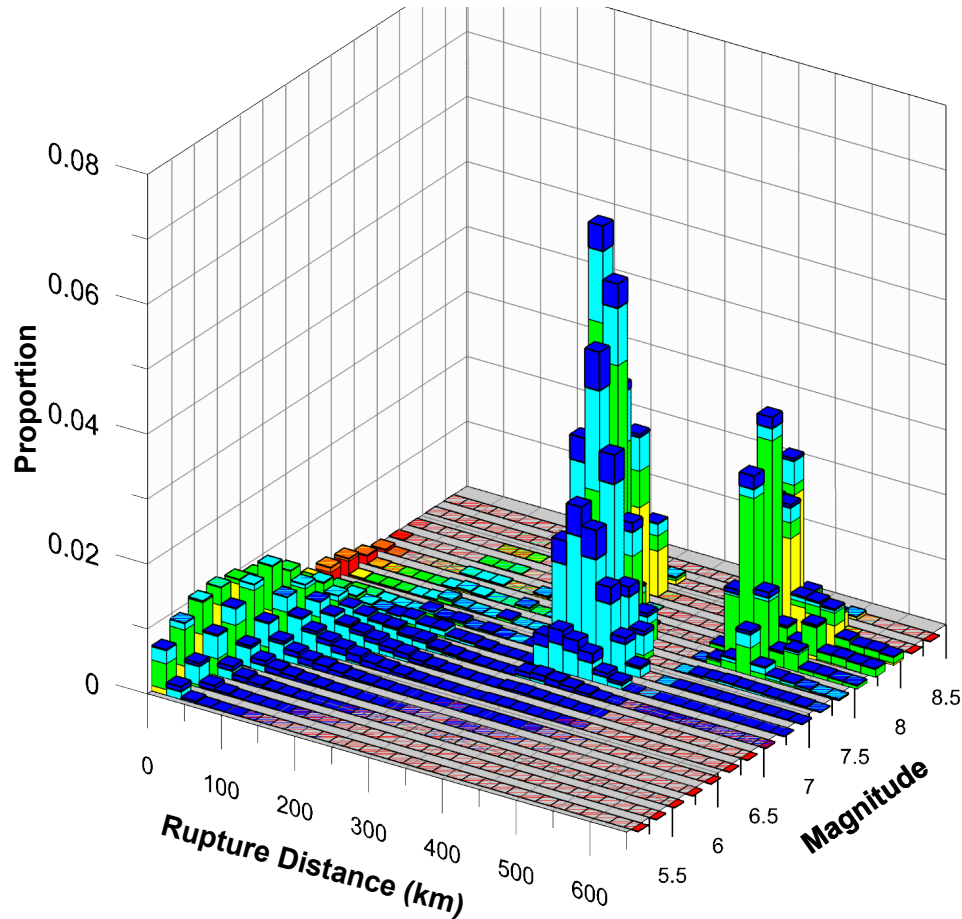
Figure 23

### 475-Year Return Period, 1.0 Sec

Modal **M**, Rrup: 7.30, 330 km

Mean **M**, Rrup ( $\leq 300$  km): 6.13, 62 km

Mean **M**, Rrup ( $> 300$  km): 7.38, 416 km



#### Epsilon

- > 2
- 1 to 2
- 0 to 1
- 1 to 0
- 2 to -1
- < -2

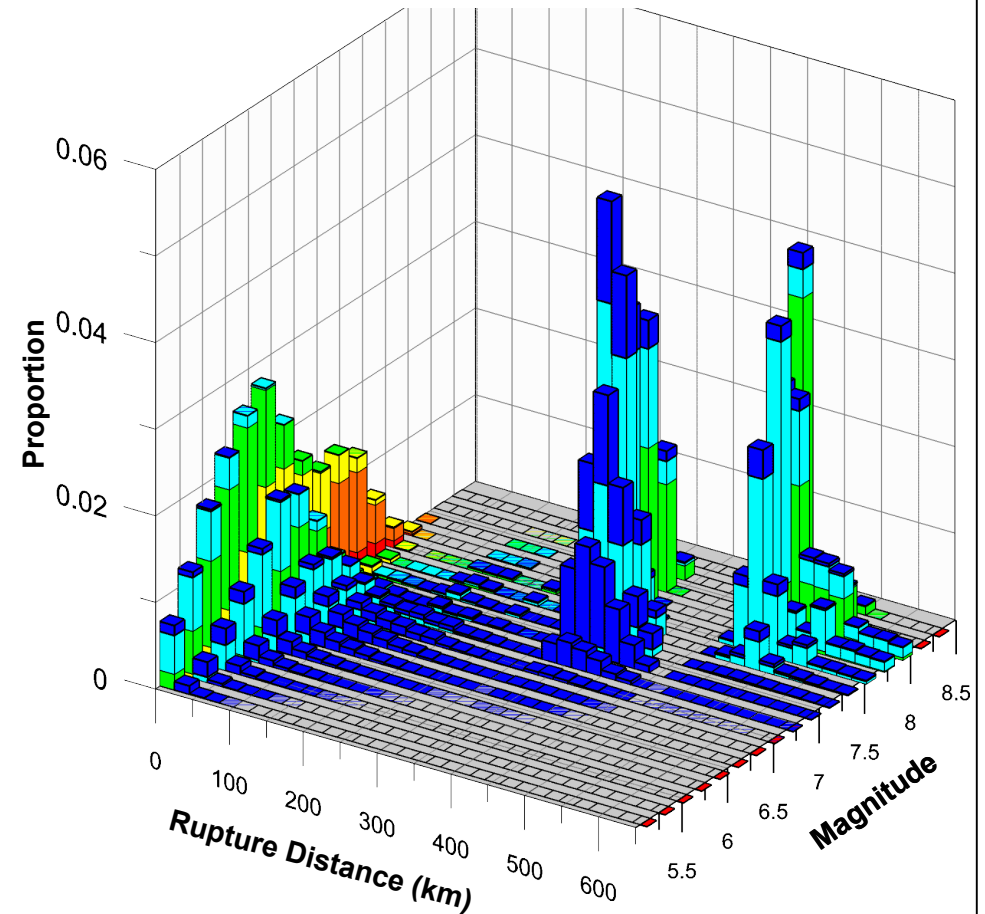
$V_{s30} = 1,200$  m/s

### 2,475-Year Return Period, 1.0 Sec

Modal **M**, Rrup: 7.30, 330 km

Mean **M**, Rrup ( $\leq 300$  km): 6.23, 36 km

Mean **M**, Rrup ( $> 300$  km): 7.51, 429 km



Magnitude and Distance Contributions to the  
Mean 1.0 Sec Horizontal Spectral Acceleration  
Hazard at 475 and 2,475-Year Return Periods  
for  $V_{s30}$  1,200 m/sec

ROSEMONT COPPER WORLD PROJECT, ARIZONA



Lettis Consultants International, Inc.

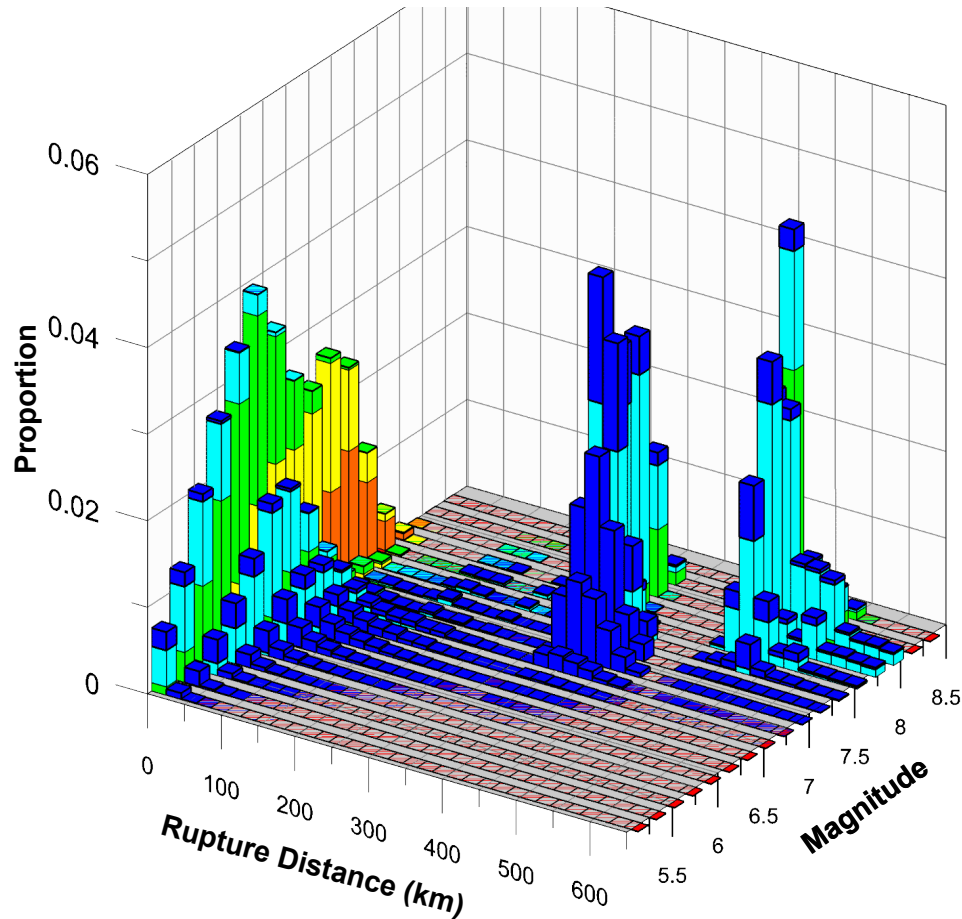
Figure 24

### 5,000-Year Return Period, 1.0 Sec

Modal **M**, Rrup: 8.10, 490 km

Mean **M**, Rrup ( $\leq 300$  km): 6.30, 28 km

Mean **M**, Rrup ( $> 300$  km): 7.56, 433 km



#### Epsilon



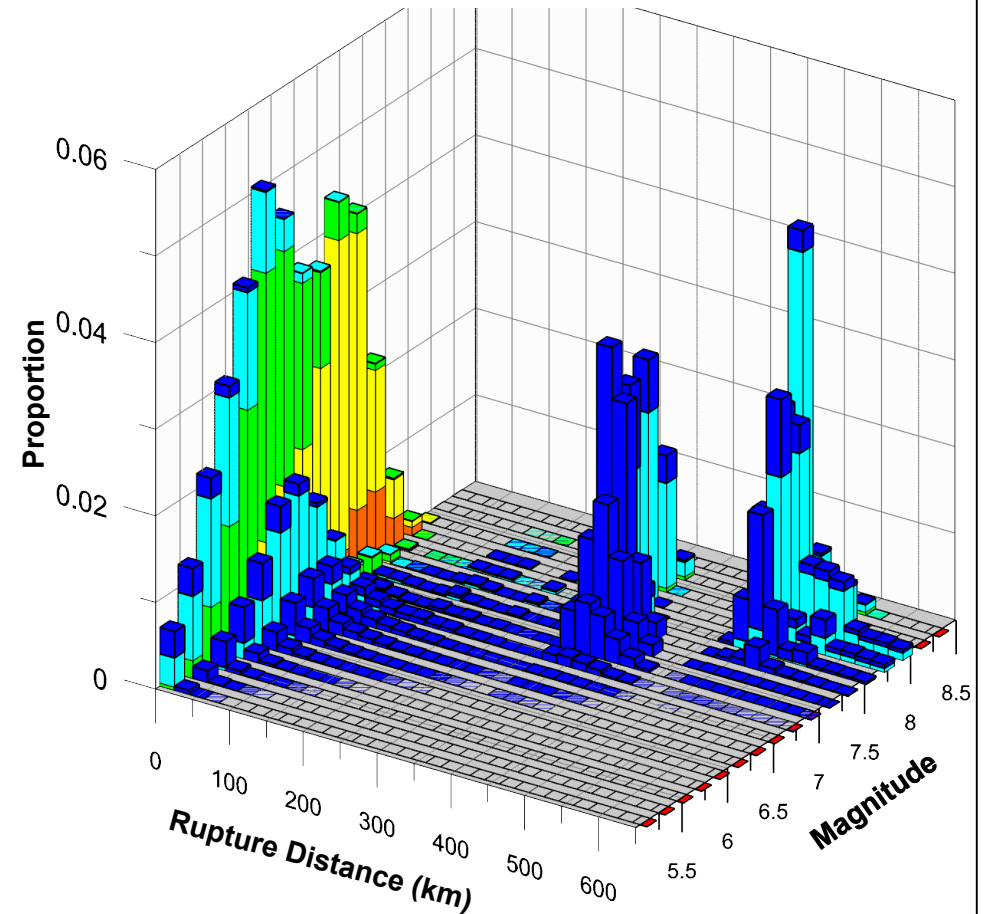
$V_{s30} = 1,200$  m/s

### 10,000-Year Return Period, 1.0 Sec

Modal **M**, Rrup: 6.10, 10 km

Mean **M**, Rrup ( $\leq 300$  km): 6.38, 22 km

Mean **M**, Rrup ( $> 300$  km): 7.60, 437 km



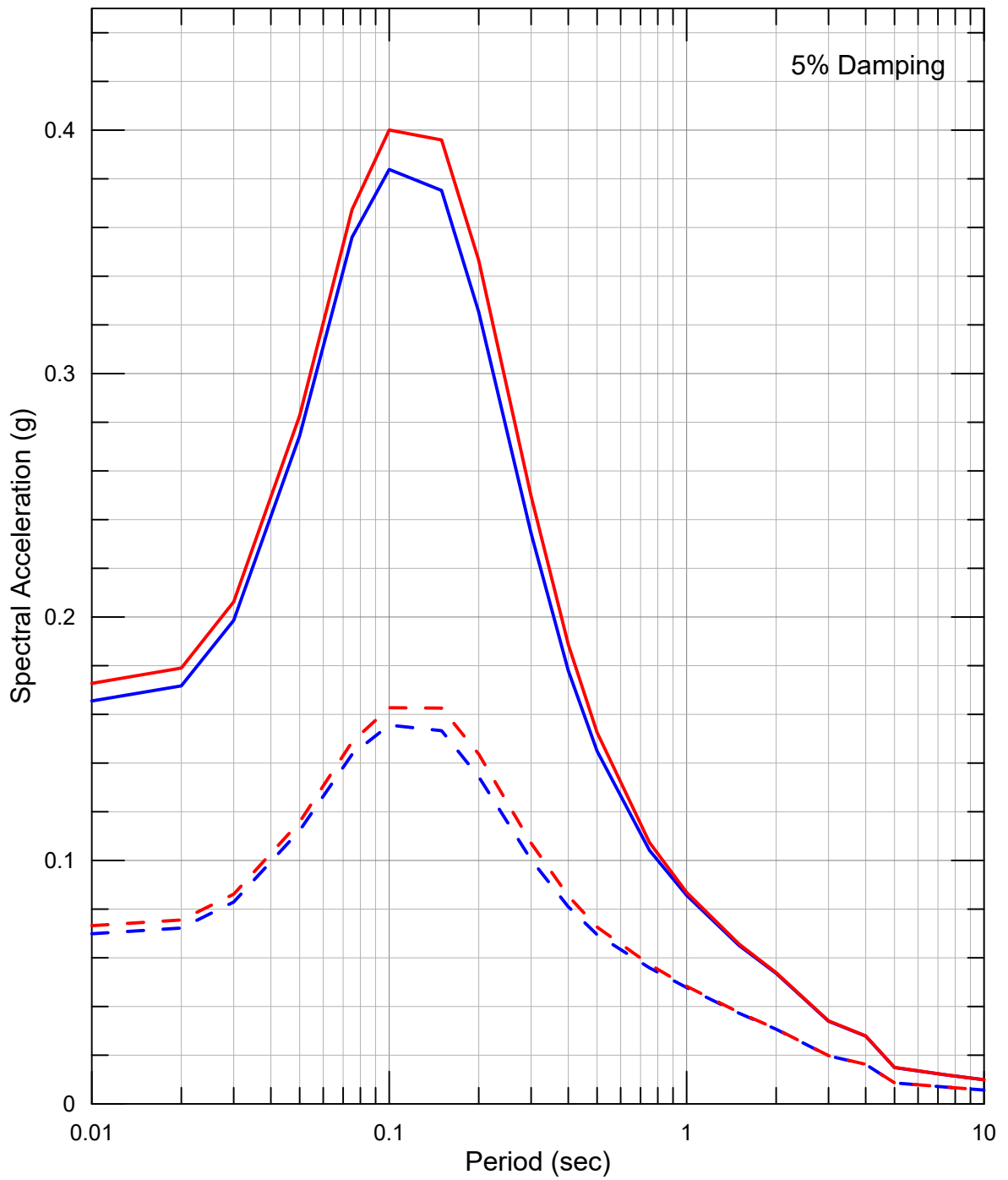
Magnitude and Distance Contributions to the  
Mean 1.0 Sec Horizontal Spectral Acceleration  
Hazard at 5,000 and 10,000-Year Return Periods  
for  $V_{s30}$  1,200 m/sec

ROSEMONT COPPER WORLD PROJECT, ARIZONA



Lettis Consultants International, Inc.

Figure 25



**2,475-Year UHS**      **10,000-Year UHS**

- - 1,200 m/sec      — 1,200 m/sec  
 - - 1,400 m/sec      — 1,400 m/sec

**Sensitivity of Uniform Hazard Spectra to  $V_{s30}$   
at 2,475 and 10,000-Year Return Periods**

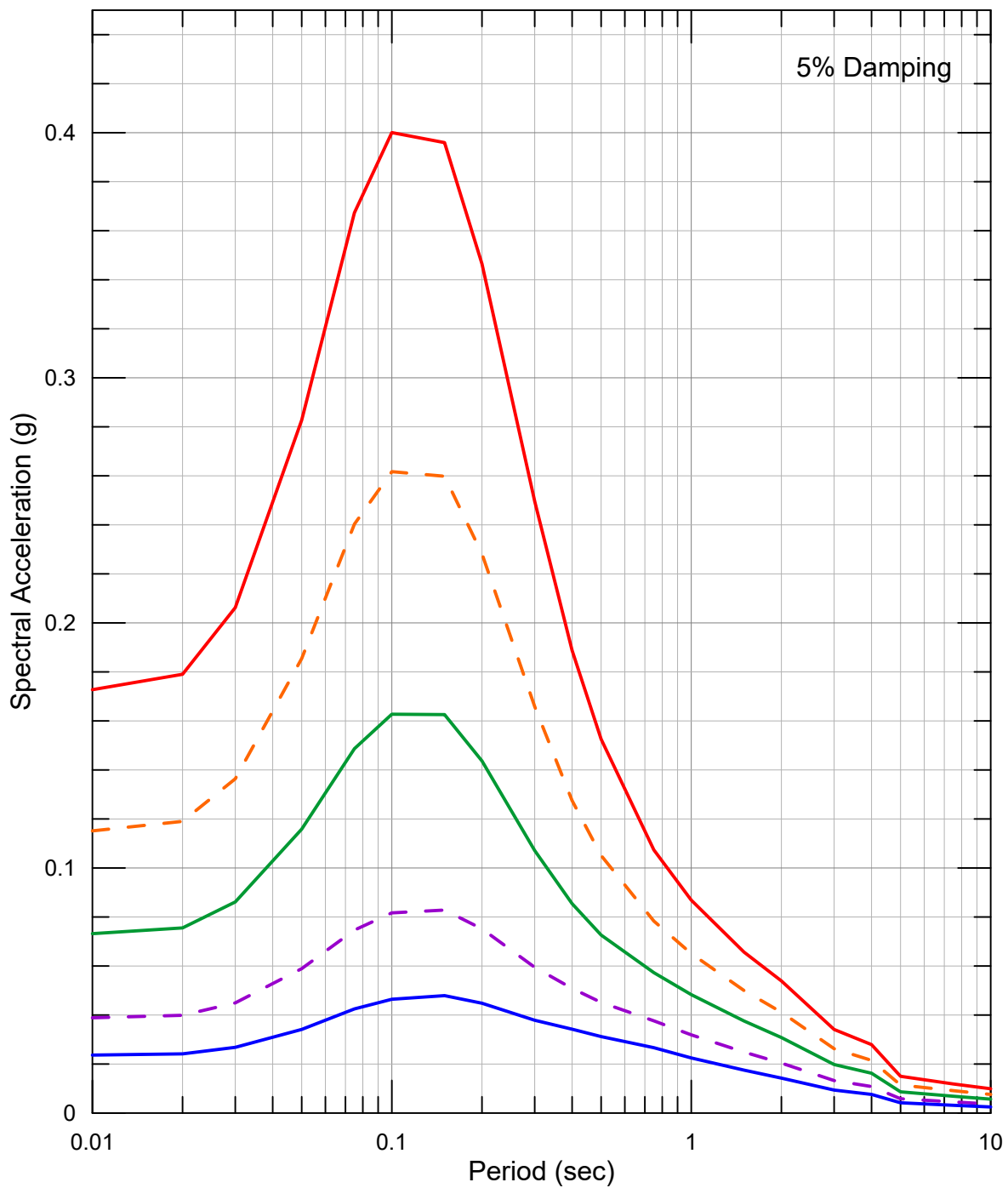
**ROSEMONT COPPER WORLD PROJECT, ARIZONA**



Lettis Consultants International, Inc.

Figure **26**





**Return Period (Years)**

- 475
- - 975
- 2,475
- - 5,000
- 10,000

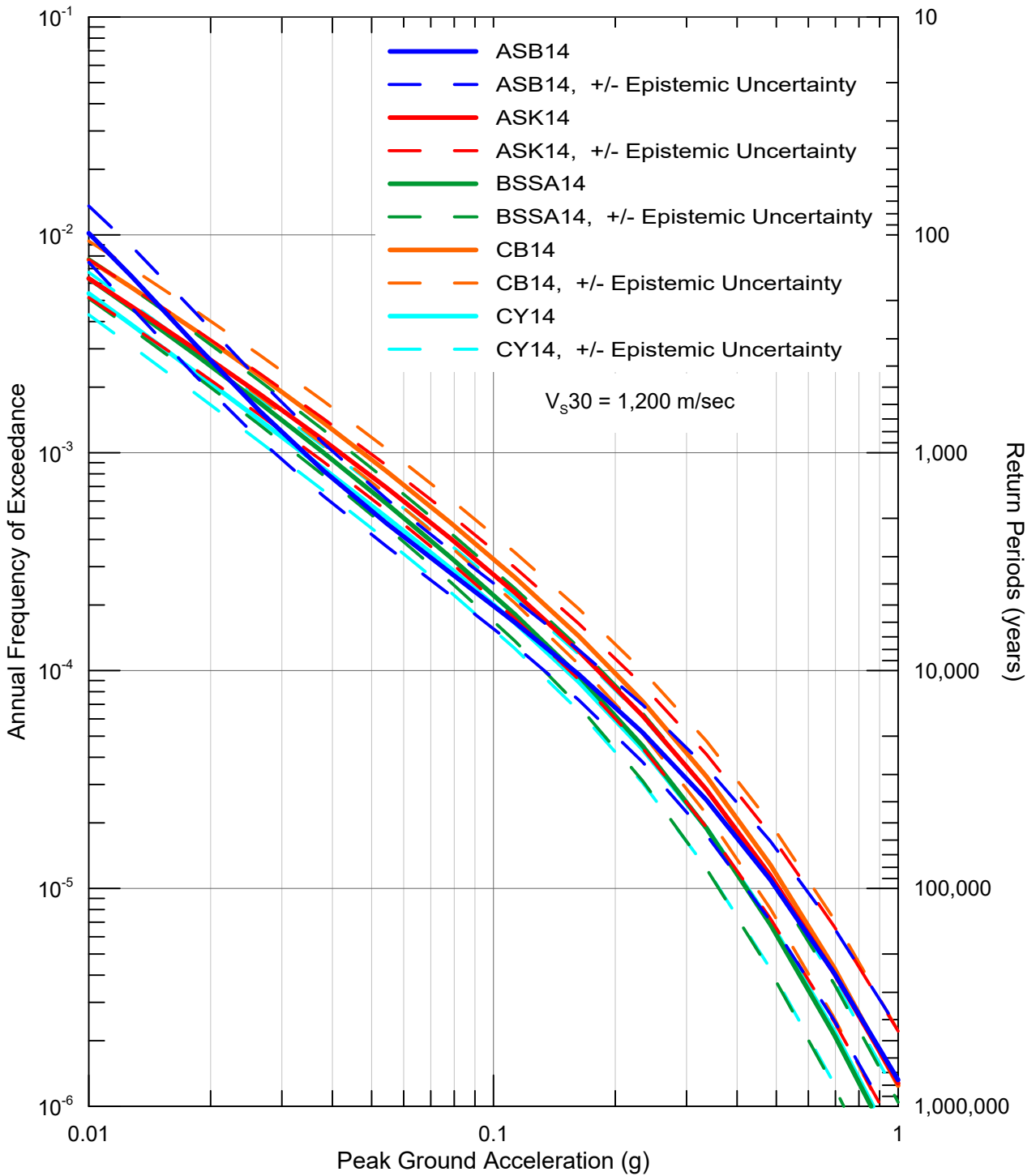
**Enveloped Uniform Hazard Spectra at  
475, 975, 2,475, 5,000 and 10,000-Year  
Return Periods**

**ROSEMONT COPPER WORLD PROJECT, ARIZONA**



Lettis Consultants International, Inc.

Figure **27**



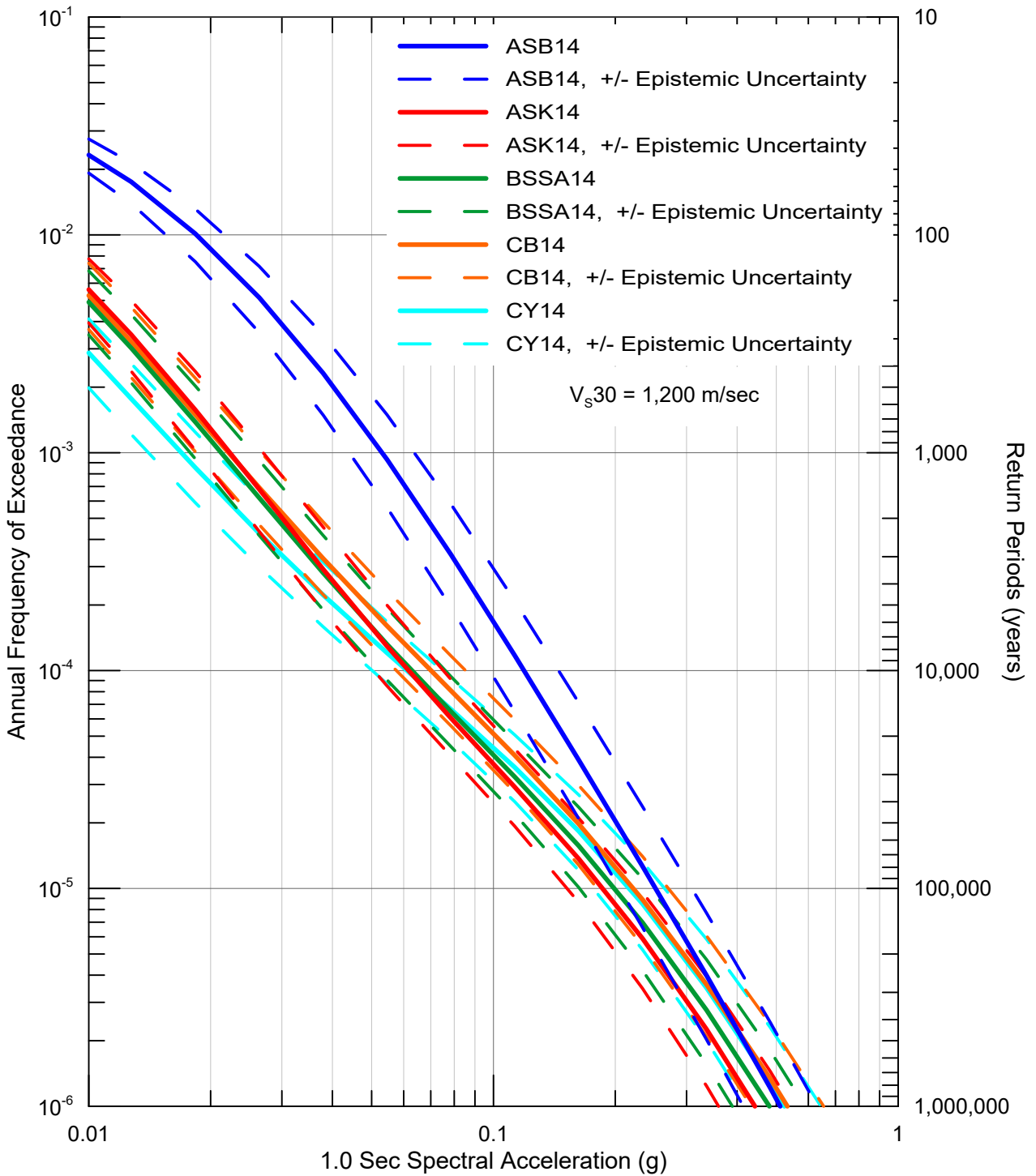
**Sensitivity of Mean Peak Horizontal Acceleration  
Hazard to GMMs for  $V_{s30}$  1,200 m/sec**

**ROSEMONT COPPER WORLD PROJECT, ARIZONA**



Lettis Consultants International, Inc.

Figure 28



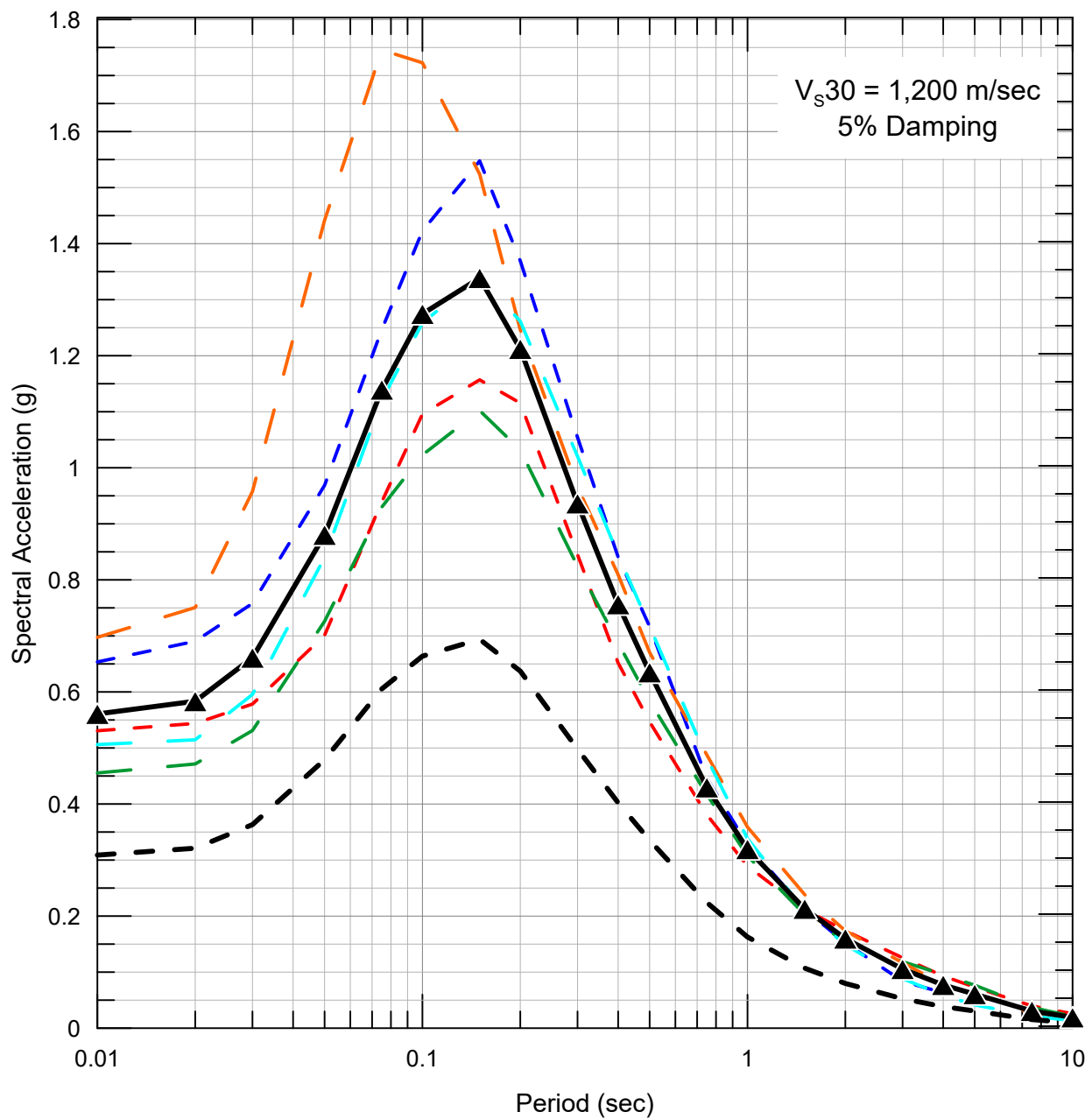
**Sensitivity of Mean 1.0 Sec Horizontal  
 Spectral Acceleration Hazard to GMMs  
 for  $V_{s30}$  1,200 m/sec**

**ROSEMONT COPPER WORLD PROJECT, ARIZONA**



Lettis Consultants International, Inc.

Figure 29



Geometric Mean (Santa Rita Fault , M 7.2, 4.9 km)

▲ — ▲ 84<sup>th</sup> Percentile

- - - Median

84th Percentile Ground Motion Models

- - - Akkar *et al.* (2014)

- - - Abrahamson *et al.* (2014)

- - - Boore *et al.* (2014)

- - - Campbell and Bozorgnia (2014)

- - - Chiou and Youngs (2014)

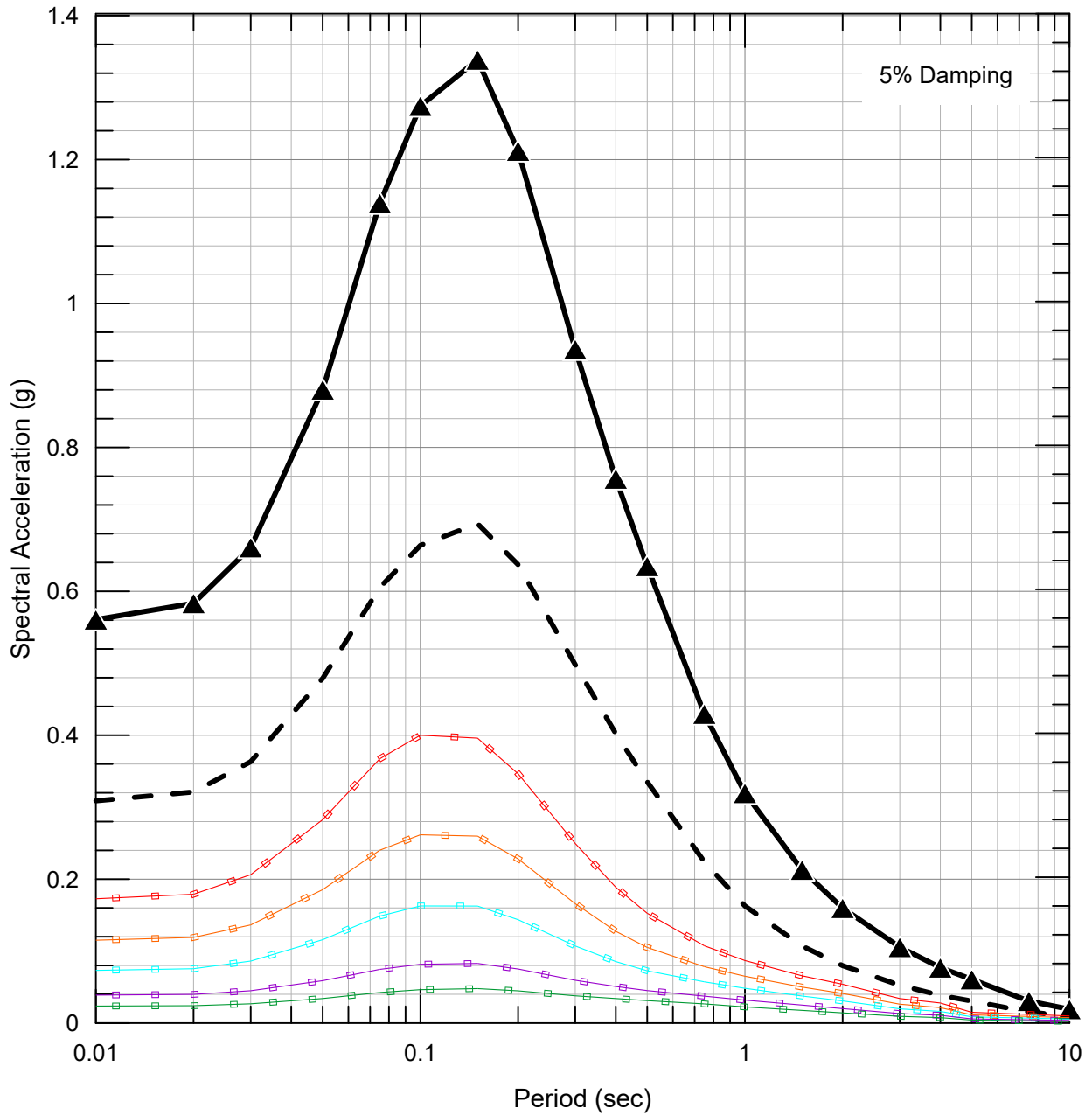
**Sensitivity of 84<sup>th</sup> Percentile Deterministic  
Spectrum for M 7.2 Santa Rita Fault  
Earthquake to GMMs**

**ROSEMONT COPPER WORLD PROJECT, ARIZONA**



Lettis Consultants International, Inc.

Figure 30



**Deterministic Spectra - Santa Rita Fault (M 7.2, 4.9 km)**

- Median
- ▲---▲ 84<sup>th</sup> Percentile

**UHS**

- 475-Year Return Period
- 975-Year Return Period
- 2,475-Year Return Period
- 5,000-Year Return Period
- 10,000-Year Return Period

**Comparison of Deterministic Spectra and Uniform Hazard Spectra**

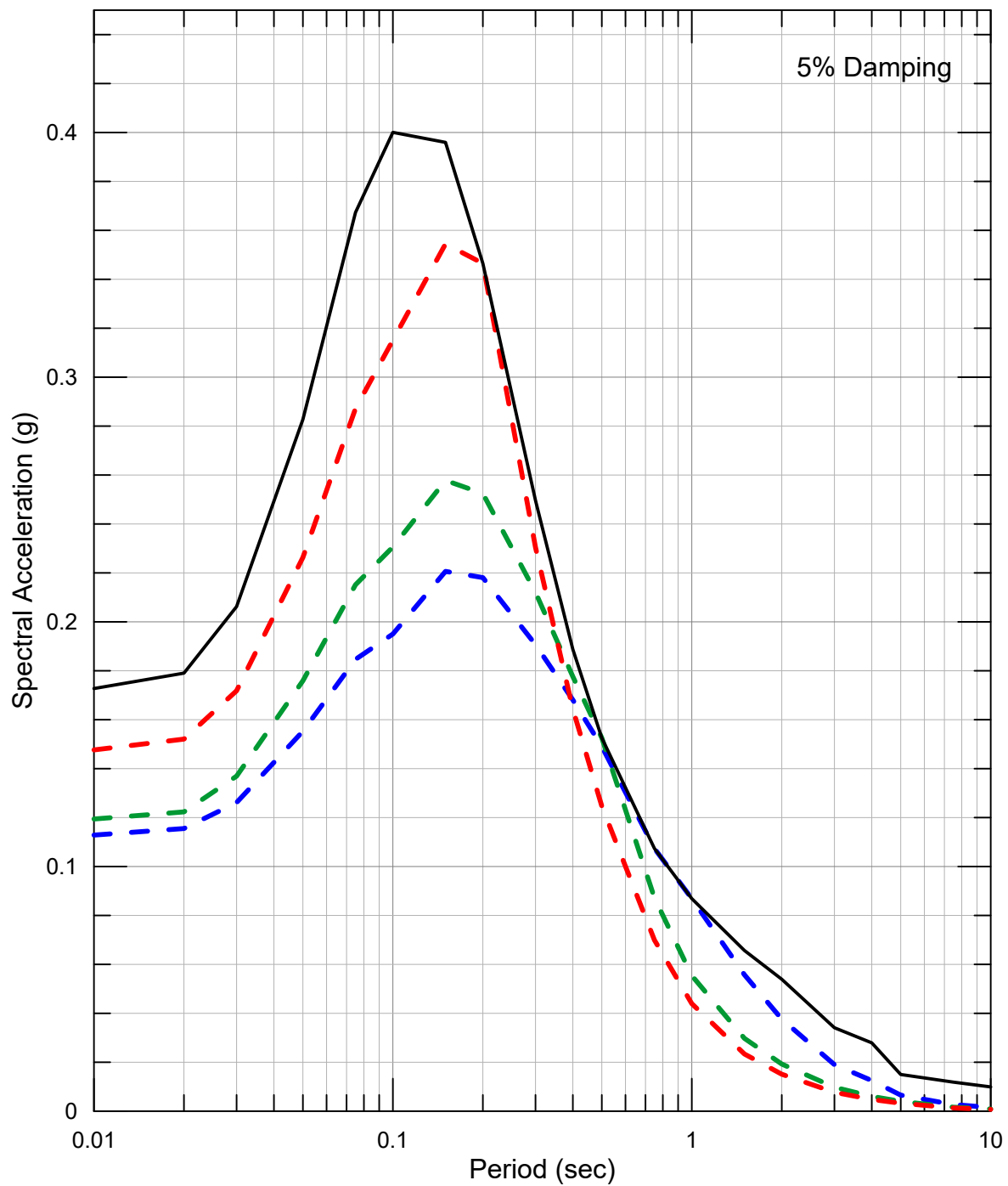
**ROSEMONT COPPER WORLD PROJECT, ARIZONA**



Lettis Consultants International, Inc.

Figure 31





- 10,000-Year UHS
- - CMS  $T^* = 0.2$  sec
- - CMS  $T^* = 0.5$  sec
- - CMS  $T^* = 1.0$  sec

**Uniform Hazard Spectrum at 10,000-Year  
Return Period and CMS Conditioned  
at 0.2, 0.5, and 1.0 sec**

**ROSEMONT COPPER WORLD PROJECT, ARIZONA**

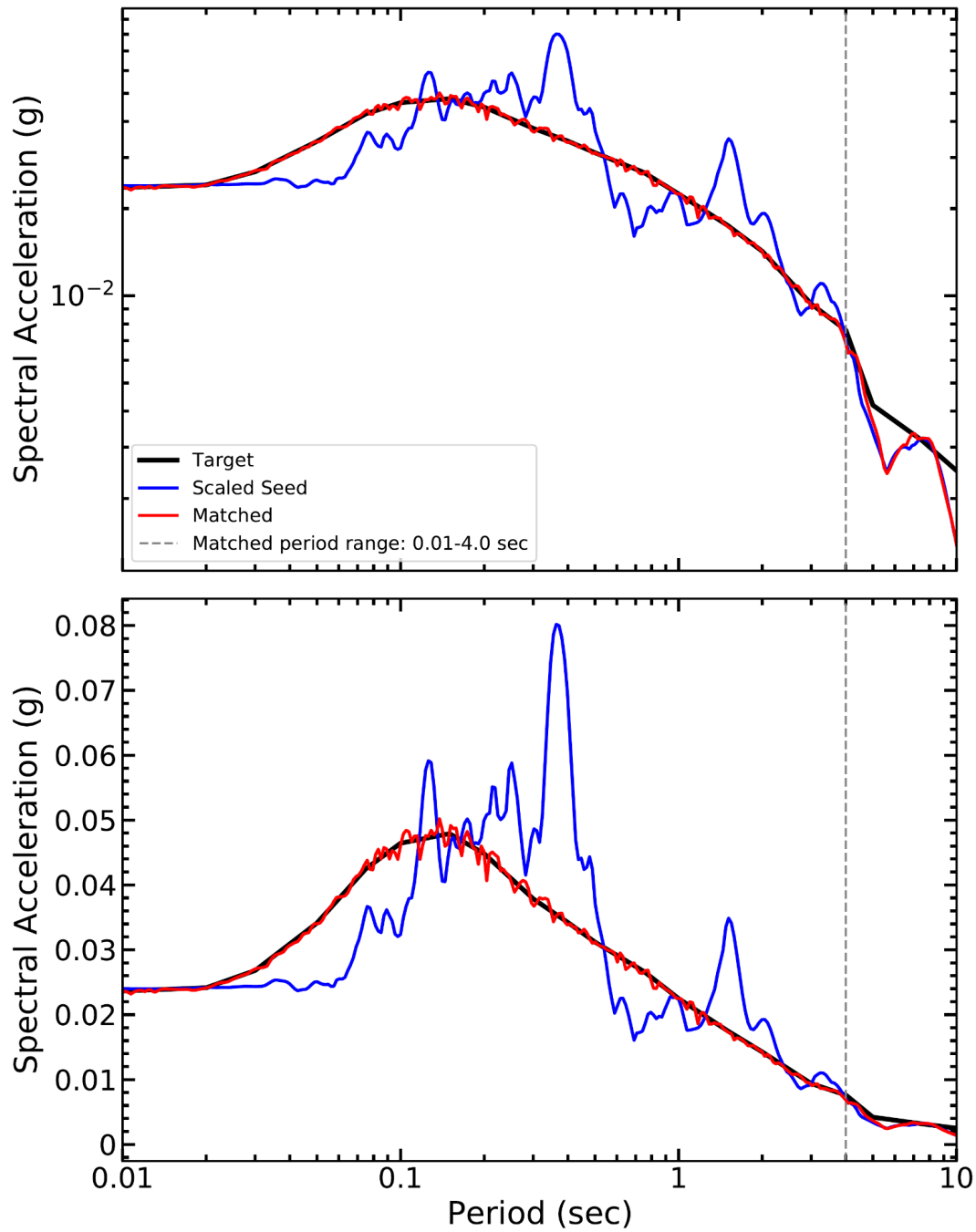


Lettis Consultants International, Inc.

Figure

**32**

## RSN295\_ITALY\_B-AUL270



Response Spectra for Time History Spectrally  
Matched to 475-Year Return Period UHS -  
1980 Irpinia, Italy-02 Earthquake  
- AUL270 Seed (RSN 295)

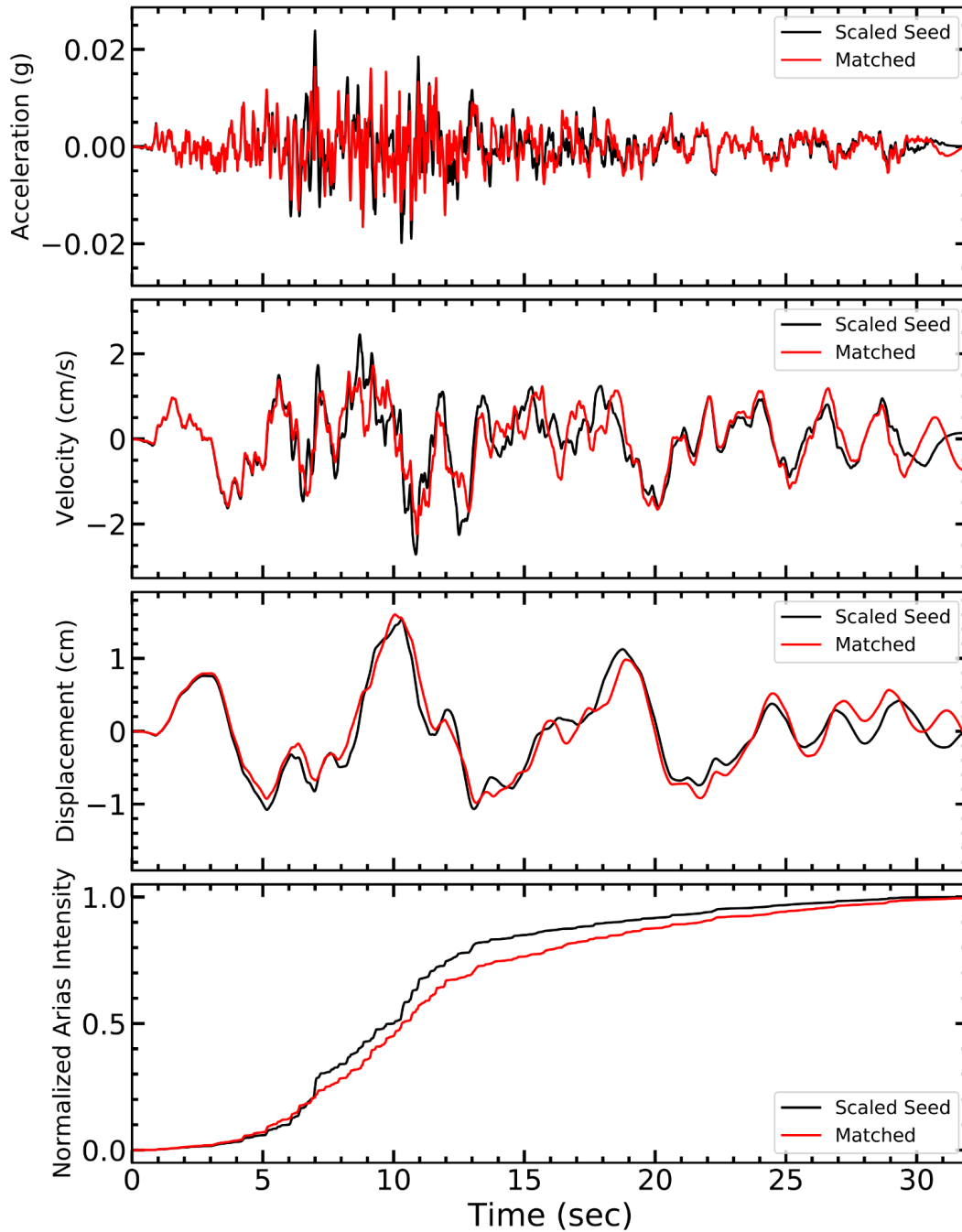
ROSEMONT COPPER WORLD PROJECT, ARIZONA



Lettis Consultants International, Inc.

Figure 33

# RSN295\_ITALY\_B-AUL270



**Time History Spectrally Matched to 475-Year  
Return Period UHS - 1980 Irpinia, Italy-02  
Earthquake - AUL270 Seed (RSN 295)**

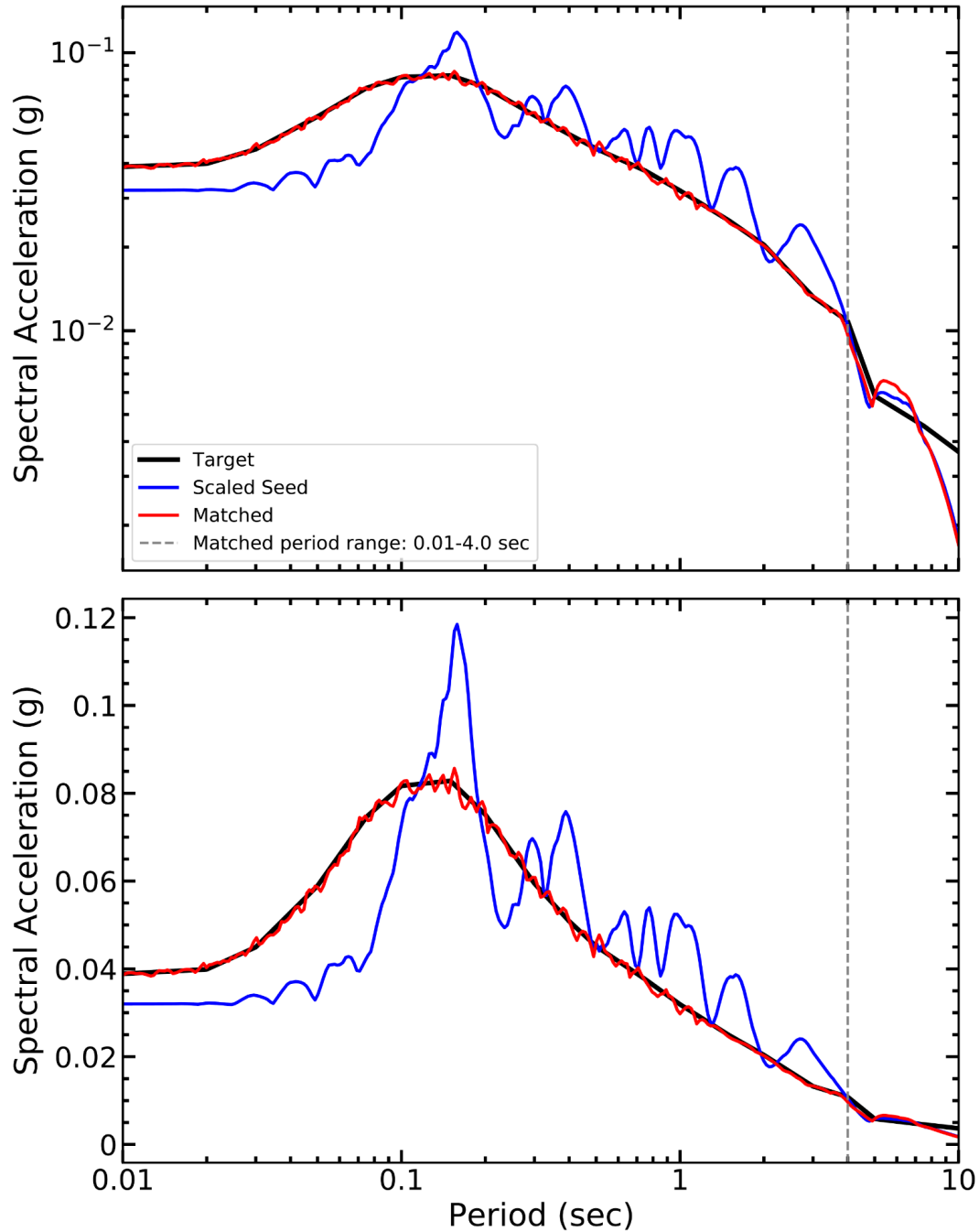
**ROSEMONT COPPER WORLD PROJECT, ARIZONA**



Lettis Consultants International, Inc.

Figure 34

# RSN2654\_CHICHI.03\_TCU120E



Response Spectra for Time History Spectrally  
Matched to 975-Year Return Period UHS -  
1999 Chi-Chi, Taiwan-03 Earthquake  
- TCU120E Seed (RSN 2654)

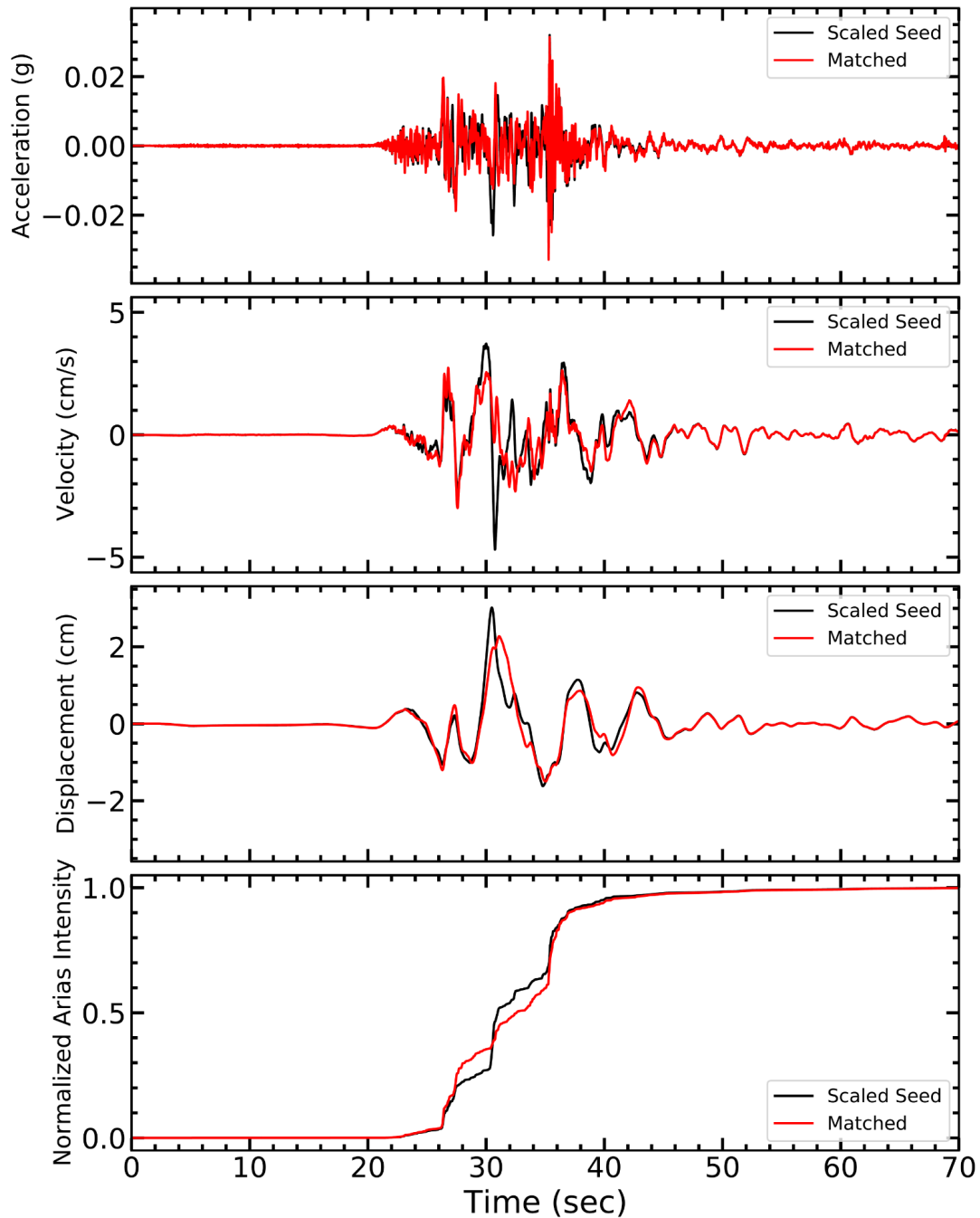
ROSEMONT COPPER WORLD PROJECT, ARIZONA



Lettis Consultants International, Inc.

Figure 35

# RSN2654\_CHICHI.03\_TCU120E



**Time History Spectrally Matched to 975-Year  
Return Period UHS - 1999 Chi-Chi, Taiwan-03  
Earthquake - TCU120E Seed (RSN 2654)**

**ROSEMONT COPPER WORLD PROJECT, ARIZONA**

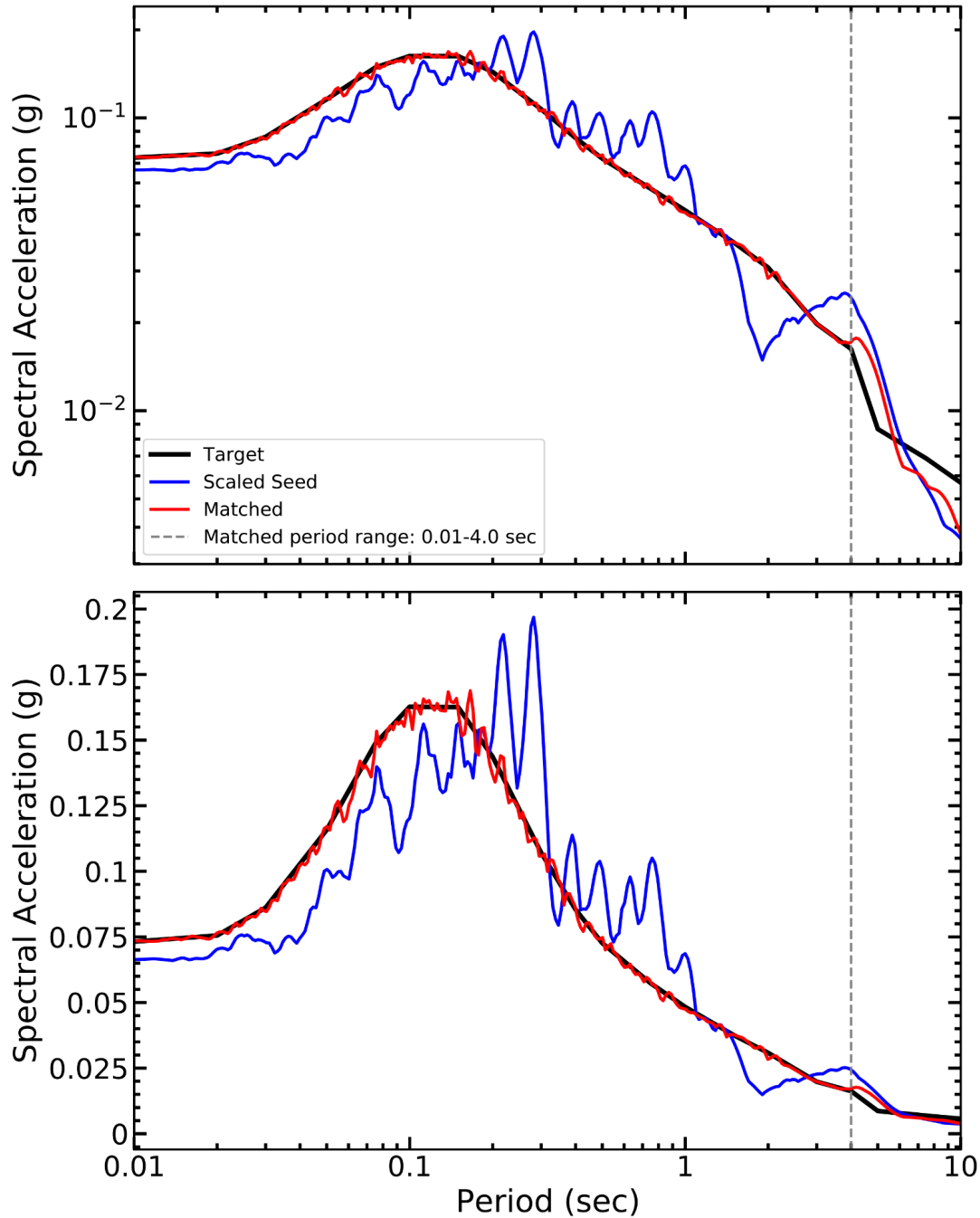


Lettis Consultants International, Inc.

Figure **36**



# RSN4478\_L-AQUILA\_GE146YLN



Response Spectra for Time History Spectrally  
Matched to 2,475-Year Return Period UHS -  
2009 L'Aquila, Italy Earthquake  
- GE146YLN Seed (RSN 4478)

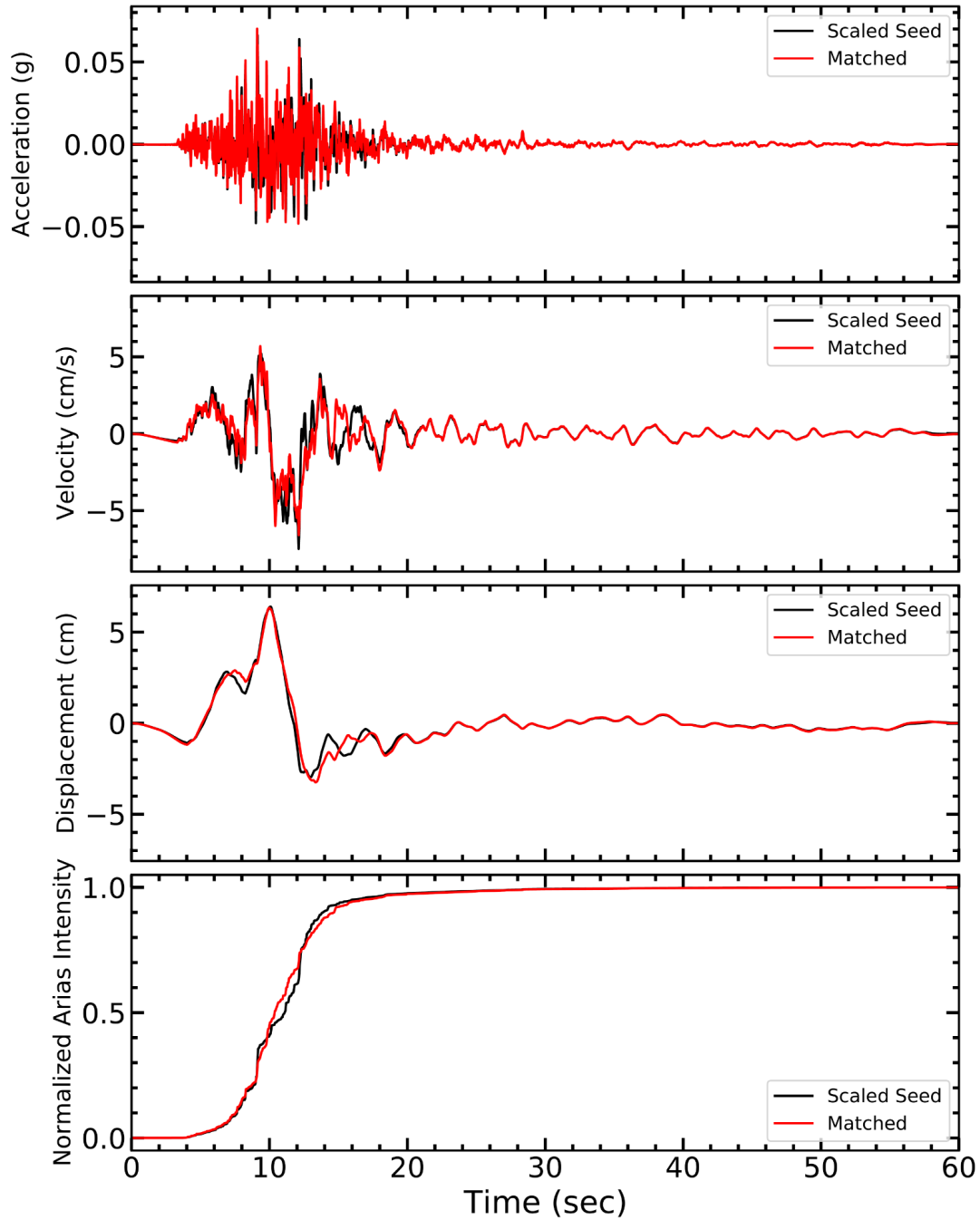
ROSEMONT COPPER WORLD PROJECT, ARIZONA



Lettis Consultants International, Inc.

Figure 37

# RSN4478\_L-AQUILA\_GE146YLN



**Time History Spectrally Matched to 2,475-Year  
Return Period UHS - 2009 L'Aquila, Italy  
Earthquake - GE146YLN Seed (RSN 4478)**

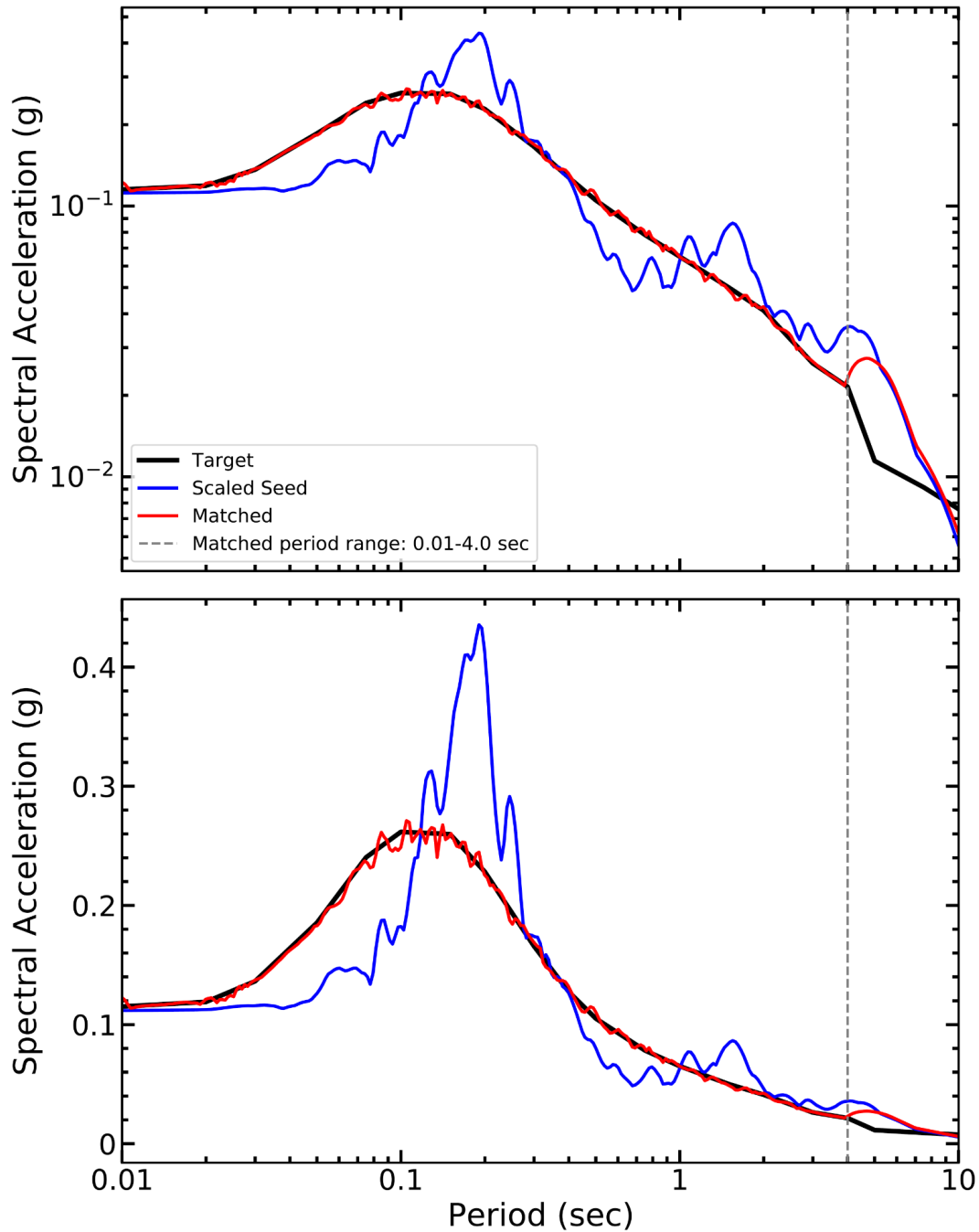
**ROSEMONT COPPER WORLD PROJECT, ARIZONA**



Lettis Consultants International, Inc.

Figure 38

# RSN4016\_SANSIMEO\_SLO090



Response Spectra for Time History Spectrally  
Matched to 5,000-Year Return Period UHS -  
2003 San Simeon, CA Earthquake  
- SLO090 Seed (RSN 4016)

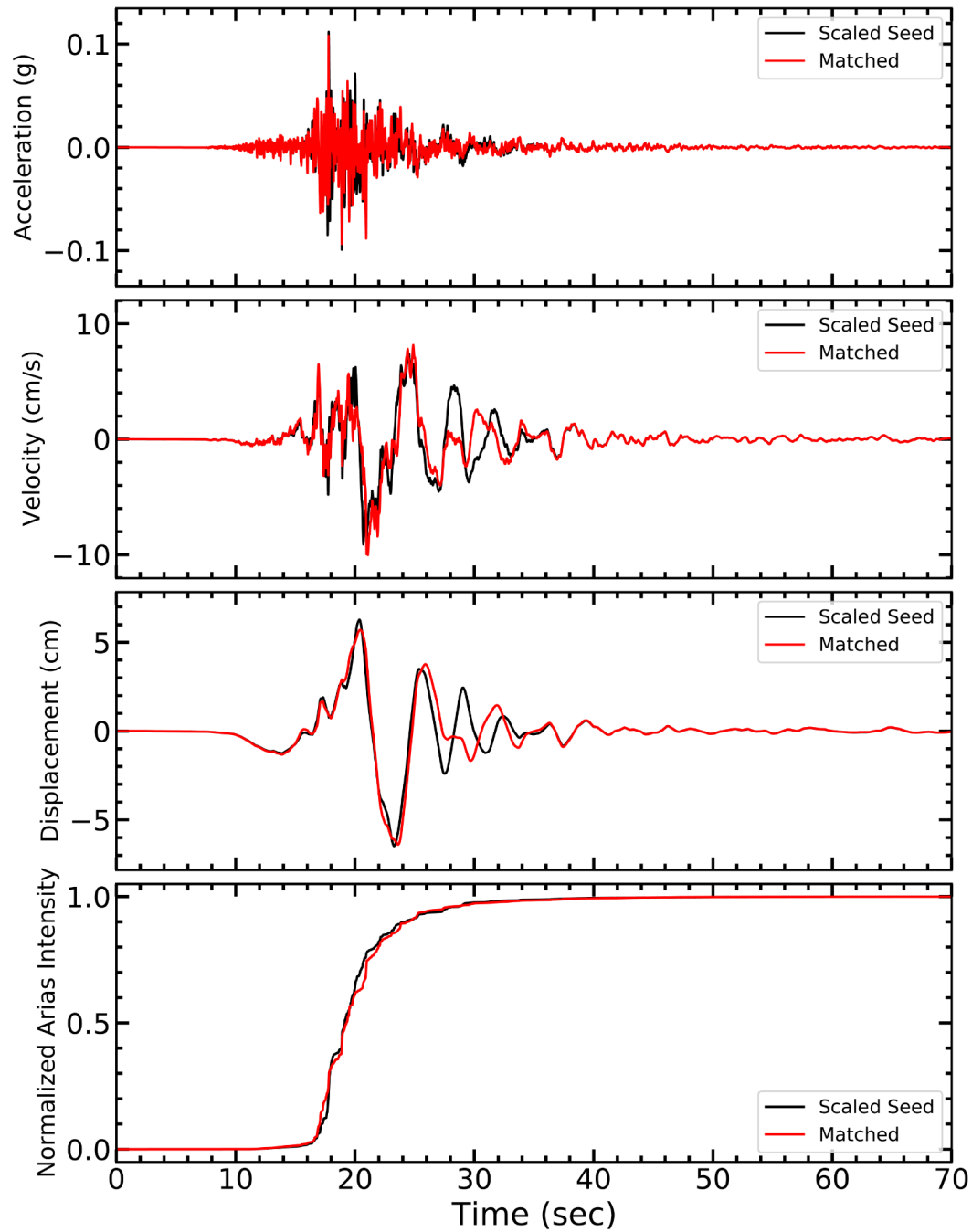
ROSEMONT COPPER WORLD PROJECT, ARIZONA



Lettis Consultants International, Inc.

Figure 39

## RSN4016\_SANSIMEO\_SLO090



**Time History Spectrally Matched to 5,000-Year  
Return Period UHS - 2003 San Simeon, CA  
Earthquake - SLO090 Seed (RSN 4016)**

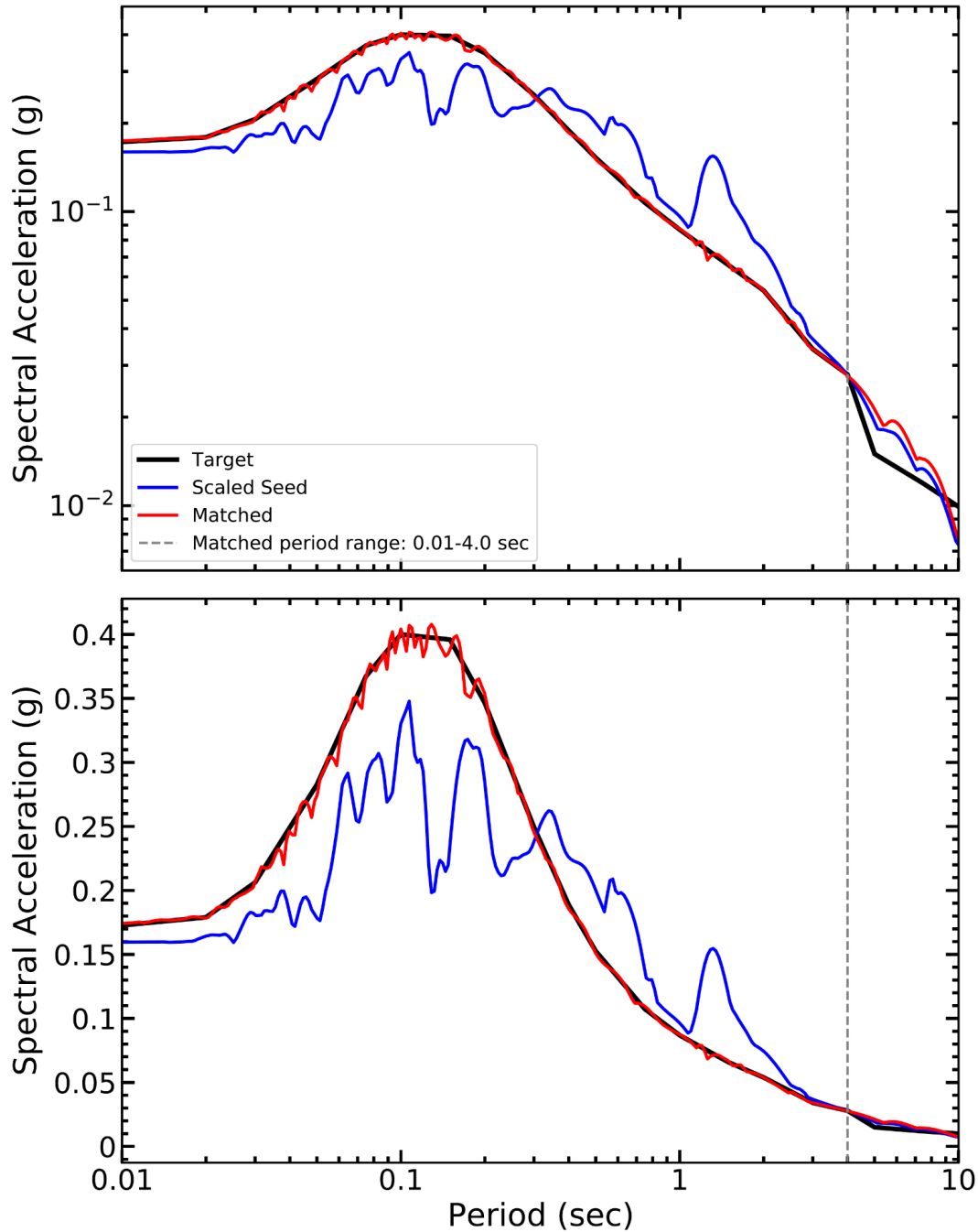
**ROSEMONT COPPER WORLD PROJECT, ARIZONA**



Lettis Consultants International, Inc.

Figure **40**

# RSN183\_IMPVALL.H\_H-E08140



Response Spectra for Time History Spectrally  
Matched to 10,000-Year Return Period UHS -  
1979 Imperial Valley-06 Earthquake  
- H-E08140 Seed (RSN 183)

ROSEMONT COPPER WORLD PROJECT, ARIZONA

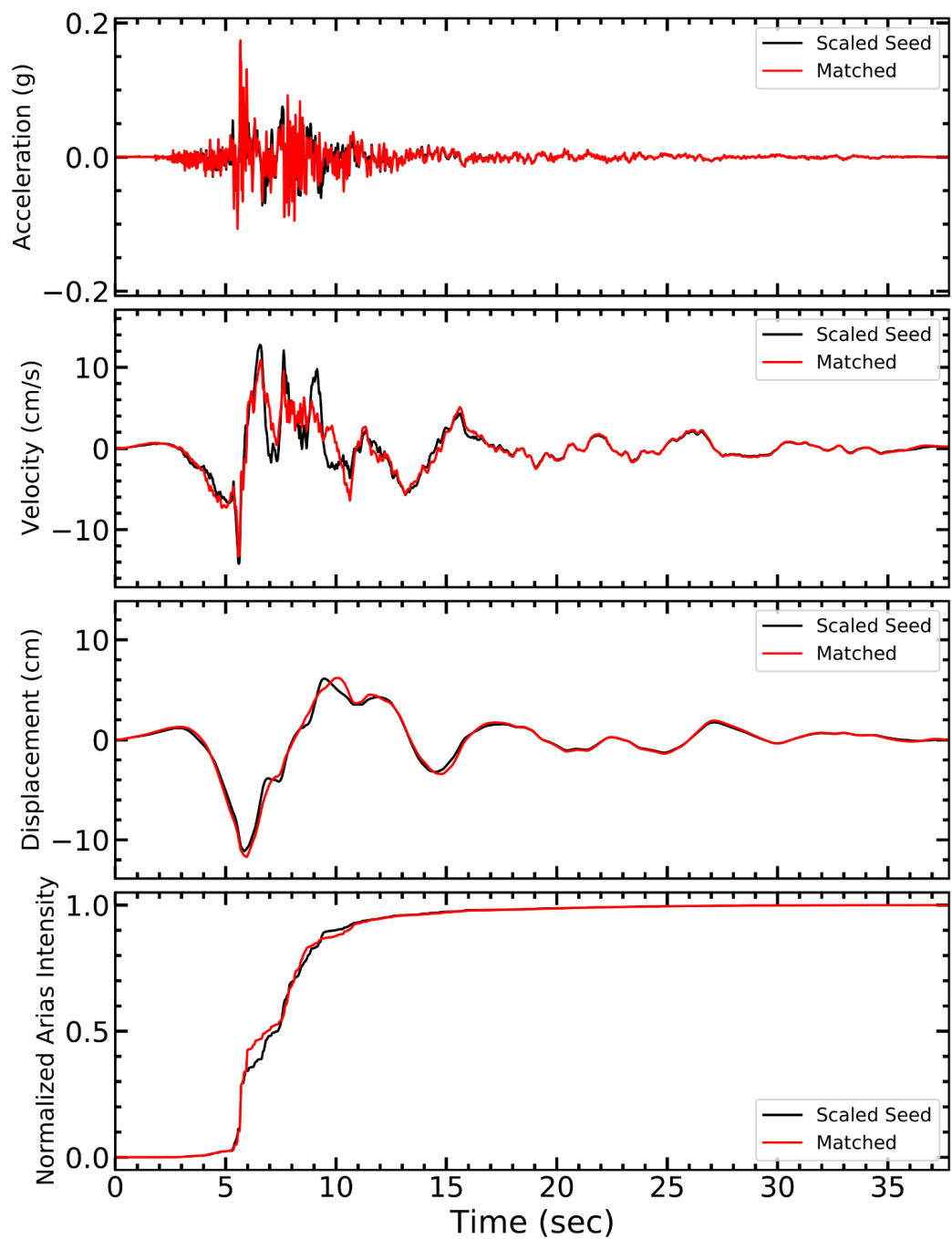


Lettis Consultants International, Inc.

Figure 41



RSN183\_IMPVALL.H\_H-E08140



Time History Spectrally Matched to 5,000-Year  
Return Period UHS - 1979 Imperial Valley-06  
Earthquake - H-E08140 Seed (RSN 183)

ROSEMONT COPPER WORLD PROJECT, ARIZONA

LCI Lettis Consultants International, Inc.

Figure 42

**APPENDIX B.4**  
**PROJECT DESIGN CRITERIA**



<b>Rosemont Copper World Project</b> <b>Pima County, Arizona</b>	<b>Civil &amp; Geotechnical</b> <b>DESIGN CRITERIA</b>	Page <b>2</b> of <b>12</b>	
		<b>DOC. NO.:</b> <b>1</b> ROSEMONT COPPER WORLD PROJECT DESIGN CRITERIA	
<b>PROJECT NO: 1720214024</b>		<b>DATE:</b> (ORIGINAL - 5/25/2021)	
		<b>REVISION:</b> <b>DATE:</b>	RW 09/01/2022

## TABLE OF CONTENTS

1.0	GENERAL .....	3
1.1	Site Location.....	3
1.2	Information Sources.....	3
1.3	Codes, Standards, and Regulations .....	4
1.4	Units and Symbols.....	4
2.0	SOILS, TAILINGS, AND SLURRY PROPERTIES.....	4
3.0	METEOROLOGICAL/CLIMATOLOGICAL DATA .....	4
4.0	HEAP LEACH PAD AND PONDS.....	5
5.0	GENERAL TAILINGS STORAGE FACILITIES INFORMATION .....	8
6.0	WASTE ROCK FACILITY .....	9
7.0	DIVERSION CHANNELS AND STORMWATER MANAGEMENT .....	9
8.0	GEOTECHNICAL STUDIES .....	10

Rosemont Copper World Project  Pima County, Arizona	Civil & Geotechnical  DESIGN CRITERIA	Page 3 of 12	
		DOC. NO.:1 ROSEMONT COPPER WORLD PROJECT DESIGN CRITERIA	
DATE: (ORIGINAL - 5/25/2021)			
PROJECT NO: 1720214024		REVISION: RW DATE: 09/01/2022	

## 1.0 General

This document defines the general design basis for civil and geotechnical work associated with the Tailings Storage Facilities (TSFs), Heap Leach Pad (HLP) and Water Management Pre-Feasibility Study at the proposed Rosemont Copper World Project (Project). All design work will be completed in general accordance with applicable requirements of Arizona Department of Environmental Quality (ADEQ) Aquifer Protection Permit's (APP) Program and its Arizona Mining Guidance Manual Best Available Demonstrated Control Technology (BADCT), which describes applicable regulations and commonly accepted industry standards and practices.

### 1.1 Site Location

The Project site is in Pima County, Arizona, approximately 28 miles southeast of Tucson at an average elevation of approximately 4,300-feet above mean sea level on the western slopes of the Santa Rita Mountains. The main mine facilities and operations will be located within Township 18 South, Range 15 East, including Sections 10,13,14,15,22,23,24,25,27, and 36 and Township 18 South, Range 16 East including Sections 19, 30 and 31. The project operation is centered near coordinates 31°51' N and 110°46' W.

### 1.2 Information Sources

The following source code letters refer to the origin of each criterion:

<b>Code</b>	<b>Description</b>
A	Criteria/Data provided by Hudbay
B	Wood
C	Manufacturer's standard
D	BADCT Guidance Manual and Other State Regulations/ ADWR
E	Standard Engineering Practice & Regulatory Standards & Code / International Tailings Standards
F	Existing Permits
G	Calculated
H	Studies by Other Consultants (Piteau, Bowman)
I	Assumed Data
J	



Rosemont Copper World Project  Pima County, Arizona	Civil & Geotechnical  DESIGN CRITERIA	Page 4 of 12	
		DOC. NO.:1 ROSEMONT COPPER WORLD PROJECT DESIGN CRITERIA	
DATE: (ORIGINAL - 5/25/2021)			
PROJECT NO: 1720214024		REVISION: RW DATE: 09/01/2022	

### 1.3 Codes, Standards, and Regulations

The design, as applicable, shall conform to the requirements of the latest issues of the following codes, standards, and regulations:

- ASTM American Society for Testing and Materials
- MSHA Mine Safety and Health Administration
- GRI Geosynthetic Research Institute
- NSF National Sanitation Federation
- AASHTO American Association of State Highway and Transportation Officials
- FTMS Federal Test Method Standards
- SCS Soil Conservation Service
- WRCC Western Regional Climate Center
- ADWR State of Arizona, Department of Water Resources
- ADEQ State of Arizona, Department of Environmental Quality
- APP Aquifer Protection Permit
- BADCT Best Available Demonstrated Control Technology Standards

### 1.4 Units and Symbols

US Imperial units will be used for all design work, calculations, and drawings.

## 2.0 Soils, Tailings, and Slurry Properties

Material properties will be generated from previous geotechnical investigations and test work.

## 3.0 Meteorological/Climatological Data

DESCRIPTION	VALUE	COMMENT	SOURCES
<b>CLIMATOLOGICAL FACTORS</b>			
Average annual precipitation, inch	19.73	The climate data will be based on average values of weather databases from the Helvetia (precipitation data) or Nogales (evaporation data). The Helvetia station is located near the project site and the Nogales station is located at the same approximate elevation as the lower portions of the project site	Helvetia Station
Average annual precipitation over 10-year period, inch	19.73		Helvetia Station
Minimum annual precipitation, inch	9.46		Helvetia Station
Average monthly precipitation, inch	1.64		Helvetia Station
Maximum monthly precipitation, inch			Helvetia Station

Rosemont Copper World Project  Pima County, Arizona	Civil & Geotechnical  DESIGN CRITERIA	Page 5 of 12	
		DOC. NO.:1 ROSEMONT COPPER WORLD PROJECT DESIGN CRITERIA	
DATE: (ORIGINAL - 5/25/2021)			
PROJECT NO: 1720214024		REVISION: RW DATE: 09/01/2022	

DESCRIPTION	VALUE	COMMENT	SOURCES
Maximum monthly precipitation, inch	3.53		Helvetia Station
Minimum monthly precipitation, inch	0.11		Helvetia Station
Average annual evaporation by average elevation, inch	91.2		Nogales Station
100-year/24-hour storm event	4.64		H
500-year/24-hour storm event			H
1000-year/24-hour storm event	6.42		H

- Rosemont Copper World Project Baseline and Final Configuration Hydrology (Bowman, Dated 9/18/22)

#### 4.0 Heap Leach Pad and Ponds

DESCRIPTION	VALUE	COMMENT	SOURCE
<b>GENERAL CRITERIA</b>			
Density of ore for sizing leach pad			
<b>HEAP LEACH PAD CONFIGURATION</b>			
Nominal lift height	30 feet		
Ultimate Maximum heap height	375 feet	103.8 million tons (MT) Capacity (per latest design)	H.31
Maximum overall heap slope	2.3H:1V	Actual ore heap slopes will include 30-foot Run-of-Mine (ROM) ore lifts stacked at the angle of repose estimated at about 1.4H:1V	H.31
Closure overall heap slope	2.3H:1V or flatter		
Individual lift slopes	1.3H:1V		
Bench width	30 feet		
Minimum slope for base pad grading	3%	Sloped toward the west side of the pad	H.31

Rosemont Copper World Project  Pima County, Arizona	Civil & Geotechnical DESIGN CRITERIA	Page 6 of 12	
		DOC. NO.:1 ROSEMONT COPPER WORLD PROJECT DESIGN CRITERIA	
DATE: (ORIGINAL - 5/25/2021)			
PROJECT NO: 1720214024		REVISION: RW DATE: 09/01/2022	

DESCRIPTION	VALUE	COMMENT	SOURCE
Minimum heap set-back from toe of heap to toe of perimeter berm	6 feet		H.31
<b>BASE MAPPING</b>			
Horizontal coordinate system		NAD83 UTM Zone 12 (at ground)	
Vertical datum		Same as above	
<b>OPERATIONAL PARAMETERS</b>			
Loading rate	30,000 ton/day (tpd) Years 1-4 45,000 tpd Years 5-9	45K tpd for HLP and 60K tpd for TSFs	A
Application rate (Average)	0.004 gallons per minute per square foot (gpm/sf)	By drip emitters	
Normal operational flow rate (target)	2,500 gpm	(3,000 gpm design)	H.31
Maximum operational flow rate	3,000 gpm		
Average leach cycle	45 days/90 days		H.31
Maximum road grade for on the pad	12%		A
<b>HEAP LEACH PAD</b>			
Prepared subgrade thickness	A minimum 12-inch-thick layer of prepared subgrade		
Low permeability layer (geosynthetic clay liner (GCL) material)	Saturated hydraulic conductivity (K) no greater than $1 \times 10^{-6}$ centimeter/second (cm/sec)	BADCT	
Geomembrane	80-mil linear low density polyethylene (LLDPE)	Liner will have double textured surfaces for stability and puncture strength	H.31
Overliner source	Overline drain fill (ODF) (minus 1.5-inch free-draining crusher rock)	<ul style="list-style-type: none"> <li>• BADCT</li> <li>• Puncture analyses for 60-, 80-, and 100-mil LLDPE</li> <li>• Geotech drilling and/or excavation studies to verify</li> </ul>	
Overliner layer thickness	A minimum 3-feet layer of ODF		

Rosemont Copper World Project  Pima County, Arizona	Civil & Geotechnical DESIGN CRITERIA	Page 7 of 12	
		DOC. NO.:1 ROSEMONT COPPER WORLD PROJECT DESIGN CRITERIA	
DATE: (ORIGINAL - 5/25/2021)			
PROJECT NO: 1720214024		REVISION: RW DATE: 09/01/2022	

DESCRIPTION	VALUE	COMMENT	SOURCE
Drainage aggregate source		Geotech drilling and/or excavation studies – preferred material (Qtz Monzonite)	
Solution collection pipe	ADS N-12 Corrugated High Density Polyethylene pipe	Industry Standard Design	
<b>PROPOSED OPERATIONAL AND NON-STORMWATER PONDS</b>			
Raffinate Pond capacity	18.2 acre-feet (ac-ft)	Assumption for design is to store up to 8 hours of operational flows and 100-yr 24- hr storm event criteria, including 24 hours of standby drain down flows. Double-lined with GCL and prepared subgrade	H.31
Reclaim Pond capacity	18.3 ac-ft		H.31
PLS Pond capacity	43.7 ac-ft		H.31
Primary Settling Pond capacity	43 acre-feet (primary cell) 7.7 acre-feet (secondary cell)	Assumption for design is to store 100-yr 24-hr storm event criteria, including 24 hours of standby drain down flows. Double-lined with GCL and prepared subgrade	H.31
Prepared subgrade (GCL) source	Sodium bentonite GCL	Wood will evaluate potential clay sources or other sources (i.e., Gila Conglomerate) **	H.31
Geomembrane	80-mil high density polyethylene (HDPE) primary liner 80-mil HDPE secondary liner	Primary pad liner will have a smooth texture.	H.31
Heap Leach Facility (HLF) North and South Stormwater Ponds capacity	Each pond with 44 acre- feet capacity	100 year/24-hour event (assuming standby generator and pumps). Single-lined with 80-mil HDPE with GCL and prepared subgrade	H.31
Process Area Stormwater Pond capacity	18 ac-ft capacity	100-year/24-hour event (assuming standby generator and pumps). Single-lined with 80-mil HDPE with GCL and prepared subgrade	H.31
Freeboard	2 feet (or 3 feet), see comment	Dry freeboard above design pond levels (BADCT)	H.31
<b>HAULAGE ROADS AND RAMP</b>			
Haul road maximum slope	10%		A
Haul road width	125 feet	Including ditch & safety berm	A
<b>LIGHT VEHICLE ROADS/PAD PERIMETER ROAD</b>			
Light vehicle perimeter road maximum slope	13%		A

Rosemont Copper World Project  Pima County, Arizona	Civil & Geotechnical  DESIGN CRITERIA	Page 8 of 12	
		DOC. NO.:1 ROSEMONT COPPER WORLD PROJECT DESIGN CRITERIA	
DATE: (ORIGINAL - 5/25/2021)			
PROJECT NO: 1720214024		REVISION: RW DATE: 09/01/2022	

DESCRIPTION	VALUE	COMMENT	SOURCE
Light vehicle perimeter road width	20 feet	Minimum road crest width along downhill side adjacent to collection ditch	A
<b>ORE PROPERTIES</b>			
Fresh ore moisture content	3.5%	Typical as-mined or as-placed on HLF (by dry weight), Column Test Data	
Moisture content under leach	TBD	Dynamic Moisture Retention (by dry weight), Column Test Data	
Water permanently loss due to ore wet up	7%	Final moisture – Fresh ore Moisture (by dry weight), Column Test Data	G
Ore dry density	125 pcf bulk density	Column Test Data	A

## 5.0 General Tailings Storage Facilities Information

DESCRIPTION	VALUE	COMMENT	SOURCE
<b>TSF DESIGN CRITERIA</b>			
Average Settled Density of Tailings	90 pcf		A
Facility Design Storage	277 million tons		A
Daily Production Rate	30,000 tpd Years 1-4 60,000 tpd Year 5-15	30K tpd for-4 years, 60K tpd starting Year 5.	A
Annual Production Rate	30M/60M tons / year		A
Operational Life	15 Years		A
<b>OPERATION/CONSTRUCTION LIMITATION</b>			
Maximum downstream face slope of Tailings Raise	3.0H:1V	Based on closure, confirmed by Stability	G
Maximum downstream face slope of Starter and Boundary Dams	2.5H:1V		
Minimum Starter/Boundary Dam Width	50 feet	Crest width	
Starter/Boundary Dam Material Source		Local Cut to Fill	
<b>TSF CLOSURE CRITERIA</b>			
Maximum Regraded Slope	3.0H:1V		



Rosemont Copper World Project  Pima County, Arizona	Civil & Geotechnical  DESIGN CRITERIA	Page 9 of 12	
		DOC. NO.:1 ROSEMONT COPPER WORLD PROJECT DESIGN CRITERIA	
DATE: (ORIGINAL - 5/25/2021)			
PROJECT NO: 1720214024		REVISION: RW DATE: 09/01/2022	

--	--	--	--

## 6.0 Waste Rock Facility (WRF)

DESCRIPTION	VALUE	COMMENT	SOURCE
<b>WASTE, ROCK, L DESIGN CRITERIA</b>			
Average Placed Density of Waste	125 pounds per cubic foot (pcf)		
Facility Design Storage	477 MT	Mine Plan	A
Nominal Lift Height	100 feet		
Maximum Dump Height	820 feet		
Maximum Overall Dump Slope	2.2H:1V		
Maximum Inter-Bench Finish Slope	1.4H:1V		
Minimum Inter-Bench Finish Slope	1.4H:1V		
Minimum Width of Operating Platform	100 feet		

## 7.0 Diversion Channels and Stormwater Management

DESCRIPTION	VALUE	COMMENT	SOURCE
<b>DIVERSION CHANNELS AND CULVERT</b>			
Storm event for depth sizing (permanent)	1,000-year/24-hour	-	D
Storm event for depth sizing (temporary)	100-year/24-hour	-	
Storm event for erosion control lining depth (permanent)	1,000-year/24-hour	-	D
Storm event for erosion control lining (temporary)	100-year/24-hour	-	
Freeboard (permanent and temporary)	1 foot (temporary) 2 feet (permanent) minimum	BADCT	D
Erosion Protection -	Riprap, gabions, articulating concrete blocks (ACB), shotcrete, drop structures, liners, fabrics	-	D

Rosemont Copper World Project  Pima County, Arizona	Civil & Geotechnical  DESIGN CRITERIA	Page 10 of 12	
		DOC. NO.:1 ROSEMONT COPPER WORLD PROJECT DESIGN CRITERIA	
DATE: (ORIGINAL - 5/25/2021)			
PROJECT NO: 1720214024		REVISION: RW DATE: 09/01/2022	

DESCRIPTION	VALUE	COMMENT	SOURCE
Culverts	1,000-year/24-hour		
Diameter requirement	> 18 inches	ADEQ Requirement Use multiple culverts if necessary	
Culvert material type	Corrugated metal pipe (CMP), HDPE	Depending on availability	A
<b>FLOOD STORAGE</b>			
Sediment Basins	10-year, 24-hour		D
Other Stormwater Containment (if required)	100-year/24-hour		D

## 8.0 GEOTECHNICAL STUDIES

DESCRIPTION	VALUE	COMMENT	SOURCE
<b>TAILINGS AND DUMP STORAGE FACILITY STABILITY</b>			
Tailings Stability – static minimum safety factor for final construction stage (without support of testing data)	1.5		D
Tailings Stability – static minimum safety factor for final construction stage (with support of testing data)	1.3		D
Tailings Stability – static minimum safety factor for Intermediate Stage	1.3		D
Tailings Stability – pseudo-static minimum safety factor for final construction stage (without support of testing data)	1.1		D
Tailings Stability – pseudo-static minimum safety factor for final construction stage (with support of testing data)	1.0		D
Tailings Stability – pseudo-static minimum safety factor for Intermediate Stage	1.0		D
Peak ground acceleration (g)	Subconsultant	Analysis completed; see Seismic Design Event	B, H
HLP Stability – static minimum safety factor for final construction stage (without support of testing data)	1.5		D

<b>Rosemont Copper World Project</b>  <b>Pima County, Arizona</b>	<b>Civil &amp; Geotechnical</b>  <b>DESIGN CRITERIA</b>	Page <b>11</b> of <b>12</b>	
		<b>DOC. NO.:1</b> ROSEMONT COPPER WORLD PROJECT DESIGN CRITERIA	
<b>DATE:</b> (ORIGINAL - 5/25/2021)			
<b>PROJECT NO: 1720214024</b>		<b>REVISION:</b> <b>DATE:</b>	RW 09/01/2022

DESCRIPTION	VALUE	COMMENT	SOURCE
HLP Stability – static minimum safety factor for final construction stage (with support of testing data)	1.3		D
HLP Stability – static minimum safety factor for Intermediate Stage	1.3		D
HLP Stability – pseudo-static minimum safety factor for final construction stage (without support of testing data)	1.1		D
HLP Stability – pseudo-static minimum safety factor for final construction stage (with support of testing data)	1.0		D
HLP Stability – pseudo-static minimum safety factor for Intermediate Stage	1.0		D
Peak ground acceleration (g) TBD	Subconsultant	Analysis completed; see Seismic Design Event	B, H
WRF Stability – static minimum safety factor for final construction stage (without support of testing data)	1.5		D
WRF Stability – static minimum safety factor for final construction stage (with support of testing data)	1.3		D
WRF Stability – static minimum safety factor for Intermediate Stage	1.3		D
WRF Stability – pseudo-static minimum safety factor for final construction stage (without support of testing data)	1.1		D
WRF Stability – pseudo-static minimum safety factor for final construction stage (with support of testing data)	1.0		D
WRF Stability – pseudo-static minimum safety factor for Intermediate Stage	1.0		D
Peak ground acceleration (g)	Subconsultant	Analysis completed; see Seismic Design Event	B, H

Rosemont Copper World Project  Pima County, Arizona	Civil & Geotechnical DESIGN CRITERIA	Page 12 of 12	
		DOC. NO.:1 ROSEMONT COPPER WORLD PROJECT DESIGN CRITERIA	
DATE: (ORIGINAL - 5/25/2021)			
PROJECT NO: 1720214024		REVISION: RW DATE: 09/01/2022	

DESCRIPTION	VALUE	COMMENT	SOURCE
Seismicity Design Event	Subconsultant	TSF: Design earthquake with 10,000-year return interval. Maximum credible earthquake (MCE) also considered to evaluate potential impact on the public safety and human life  HLF/WRF: Design earthquake with 2,475-year return interval	D
<b>GEOHAZARDS</b>			
Geological Mapping Data	Subconsultant	Including fault information	B